

# Remote Sensing and Modelling of Wind Waves in Semi-Enclosed Seas

Fatemeh Najafzadeh

TALLINN UNIVERSITY OF TECHNOLOGY  
DOCTORAL THESIS  
64/2022

# **Remote Sensing and Modelling of Wind Waves in Semi-Enclosed Seas**

FATEMEH NAJAFZADEH



TALLINN UNIVERSITY OF TECHNOLOGY  
School of Science  
Department of Cybernetics  
Wave Engineering Laboratory

This dissertation was accepted for the defence of the degree 01/11/2022

**Supervisor:** Prof. Dr. Tarmo Soomere  
Department of Cybernetics, School of Science  
Tallinn University of Technology  
Tallinn, Estonia

**Opponents:** Prof. emer. Matti Leppäranta  
Institute for Atmospheric and Earth System Research  
University of Helsinki  
Finland

Dr. Joanna Staneva  
Department of Hydrodynamics and Data Assimilation  
Helmholtz Zentrum Hereon  
Geesthacht, Germany

**Defence of the thesis:** 02/12/2022, Tallinn

**Declaration:**

Hereby I declare that this doctoral thesis, my original investigation and achievement, submitted for the doctoral degree at Tallinn University of Technology has not been submitted for doctoral or equivalent academic degree.

Fatemeh Najafzadeh

-----  
signature



European Union  
European Regional  
Development Fund



Investing  
in your future

Copyright: Fatemeh Najafzadeh, 2022  
ISSN 2585-6898 (publication)  
ISBN 978-9949-83-917-9 (publication)  
ISSN 2585-6901 (PDF)  
ISBN 978-9949-83-918-6 (PDF)  
Printed by Auratrükk

TALLINNA TEHNIKAÜLIKOOL  
DOKTORITÖÖ  
64/2022

# Tuulelainete kaugseire ja modelleerimine poolsuletud merealadel

FATEMEH NAJAFZADEH





# Content

<b>List of publications .....</b>	<b>6</b>
<b>Author's contribution to the publications .....</b>	<b>6</b>
<b>Introduction .....</b>	<b>7</b>
Wind climate .....	9
Wave properties from models and satellite altimetry .....	10
The technique of Empirical Orthogonal Functions.....	11
Ice season duration .....	12
Interplay of wind anisotropy, loss of ice and local features.....	13
The objective and outline of the thesis.....	14
<b>1 Applicability of the EOF technique for satellite data in the Baltic Sea.....</b>	<b>17</b>
1.1 Wave properties in the Baltic Sea .....	17
1.2 Atmospheric circulation in the Baltic Sea.....	18
1.3 Empirical Orthogonal Functions .....	20
1.4 Satellite altimetry data.....	21
1.5 Seasonal variability and averaging errors.....	25
1.6 Sensitivity of the Empirical Orthogonal Function technique.....	25
<b>2 Links between large-scale forcing and the Baltic Sea wave climate .....</b>	<b>31</b>
2.1 Evidence about teleconnection patterns .....	31
2.2. Spatial variations in the wave fields .....	32
2.3 Reliability of spatial patterns.....	34
2.4 Wave climate pattern and its links with atmospheric circulations.....	35
2.5 Time variable correlation with climatic indices .....	36
<b>3 The effects of seasonal ice cover on wave fields.....</b>	<b>38</b>
3.1 The decreasing influence of ice on wave impact.....	38
3.2 Sea ice and wave data .....	41
3.3 Wave climate during ice-free times.....	45
3.4 Impact of the presence of ice on average wave properties .....	48
3.5 The role of ice season duration .....	50
<b>4 Directional effects in the nearshore .....</b>	<b>53</b>
4.1 Wave fields in the Gulf of Riga and near Ruhnu.....	53
4.2 Simulation of local wave patterns .....	56
4.3 Refraction-driven redirection of storm waves near Ruhnu.....	58
<b>Conclusions .....</b>	<b>61</b>
Summary of the results .....	61
Main conclusions proposed to defend .....	63
Recommendations for further work.....	64
<b>References .....</b>	<b>65</b>
<b>Acknowledgements.....</b>	<b>77</b>
<b>Abstract .....</b>	<b>78</b>
<b>Lühikokkuvõte .....</b>	<b>79</b>
<b>Appendix: Papers constituting the thesis .....</b>	<b>81</b>
<b>Curriculum Vitae .....</b>	<b>130</b>
<b>Elulookirjeldus .....</b>	<b>132</b>

## List of publications

The list of author's publications, on the basis of which the thesis has been prepared:

- Paper I      **Najafzadeh F.**, Kudryavtseva N., Soomere T. 2021. Effects of large-scale atmospheric circulation on the Baltic Sea wave climate: application of the EOF method on multi-mission satellite altimetry data. *Climate Dynamics* 57(11), 3465–3478, doi: 10.1007/s00382-021-05874-x.
- Paper II      **Najafzadeh F.**, Kudryavtseva N., Soomere T., Giudici A. 2022. Effect of ice cover on wave statistics and wave-driven processes in the northern Baltic Sea. *Boreal Environment Research*, 27, 97–116.
- Paper III     Männikus R., Soomere T., **Najafzadeh F.** 2022. Refraction may redirect waves from multiple directions into a harbour: a case study in the Gulf of Riga, eastern Baltic Sea. *Estonian Journal of Earth Sciences*, 71(2), 80–88, doi: 10.3176/earth.2022.06.

## Author's contribution to the publications

Contribution to the papers in this thesis are:

- I    I retrieved the time series of various teleconnection indices, performed the relevant statistical analysis, produced the images, and wrote about 60% of the text.
- II   I provided the idea for the research, designed the framework of visualisation, retrieved the ice observation data from the SMHI database, performed the analysis of wave and ice data, produced the images, wrote about 70% of the text, and acted as the corresponding author.
- III  I performed part of the calculations, created the relevant images, developed interpretation of the results in the context of climate change, and wrote the associated parts of the manuscript.

## Introduction

The oceans and seas are the main sources of heat absorption received by the Earth from the Sun. Differential heating between the equator and the poles drives motions in the atmosphere. In turn the wind transmits kinetic energy from the atmosphere to the oceans in the form of driving surface currents and waves. The amount of absorbed heat has been increasing over the last decades (Levitus et al., 2005; Lindsey and Dahlman, 2020), which has amplified the variations in both land and sea surface temperature. This has led to stronger winds (Reguero et al., 2019) and also the intensification and reshaping of both large-scale wind systems and individual storms. An increase in wind speed generally means that the surface waves induced by wind carry more energy. This change has an essential contribution to many aspects of offshore and coastal management, including shaping shorelines (e.g., Łabuz, 2015; Kelpšaitė-Rimkienė et al., 2021), coastal erosion (Ryabchuk et al., 2011a; Suursaar et al., 2014; Harff et al., 2017), increase in local sea-level extremes (e.g., Kudryavtseva et al., 2021), and issues with safety of navigation and shipping (Goerlandt et al., 2017; Lensu and Goerlandt, 2019; Barbariol et al., 2019).

A direct consequence of oceanic (climate) warming is an increase in wave energy flux or power (Reguero et al., 2019), which is harnessed by waves produced via the interaction between wind and the sea-surface. In many situations, wave energy flux provides more information than other parameters of wave conditions since it takes into account both wave height (wave energy) and wave period over the duration of time. There is a similar increase in the mean wave height and, an even larger increase in the extreme wave height (Wang and Swail, 2002; Young et al., 2011). These changes not only endanger offshore and coastal infrastructure (e.g., Weisse et al., 2012) but may also reshape alongshore sediment transport (Soomere et al., 2015; Masselink et al. 2016) and increase the vulnerability of the coastal zone.

Climate change is also one of the main accelerators of wave climate variability. In order to better comprehend the effects of this, it is essential to investigate the large-scale atmospheric circulation patterns (often called teleconnection patterns). The term “teleconnection pattern” specifies the anomalies of the large-scale pattern of atmospheric pressure at a certain height (measured, e.g., at 500-hPa geopotential height). The effects of these patterns may last from several weeks to several years and may stretch over continents and oceans. For instance, the consequences of El Niño–Southern Oscillation and North Atlantic Oscillation span the North Pacific Ocean, and from eastern North America to northern Europe and Scandinavia, respectively. Different phases of teleconnection patterns affect the wave properties. The impact of these patterns can be explained in terms of climate change (Wang et al., 2004). There is a robust connection between the interannual extreme wave conditions in the North Atlantic and the climatic indices of North Atlantic Oscillation and Arctic Oscillation (Izagirre et al., 2011). Thus, long-term wave climate variability and its effect on coastal process can be to a certain extent assessed by the properties of teleconnection patterns.

Semi-enclosed marginal seas, such as the Baltic Sea, are particularly sensitive to climate change driven variations in the large-scale circulation patterns. First of all, such patterns govern the predominant wind and wave direction and may thus give rise to asymmetry of wave fields. Further, changes to these patterns may strongly affect the number and typical trajectories of cyclones crossing such seas. These variations also

affect the amount of heat carried into the region and induce changes in the predominant directions in local storms. For example, multi-decadal variations in the typical locations of low-pressure areas in the northern Baltic Sea region (Bärring and von Storch, 2004) have apparently affected the spatial and directional distribution of surface wave energy at the downwind shores (Kelpšaitė and Dailidienė, 2011). As the wave fields of the Baltic Sea are locally generated and swells are usually infrequent and weak (Broman et al., 2006; Björkqvist et al., 2021), modifications in the trajectories of storm cyclones may lead to substantial changes in wave approach directions for some coastal segments, with possibly extensive consequences on sedimentary landforms (Viška and Soomere, 2012).

Changes to the extent and duration of the ice cover may greatly alternate the magnitude of wave power in many segments of seasonally ice-covered seas, such as the Baltic Sea. Climate change has led to a shorter ice season in the Arctic (Overeem et al., 2011) and, partially as a consequence, in the Baltic Sea (Omstedt et al., 2004; Haapala et al., 2015). Sea ice, with its albedo within a range of 0.5–0.7, is one of the main factors that determines solar heat exchange in polar oceans. When the sea ice melts, the albedo decreases to the level of 0.06, and the distance over which wind can interact with the sea surface to produce waves (the fetch) increases. This results in higher and longer the sea waves.

The variation in sea ice influenced by the climate change might be one of the vital elements that determine the future of the wave climate in polar and seasonally ice-covered seas. Correspondingly, the combination of the greater heat absorption and weaker ice field exposes the open water and coastal areas to more severe wave conditions in these basins. The associated changes to wave properties involve not only an increase in the wave height, energy and power, and possibly changes in the propagation direction, owing to longer fetch, but also changes in the refraction properties because of associated changes in wave periods. These consequences may add to the variation of regional wave climate and make it more challenging to understand.

Therefore, climate change and the increasing trend of ocean heat content have led to a complicated, multi-step cascade of impacts in some parts of the World, such as more frequent and powerful storms, an increase in wave heights, and changes in the predominant wave direction. This cascade is complemented by changes driven by the loss of sea ice in polar and subpolar seas, for example the Baltic Sea. A natural consequence is an increased probability of partially wave-driven flooding (e.g. wave set-up, Pindsoo and Soomere, 2015) and more erosive energy potential for coastlines (Orviku et al., 2003; Ryabchuk et al., 2011b). An understanding of wave climate and its spatio-temporal variations is essential to mitigate coastal threats, minimize economic losses, and provide adequate information for engineering and coastal planning (e.g., Hemer et al., 2013) in the future.

This thesis makes an attempt to quantify three steps of this cascade that are less commonly addressed in the international literature. First, the properties of spatial patterns of wave height in the wider Baltic Sea, such as the east-west pattern and the related anisotropy of wave fields, and their background driving mechanisms are investigated using satellite wave height data and the technique of Empirical Orthogonal Functions. Second, the consequences of further loss of ice on these coastal segments are evaluated using satellite information about ice and model data about wave properties. Finally, the joint consequences of this anisotropy and depth-induced refraction in Estonian waters from the viewpoint of one small port is explored.

## Wind climate

Most of the temporal variations in wave properties stem from the wind field. The features of wind waves depend on the wind speed and duration, as well as the fetch length. Due to the relatively small dimensions of the Baltic Sea, the waves in this basin are fetch-limited and classic long-period regular swells are rarely produced (Broman et al., 2006; Björkqvist et al., 2021). Therefore, the waves mostly reflect features of the local wind climate (Suursaar, 2013; 2015). The Baltic Sea has a strongly elongated shape, as do the Gulf of Finland and the Sea of Bothnia which are its large subbasins. This means that even a slight change in the wind direction which affects the fetch length can cause substantial variations in the wave properties, such as wave height, period, and direction.

The wind fields over the Baltic Sea have strong seasonal and annual variations. The wind climate over the Baltic Sea also contains extensive regional variations. The overall wind speed has not changed substantially during the last century (Hünicke et al., 2015), however, there is a clear increase in the mean geostrophic wind speed in winter and to a lesser degree in spring (Lehmann et al., 2011). This increase is also associated with a change in the wind direction to more westerly than north-westerly (Keevallik and Soomere, 2008) in the easternmost Baltic Sea.

The presence of a predominant strong wind direction greatly affects the formation and properties of the wave climate. The most frequent wind directions in the northern section of the main part of the Baltic Sea (Baltic proper) are south-west and north-north-west (Soomere and Keevallik, 2001). While the weak winds ( $\leq 5$  m/s) are usually more or less isotropic, the moderate (6–10 m/s) and strong ( $>10$  m/s) winds exhibit high anisotropy in this region. Strong winds usually blow from south-west and west from where winds are most frequent. The strongest winds ( $>10$  m/s), however, may blow from north-north-west. This property of wind fields in the north-east of the Baltic Sea was established based on relatively limited evidence (Soomere, 2001) but was recently confirmed by evidence of exceptional wave heights in the Sea of Bothnia (Björkqvist et al., 2020). As fetch length for these wind directions is different, northern storms usually result in shorter waves in Estonian waters. The anisotropy in the wind and wave fields has large effects on the local sea level (Orviku et al., 2003; Männikus et al., 2019) and sediment transport in shallow areas (Jönsson et al., 2005).

The wind climate of the Baltic Sea has undergone large variations in the past. Omstedt et al. (2004) identified a significant change in cyclonic circulation at the end of the 19th century. The analysis of Bärring and von Storch (2004) indicates similar large variations in the low-pressure regime. These variations can be to some extent related to and quantified by the concept of large-scale teleconnection patterns, such as the North Atlantic Oscillation (NAO) or the Arctic Oscillation (AO), that to a large extent govern wind properties over the Baltic Sea. The time series of the relevant indices also show clear correlation with the Baltic Sea water level records (Andersson, 2002; Wakelin et al., 2003; Jevrejeva et al., 2005; Suursaar and Sooäär, 2007), temperature (e.g., Jacobeit et al., 2001), and ice conditions (e.g., Jevrejeva et al., 2003). It is therefore natural to expect a similar relationship between such indices and wave climate in the Baltic Sea. This is to some extent explored in Paper I, based on wave properties evaluated using satellite altimetry.

## Wave properties from models and satellite altimetry

The Baltic Sea is a challenge for studies of wave climate. Even though it is practically isolated from the rest of the World Ocean in terms of wind waves, its complex shape, extensive variability of wind properties and seasonal presence of ice cover make both wave measurements and simulations an extremely complicated task. Lack of reliable large-scale wave height measurements leads to gaps in the knowledge of wave climate variations in the Baltic Sea, and their drivers.

There exist several ways to acquire and compile information about wave properties. The longest times series are provided by visual wave observations (Soomere, 2013). Their accuracy and spatio-temporal resolution are not sufficient to create an adequate perception of wave fields in larger sea areas.

Instrumental *in situ* wave measurements provide high-quality information in time. This information represents only a specific location and does not have a good spatial coverage. The most common *in situ* measurement devices, waverider buoys, are removed from the sea before the start of the ice season (Tuomi et al., 2011). This leads to major gaps in the information about waves in parts of the sea that have extensive seasonal ice cover. In particular, the strongest wave events could be easily lost in the climate of the Baltic Sea where the strongest storms occur during the cold season (Björkqvist et al., 2017).

Contemporary wave models provide very good spatial and temporal resolution of the wave fields of the Baltic Sea (Soomere, 2022). The third-generation wave models such as WAM (Hasselmann et al., 1988; Komen et al., 1994; Cavaleri, 1997) and SWAN (Booij et al., 1999) are widely used for the forecast and hindcast of wave properties in the Baltic Sea (Soomere et al., 2008; Cieřlikiewicz and Paplińska-Swerpel, 2008; Björkqvist et al., 2018; Tuomi et al., 2019). The consistent coverage of wave models makes it feasible to investigate spatial, seasonal and decadal variations in the main wave properties (Soomere and Räämet, 2014). However, the quality of their output substantially depends on the adequacy of the forcing wind data, information about ice, and the ability to resolve or parameterise wave propagation in archipelagos (Tuomi et al., 2011; Soomere and Räämet, 2011; Björkqvist et al., 2018; Räämet and Soomere, 2021).

For the listed reasons satellite information is gradually becoming one of the most important methods to retrieve instantaneous wave properties in single locations. The increase in the coverage of this kind of information has made it possible to estimate spatial patterns of wave fields, and to evaluate changes to these patterns (Young and Ribal, 2022) and their links to atmospheric circulation patterns on a global scale (Hannachi, 2004). This approach also works well in regional applications, for example, at the scale of the North Atlantic where Izaguirre et al. (2011) analysed interrelations of several climate indices and interannual changes to average and extreme wave heights.

There are several options for retrieving wave properties from satellite-based remote sensing systems. For example, Synthetic Aperture Radar (SAR) information is used for the evaluation of wind and wave properties over the Baltic Sea (Rikka et al., 2018). It works properly up to about 2 km from the coast (Dinardo et al., 2018). However, the SAR images are taken infrequently and they usually cover only a short period of time and a limited sea area.

An important source of information about wave fields that can be used to reconstruct long-term wave climate variability is provided by satellite altimetry. Satellite altimetry

measures the topography of the sea surface by the time it takes for a pulse to travel from the satellite to the sea surface and back to the satellite. Combined with the precise location of the satellite, altimetry measurements determine the height of sea surface with high accuracy. The amplitude and waveform of the returned signal provides information about the wave conditions.

Advances in technology since the introduction of remote sensing in the 1970s have made satellite altimetry an effective tool for measuring significant wave heights. Several validation studies of satellite altimetry data against buoy measurements indicate the high quality of altimeter data at global (Young et al., 2011), regional (e.g., the Mediterranean Sea, Galanis et al., 2012) and local scales (e.g., the Caspian Sea, Kudryavtseva et al., 2019; Rakisheva et al., 2019).

The information inferred from satellite altimetry may be contaminated by the presence of ice and the influence of coastal areas (e.g., Passaro et al., 2015; Brenner et al., 1983). As the relevant distortions cannot be corrected, the possibly contaminated records are usually discarded. For this reason, satellite altimetry is only infrequently used to estimate wave properties in small and/or ice-covered water bodies, like the Baltic Sea. Some recent studies have addressed the challenge of making the satellite altimetry data more useable for these regions (Wiese et al., 2018). Altimetry data tend to slightly overestimate the significant wave height values retrieved from *in situ* measurements (Wiese et al., 2018). A systematic and long-term validation of satellite altimetry data against *in situ* measurements for the whole Baltic Sea (Kudryavtseva and Soomere, 2016) specified more clearly which significant wave height data are adequate. The resulting data set has provided good temporal and spatial coverage and allows the analysis of spatio-temporal variations of the Baltic Sea wave climate in recent decades.

In comparison to the other sources of wave height, satellite altimetry can provide high-resolution and global coverage (along-track) information about the significant wave height. A large number of significant wave height measurements by different satellite altimetry missions with extensive spatial coverage over the Baltic Sea makes it possible to scrutinize in great detail features of the variability in wave climate, such as spatial patterns of changes in wave properties and their likely causes (Paper I).

## **The technique of Empirical Orthogonal Functions**

A combination of the complex shape of the Baltic Sea and the extensive variability in wind properties in the entire region gives rise to large spatio-temporal variations in wave properties (e.g., Jönsson et al., 2003; Soomere and Räämet, 2011). Even though there seem to be no major trends in the average wave properties in this water body (Björkqvist et al., 2018), several interesting basin-scale patterns of changes have been identified using satellite altimetry data (Kudryavtseva and Soomere, 2017). These patterns were explained by a rotation of strong wind directions. This change may have a large impact on wave properties in elongated water bodies, such as the Baltic Sea. In light of this, one of the major goals of this work is to identify the main drivers behind basin-wide changes of this kind.

As the wind fields are strongly asymmetric in the region, with two predominant wind directions from the south-west and north-north-west in the northern Baltic proper, this asymmetry hints that the patterns of changes in wave properties are likely to have a similar structure. To further examine this, a technique to extract such large-scale patterns, the Empirical Orthogonal Function (EOF) analysis (Hannachi, 2004), is employed.

This technique defines the data in an expansion in terms of spatially varying orthogonal functions. Such an expansion provides an option to separate individual orthogonal (and thus uncorrelated) modes of spatial and temporal variabilities in the field of interest (von Storch and Navarra, 1999). This decomposition often makes it possible to link certain kinds of variability with clearly identifiable drivers, patterns or changes in the system. Even though such links are usually expressed in terms of correlations between certain elements of the system, they still provide a powerful tool towards a deeper understanding of complex weather systems and their interrelations with oceanographic quantities.

This technique expedites the analysis of variability in a large space-time data set in a consistent manner. For this reason, it has become a widely-used method in atmospheric science and oceanography to reveal various teleconnection patterns at global (e.g., for study of the NAO and the El Niño indices, Nezlin and McWilliams, 2003), ocean-wide (e.g. Minobe and Mantua, 1999) and regional scales (e.g., Church et al., 2004), for the analysis of the variance of the significant wave height field, including in the North Sea and Baltic Sea during an extreme event (Wiese et al., 2018). It has also been applied to identify links between wave properties and atmospheric indices at various scales. The dominant spatial patterns of wave height variability during winter in the northern hemisphere (in terms of monthly averages) (Shimura et al., 2013), and variability of directional wave energy flux in the southern hemisphere (Hemer et al., 2010), have been quantified using the EOF technique.

The effect of teleconnection patterns on the wave climate in the North Atlantic has been extensively addressed over the past two decades. The general perception is that phenomena behind the NAO climatic index are particularly influential in the affected water bodies. This viewpoint is backed up by the robust link between this index and the increasing trend of wave height in the North Atlantic and the North Sea (Woolf et al., 2002; Wolf and Woolf, 2006; Bertin et al., 2013). A similar link can be traced at the same scale of phenomena between the Southern Annular Mode and the wave climate of the Southern Ocean (Hemer et al., 2010). On the regional scale, this method has been used to reveal connections between the wave climate in the Mediterranean Sea and the NAO (Cañellas et al., 2010) and the Indian Monsoon (Lionello and Sanna, 2005).

The possible links between such indices and the trends of wave height in the Baltic Sea are addressed for the first time in Paper I and in this thesis. Following the line of thought in Shimura et al. (2013), in this thesis the EOF technique is applied to monthly-averaged wave heights retrieved from satellite altimetry.

## **Ice season duration**

Waves impact the shores when substantial amounts of wave energy flux reach the nearshore. The core driver of the wave field is atmospheric forcing, the links of which with large-scale teleconnection patterns and wave properties are addressed in Chapters 1 and 2. Apart from the geometry and bathymetry of the sea, the possible presence of sea ice may have great influence on wave properties and, in particular, on the impact of waves on nearshore and coastal processes. The main properties of the ice season in the Baltic Sea and evidence about its current changes are described in detail in the literature (e.g., Granskog et al., 2006; Omstedt et al., 2014; Käyhkö et al., 2015). Both wave and ice regimes have considerable seasonal and interannual variations in the Baltic Sea and therefore jointly impact the nearshore in a complicated manner.

The extent and duration of ice cover vary greatly in the Baltic Sea (Haapala and Leppäranta, 1997). A typical ice season in the Baltic Sea starts in late autumn and continues until the spring of the following year. The northern parts of the sea, such as the Bay of Bothnia, the Archipelago Sea, and some parts of the Gulf of Finland are ice covered every year for several months. Usually ice is observed in almost half of the sea and in very cold years the entire sea may freeze (Jevrejeva, 2001; Leppäranta and Myrberg, 2009).

Most of the extreme wave events and thus conditions that provide large portions of wave energy flux occur from September to February (e.g., Björkqvist et al., 2018). Therefore, the windiest months often overlap with the ice season in the northern Baltic Sea. For this reason, even small changes in the starting date or duration of the ice season may lead to considerable changes in the wave impact at some locations (Omstedt and Nyberg, 1996). These changes largely follow variations in air temperature. An increase in the average winter temperature by about 2–3°C since the 1970s has the potential to reduce the ice season length by more than a month (Leppäranta, 2012).

Climate warming occurs much faster in the Arctic and at the latitudes of the Baltic Sea than at lower latitudes. It has already led to a much shorter ice season in many parts of the Arctic (Overeem et al., 2011) and created increasing pressure on its shores (Barnhart et al., 2014). However, the shortening of the ice season in the Baltic Sea (Omstedt et al., 2004; Käyhkö et al., 2015) is slower at high latitudes (e.g., Bay of Bothnia) than in the temperate latitude areas, such as the northern Baltic proper or the Gulf of Finland (Haapala and Leppäranta, 1997; Jevrejeva et al., 2004). The number of days with ice has decreased by 18 in the northern Bay of Bothnia and by 47 in southern Sea of Bothnia during the last century (Haapala et al., 2015). This process has shortened the ice season by 30 days per century on the northern shores of the Gulf of Finland (Merkouriadi and Leppäranta, 2014).

The fastest change has been identified for the West Estonian Archipelago where the duration of the ice season has become shorter by 6–10 weeks in 1950–2005 (Sooäär and Jaagus, 2007). If this process continues, it is likely that by 2050 ice cover will systematically exist only in the Bay of Bothnia, the Archipelago Sea, the eastern Gulf of Finland, and on the Estonian west coast (Haapala and Leppäranta, 1996; Käyhkö et al., 2015).

This extensive loss of sea ice generally occurs owing to both later freezing and earlier break-up (Sooäär and Jaagus, 2007). In particular, the later freezing means that more wave energy created by autumn and winter storms reaches the nearshore of the affected areas. Such storms often create strongly elevated water levels during which strong waves may reach unprotected and unfrozen sediment that is out of reach during other seasons. This process has already led to much faster erosion of Estonian shores (Orviku et al., 2003) and several sections of shores of the eastern Gulf of Finland (Ryabchuk et al., 2011a) during mild but windy winters. In this context it is important to map which regions or areas are under the largest pressure owing to increased exposure to strong waves during additional ice-free time.

### **Interplay of wind anisotropy, loss of ice and local features**

Both the described anisotropy of wind and wave fields and the presence of ice have considerable effect on wave properties of the Baltic Sea. First of all, the wave energy flux and thus the potential impact of waves on coasts and coastal engineering structures is generally much larger in the downwind eastern parts of the sea. A change

in the predominant wave approach direction may change the overall pattern of wave-driven alongshore sediment transport over long coastal segments (Soomere et al., 2015). It may also endanger the seemingly stable beaches that have been protected in the past (Ryabchuk et al., 2011a), drive the instability of sandy shores and landforms (Ashton et al., 2001), and affect various coastal engineering structures. Locally, changes in the wave approach direction may relocate erosion and accumulation areas. Such changes are particularly inconvenient when, for some reason waves start carrying sediment to a fairway or create dangerous conditions in the port interior.

These variations in the wave field are often amplified by the loss of local protecting ice cover (Orviku et al., 2003; Ryabchuk et al., 2011a). Climate change driven loss of sea ice affects wave fields in many ways. A direct consequence is the increase of the air-sea interface area. This change generally leads to an increase in the transfer of energy and momentum from the airflow to the water surface. This process generally leads to the generation of stronger waves. A shorter ice season, weaker ice cover and smaller ice concentration provide less direct protection to beaches and coastal engineering structures.

A more subtle effect is that the loss of sea ice and the associated extension of fetch length generally leads to the generation of longer waves. The more frequent presence of longer waves provides more energy to the shore and to coastal engineering structures, in particular to the port areas. This kind of effect of ice loss on the offshore wave energy and its flux is addressed in Chapter 3.

An even finer effect is connected with different refraction properties of waves with different length. Wave refraction is a classic phenomenon that often reshapes nearshore wave fields in an unexpected manner. The properties of wave refraction along single segments of a complex shoreline are influenced by the features of sea floor, such as the beach slope and the angle at which the waves arrive from offshore. In particular, it may cause substantial variation in wave heights along the shores of the open ocean (Kinsman, 1965) and the Baltic Sea (Kovaleva et al., 2017). It is likely that the associated changes in wave approach direction to beaches or coastal engineering structures may be even larger than those driven by changes in the directional structure of moderate and strong winds. These effects are usually local in the study area as the properties of coastal profiles and thus their impact on wave refraction vary greatly along the Estonian coasts (Didenkulova et al., 2013).

From the engineering viewpoint, changes to the refraction properties may lead to unexpected and dangerous situations, e.g., high water levels owing to wave set-up in certain shore segments or penetration of strong waves into ports. To evaluate such outcomes in the study area, Paper III and Chapter 4 report several unexpected effects of refraction of storm waves around the island of Ruhnu in the hypothetical ice-free climate using high-resolution wave simulations.

## **The objective and outline of the thesis**

The central goal of the thesis is to identify core patterns of spatio-temporal variations of wave properties in the Baltic Sea and their links to major circulations patterns using information about wave heights retrieved from satellite altimetry and using the technique of Empirical Orthogonal Functions (EOF). Satellite-derived information about ice concentration is used to analyse the impact of climate change driven loss of sea ice on wave loads in the northern Baltic Sea, and to provide an engineering-level example of wave-induced threats to a small port.

The main objectives are to:

- analyse the applicability and sensitivity of the EOF technique to retrieve patterns of changes to wave properties using satellite altimetry in the small semi-enclosed and seasonally ice-covered Baltic Sea;
- quantify the core patterns of changes to wave heights in the Baltic Sea during the satellite era and to link these changes to the temporal course of the major teleconnection patterns in the area;
- employ satellite-derived information about ice properties and modelled wave fields to evaluate the current and potential impact of the loss of sea ice on wave loads in the north-eastern part of the sea;
- provide an example of concealed threats to coastal engineering structures driven by the strongly anisotropic wave climate in the case of total loss of sea ice.

To meet these objectives, Chapter 1 provides a short introduction to the known properties of the Baltic Sea waves retrieved using satellite altimetry, the major teleconnection patterns in the area and the EOF technique, and to the selection procedure for optimum parameters for data gridding for the EOF analysis. A core development is the specification of the interrelations between the smallest identifiable pattern of changes and the acceptable level of noise (equivalently, measurement uncertainties).

The main task of Chapter 2 is to identify patterns of spatial and temporal variations in the wave height of the entire Baltic Sea in terms of the first three modes of two-dimensional EOF. Further analysis provides quantitative estimates of the reliability of these patterns and establishes several links (on the level of statistically significant correlations) between the retrieved quantities and three major teleconnection patterns in the area. The new material presented in Chapter 1 and Chapter 2 mostly follows Paper I.

Chapter 3 proceeds with the further analysis of joint implications of climate driven changes in ice properties. The focus is on the downwind regions of the sea that are currently seasonally ice-covered. The analysis is performed via comparison of average and cumulative wave properties in the current climate and in a hypothetical ice-free climate simulated using the wave model WAM. The presented new material follows Paper II.

Chapter 4 converts knowledge about possible changes to wave properties in a warmer climate into the context of coastal engineering. The analysis is performed for the Port of Ringsu on the island of Ruhnu in the Gulf of Riga in terms of the danger to the port of intense refraction of storm waves simulated using the SWAN model in the hypothetical ice-free climate. The new material follows Paper III.

### **Presentation of the results to scientific community**

The basic results described in this thesis have been presented by the author at the following scientific events:

#### **Oral presentations:**

Giudici A., Männikus R., **Najafzadeh F.**, Jankowski M.Z., Soomere T., Suursaar Ü. 2022. High-resolution wave model for coastal management and engineering in the eastern Baltic Sea. *4<sup>th</sup> Baltic Earth Conference Assessing the Baltic Sea Earth System*. (30 May to 3 June 2022, Jastarnia, Poland. Presented by M.Z. Jankowski).

**Najafzadeh F.**, Kudryavtseva N., Giudici A., Soomere T., 2020. Estimating the wave statistics bias in the partially ice-covered regions of the Baltic Sea. *3<sup>rd</sup> Baltic Earth Conference Earth system changes and Baltic Sea coasts*. (2–3 June 2020, online).

**Najafzadeh F.**, Kudryavtseva N., Soomere T. 2019. Baltic Sea wave climate variability and its connection with climatic indices deduced from Empirical Orthogonal Functions. *Baltic Sea Science Congress 2019* (19–23 August 2019, Stockholm, Sweden).

**Najafzadeh F.**, Kudryavtseva N., Soomere T. 2018. Application of empirical orthogonal functions reveals multiple modes of variations in the Baltic Sea wave climate. *7<sup>th</sup> IEEE/OES Baltic Symposium Clean and Safe Baltic Sea and Energy Security for the Baltic countries* (12–15 June 2018, Klaipėda, Lithuania).

**Poster presentations:**

**Najafzadeh F.**, Giudici A., Soomere T., Männikus R., Jankowski M.Z. 2021. High-resolution wave climate calculations in the Baltic Sea using SWAN with a 3-nested grid system. *The Gulf of Finland Science Days* (29–30 November 2021, Tallinn, Estonia).

**Najafzadeh F.**, Kudryavtseva N., Soomere T. 2020. Contribution of atmospheric teleconnections in regional wave climate variability based on EOF application: Baltic Sea case. *AGU Advancing Earth and Space Science* (11–17 December 2020, online).

**Najafzadeh F.**, Kudryavtseva N., Soomere T. 2019. Effects of the sampling bias on retrieved modes of wave climate variations from satellite altimetry: Baltic Sea case study. *ESA Living Planet Symposium* (13–17 May 2019, Milan, Italy).

**Najafzadeh F.**, Kudryavtseva N., Soomere T. 2018. Baltic Sea wave climate via empirical orthogonal function analysis. *Baltic Earth Workshop on Multiple drivers for Earth system changes in the Baltic Sea region* (26–27 November 2018, Tallinn, Estonia).

# 1 Applicability of the EOF technique for satellite data in the Baltic Sea

In this chapter a short insight into the core features of the wave climate in the Baltic Sea, as well as the relevant climatic indices and their possible effects on the Baltic Sea, is provided. An introduction to satellite altimetry data and the Empirical Orthogonal Function (EOF) method is followed by a description of the analysis of its sensitivity to the spatial and temporal distribution of altimetry data. This sensitivity is compared for meridional and zonal variations in wave fields. The goal is to identify the smallest detectable patterns using the EOF technique. The material follows the sensitivity analysis part of Paper I that was implemented using the software package “spacetime” (version 1.2-1) in R (version 3.4.4).

An issue that deserves specific attention is that applications of the EOF method on the satellite-measured data generally yield relatively low variability in the data (Woolf et al., 2002; Hemer et al., 2010). This is usually just noted but neither addressed in detail nor explained qualitatively. To shed some more light on this aspect of the EOF method, Chapter 1 also provides an examination of the impact of measurement noise (or uncertainty) on the level of retrieved variability of the employed EOF modes.

## 1.1 Wave properties in the Baltic Sea

The Baltic Sea is an almost closed arm of the North Atlantic Ocean, extending from 53° to 66°N latitudinally and from 10° to 30°E longitudinally. It is a comparatively small basin with a complicated shape, extensive archipelago areas, and shallow nearshore regions. The combination of these features with the complexity of wind patterns in the area makes the Baltic Sea a fascinating area for wave climate researchers. Due to its limited size, the wave fields in this basin are mostly dominated by features of the wind. Even small changes in the directional structure of predominant winds may cause substantial variations in the associated wave properties (e.g., Jönsson et al., 2003; Soomere and Räämet, 2011; Kudryavtseva and Soomere, 2017; Kudryavtseva et al., 2019) and the course of coastal processes (Soomere et al., 2015). Therefore, the quantification of temporal and spatial variations in the wave fields of the Baltic Sea is both a great challenge and an important task for many offshore and coastal applications.

Wave properties of the Baltic Sea have varied substantially in recent decades (Soomere and Räämet, 2014; Suursaar and Kullas, 2009; Różyński, 2010). For instance, average wave heights were lower than the long-term average in the northern Baltic proper in the beginning of 1980s. During this time, wave heights increased to some extent near Lithuania (Kelpšaitė et al., 2008). For this reason, estimates of the long-term average wave properties depend on the particular method and time period. The largest values of average wave height are provided by satellite altimetry data. During the period 1993–2015, the average significant wave height (SWH) retrieved from this source in the Baltic Sea varied in the range of 0.44–1.94 m (Kudryavtseva and Soomere, 2016). These values are apparently overestimated because satellite altimetry usually does not adequately sense low wave heights. However, a statistically significant increasing trend of SWH by 0.005 m/yr (Kudryavtseva and Soomere, 2017) is an important feature of the wave fields.

The wave modelling efforts have indicated the greatest mean SWH levels of about 1.2 m (Nikolkina et al., 2014; Björkqvist et al., 2018) in the eastern Baltic proper. Slightly lower values have been found for the Sea of Bothnia (Nilsson et al., 2019) where ice cover limits the generation of wave height in some seasons (Tuomi et al., 2011). Smaller semi-sheltered subbasins (the Bay of Bothnia, the Gulf of Finland, the Gulf of Riga) have an average SWH in the range of 0.5–1 m (Tuomi et al., 2011; Nikolkina et al., 2014).

The largest single wave was observed in the northern part of the Baltic Sea with a height of more than 14 m (EUMETSAT, 2017) in January 2017. It was called a “monster” wave by Rutgersson et al., (2022). The highest recorded SWH was 8.2 m in the northern Baltic proper during a wave storm in December 2004 (Tuomi et al., 2011; Björkqvist et al., 2018). The maximum measured SWH was 7.2 m in the northern Baltic proper in January 2005. Later simulations suggested that the SWH probably reached 9.5 m to the west of Latvia in this storm (Soomere et al., 2008). An exceptional storm in January 2019 created a new maximum SWH of 8.1 m in the Sea of Bothnia (Björkqvist et al., 2020).

The wave climate has strong seasonal and spatial variation. The majority of the extreme SWHs (top 0.1 percentile of which is 6.9 m) happen between November and January. Such wave conditions mostly occur in the south-eastern and north-eastern Baltic proper (Björkqvist et al., 2018). Contrary to mean SWH retrieved from satellite altimetry that exhibits a statistically significant trend (Kudryavtseva and Soomere, 2017), the modelled severe wave heights (90–99%-ile) in the Baltic Sea do not have a clear trend (Soomere et al., 2012). The longest wave periods for storm waves can reach 10–12 s in the northern part of the Baltic proper (Tuomi et al., 2011) and Sea of Bothnia (Björkqvist et al., 2020), and 8–11 s in the Gulf of Finland.

## 1.2 Atmospheric circulation in the Baltic Sea

Waves generated in the North Sea almost do not penetrate into the Baltic Sea. Changes in the wave climate of the Baltic Sea are, therefore, driven by alterations in the properties of local storms. Their frequency, strength, location and trajectory are determined mainly by the conditions of large-scale atmospheric circulation that affect the generation of storm cyclones in the North Atlantic and their motion over the Baltic Sea region. In other words, the effects of teleconnection patterns that link the situation in the cyclone generation areas and the impact of these cyclones to the Baltic Sea waves are important for understanding wave climate and its changes in the basin.

The Baltic Sea is located in an area that is strongly impacted by processes in the North Atlantic Ocean that carry heat and moisture along the North Atlantic storm track and towards the continental area of Eurasia. It is therefore likely that teleconnection patterns in these regions have great influence on the wind regime and wave climate of this water body (Fig. 1). The main patterns of this type are the North Atlantic Oscillation (NAO), Arctic Oscillation (AO), and Scandinavia pattern (SCAND), and relevant climate indices. The SCAND pattern was previously called Eurasia-1 (Barnston and Livezey, 1987).

The characteristics of the NAO are among the main drivers that link the teleconnection patterns to the regional climate of Europe and the Baltic Sea (e.g., Walker and Bliss, 1932; Hurrell et al., 2003; Bednorz et al., 2018). This pattern has two centres of actions, one is located over the Greenland/Iceland and the other is over the Azores. The NAO climatic index is obtained from the anomalies of monthly mean at the 500 mb height between those centres. The base of anomalies is calculated over the period 1950–2000.

The NAO pattern seems to greatly affect wind direction, especially in winter (December to February, Rózyński, 2010). Even though the westerly wind is the most prominent in the Baltic Sea region, its frequency and strength reflects variations in the NAO. The positive phase of the NAO is characterised by stronger westerly winds while during the negative phase, easterly and north-easterly winds are more frequent (Trigo et al., 2002). This feature together with the sensitivity of the Baltic Sea wave fields to wind direction described above, suggests that the increase in extreme wave energy flux (Mentaschi et al., 2017) is caused by the variation of the NAO index.

The pattern of AO is retrieved from the anomalies of monthly mean at the 1000 hPa height between the Arctic and mid-latitudes. It describes features of the wind circulating zonally (anticlockwise) around the Arctic at latitude of 55° N (e.g., Thompson and Wallace, 1998). In the positive phase of the AO, there is a strong low-pressure system in the Arctic, while the high-pressure system is located at mid-latitudes. The high pressure at mid-latitudes guides ocean storms further north.

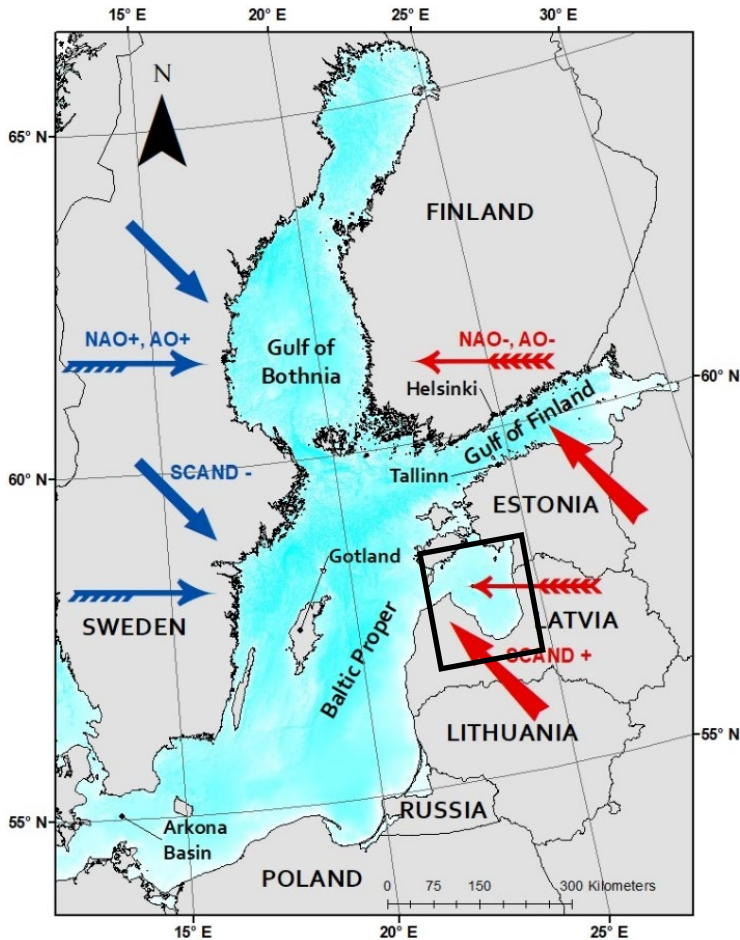


Figure 1. The predominant wind direction in the study area during the positive (red) and negative (blue) phases of the SCAND, and the positive (blue) and negative (red) phases of NAO and AO patterns. The black box shows the detailed study area in the Gulf of Riga in Chapter 4. Modified from Paper I.

This process causes fast-moving westerly winds at the latitudes of the Baltic Sea which trap the cold air in the Arctic. In terms of strong westerly winds, this phase of AO is similar to the analogous phase of NAO. During the negative phase of AO, the polar vortex is weak. The average pressure is higher in the Arctic than during the positive phase, and the pressure at mid-latitudes is lower. The resulting smaller North-South pressure gradient force causes weaker zonal flow of air. This allows the cold arctic air to proceed southward and creates more frequent easterly winds. Weather patterns of these two phases are, in general, reflections of each other. The AO has shown significant variation in winters; therefore, its patterns can represent the climate variability during this season.

Several natural phenomena in the weather and wave climate of the Baltic Sea region are extensively related to the climatic indices described above. These phenomena include (but are not limited to) sea ice conditions (Jevrejeva et al., 2003), sea level (Andersson, 2002; Jevrejeva et al., 2005; Passaro, 2015), wave storms (Surkova et al., 2015; Kudryavtseva et al., 2021), and wave height (Rózyński, 2010). The AO phases correlate with the phases of the NAO, and there is a clear relation between these two climatic indices.

The Scandinavia teleconnection pattern, SCAND, is based on anomalies of monthly mean at the 700-hPa height. It is composed of the main centre of circulation over Scandinavia and two centres of opposite sign over western Europe and eastern Russia. Its positive phase is characterized by anticyclonic circulation around Scandinavia with more frequent easterly and south-easterly winds in the Baltic Sea region (Bueh and Nakamura, 2007). In the negative phase, strong westerly and north-westerly winds are common over Scandinavia and the Baltic Sea. Similar to the NAO, it affects regional winds mostly in winter (Gao et al., 2017).

Several other teleconnection patterns, such as East-Atlantic West-Russia (EAWR), the East Atlantic (EA), the Polar-Eurasia (POL), and the Atlantic Multidecadal Oscillation (AMO) have been identified as well, and have shown to have a certain impact on precipitation patterns (Jaagus, 2009; Irannezhad et al., 2014) and coastal upwelling (Bednorz et al., 2019). In this thesis, I explore the relationships between the wave properties in the Baltic Sea and a selection of these climatic indices. The focus in Paper I and in Chapters 1 and 2 is on the most widely used indices, NAO, AO, and SCAND, which are more dominant than other indices for the wave climate variability of the Baltic Sea basin (higher correlation than uncertainty, explained in Chapter 2). For this reason, the focus of analysis in Paper I is on the impact of these climatic indices on Baltic Sea waves.

### **1.3 Empirical Orthogonal Functions**

Wave climate in sea areas of complex shape, such as the Baltic Sea, is characterized by extensive spatio-temporal variability and nonlinear reaction to changes in global atmospheric forcing patterns. In recent decades, several methods to extract patterns and identify possible driving forces from measurements of climatic variables have been developed. A more complete approach can be delivered by the EOF method. In particular, the EOF method became the most widely used technique to reduce the dimensionality of the system (Hannachi, 2004).

EOFs represent multi-dimensional patterns that explain<sup>1</sup> large parts of the observed spatio-temporal variability of measured or modelled data. These variabilities are described as a sequence of functions that are divided into time and space. With regard to the EOF analysis, the time series of the data express as

$$F(x, y, t) = \sum_{i=1}^N EOF(x, y)PC(t), \quad (1)$$

where  $F(x, y, t)$  is the analysed data set,  $N$  is the number of the modes, and  $EOF(x, y)$  represent the eigenvectors of the correlation matrix of this data set. The expression  $PC(t)$  stands for the time series associated with the EOF explaining the temporal variations (Principal Component). Each spatial pattern that is decomposed using the EOF method contains a certain time variability. By construction, the modes of EOF are orthogonal and the related time variabilities (the relevant  $PC(t)$ ) are uncorrelated. The lower modes of EOF usually incorporate the highest temporal variability, while the upper modes typically reflect a smaller amount of variability or occasionally mirror the existing noise.

This technique is mainly used for the analysis of spatial correlations of the field, which is an essential feature of climate data. They are often used in climate science because the relevant operations are straightforward and well defined. They can be effectively applied to describe processes at local spatial scales (e.g., the patterns of sea surface temperature in the Baltic Sea, Zujev et al., 2021) and relatively short temporal scales (e.g., inter-seasonal variations, Patra and Bhaskaran, 2016). They have been successfully applied to analyse spatio-temporal patterns of wave properties in the Mediterranean Sea (Lionello and Sanna, 2005; Sartini et al., 2017) and in Chesapeake Bay (Niroomandi et al., 2018).

The first application of this method to the study of wave properties in the Baltic Sea (Mietus and von Storch, 1997) was based on a short (5-year) modelled data set in 1988–1993. The outcome revealed a SWH anomaly in the eastern part of the Baltic Sea that could be associated with larger wave heights in this part of the sea. The second EOF mode revealed another pattern of wave heights that extended from the southwest to the northeast parts of the sea. The third mode indicated the presence of a certain zonal pattern between the eastern and western parts of the basin. Given this extensive range of applications of the EOF technique, it is safe to assume that EOF analysis is a robust tool to determine the correlations between wave climate and climatic indices.

## 1.4 Satellite altimetry data

The whole Baltic Sea has been regularly observed by several generations of satellite altimetry missions. The analysis in Paper I makes use of SWH data from GEOSAT, ERS-1, TOPEX, ERS-2, ENVISAT, JASON-1, JASON-2, CRYOSAT-2, and SARAL. The relevant data set for 24 years (from 1992 to 2015) contains about 700,000 single measurements retrieved from the Radar Altimeter Dataset System database (Scharroo, 2012; Scharroo et al., 2013) (RADS, <http://rads.tudelft.nl/rads/rads.shtml>).

---

<sup>1</sup>Strictly speaking, the EOF and similar methods evaluate correlations and do not establish dynamic or causal relationships that govern the measured patterns. However, for simplicity I follow the widely used notion of “explaining” the pattern.

Several phenomena, such as rain, may greatly affect the accuracy of satellite data. The presence of ice or dry land in the footprint of a particular altimeter may render the estimate of the SWH completely inadequate (Brenner et al., 1983; Madsen et al., 2007). This method has large uncertainty for situations with small wave heights. Thus, SWH data retrieved from satellite altimetry devices has been used infrequently in relatively small inland seas, such as the Baltic Sea and the Caspian Sea.

The analysis in Paper I relies on the examination of the quality of the RADS SWH data set for the Baltic Sea conditions in Kudryavtseva and Soomere (2016). According to their recommendations, first of all, the data with a backscatter coefficient  $>13.5$  cdb (which relate to the low wind speed) and with normalised standard deviation of SWH  $>0.5$  m were excluded. To ensure that the snapshots are not contaminated by the presence of dry areas, the snapshots with their centres closer than  $0.2^\circ$  to the land were removed. Finally, the snapshots over the areas with ice concentration  $>30\%$  are likely erroneous and were also omitted from the data set. The final data set was checked for possible biases and errors and validated by Kudryavtseva and Soomere (2016).

The entries in this data set are thoroughly cross-validated with *in situ* measurements, corrected for ice cover, and biases between different missions, and have been filtered based on the distance of the centre of the measurement footprint from the land, as also described in Paper I. An earlier outcome of this validation is the set of SWH measurements over more than two decades for the whole Baltic Sea (Kudryavtseva and Soomere, 2016). The massive number of measurements with proper spatial and temporal coverage of the Baltic Sea has been used for the analysis of the wave climate in this basin in Kudryavtseva and Soomere (2017).

The technology of satellite altimetry has made the collection of data over a vast area possible. However, the phenomena under investigation are measured along a straight line during each pass of the satellite. Each satellite has a unique orbit and subsequent passes of the satellite over the same region do not necessarily cover exactly the same area. Therefore, the measured data from different passes and missions usually do not

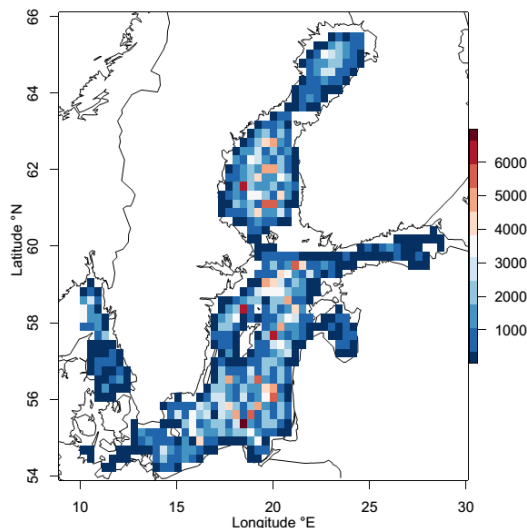


Figure 2. Spatial distribution of the number of satellite altimetry SWH data in the Baltic Sea for the period 1992–2015. From Paper I.

*Table 1. The threshold of the number of SWH snapshots for cells that were included in the analysis for different grid sizes and percentile cut-offs.*

Grid size	1%-ile	2%-ile	3%-ile	4%-ile	5%-ile
0.2°	40	120	160	200	399
0.4°	93	279	372	465	929
0.6°	149	447	596	745	1489
0.8°	215	645	860	1075	2149

have a uniform coverage and may contain some gaps. A better coverage in both time and space can be achieved by combining the data from different satellite altimeters.

Most applications require gridded data. In order to evaluate the density of data in the study area, the monthly average of data points for different grid sizes were calculated in Paper I. The regular rectangular longitude-latitude grid covers the area between latitudes 54.11°N to 65.57°N and longitudes 10.00°E to 28.83°E. The effect of different sizes of grid on the data coverage was examined in detail in Paper I by means of a comparison of the properties of the first EOF for different sizes of grid. The grid size was varied from 0.2° to 0.8° with a step of 0.2° (Table 1). The application of EOF did not retrieve a clear pattern for a spatial resolution much finer than 0.8°. A possible reason for this is the low coverage of data in cells of finer grids for monthly average. The application of EOF retrieved a clear pattern for the grid size of 0.8°. Hence, the grid size of 0.8°×0.8° was selected for the further analysis.

The number of single satellite altimetry snapshots greatly varies in different cells (Fig. 2). It ranges from just one data point in 11 grid cells near the coast to a maximum of 6989 data points in a single cell. The number of SWH estimates in different cells of the spatial grid has an almost uniform distribution (Paper I). The areas with several thousand snapshots per grid cell are mostly located in the central parts of the Sea of Bothnia and Baltic proper (Fig. 2). The grid points in the Gulf of Finland and the Gulf of Riga have lower number of SWH estimates. No reliable data over the Archipelago Sea are retrieved.

A distribution of the output of single measurements that is too variable and a number of SWH estimates in a cell that is too small may lead to inadequate results from the EOF analysis. To avoid such an outcome, the cells with less than a specific (threshold) number of data were discarded in Paper I. To evaluate an optimal threshold, a set of lower percentiles (from 1%-iles to 5%-iles) of the uniform distribution was employed as cut-off values (Table 1). The cells with a lower number of SWH snapshots than this threshold were removed. This procedure was applied using different grid sizes. The effect of this elimination on the results of the EOF analysis was examined in detail in Paper I for the whole data set and for single seasons. The outcome is presented in brief in Tables 2 and 3.

*Table 2. The effect of different cell size on the percentage of temporal variability retrieved by EOF (three first modes) for different cut-off thresholds.*

Temporal variability of EOFs	Grid size: 0.4°×0.4°	Grid size: 0.6°×0.6°	Grid size: 0.8°×0.8°
First EOF	0.23	0.17	0.17
Second EOF	0.16	0.11	0.13
Third EOF	0.08	0.09	0.10
Total variability	0.47	0.37	0.40

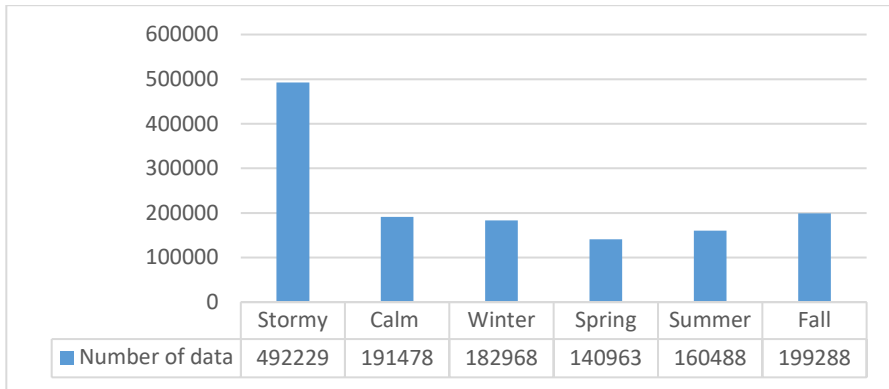


Figure 3. Total number of single estimates of SWH from all satellite altimetry missions. From Paper I.

The test indicated that the results of the EOF analyses were consistent (from 5%-ile down to the 2%-ile) until the cut-off was performed at the 2%-ile. This threshold was thus employed in the analysis. For this choice, the grid cells that contained less than 645 single measurements were discarded. Applying this threshold kept about >99.1% of the entire SWH data, and less than 0.9% of the whole data set was discarded. The same procedure was applied on the data from different seasons (Table 3).

The relevant level of cut-off is 181 (0.85% of the data removed) in winter, 141 (0.86%) in spring, 145 (0.73%) in summer, 180 (0.71%) in autumn, 469 (0.74%) in windy season and 176 (0.62%) in calm season. The majority of the removed cells were from the relatively narrow Gulf of Finland. Other removed grid cells were randomly distributed. It is thus likely that this operation did not considerably impact spatial patterns in the first EOF. The seasonal distribution of discarded grid cells is also random. Therefore, it can be assumed that removing these cells did not distort the temporal variabilities of EOFs.

The impact of the particular choice of the grid size on the entire analysis was additionally evaluated based on changes to the percentage of temporal variability retrieved by the first three modes of EOF analysis (Table 2). The total variance of temporal variability did not show any significant dependence on the increased size of cells.

Paper I provides estimates of the temporal variability of the first three EOF modes and the entire variability (in percentage) for different seasons and for the whole set of years of the study period (Table 3). The winter season is characterised by the highest

Table 3. The level of temporal variability explained by EOF modes for different seasons. The percentage of retrieved variability for the first three EOFs and the total variability are shown in each column. From Paper I.

Seasons	First EOF (%)	Second EOF (%)	Third EOF (%)	Total variability (%)
Winter	27	9	8	44
Spring	17	14	12	43
Summer	22	09	8	39
Autumn	23	09	7	39
Stormy	19	12	8	39
Calm	17	11	10	38
All seasons	17	13	10	40

temporal variability for the first mode (27%) and total variability (44%) among all the seasons and the entire years. The smallest temporal variability of the first three EOFs, 38%, is related to the calm season. The estimate of the total variability retrieved by the first three EOFs, both at annual and seasonal scales, is at the same level as in comparable studies based on satellite altimeter data: it varied between 36% and 42% in Hemer et al. (2010), and it was 69% in Woolf et al. (2002).

## 1.5 Seasonal variability and averaging errors

There are two distinct seasons in terms of water level in the Baltic Sea. The relatively windy season (called “stormy” season here), includes the months from January to March and from August to December. The relatively calm season (called “calm” season here) spans from April to July (Johansson et al., 2001; Suursaar et al., 2002; Jaagus and Suursaar, 2013; Soomere and Pindsoo, 2016; Männikus et al., 2020). A similar variation is typical for wave fields in the Baltic proper (Broman et al., 2006; Soomere and Räämet, 2011). This is clearly evident in the pattern of the highest waves: most of the wave events with SWH more than 7 m occurred from November to January (Björkqvist et al., 2017). For this reason, the seasonality of the outcome of the EOF estimates was estimated based on stormy and calm seasons, along with the traditional seasons (spring, summer, autumn, winter). The number of data points in stormy seasons (8 months) is about twice as large as in the calm season (Fig. 3). The number of data points in winter, spring, summer and fall (3 months each) varies within  $\pm 17.5\%$  from the average value (about 170,000). The fall and spring seasons have the largest and the least number of data points, respectively.

To provide a more suitable data set as input for the EOF method, the monthly average of SWH at each cell of the data set was computed in Paper I. As wave properties have extensive temporal variability in this basin (Soomere and Eelsalu, 2014), the average wave height for time intervals less than one month may strongly depend on one or two wave storms and therefore is not necessarily representative of this time interval in a longer perspective. To investigate the level of uncertainty of the estimated average wave height (that may affect further analysis), the error of the mean is calculated as

$$SE = \frac{sd(SWH_i)}{\sqrt{N}}. \quad (2)$$

Here,  $sd$  is the (sample) standard deviation of single estimates of wave height,  $SWH_i$  is the average of single estimates of SWH in a grid cell over one month, and  $N$  is the total number of SWH estimates in this cell during that specific month. The median of the resulting estimates of uncertainty  $SE$  in single cells for the whole data set,  $SE_\sigma$ , can be interpreted as a characteristic error of the mean for the entire data set. This median value was about 9%.

## 1.6 Sensitivity of the Empirical Orthogonal Function technique

As the EOF technique was applied to the analysis of the structure of Baltic Sea wave fields for the first time in Paper I, it was necessary to systematically estimate the sensitivity of this technique with respect to possible noise, uncertainties and gaps in the satellite altimetry data. The omitted data in the vicinity of land and during the ice season cause temporal and spatial gaps in the data set. The variations of the orbits of

satellite missions may introduce inhomogeneity in terms of the actual location of the area in which the SWH is evaluated. The presence of the gaps and inhomogeneity may introduce biases to the evaluation of EOFs. To understand their role, a detailed analysis of the temporal gaps and spatial inhomogeneity of the multi-mission satellite altimetry data set on the outcome of EOFs was performed in Paper I by means of simulating data sets with three different scenarios.

To estimate the ability of the EOF technique to reveal trends in the data set, two distinct patterns were simulated. One comprised of a linear increasing trend of 0.005 m/yr. The other did not contain any persistent variations. The assigned trend has a magnitude of the detected increase in the SWH in the Baltic Sea (Kudryavtseva and Soomere, 2017). The synthetic data sets were made up of these two patterns. Three scenarios that were meant to check whether the technique identifies changes in the north-south direction (zonal pattern, scenario A), east-west direction (meridional pattern, scenario B), or within a limited rectangular area (scenario C) were analysed. Scenarios A and B were thoroughly discussed in Paper I.

In scenario A, a linear trend of 0.005 m/yr was prescribed to occur in the SWH in half of the Baltic Sea north of the latitude of 59°N. To the south of this latitude, no long-term variation was applied. The entire Gulf of Bothnia, Gulf of Finland, Archipelago Sea, and Åland Sea were located in the northern section, and the rest of the Baltic Sea (the Gotland Basin, the Gulf of Riga, the Bornholm Basin and the Arkona Basin) was in the southern part.

In scenario B, a linear trend of 0.005 m/yr was prescribed to occur in the SWH from the longitude of 19.4°E to the west. To the east of this longitude, no long-term variation was applied. The Bay of Bothnia, the eastern parts of Sea of Bothnia, the Gulf of Finland, the Gulf of Riga and the Eastern Gotland Basin were in the eastern zone.

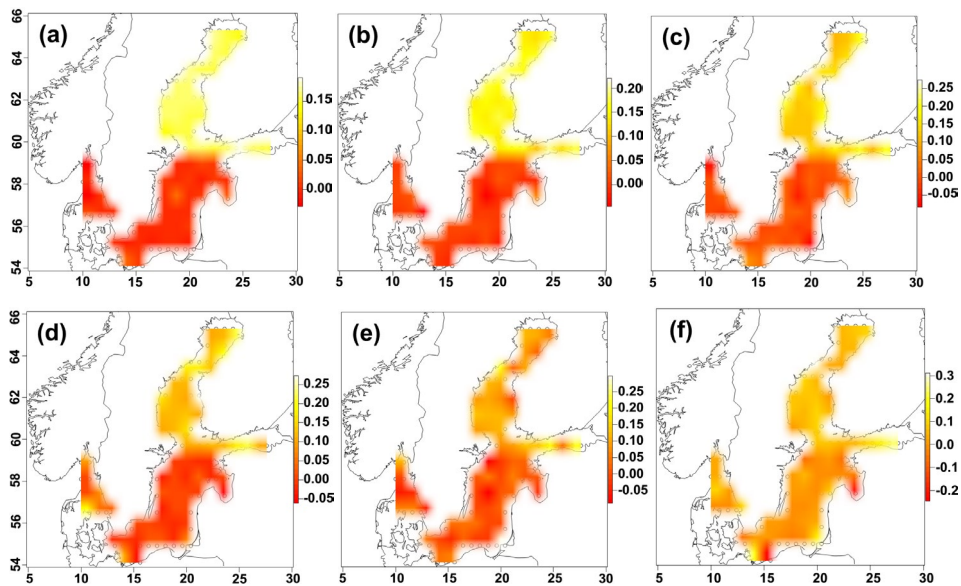


Figure 4. The first EOF patterns for simulated data sets with an increase in the SWH in the northern Baltic Sea (scenario A) with introduced random noise at the level of 5% (a), 10% (b), 20% (c), 25% (d), 27% (e), and 30% (f). The data were interpolated for ease of interpretation. Modified from Paper I.

In order to identify the smallest pattern which can be detected from the multi-mission satellite altimetry data with the EOF method, a synthetic data set with a SWH following the linear trend only in a limited rectangular area was created (scenario C). As this scenario was not reflected in Paper I, I present here its analysis in more detail. The centre of the rectangle was located at 56.3°N and 18.8°E. The datapoints exterior to the rectangle area were introduced to the pattern with no variation. Different spatial sizes of the rectangle area (varied from 1.5°×1.5° to 3.5°×3.5°, Table 4) were investigated.

The synthetic sets of SWH data of these scenarios contained entries exactly at the times and coordinates of the satellite altimetry snapshots. To evaluate the performance of the EOF technique, Gaussian random noise with zero mean was introduced to the data. The width of the relevant distribution (at half maximum  $x = 2\sqrt{2\ln 2}\sigma$ , where  $\sigma$  stands for the standard deviation of the corresponding Gaussian distribution) was from 5% to 30% of the total average of the simulated SWH.

The EOF analysis (Fig. 4, 5) indicates that both the zonal and meridional spatial patterns introduced in scenarios A and B are discernible in the first EOF mode with the noise level below 30%. Both patterns become visually indistinguishable if the noise level is  $\geq 30\%$ . Based on these results, it is concluded in Paper I that the presence of gaps in the satellite SWH data sets (including those stemming from the removal of less populated grid cells) do not considerably affect the information retrieved using EOF analysis for global trends in the Baltic Sea basin. Also, the results of this kind of analysis are reasonably susceptible to noise, which should not increase above 25% of the average SWH.

The performance of the EOF technique in detecting smaller-scale patterns can be estimated using the results of the first EOF for such patterns introduced into the simulated data set (scenario C) together with different noise levels (from 5% to 30%).

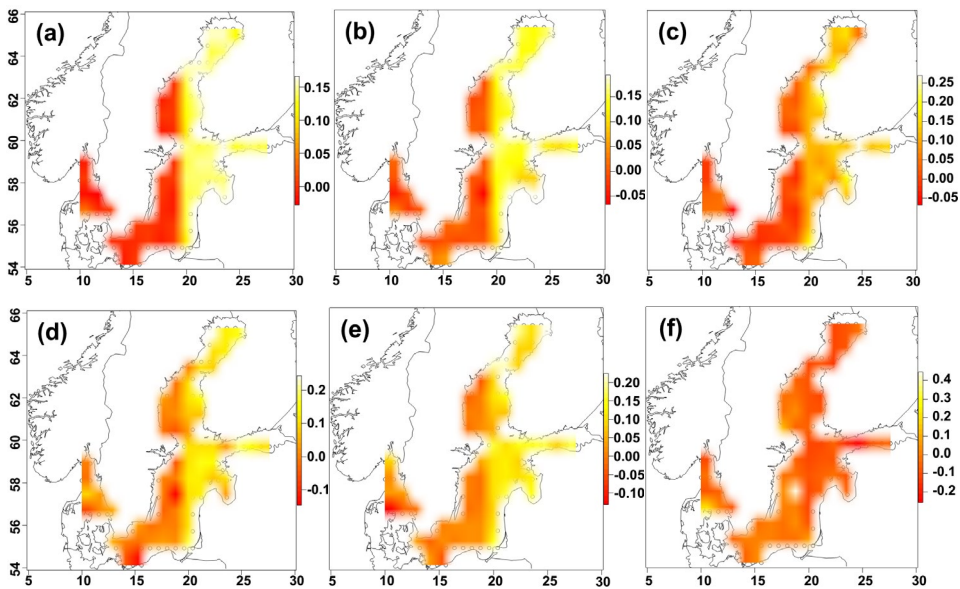


Figure 5. The first EOF patterns for simulated data with an increase in the SWH in the northern Baltic Sea (scenario B) with introduced random noise at the level of 5% (a), 10% (b), 20% (c), 25% (d), 27% (e), and 30% (f). The data were interpolated for ease of interpretation. Modified from Paper I.

For small noise levels (5%), the introduced patterns with a size of  $2.5^\circ \times 2.5^\circ$  and larger are clearly visible (Fig. 6a). The EOF technique did not reveal visually detectable signals of smaller patterns than  $1.5^\circ \times 1.5^\circ$  (Fig. 6b). An increase in the noise (e.g., 10%, Fig. 7) leads to the inability of the EOF technique to reveal patterns of the size of  $1.5^\circ \times 1.5^\circ$ .

In this case the minimum visually-detected pattern must be larger than  $2.2^\circ \times 2.2^\circ$  (Fig. 6d). The presented analysis additionally supports the ability of the EOF technique to retrieve relatively large patterns even from a fairly noisy signal. The size of the pattern and the level of noise have a significant effect on the ability to retrieve the inserted EOF patterns.

As expected when the level of noise increases, the smallest detectable pattern size increases as well. This increase is roughly linear (Fig. 7). At a 30% level of noise, only patterns larger than  $5.6^\circ \times 5.6^\circ$  can be detected.

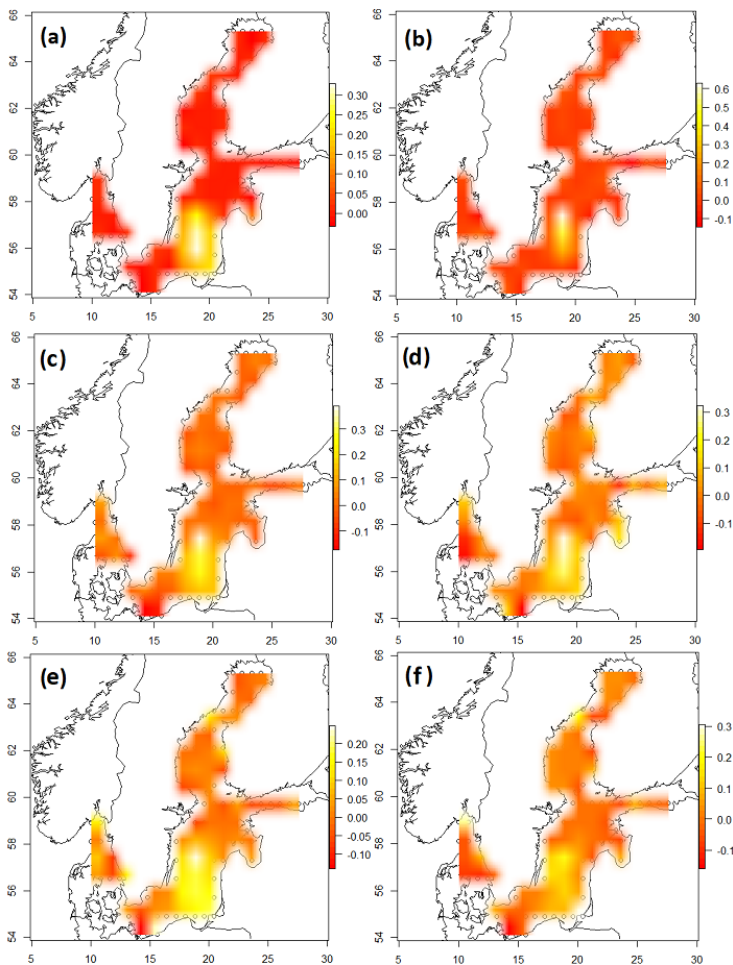


Figure 6. Upper row: First EOF patterns for simulated data with 5% level of noise and for pattern size of (a)  $2.5^\circ \times 2.5^\circ$ , (b)  $1.5^\circ \times 1.5^\circ$ . Medium row: 10% level of noise, sizes, (c)  $2.5^\circ \times 2.5^\circ$ , (d)  $2.2^\circ \times 2.2^\circ$ . Bottom row: 20% level of noise, (e)  $3.5^\circ \times 3.5^\circ$ , (f)  $3^\circ \times 3^\circ$ .

It is interesting to estimate the impact of added noise on the ability of the EOF technique to reveal the actual variability of the wave fields. The extension of one degree along longitudes is about half of that along latitudes in the northern Baltic proper and the Gulf of Finland. This difference may impact the ability of the EOF technique to reveal some patterns. The temporal variability of the first EOF mode showed a high sensitivity to the level of noise in the data set (Fig. 8). An increase in the magnitude of the introduced noise rapidly reduced the percentage of revealed temporal variability.

When the level of noise was increased from 5% to 30%, the percentage of retrieved variability decreased from about 90% to 29% for the meridional pattern (scenario A) and from about 80% to 18% for the zonal pattern (scenario B). The rate of decrease is almost the same for both cases. Still, the spatial patterns of the first EOF in Fig. 4d, 4e and Fig. 5d, 5e are apparent, even though the method recovers only 20% and 35% of the actual variability for scenarios A and B, respectively. This result suggests that despite the low percentage of retrieved variability, the application of EOF is still capable of correctly recovering the basic patterns in the data set.

Since only one pattern was applied to the simulated data sets in scenarios A and B, any variability presented by the second and third modes of EOF is generated by the introduced random noise and thus is not genuine. These modes of EOF retrieved less than 10% of the variability. This level of retrieved variability is employed in Paper I as an indirect indicator of the reliability of the information presented by the EOF modes. Following this conjecture, all results of the EOF analysis that retrieved less than 10% variability were considered untrustworthy.

In order to examine the possibly different performance of the EOF method in exposing the meridional and zonal patterns (scenarios A and B) depending on the level of noise, a comparison between the retrieved variability associated with these patterns was conducted. The difference for this indirect indicator of the performance reached its maximum (21%) for the noise level of 20% and was the smallest (about 10%) for very small (5%) and very large (30%) noise levels (Fig. 8). In general, the method shows a slightly better performance in discerning the meridional pattern than in discerning the zonal pattern. This might be because of the unequal lengths of the borders of longitude-latitude grid cells. It may also reflect the greater number of satellite altimeter measurements in the east-west direction order at the latitudes of the Baltic Sea.

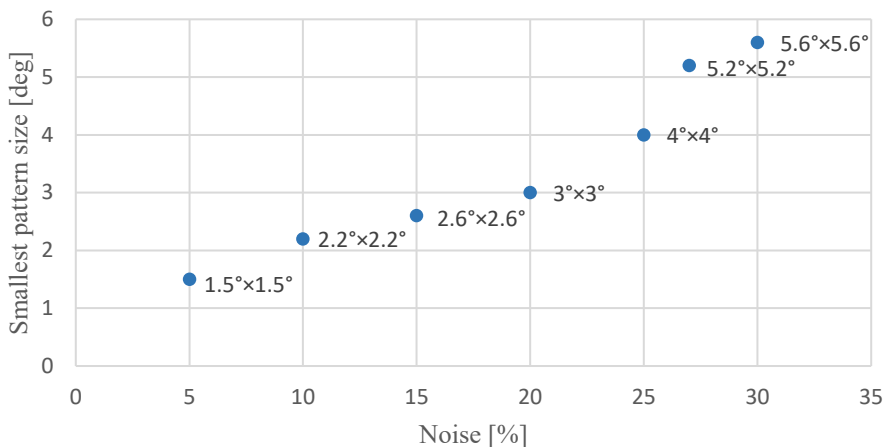


Figure 7. Smallest detectable pattern size for different levels of introduced noise.

Table 4. Temporal variabilities of different pattern sizes for different level of introduced noise.

Introduced noise	Pattern size, Temporal variability	Smallest detectable pattern size, Temporal variability
5%	2.5°×2.5°, 91%	1.5°×1.5°, 77%
10%	2.5°×2.5°, 74%	2.2°×2.2°, 69%
20%	3.5°×3.5°, 46%	3°×3°, 46%

It is natural to assume that the performance of the EOF method in terms of detection of small patches also depends on the level of noise. As with the meridional and zonal patterns, random noise was introduced to all the data in experiments with a small pattern in the Baltic proper (scenario C). Different error levels from 5% to 30% with different pattern sizes were applied to the synthetic data set.

The ability of the EOF method to recognize patterns thus significantly depends on the size of the pattern and the level of noise in the signal. Table 4 illustrates the temporal variabilities of each pattern size and the smallest detectable pattern for each noise level. At 5% noise level, their percentages are 91% and 77%, for the pattern sizes of 2.5°×2.5° and 1.5°×1.5°, respectively. The retrieved percentage of temporal variability explained by the first EOF mode decreases when the noise becomes stronger. For 10% level of noise, the retrieved temporal variabilities are 74% (Fig. 6c) and 69% (Fig. 6d). For the smallest detectable pattern this percentage drops from 77% to 46% when the noise level changes from 5% to 20% (Table 4).

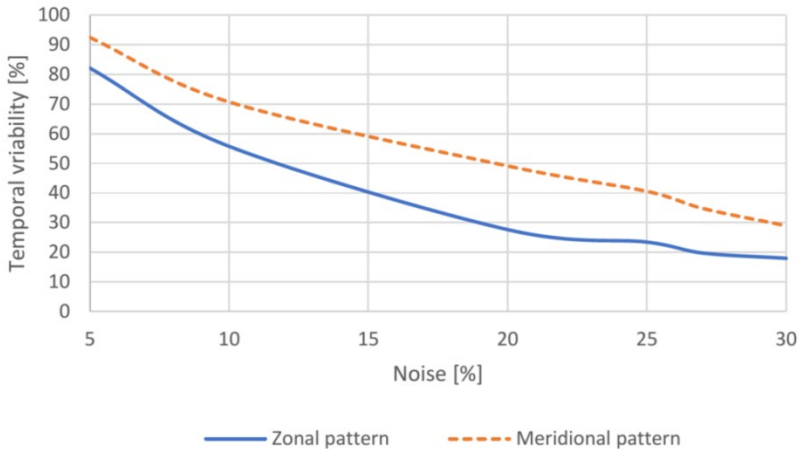


Figure 8. Reconstructed percentage of variability of the first EOF mode versus a percentage of introduced level of noise in the synthetic data sets. The blue solid line represents the data set with the introduced zonal pattern (scenario A), and the orange dashed line is the data set with the meridional pattern (scenario B). From Paper I.

## 2 Links between large-scale forcing and the Baltic Sea wave climate

The previous chapter demonstrated that the EOF technique is sensitive enough to identify fairly weak trends in the Baltic Sea wave properties from the satellite altimetry SWH data. More importantly, this technique is capable of recognition of spatial patterns in wave heights that cover more than a few degrees along latitudes and longitudes. The outcome is generally robust with respect to a fairly large level of noise and thus also robust with respect to uncertainties in the values of SWH snapshots.

In this chapter, this technique is applied to the set of SWH data for the Baltic Sea basin from all available satellite altimetry missions which is cleaned and validated against wave measurements. The goal is to reveal hidden patterns of changes to the wave heights in the Baltic Sea basin, quantify these changes in terms of EOFs and reveal the possible connection of these results with widely used climatic indices. The presentation follows Paper I where the EOF technique is applied to reveal various patterns of monthly averages of the SWH. The results of this analysis are explored to reveal correlations between the EOF modes and the most important climatic indices.

### 2.1 Evidence about teleconnection patterns

Several earlier studies have made attempted to establish connections between the wind wave climate in the Baltic Sea and the main teleconnection patterns SCAND, AO and NAO. These links and the level of explained variability are state of the art for the relevant knowledge and implicitly provide information about the reliability of the analysis performed in Paper I.

Myslenkov et al. (2018) compared numerically modelled wave properties in specific storms in the Baltic, White and Barents Seas with SCAND, AO and NAO climatic indices. They employed results of a model that uses rectangular and unstructured grids and the NCEP/CFSR reanalysis (Medvedeva et al., 2016). They found a strong negative correlation ( $-0.59$ ) between the number of storms with the SWH higher than 2 m in a year and the SCAND index. The correlation was positive but much weaker (coefficient 0.32) with the AO and almost non-existent (0.12) with the NAO index.

Correlations of similar magnitude (slightly stronger for the NAO and AO but weaker for SCAND) were obtained for the annual number of storms in which SWH exceeded 4 m for years 1950–2010 (Surkova et al., 2015). This match of the two data sets suggests (not unexpectedly) the presence of a fairly strong correlation of storms that produce a substantial part of annual wave energy and its flux on the Baltic Sea shores. Based on the description of the nature of the SCAND index it is also natural that the described correlation is strongly negative for this index as its large values correspond to weaker westerly winds.

The links between selected teleconnection patterns and wave properties have been explored at a few locations with *in situ* wave measurements. The SWH data simulated for 1966–2006 with a locally calibrated fetch-based model and one-point wind information for a location on the western shore of the West Estonian Archipelago near the island of Vilsandi has a much stronger correlation (coefficient 0.48 for all months and 0.72 for December–March) with the Iceland-Gibraltar version of the NAO index (Suursaar and Kullas, 2009). The situation was completely different in the southern Baltic Sea.

The connection between these two parameters (SWH and NAO index) is much lower in the southern part of the Baltic Sea for the time series reconstructed using the WAM model and REMO winds from German Weather Forecast Service (DWD) for a coastal location at Lubiatowo in Poland for 1958–2002 (Różyński, 2010). For example, the correlation coefficient for February was only 0.092. No coupling was detected for November and December and only January had a higher correlation coefficient of 0.381. Still, the explained variability was only 14% (Różyński, 2010).

The described results suggest that the influence of the main climatic indices, including the NAO index, on the wave climate of the Baltic Sea strongly depends on the particular area and time period. This feature may reflect a spatially strongly varying match of the geometry of the Baltic Sea with the directions of strong winds. While the location at Vilsandi is open to all directions of predominant strong winds, the nearshore at Lubiatowo is partially sheltered against south-westerly winds. It is likely that the application of the EOF technique would be able to reveal also several aspects of this variability that largely depends on the shape of the water body.

## 2.2. Spatial variations in the wave fields

The pattern of SWH anomaly for the entire set of years in the Baltic Sea is evaluated by the first mode of EOF (Fig. 9a). The eastern and southern areas of the Baltic proper, from the Gulf of Bothnia clockwise over the Gulf of Riga to the Danish straits, have higher values of the first EOF mode. This outcome is similar to the results of Mietus and von Storch (1997), where the application of EOF was applied on the modelled wave data.

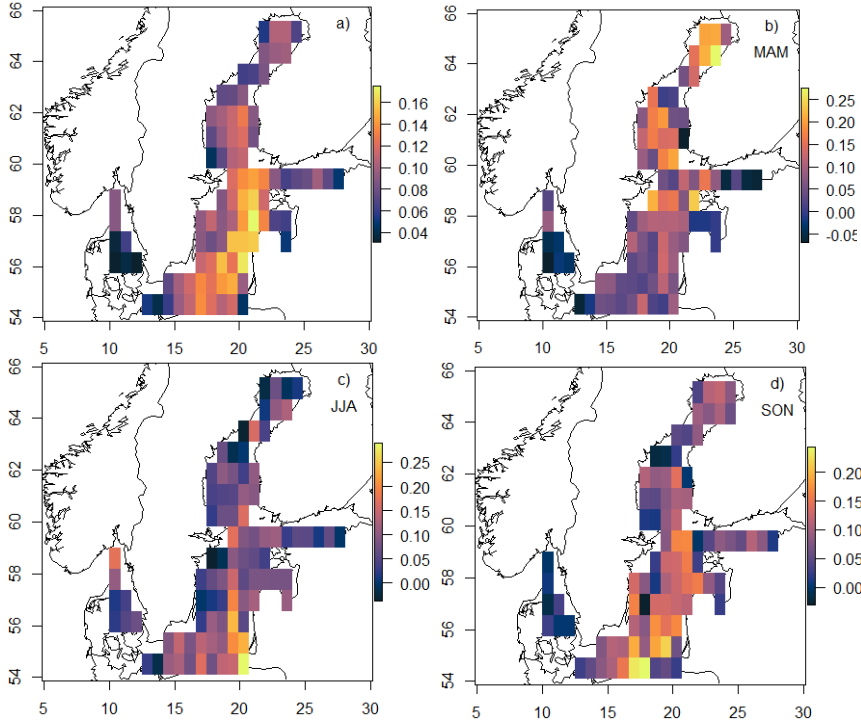


Figure 9. First EOFs describing the main patterns in the Baltic Sea wave heights retrieved for the entire SWH data set (a), spring (b), summer (c), and autumn (d) seasons. From Paper I.

The seasonal variation of the wave patterns is calculated separately for the stormy and calm seasons (see Section 1.5), as well as for conventional seasons; winter (DJF, Fig. 10a), spring (MAM, Fig. 9b), summer (JJA, Fig. 9c), and autumn (SON, Fig. 9d). The first EOF values have a clear asymmetry in the north-south direction for spring and autumn. In spring the first EOF values are larger in the north, in the Bay of Bothnia, and the lowest values are in the south (Fig. 9b). This arrangement of EOF is reversed for the autumn season when the first EOF maxima are in the southern Baltic proper (Fig. 9d). While spring and autumn have the largest and the smallest number of SWH estimates (Fig. 3), it is unlikely that this difference causes such an asymmetry. No similar large-scale pattern of wave climate in terms of the first EOF that is characterised by smaller-scale patchiness was found for the summer season (Fig. 9c).

The strongest spatial signal revealed in the first EOF is evident in the winter season (Fig. 10a). Unlike the variability in other seasons, this EOF mode has a prominent meridional pattern (Fig. 10a) that involves both positive and negative values. It shows very small positive values in the western parts of the Sea of Bothnia and Baltic proper and large negative values (with magnitude comparable to the largest positive values for other seasons) in the eastern regions of these water bodies. Not unexpectedly, this pattern resembles the spatial pattern of linear trends of pointwise estimated SWH (Fig. 10b; see also Kudryavtseva and Soomere, 2017).

To quantify the similarity of the spatial structure of the first EOF mode in winter with the meridional pattern of SWH changes established in Kudryavtseva and Soomere, (2017), the linear trends of SWH in the Baltic Sea were recalculated in Paper I using the same grid size that was applied in the EOF analysis ( $0.8^{\circ} \times 0.8^{\circ}$ ). This was done using the seasonal average of SWH values in each cell. Fig. 10b provides information about locations where these trends were statistically significant at a  $>95\%$  confidence level.

It is also carefully checked in Paper I if the significant trends of SWH and high values of the first EOF occur at the same locations. This was done by applying different cut-off values of the first EOF. The choice of  $-0.07$  as the cut-off value leads to the highest

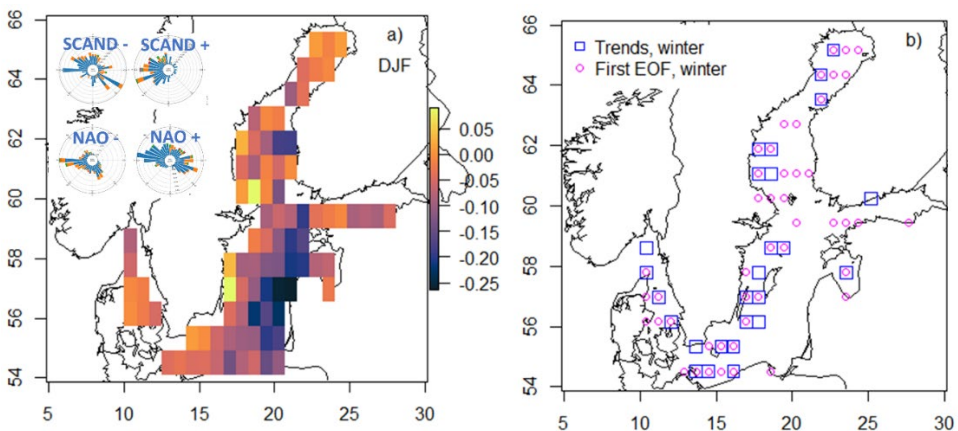


Figure 10. (a) The first EOF for the winter season (DJF). The wind roses show typical winter wind direction during the SCAND positive (01.12.1998–06.02.1999) and negative (01.12.2005–28.02.2006) phases and the NAO positive (01.12.1994–28.02.1995) and negative (01.12.1995–28.02.1996) phases at Hultsfred station  $57.53^{\circ}\text{N}$ ,  $15.82^{\circ}\text{E}$ . (b) The spatial coincidence of the linear trends in SWH in winter and the first EOF mode in winter. The statistically significant trends of SWH in winter over the 1996–2015 period has the same grid size as the EOF method and are shown by blue squares. EOF values above  $-0.07$  are shown by pink circles. From Paper I.

probability of coincidence of these two features. For this cut-off value, 77% of grid cells where a trend of SWH was detected coincide with the locations where the first winter EOF exceeds the value  $-0.07$ .

This synchronisation of locations of the two quantities suggests that the established spatial pattern of the first winter EOF reflects the pattern of linear trends in SWH identified in Kudryavtseva and Soomere (2017). This feature also signals that the north-south asymmetry of the first EOF for spring and autumn could reflect decadal spatial changes in the wave intensity in the north-south direction.

## 2.3 Reliability of spatial patterns

The reliability of the identified spatial patterns can be, to some extent, estimated from the percentage of explained temporal variability. This percentage varies in different seasons but is relatively small for altimeter-based data sets in North Atlantic and Baltic Sea conditions. The temporal variability of the first EOF retrieved in Paper I for different seasons is fairly modest. It is the largest (27%, Table 3) in winter. This proportion of variability is lower than that retrieved in similar studies based on wave simulations. For example, it ranges from 57.6% to 83%, during winter and stormy seasons in the analysis of (Mietus and von Storch, 1997) and (Shimura et al., 2013).

The relatively low level of variability explained by the first EOF function is a frequent feature of analyses based on satellite altimetry data. For instance, the variability explained by the first EOF of altimeter-measured SWH in the southern hemisphere is in the range of 17–19% (Hemer et al., 2010). The level of explained variability was much larger (41%) for the North Atlantic (Woolf et al., 2002). The variability of the higher modes of EOF was at the level of 15% and 19%.

The results presented in Woolf et al. (2002) and Hemer et al. (2002) did not take into account the presence of gaps and noise in the satellite data. The analysis of the impact of noise using simulated data sets in chapter 1 sheds some light on this aspect. The main conclusion was that an increase in the level of noise considerably decreases the amount of explained variability. However, the spatial patterns of variability are generally not affected until some threshold of noise is reached (Fig. 4e, Fig. 5e, Chapter 1).

The analysis in Chapter 1 and Paper I suggests that the significant levels of noise may reduce the retrieved temporal variability to a level of 20%, even when well-defined and strong global patterns exist in the study area. The low level of retrieved variability of the first EOF in Paper I and in Hemer et al. (2010) can thus be explained by the presence of relatively strong noise in the altimeter data set.

The analysis provided in Paper I and Chapter 1 also confirms that it is still possible to capture existing patterns in the data even in the presence of substantial noise. The larger the pattern, the better it is visible against the background of increasing noise. Consequently, the meridional pattern in the first EOF in winter season (Fig. 10a) most likely exposes an actual arrangement of the wave height trends over the Baltic Sea (an increase in the SWH in the western part of the sea, Kudryavtseva and Soomere, 2017) even though the relevant first EOF only explains 27% of the temporal variability.

## 2.4 Wave climate pattern and its links with atmospheric circulations

Sections 2.1 and 2.2 presented several examples of spatial variations in the EOFs of the SWH at annual and seasonal scales. A major east-west pattern in the first winter EOF can apparently be linked to the detected trend of SWH in the Baltic Sea. It is likely that this and other features of the EOFs (equivalently, spatial patterns of wave climate) are driven by the spatio-temporally varying atmospheric circulation. To reveal potential links of these patterns with large-scale teleconnection patterns, a detailed correlation analysis between the evaluated EOFs and the major atmospheric indices was conducted in Paper I.

The analysis involved the SCAND, AO and NAO climatic indices as the main targets. Several other teleconnection patterns, such as AMO, EA, EAWR, POL (Section 1.2) were also addressed. The time series of these indices were downloaded from the Climate Prediction Centre, National Oceanic and Atmospheric Administration (NOAA). The analysis was performed for the first three modes of EOF in terms of monthly means as in Chapter 1 and Sections 2.1, 2.2. The focus was on the correlations that were nonzero with probability of  $\geq 0.95$ . To select such correlations, the 95% confidence intervals of particular correlation coefficients were extensively used to acknowledge the uncertainties and to estimate the reliability of the analysis. While the EOF modes showed reliable (in this sense) correlations with the SCAND, AO and NAO indices, the results for AMO, EA, EAWR and POL almost always contained uncertainties larger than the correlation coefficients. Only the correlation coefficient of the EAWR index with the first winter EOF (0.26) is marginally larger than its uncertainty ( $\pm 0.22$ ).

The strongest correlation between the first EOF in winter and the atmospheric circulation indices was found for the SCAND index ( $-0.47 \pm 0.19$ , Table 5). This teleconnection pattern is thus the most influential for the observed spatial pattern of SWH in winter (Fig. 10). The correlation is negative and therefore high values of EOF are associated with low levels of this index. Interestingly, the correlation of the second and third EOFs was almost zero. The relevant correlation coefficients with the first EOF for other seasons were positive but had considerably smaller magnitudes:  $0.24 \pm 0.22$  in spring,  $0.38 \pm 0.20$  in summer and  $0.36 \pm 0.21$  in autumn. These positive seasonal correlations might mirror the frequent presence of south-easterly winds during these seasons.

The first winter EOF exhibits a strong positive association to the AO (correlation coefficient  $0.42 \pm 0.20$ ) and NAO indices ( $0.31 \pm 0.22$ ). The second and third EOFs for winter (Table 5) and all three EOFs for other seasons have lower magnitudes of correlation coefficients with all three indices. In other words, the estimated uncertainties were greater than the correlation coefficients and no remarkable correlation were detected.

The obtained estimates for the correlation coefficients match the results of similar correlation analysis for the number of days with very strong wave storms (SWH > 4 m) over the years 1950–2010 (Section 2.1). The correlation coefficient ( $-0.47$ ) is exactly

*Table 5. Correlation coefficients between climatic indices and first three EOFs for the winter season. The correlation of the most prominent climatic indices is presented.*

Climatic Index	First EOF	Second EOF	Third EOF
SCAND	$-0.47 \pm 0.19$	$0.01 \pm 0.24$	$-0.07 \pm 0.24$
AO	$0.42 \pm 0.20$	$0.19 \pm 0.23$	$-0.03 \pm 0.24$
NAO	$0.31 \pm 0.22$	$0.19 \pm 0.23$	$-0.09 \pm 0.24$

the same for the SCAND index and clearly higher (0.66 and 0.56) for the AO and NAO indices, respectively (Surkova et al., 2015). A similar analysis for the correlation of the number of storms generated in the Baltic Sea with SWH over 2 m and various teleconnections patterns had a correlation coefficient of  $-0.59$  with the SCAND, 0.32 with the AO, and 0.12 with the NAO index (Myslenkov et al., 2018). This difference may mirror rapid reaction of the sea surface to large values of these indices that correspond to much stronger than average westerly winds and thus large wave heights in the eastern part of this basin. The described match signals that the first winter EOF and the SWH trends might be affected by the same drivers of storminess in the area.

## 2.5 Time variable correlation with climatic indices

The correlation coefficients presented in the previous section characterise the strength of the relevant links during the entire study period. This strength may vary in time. This kind of variability of the association between the climatic indices and the wave climate of the Baltic Sea over time is estimated in Paper I using the technique of sliding (or running) correlation. The bivariate Pearson product-moment correlation, often called Pearson's  $r$ , was used for this purpose along with Kendall and Spearman correlations. All these correlation coefficients serve as a measure of the strength of linear correlation between two sets of data. Their estimates were created using the statistical programming language R version 3.4.4 `cor.test` command from the "stats" package. The procedure was applied on the three major teleconnections (SCAND, AO, and NAO) and the first winter EOF. Test runs with window lengths from 2 to 9 years with a time step of one year indicated that the lowest level of noise was delivered by the 5-year window. This window was used in the analysis of sliding correlation.

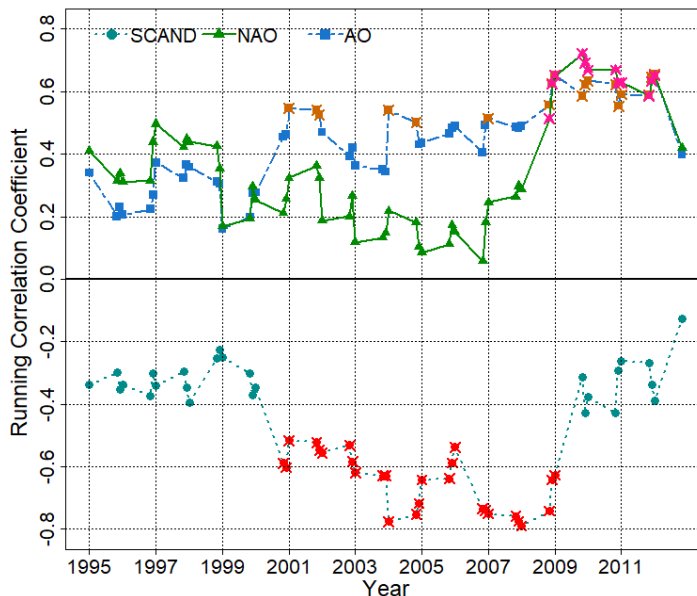


Figure 11. Sliding correlation coefficient for 5-year time periods between the first winter EOF and (a) Scandinavia pattern, (b) Arctic Oscillation, and (c) the North Atlantic Oscillation in 1993–2015. The correlations with  $>95\%$  level of statistical significance are indicated in red. Modified from Paper I.

The averages of such sliding correlation coefficients over the entire study period match the values presented in the previous section (about  $-0.5$  for SCAND and about  $0.4$  for AO and NAO, Fig. 11). Their temporal courses are greatly different (Fig. 11). This quantity for the SCAND index is in the range from  $-0.5$  to  $-0.8$  in 2000–2009. All these values represent a statistically significant correlation between the SCAND index (>95% confidence interval, that is, Pearson  $p$ -value  $<0.05$ ) and the first winter EOF within the relevant 5-year time periods. This correlation was always negative but much lower (around  $-0.3$ ) before 2000 and after 2009. This behaviour is characteristic of regime shifts.

The running correlation coefficient of the first winter EOF and the AO and NAO indices was positive during the entire study period. It increased almost linearly for the AO from about  $0.2$  (with the minimum value  $0.16$  in 1999) to the level of about  $0.6$  (with a maximum of  $0.66$  in 2012). In contrast, this coefficient for the NAO decreased almost linearly from the level of about  $0.4$ – $0.5$  at the beginning of the study period down to zero in 2007 and increased explosively to about  $0.6$ – $0.7$ , with a maximum of  $0.72$  in 2010. For both climatic indices the values of coefficients above about  $0.5$  are statistically significantly correlated at a >95% level. This kind of robust correlation was present in 2008–2012 for the AO and in 2009–2012 for the NAO. The AO index also showed statistically significant correlation for a few years between 2001 and 2008.

Therefore, strong correlation of the first winter EOF with the three dominant climatic indices occurs in certain decades for different indices. The temporal courses of all these correlations are greatly different. When the correlation with the SCAND index is strong, the similar correlation with the NAO/AO index is weak. This implies that the wave climate in the Baltic Sea is driven by either of these climatic indices (SCAND or NAO/AO) in different decades. They both signal a possible presence of a major shift in the Baltic Sea wave climate in terms of the loss of correlation with the SCAND index and largely following the NAO index in 2008–2009. The temporal course of the running correlation with the AO index has almost no similarity with the other correlations, except the presence of statistically significant correlation around 2010. This feature also deserves attention because previous research has reported similar behaviour of the AO and NAO indices (Jevrejeva et al., 2005).

### 3 The effects of seasonal ice cover on wave fields

The wind climate in the Baltic Sea basin is usually relatively windy in the autumn and winter seasons, and calmer in the spring and summer. The windy season usually begins in late autumn when temperatures drop and freezing starts. The presence of ice can protect the shore against storm surges and wave-driven erosion (Orviku et al., 2003; Ryabchuk et al., 2011a). Seasonal sea ice has a strong influence on the regional wave climate. Wave propagation and growth are restrained by the decrease in fetch length (Liu and Mollo-Christensen, 1988). The presence of floating ice enhances dissipation and reflection of wave energy (Collins et al., 2015; Mostert and Deike, 2020; Tavakoli and Babanin, 2021). Therefore, the existence of sea ice usually reduces the wave energy and the impact of waves on the shore.

The extent and duration of sea ice are greatly sensitive to the climate change driven alterations in air temperature. Therefore, it is essential to estimate possible consequences of variations in the ice conditions on the wave properties. The main purpose of research in Paper II and this Chapter was to understand how the presence of sea ice, estimated using satellite information, impacts the Baltic Sea wave fields. The commonly used average wave properties, such as average SWH, wave energy, and wave energy flux may give an inaccurate representation of the wave climate in seasonally ice-covered seas because there are several ways to represent the ice season in these quantities (Tuomi et al., 2011). For this reason, the focus is on the cumulative properties, particularly total annual wave energy flux.

The analysis in this chapter relies on the concentration of sea ice in the Baltic Sea. The ice season duration is evaluated from the relevant ice information retrieved from satellite missions since 1979 and validated using the classic ice charts. It is condensed into dates that reflect the start and end of each ice season. These time periods are matched with the hindcast of wave properties for 1980–2007. The impact of changes to ice properties on wave loads is evaluated in terms of associated changes in the mean and cumulative (total) wave energy and wave energy flux for the overlapping time of these two data sets.

#### 3.1 The decreasing influence of ice on wave impact

The climate of wind waves explored in Chapters 1 and 2 is forced by wind conditions and controlled by the geometry and bathymetry of the sea, and by the presence of ice. The relevant analysis confirms that wind properties in the Baltic Sea are to a large extent influenced by large-scale atmospheric circulation systems; such as the NAO, AO, or SCAND (e.g., von Storch et al., 2015; Paper I). Their broad variability in both space and time gives rise to widespread spatial variability, temporal intermittency and complicated patterns of decadal changes in the Baltic Sea wave fields (Soomere and Räämet, 2011) as partially described in the Introduction.

On average, the wave climate of the Baltic Sea is relatively mild. The mean SWH ( $H_s$ ) is 1–1.3 m in the Baltic proper and below 1 m in its smaller sub-basins based on both estimates from satellites (Kudryavtseva and Soomere, 2016; 2017) and from wave modelling (Björkqvist et al., 2018). The maxima of annual average SWH may reach almost 2 m (Kudryavtseva and Soomere, 2016). However, severe wave conditions, with SWH exceeding 8 m, may occur in this water body as discussed in Section 1.1.

Even though the wave climate of the Baltic Sea has substantial decadal variability (Soomere and Räämet, 2014), there is no convincing evidence about its long-term

changes. An increase in the frequency of strong westerly winds in the region (Ruosteenoja et al., 2019) has apparently not substantially altered the wave climate (Hünicke et al., 2015; Rutgersson et al., 2022). An increase in the SWH by 0.005 m/yr 1993–2015 (Kudryavtseva and Soomere, 2017) becomes evident mostly in the western part of the sea and apparently does affect its eastern sedimentary shores.

The major driver of coastal processes is wave energy flux. This quantity is particularly intermittent: half of the annual wave energy flux to the eastern shores of the Baltic Sea is generated in storms with a total duration of less than two weeks (Soomere and Eelsalu, 2014). These events are often treated as extreme storms. They have led to unexpectedly severe wave storms in the 21st century (Björkqvist et al., 2017; 2020). Such storms may become stronger (Mäll et al., 2020) and more frequent (Kudryavtseva et al., 2020).

The strongest storms in the Baltic Sea usually occur in the middle of the windy season from November to January (Suursaar et al., 2006; Björkqvist et al., 2017; 2020). A substantial part of this windy season coincides with the ice season. The presence of sea ice protects the shores both explicitly (by direct protection of the shore) and implicitly (by restricting the fetch length and damping offshore waves). Its total effect in terms of decrease in the wave energy is up to 80% in the Bohai Sea (Yellow Sea, Zhang et al., 2020).

The impact of this effect is highly variable in the Baltic Sea. Its magnitude can be roughly estimated by means of the variation of average wave properties evaluated for the ice-free and ice-included statistics. The two estimates differed by 30% in the Bay of Bothnia (Björkqvist et al., 2018). This difference decreased for more southern sea areas, and was also relatively large in the north-eastern Gulf of Finland and became negligible to the south of latitude 59.5°N.

This kind of protection is effective in the Baltic Sea regions that are ice covered during at least part of the windy season and particularly during very strong storms. The gradual decrease in the ice season length owing to climate warming (see Introduction) may weaken and even completely remove this protection.

Paper II presents an attempt to quantify the threats posed by this process in terms of an increase in the wave energy flux owing to the later appearance or earlier disappearance of the ice cover. The research questions are: (i) how much does the presence of ice reduce the wave impact, and (ii) how much has this kind of reduction changed over the years? These questions are often addressed in terms of calendar years (e.g., Zaitseva-Pärnaste and Soomere, 2013). In Paper II this analysis is undertaken for entire ice seasons. An ice season usually contains some time periods from two subsequent years. This viewpoint, similar to the one used in the analysis of sea level extremes (Männikus et al., 2019), makes it possible to link the severity of the ice seasons with properties of the entire windy season.

This task requires the use of cumulative properties of wave fields (e.g., total wave energy flux) over certain time periods (Zaitseva-Pärnaste and Soomere, 2013). Two classic approaches of average wave statistics introduced by Tuomi et al., (2011) are used for their construction. Type F statistics only includes the wave data during the ice-free season. The relevant quantities are often used in a normalised form in order to take the varying duration of the ice-free season into account. Type N statistics reflect the idealised situation of no ice during the entire period of interest. This viewpoint was common in numerical wave modelling in the past (Räämet and Soomere, 2010; Soomere, 2022). It obviously overestimates the cumulative wave properties for seasonally ice-covered seas.

A specific focus in Paper II is on the exploration of the spatial pattern of changes in the protective role of sea ice and on the identification of locations or latitudes where this change may substantially affect coastal processes. The sea ice data are derived from the OSI-450 ice concentration measurements (OSI SAF 2017; Lavergne et al., 2019) obtained from various satellite missions. Wave properties are extracted from the simulations of Dr. Andrus Räämet using the wave model WAM driven by adjusted geostrophic winds for the period of 1970–2007 (Räämet and Soomere, 2011).

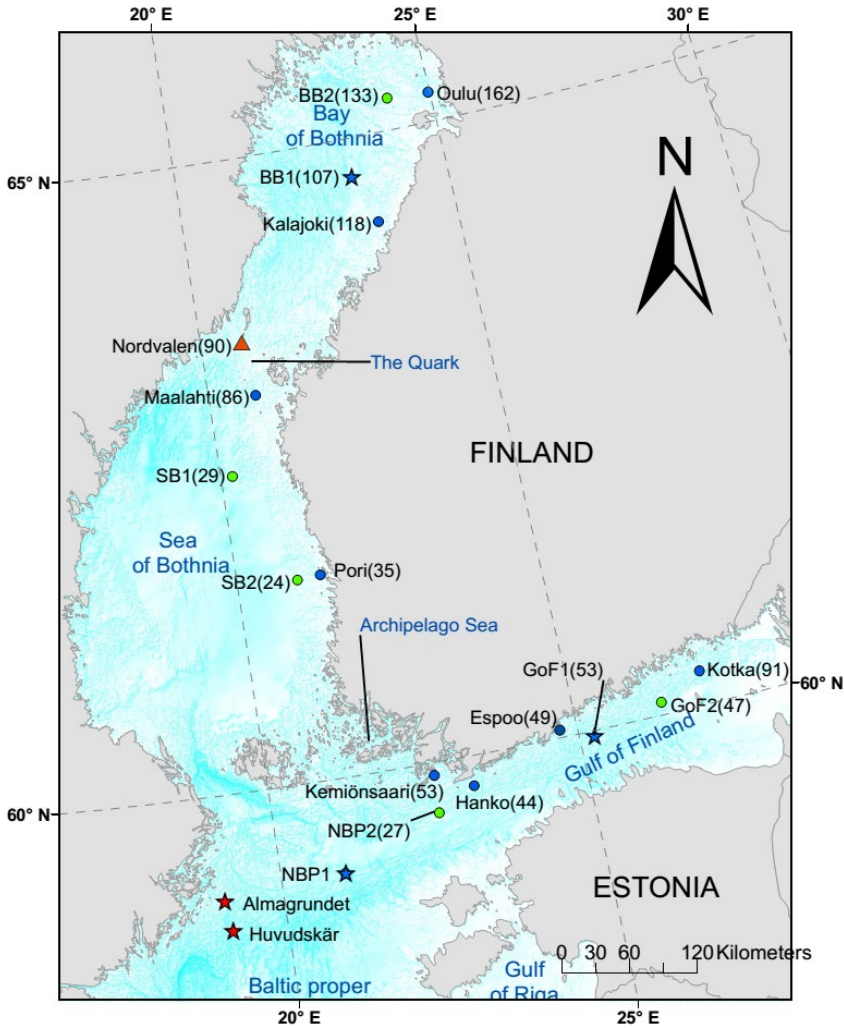


Figure 12. Map of the locations discussed in Chapter 3 and Paper II. The wave measurement devices operated by the Swedish Meteorological and Hydrological Institute (SMHI) and Finnish Meteorological Institute (FMI) are marked with red and blue stars, respectively. The locations of FMI temperature buoys are shown by blue circles, WAM model grid points used in the analysis by green circles, and the south-west SMHI location Nordvalen by a red triangle. The reasons for the choice of the particular locations and main parameters of measurement devices are described in Paper II. The numbers at selected locations indicate the average duration of ice season during the study period. From Paper II.

### 3.2 Sea ice and wave data

Both modelling and observation of waves that occur in the presence of sea ice involve large uncertainties, especially when ice covers only part of the study area. Wave simulations with different ice information have led to differences up to 3.2 m in the monthly maximum values of SWH in the northern Baltic Sea (Tuomi et al., 2019). Such differences reflect offshore ice conditions in single storms that could be highly variable depending on ice drift. However, it is likely that this sort of variability does not substantially impact the annual (or ice-season) cumulative properties of waves in the nearshore.

This assumption is apparently reasonable for most of the northern Baltic Sea, especially for regions to the north of the latitudes of the Gulf of Finland and along large sections of the Swedish shore. These regions have extensive archipelago areas, such as the Åland Archipelago. The coastline is extremely rugged in this region. The nearshore has numerous small islands and many peninsulas and bays. As a consequence, this region normally has a wide belt of non-moving (landfast) ice at the shore during the entire ice season (defined as the time period when high concentrations of ice are observed in the open sea). This landfast ice effectively protects the coastal area against wave energy. Consequently, the amount of wave energy that reaches the nearshore is limited by the duration of the ice season. For this reason, the analysis in Paper II focuses on the determination of the start and end of the ice season based on the available *in situ* ice observations and the relevant information from satellites.

The core source of satellite information used to estimate sea ice concentration in the study area is the OSI-450 (EUMETSAT Ocean and Sea Ice) database (Tonboe et al., 2016) kept by the Norwegian and Danish Meteorological Institutes. Its current version has a spatial resolution of  $25 \times 25$  km and employs a new Open Water (Weather) Filter (Gloersen and Cavalieri, 1986; Buehner et al., 2016). This filter removes false ice readings generated by weather-induced noise and enables the measurement of small values of ice concentration. It also receives the input data from new instruments (from the EUMETSAT Climate Monitoring Satellite Application Facility) and uses more precise algorithms to evaluate ice concentration (Lavergne et al., 2019). It provides daily records of sea ice concentration for 1979–2015 in terms of the percentage of the grid area covered by ice together with various service information, such as flags and uncertainty estimations. The analysis in Paper II only uses entries from OSI-450 with the flag equal to 0, indicating that they are the most reliable.

Based on the arguments presented and following the usual definition of the duration of the ice season (e.g., Jevrejeva, 2001), the analysis in Paper II relies on two important dates: the beginning and end of offshore ice cover for each winter. These dates are used to define the duration of the ice season. The notion of offshore is understood here as the sea area in which satellite information on ice cover is provided.

This definition requires specification of a threshold for the offshore ice concentration, the reaching (or falling below) of which is interpreted as the beginning (or end) of the ice season. The beginning is actually more important for the analysis in Paper II as the spring season provides much less wave energy. The analysis in Tuomi et al. (2019) suggests that the exact value of this threshold is not critical and its variations from 30% to 70% changes wave statistics insignificantly.

A suitable threshold was specified in Paper II based on a comparison of two sets of estimates for the ice season duration at the location Maalahti (Fig. 12) and based on different thresholds. One of these was derived based on the information from the

OSI-450 database and the other using the ice charts by Swedish Meteorological and Hydrological Institute (SMHI). The SMHI data set reflects, in addition to satellite images, information presented by ice observers, coastguard, pilot stations, and icebreakers. It is therefore natural that the start and end of the ice season based on all this material may differ from that retrieved from satellites only. The best match of these estimates (correlation coefficient 0.91, bias 10.35 days and root mean square deviation 21.35 days) was achieved using the threshold  $\zeta = 50\%$  of the ice concentration. This threshold was used in the analysis.

The estimates of the start and end dates of the ice season based on the OSI-450 data set and the threshold of 50% of ice concentration were additionally compared with similar estimates using the SMHI ice charts for a different location. A comparison of the two estimates of the ice season duration was made for an SMHI observation location near Nordvalen (63.54°N, 20.73°E) and at the nearest OSI-450 grid point (63.54°N, 20.76°E) (Fig. 13). The match of these estimates was sound, with correlation coefficient 0.94 and intercept of the linear regression line at 4.7 days. *In situ* estimates tended to provide about 10% longer ice seasons (expressed by the slope 0.88 of the linear regression line). This is because the ice season according to *in situ* observations is counted from the first observation of ice until the last observation of ice (cf. SMHI and FIMR, 1982; Jaagus and Sooäär, 2007). Therefore, the ice season duration based on such observations is generally longer than the one derived from satellite information using the threshold of 50% of ice concentration and used in this analysis.

The properties of ice seasons retrieved from the OSI-450 database show extensive variability in the north-south direction (Fig. 14). The average ice season in the Bay of Bothnia (BB1) (107 days) is about 2 months longer than the ice season in the middle of Gulf of Finland (GoF1) (53 days), or at Kemiönsaari (Kalvören) at the northern margin of the Baltic proper (53 days).

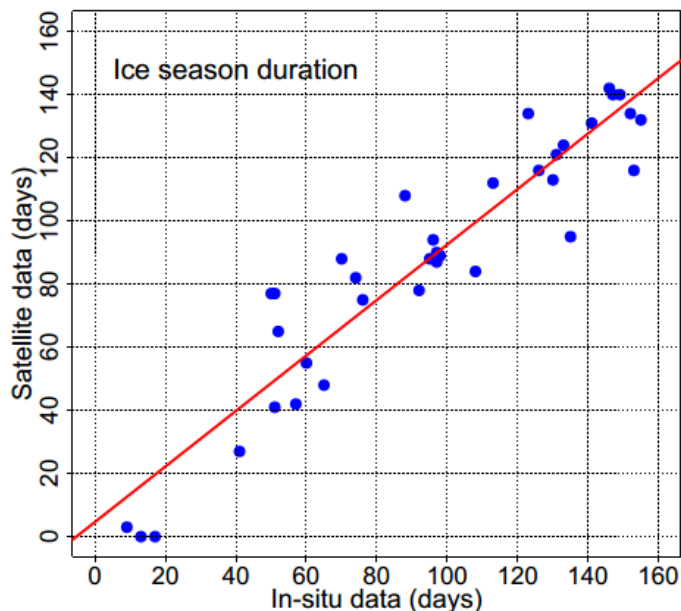


Figure 13. Satellite-derived ice season duration from OSI-450 ( $\zeta = 50\%$ ) versus *in situ* ice season duration observed at SMHI Nordvalen station. The red line represents the linear regression line. From Paper II.

The performed analysis showed that the western parts of the Baltic proper do not have any extensive ice season in typical years and the sea is ice-covered during colder than usual and severe winters. The ice season duration is zero in these locations in most of the years. Consequently, climate-driven changes to the effect of sea ice on wave loads are apparently small at such locations. For this reason, Paper II focuses on locations where this sort of change can be identified from the OSI-450 data set. While this data set covers 27 years, for an adequate estimate it is necessary to have at least 20 partially ice-covered winters (Paper II). The areas where this condition is met are located in the north-eastern part of the Baltic Sea. They include the Gulf of Finland, Sea of Bothnia and Gulf of Bothnia, and several regions of the north-eastern Baltic proper.

To link the analysis in Paper II with hydrometeorological measurements, the locations for analysis were chosen from the locations of eight Finnish Meteorological Institute (FMI) buoy stations (Fig. 12). Two of them are in the Bay of Bothnia, one in the Quark area, one in the Sea of Bothnia, two at the north-eastern margin of the Baltic proper, and two in the Gulf of Finland. Some of these sites are located at a water depth of 3–6 m (Paper II) or near the shore. Numerically replicated wave data may provide a distorted picture of wave properties in such locations because of the limited resolution of the wave model used (about 3 nautical miles, Räämet and Soomere, 2010).

The location of the FMI wave buoy in the Gulf of Finland (GoF1 in Fig. 12) and another similar location in the middle of the Bay of Bothnia (BB1) were added to compare the identified changes in the far offshore and near the shore to some extent. The analysis also made use of modelled wave data in several other arbitrarily chosen offshore locations in the Bay of Bothnia (BB2), and in the Sea of Bothnia (SB1 and SB2), one location in the northern Baltic proper (NBP2), and one in the Gulf of Finland (GoF2, Fig. 12). The available instrumentally measured wave data at Almagrundet, Huvudskär, and in the northern Baltic proper (NBP1) were used for testing. See detailed information about all locations in Paper II.

Wave data exists at much finer resolution than ice observations. The horizontal resolution of wave modelling studies for the entire Baltic Sea has varied from about 20 km in the 1990s (Soomere, 2022) up to 1.1–1.85 km in contemporary studies (Nilsson et al., 2019; Björkqvist et al., 2018). The small-scale spatial variations in wave properties are often missed by the models with a coarse resolution (grid size >10 km).

The study in Paper II relies on wave fields reconstructed for the entire Baltic Sea for 1970–2007 (Räämet and Soomere, 2010) using the wave model WAM (Komen et al.,

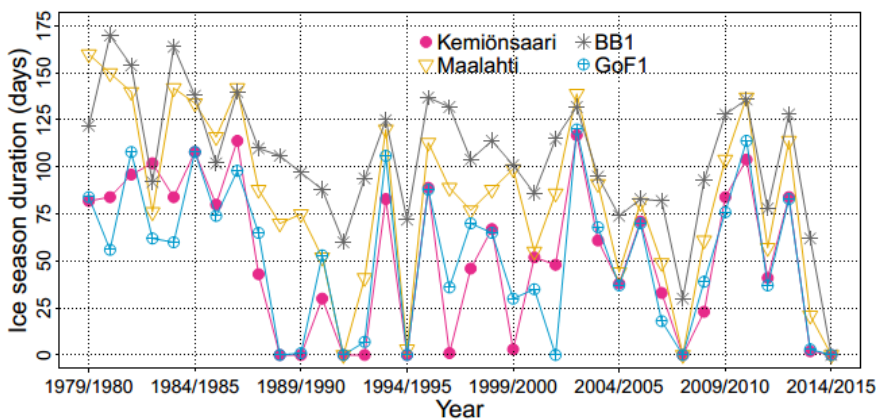


Figure 14. Ice season duration at different locations based on OSI-450 satellite data. From Paper II.

1994) forced with adjusted geostrophic winds. This wind information is not particularly realistic and leads to frequent underestimation of wave heights in the Baltic proper and low quality of reconstruction of wave properties in the southern Baltic Sea. However, the quality of the simulated wave data was acceptable in the study area and to the north of the Gulf of Finland (Räämet and Soomere, 2021). The hourly time series of SWH and peak period  $T_p$  were extracted at the nearest wave model grid point for each studied location. As most of wave energy flux is propagated onshore in coastal areas, the analysis of Paper II is based on the magnitude of wave energy flux that is calculated from the above parameters for the water depth at each selected location.

The resolution of the wave model (about 3 nautical miles or about 5.6 km) led to a typical mismatch between the centre of the relevant grid cell and the particular location by  $0.02^\circ$  on average. This data set was produced under the assumption of no sea ice in the Baltic Sea and thus represents Type N statistics. This was an intentional choice as Paper II makes an attempt to estimate the rate of the part of wave-induced impact that is currently suppressed by the presence of ice. Changes to this rate of suppression are largest in the northern Baltic Sea where the ice conditions have changed the most (Jevrejeva, 2001).

As explained above, the analysis in Paper II addresses the impact of single ice seasons on the background of longer relatively windy seasons. These seasons usually include several weeks in the late autumn of one year and the winter months of the subsequent year. This approach is standard in ice studies and has been often implemented in the analysis of water levels (e.g., Männikus et al., 2019). Paper II uses 12 month-long time periods from 01 July of a certain year to 30 June for the analysis. For simplicity, they are called stormy seasons. They cover the entire ice season in the study area for each winter and are separated by the calmest and warmest time in Baltic Sea region. The wave data during the whole duration of ice seasons is discarded from the calculation of wave energy flux in ice-free time.

The instantaneous values of the wave energy  $E$  ( $\text{KJ/m}^2$ ) are calculated in the classic manner as  $E = \rho g H^2 / 16$ , where  $\rho$  is the density of water and  $g$  is gravity acceleration (Dean and Dalrymple, 1991). The symbol  $H$  stands for the SWH of *in situ* data and for the hindcast  $H_s$  for modelled data. The density of wave energy flux  $P$  per unit of wave crest ( $\text{KW/m}$ ) is  $P = E c_g$ , where

$$c_g = \frac{\omega}{2k} \left( 1 + \frac{2kd}{\sinh 2kd} \right) \quad (3)$$

is group speed,  $\omega = 2\pi/T$  is angular wave frequency ( $\text{rad/s}$ ),  $k = 2\pi/\lambda$  is the wave number, and  $d$  is water depth (m), at the particular location. The wave number  $k$  and length  $\lambda$  are calculated from the full dispersion relation of linear water waves  $\omega^2 = gk \tanh(kd)$ . The values of peak period are used to represent the wave period  $T$ .

The classic (Type F) average wave properties used in the analysis, such as average SWH  $\bar{H}_{Sy}$ , wave energy  $\bar{E}_y$  and its flux  $\bar{P}_y$ , during the ice-free time of a single stormy season marked by subscript  $y$  are calculated over the entire set of available measured, estimated or modelled values of wave properties. For example, the average wave energy is evaluated as a simple average

$$\bar{E}_y = \frac{1}{N_y} \sum_{year} E_i, \quad (4)$$

over all  $N_y$  instantaneous values of wave energy  $E_i$  in this stormy season. The information about the particular ice season duration is given by the difference of  $N_y$  and the total number of measured or modelled wave data points during the stormy season.

The average wave properties during a stormy season only partially reflect the impact of ice on wave fields (Tuomi et al., 2011; 2019). It is likely that this impact is much better characterised by the total (cumulative) wave energy and wave energy flux (Zaitseva-Pärnaste and Soomere, 2013). Wave energy flux is expected to be a more sensitive measurement to estimate the impact of ice cover on hydrodynamic loads. While the wave energy is proportional to the squared wave height, the wave energy flux is proportional to the SWH to power of 2.5. These quantities for a stormy season (the total wave energy  $E_{tot}$  and wave energy flux  $P_{tot}$ ) are calculated as in Eq. (4) but without the multiplier  $1/N_y$ .

The time series of modelled wave data only cover years 1979–2007. The ice information in the OSI-450 database is available from 1979. The analysis in Paper II addresses the overlapping part of these data sets. The results provided here are based on data for 27 stormy seasons from 1979/1980 to 2006/2007.

### 3.3 Wave climate during ice-free times

A distinctive feature of the Baltic Sea wave climate is its large variability in space and time. This feature becomes evident also in terms of properties of wave climate during ice-free times. The stormy season average SWH during the ice-free time (Type F statistics) varies by a factor of almost two at the study sites (Fig. 15). The northernmost site, Oulu, has the lowest range of the stormy season average SWH (0.38–0.55 m). This small range apparently reflects two features. First, this site is located in a relatively

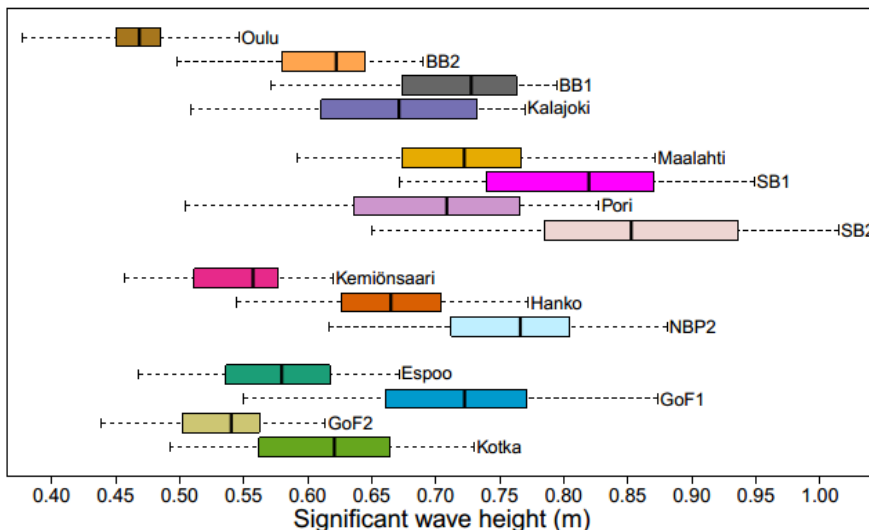


Figure 15. Boxplot of ice-free modelled mean SWH (Type F statistics) during 27 stormy seasons from 1979/1980 to 2006/2007. The coloured area reflects the two middle quartiles of the average SWH. The vertical line in this area represents the median SWH (in terms of average SWH in single stormy seasons). The sections denoted by dashed lines represent the lowest and the highest quartiles. The maximum and minimum SWH at the particular location are shown using small vertical lines. From Paper II.

sheltered area. Second, it may be covered by ice during a considerable part of windy autumn and winter seasons. The stormy season average SWH at three nearby stations (BB1, BB2, and Kalajoki) varied between 0.50 m and 0.77 m. The somewhat larger average SWH at BB1 (0.72 m) evidently reflects its more open position compared to Kalajoki.

Sites to the south of the Bay of Bothnia have larger stormy season average SWH (0.51–1.01 m). It is not clear from the analysis in Paper II whether this feature stems from a shorter ice season than in the Bay of Bothnia or from the larger size of the Sea of Bothnia. The larger stormy season average SWH at the more offshore locations SB1 and SB2 than at Maalahti and Pori evidently reflects the wider openness of SB1 and SB2. Similarly, the relatively low average wave intensity at Kemiönsaari (the second-lowest average SWH in the range 0.46–0.62 m) apparently reflects its sheltered location in the Archipelago Sea (Fig. 12). This conjecture is supported by much higher average SWH values (0.54–0.77 m) at Hanko that is open to the predominant winds over the Baltic proper.

Clearly a more severe wave climate is characteristic of the northern Baltic proper (NBP2) and of the Gulf of Finland with the largest average SWH 0.55–0.87 m (GoF1) in the gulf. We conjecture that the farther the particular site is located from the coast, the higher the averages at that site. This feature becomes evident in each sub-basin, except for the GoF2 location. The estimates of the average SWH presented in Paper II are consistent with the results of a 41-year SWAN model hindcast (Björkqvist et al., 2018).

The main conclusion of the presented analysis is that variations in the length of the ice season duration generally have a smaller impact on the “classic” (Type F) statistics of wave climate than the location of the particular site offshore or in a sheltered nearshore region.

The spatial patterns of interannual variations in the Type F stormy season average wave energy and wave energy flux for ice-free times, estimated from the modelled wave data, qualitatively follow the described pattern for the average SWH very closely and are almost identical at all locations (Paper II). An expected difference is that the stormy season average wave energy and its flux have much larger interannual and spatial variation than the average SWH. The annual average ice-free wave energy varies by a factor of up to 3 at some locations. It reaches the level 0.79 KJ/m<sup>2</sup> at GoF1 and is only 0.2–0.3 KJ/m<sup>2</sup> at Kemiönsaari (Fig. 16). The average wave energy flux over the entire study area also varies by a factor of up to 3.

Similar interannual variations in the ice-free (Type F) stormy season average wave energy flux are even larger (Fig. 16), but qualitatively follow almost exactly the interannual variations in wave energy. This similarity apparently signals that wave periods in the strongest storms that provide the largest contribution to the wave energy flux do not vary significantly. In other words, severe wave fields in the study area are generally fetch-limited. The long-term average of the local wave energy flux is about 1 KW/m at Kemiönsaari and up to 2.5 KW/m at Maalahti, BB1 and GoF1. The presented values match well the similar values in idealised ice-free conditions in the western Baltic proper (Soomere and Eelsalu, 2014).

The cumulative properties of waves during ice-free times more explicitly take into account the duration of the ice season. This is apparently the main reason why these properties vary even more extensively in time. The largest variation, as expected, is from the cumulative wave energy flux  $P_{tot}$ . At the GoF1 it varies by almost a factor of 6

in individual stormy seasons (Paper II). Together with information presented in Fig. 16, such extensive variability signals that the widespread intermittency of wave energy flux (and thus the impact of waves on nearshore processes) extends from single storms and seasons (Soomere and Eelsalu, 2014) to different years. At the same time, spatial differences in the stormy season wave energy flux at single locations are smaller than those for the average wave energy or wave energy flux. The Type F cumulative wave energy flux  $P_{tot}$  varies by about a factor of 2 at the sites in the study area.

This feature could be interpreted as a consequence of the (usually) fetch-limited nature of the wave fields in this water body. In such conditions, the most severe storms have a fixed fetch length for each wind direction and the wave periods mostly depend on the wind speed. A much smaller spatial variability in the cumulative wave energy flux may result from the very large contribution of a few of the strongest wave storms

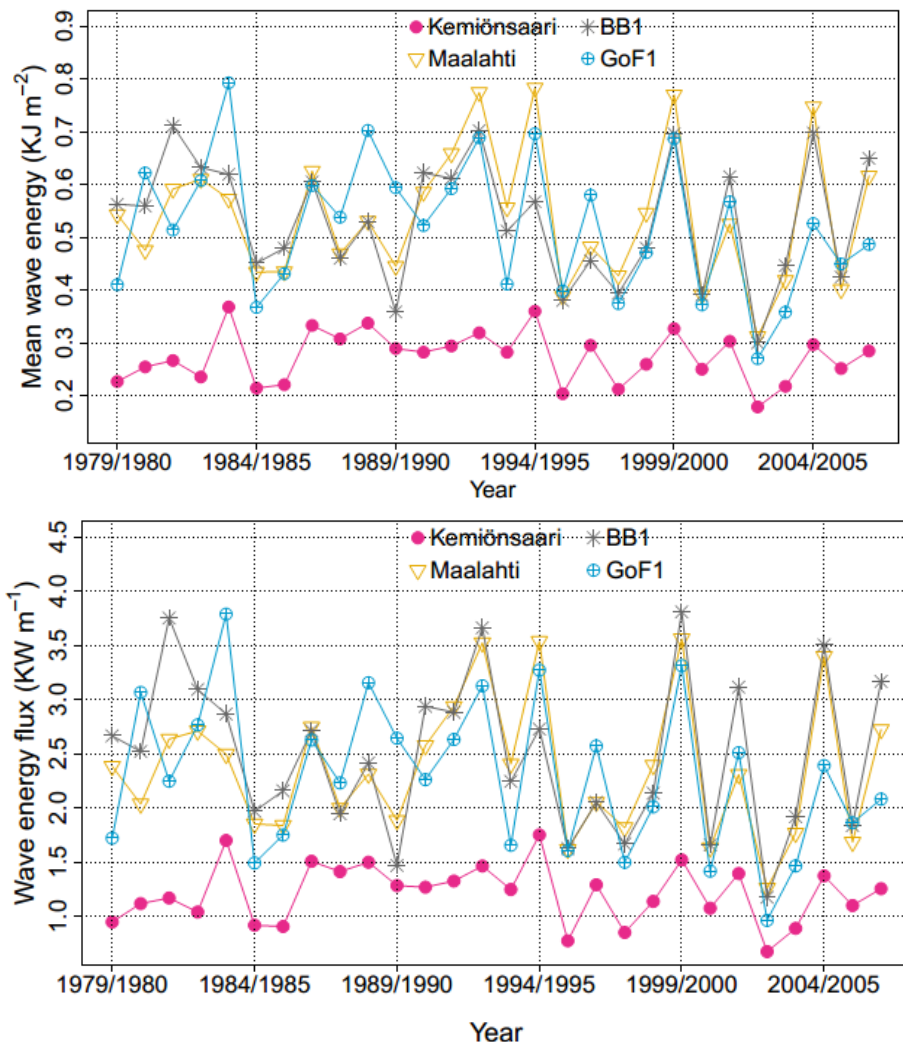


Figure 16. Mean ice-free wave energy (upper panel) and wave energy flux (lower panel, both Type F statistics) evaluated from the WAM model output during stormy seasons 1979/1980–2006/2007. From Paper II.

in the area into the total wave energy flux. Such storms usually cover large sea areas and thus impact simultaneously all locations in Fig. 12.

In Paper II the statistical properties derived from the described wave simulations were compared with similar properties evaluated using time series from instrumental wave measurements. This type of statistics is denoted as Type M in Tuomi et al., (2011). The duration of the ice season was the same as for the modelled wave data. The instrumental measurement season is often much shorter than the ice-free season because wave buoys are removed well before the ice season starts. The measurement period is typically from May to December in the northern Baltic proper, Gulf of Finland and Sea of Bothnia (Tuomi et al., 2019).

As a consequence, only a few sites and years were suitable for a comparison in Paper II. The most reliable data for this purpose comes from the Gulf of Finland. This site frequently has a long ice season and also has an overlap of 5 years (2001/2002–2006/2007) with our model and the OSI-450 data set. The ice season length varied from zero to 120 days (in 2002/2003) in these years. The Type F and Type M wave properties during the ice-free time largely varied during these years. The difference in the wave energy flux was in the range of 3% to 48%.

The difference of similar estimates for single stormy seasons at Almagrundet was 62% (1994/1995, ice season 22 days), 47% at Huvudskär (2002/2003, 12 days) and 34% at the FMI buoy (NBP1) location in the northern Baltic proper (2002/2003, 34 days). These differences match a similar estimate for the Bay of Bothnia (Björkqvist et al., 2018). Even though the presented estimates could be only characteristic of long ice seasons, the obtained match could be considered acceptable under many uncertainties.

### **3.4 Impact of the presence of ice on average wave properties**

The difference between average and cumulative wave properties evaluated for the ice-free season and for the entire stormy year characterises to some extent the impact of the presence of sea ice cover on wave properties. The wave properties in the hypothetical ice-free climate can be interpreted as a proxy of those that would happen in a much warmer climate. A shortcoming of this comparison is the implicit assumption that the future climates with less sea ice will have the same wind and wave climate that exists today. The relevant difference in modelled Type F and Type N wave statistics is analysed in Paper II from the viewpoint of the average SWH, average and cumulative wave energy, and average and cumulative wave energy flux. The qualitative patterns of variations between the Type F and Type N statistics are very similar for all these quantities.

The average SWH in the hypothetical ice-free conditions exceeds the similar value for the current climate at almost all selected locations (Fig. 17). Only at Pori, the total loss of ice would lead to very small decrease (by 0.25%) of the average SWH. The increase would be small (<1%) in the offshore locations in the Sea of Bothnia (SB1, SB2), at the margins of the Baltic proper (Kemiönsaari, Hanko) and in the western and central Gulf of Finland (Espoo, GoF1 and GoF2). As all these sites have relatively short ice seasons, it is likely that a substantial part of autumn and winter storms occur before the ice season starts. The complete loss of sea ice would lead to an increase by 2–4% in the average SWH at sites with a longer ice season, such as BB1, Kalajoki, Maalahti and Kotka. The largest increase in the mean SWH (7–11%) is likely to happen at BB2 and at Oulu in the Bay of Bothnia.

While changes in the annual (stormy year) average SWH are fairly small and generally less than the uncertainties in numerical reproductions of wave properties (estimated as the bias, Björkqvist et al., 2018), the loss of sea ice would lead to a much stronger increase in the average SWH in single stormy seasons (Fig. 17). This increase could be in the range of 23–28% at Oulu, Kalajoki and BB1.

The average single stormy season SWH may be smaller in the ice-free climate than in the current climate. This feature once more stresses the huge variability of the wind and wave climate in the Baltic Sea. Also, it once more confirms the perception that the potential impact of the loss of sea ice strongly depends on the (mis)match of the relatively windy season with the ice season. The rates of change in average values of wave energy flux in the stormy season (Fig. 17) are qualitatively similar than the changes in the average wave energy. The loss of sea ice almost does not change the average of these quantities at Pori and in the open part of the Sea of Bothnia (SB1, SB2). Small changes are characteristic to all sites with a relatively short ice season.

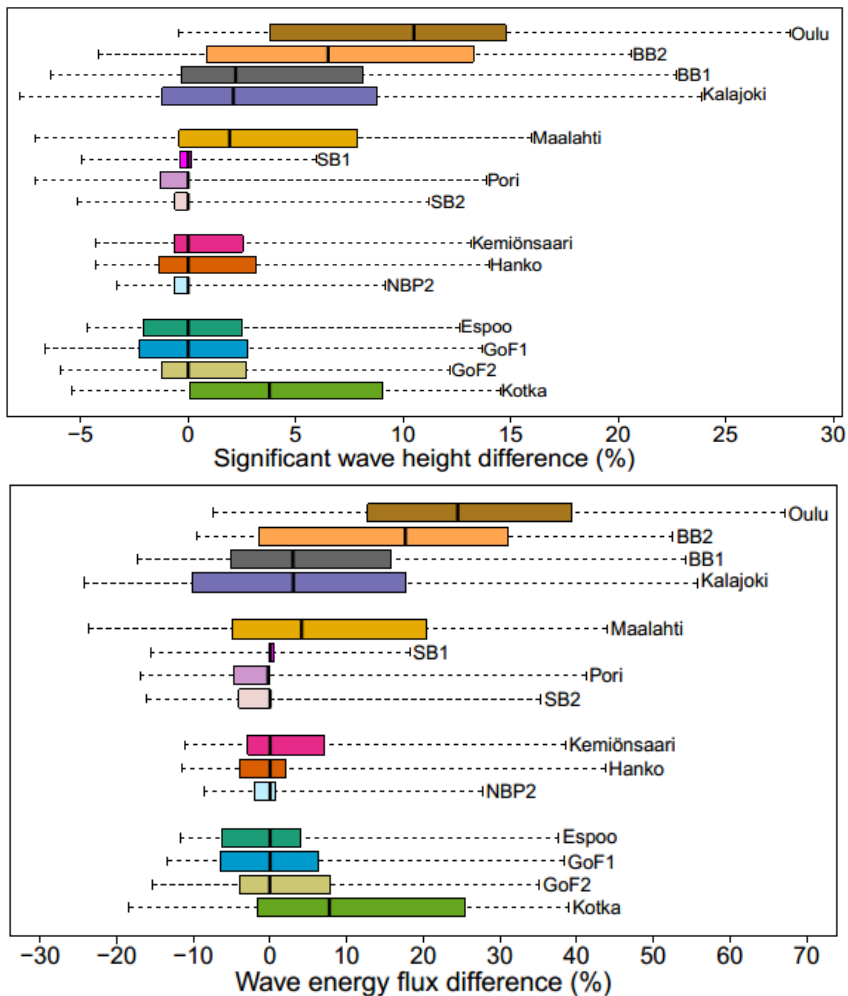


Figure 17. The difference of Type F and N estimates of average SWH (upper panel) and wave energy flux (lower panel) in single stormy seasons 1979/1980 to 2006/2007. From Paper II.

The magnitude of changes increases towards the northern and eastern end of the Baltic Sea and generally follows the ice season duration. The difference is largest in the coastal area of the Bay of Bothnia. For example, at Oulu, the mean wave energy in the ice-free climate would be 20% larger than it is now (Fig. 17). The rates of increase in the stormy season average wave energy flux differ from those for average wave energy by only a few percent (Paper II).

It can therefore be concluded that the Type F estimates of annual average wave height, wave energy and wave energy flux also adequately represent (within an accuracy of a few per cent) the hypothetical ice-free situation in the northern Baltic Sea as indicated also by Björkqvist et al. (2018). Only in the northernmost (Bay of Bothnia) and easternmost (Gulf of Finland) regions do Type F statistics considerably (by 20–30%) underestimate the annual wave energy and wave energy flux. This type of statistics does not overestimate any of the addressed properties. It is likely that the total loss of sea ice would lead to enhanced variability in wave energy and wave energy flux in single (stormy) years in areas that are seasonally ice-covered in the current climate.

### 3.5 The role of ice season duration

The cumulative properties of the wave climate, estimated in the manner described above as Type F statistics for single stormy years, can only increase when the ice season becomes shorter. Only in years with no ice can the Type F and Type N cumulative properties be equal. As the cumulative wave height is usually not used in applications, the analysis in Paper II focuses on cumulative wave energy flux. It is an important parameter in wave energy matters (Soomere and Eelsalu, 2014) and also characterises the impact of waves on beach sediments. It also provides an insight into changes in the cumulative wave energy. The difference in the properties of Type F and Type N statistics for cumulative wave energy flux  $P_{tot}$  is almost the same for cumulative wave energy  $E_{tot}$ . As discussed above, this feature may be interpreted as indicating weak dependence of wave energy flux on the variation of wave periods in strong storms.

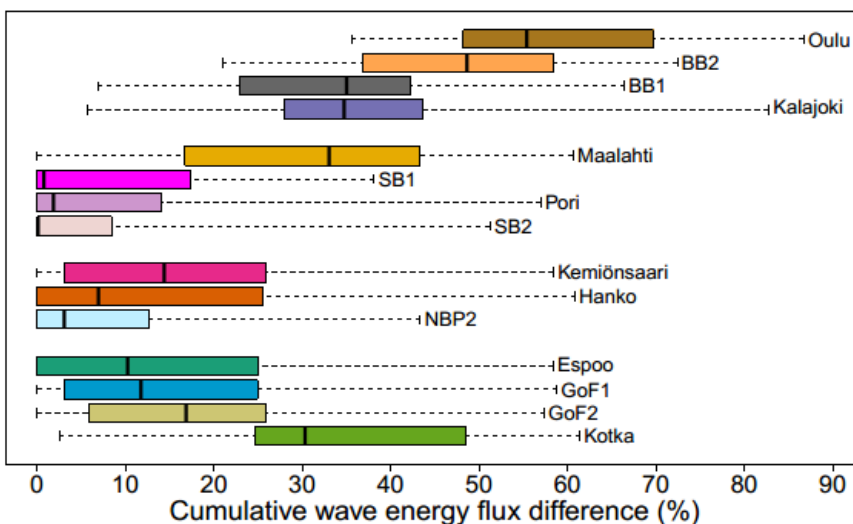


Figure 18. The difference of Type F and N estimates of cumulative wave energy flux in single stormy seasons 1979/1980 to 2006/2007. From Paper II.

The difference between the typical stormy season cumulative wave energy flux in the current (Type F) and hypothetical ice-free conditions (Type N) is largest (56%) at Oulu. Large differences (30–50%) are characteristic for other locations in the Bay of Bothnia (BB1, BB2 and Kalajoki), Maalahti in the northern part of the Sea of Bothnia and at Kotka in the eastern Gulf of Finland. These locations have the longest ice seasons. The difference is much larger, up to 87%, for single stormy seasons (Fig. 18). It is not clear why this difference is fairly small (below 15% on average) at several sites in the Sea of Bothnia (e.g., 8.5% at SB1) and the Gulf of Finland. A likely reason is the short ice season at these sites (only 24 days at SB2 whereas it is 162 days at Oulu).

The main conclusion from the presented material is that the hypothetical ice-free (Type F) statistics usually provide an acceptable estimate of average wave properties in the current (seasonally ice-covered) climate. A likely reason for this outcome is that the ice season often involves both relatively windy (autumn and early winter) months as well as much calmer spring months. However, the cumulative wave energy and wave energy flux would be much larger in ice-free climates. This dependence is generally robust: the longer the ice season, the larger the difference. The analysis hints that the loss of sea ice may increase the level of wave energy flux in the nearshore by 30–50% in the Bay of Bothnia and the eastern Gulf of Finland. This might be beneficial for wave energy converters but could also lead to erosion of sedimentary coasts.

The interrelations between the ice season duration and the mean SWH, wave energy and wave energy flux are more complicated. The average length of ice seasons varies from 24 (SB2) to 162 (Oulu) days. A longer ice season generally corresponds to a lower stormy season average SWH, wave energy and wave energy flux (Fig. 19). Therefore, interannual variations in the average wave properties are in counter-phase with the severity of the ice season duration.

The analysis in Paper II reveals that the stormy year average SWH at all addressed sites is systematically smaller for longer ice seasons (see Table 2 in Paper II). The relationships between the ice season duration and the average SWH, wave energy and wave energy flux for the ice-free season are statistically significant at a 99% level at Espoo, Hanko, Kemiönsaari, NBP2 and at three locations of the Gulf of Finland (GoF1, GoF2<sup>2</sup>, Kotka). All these sites are located in, or to the entrance of, the Gulf of Finland.

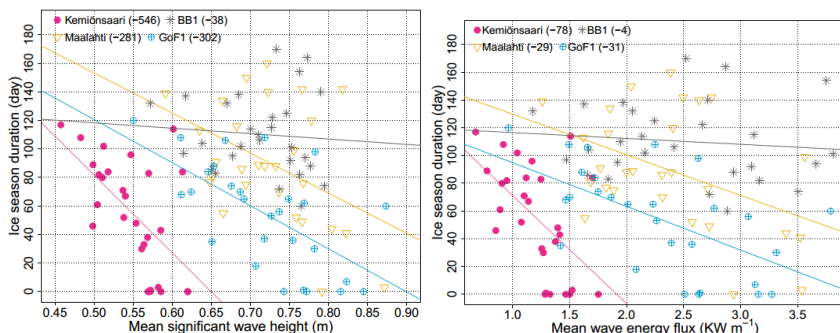


Figure 19. Scatter diagram of ice season duration and average SWH (left panel) and wave energy flux (right panel) during ice-free times of single stormy years at four locations of Fig. 12. The slopes of the relevant regression lines are presented in the legend. From Paper II.

<sup>2</sup> The text in Paper II does not mention NBP2 and GoF2. The relationship for wave energy flux is statistically significant at a 98% level at GoF2.

The relevant correlation coefficients range from 0.48 to 0.63 and are also almost the same for SWH, wave energy and wave energy flux (except at Oulu where the correlations for energy and energy flux are clearly stronger than for SWH). These correlations are weak at Maalahti (ice season about 90 days), Oulu, Pori, BB1 (~110 days) and Kalajoki.

The described feature, in essence, reiterates a similar conjecture based on modelled data at three locations in the eastern Baltic Sea (Zaitseva-Pärnaste and Soomere, 2013). A direct consequence is that the Type F statistics of average wave properties apparently will not remain adequate in an even slightly warmer future climate at the latitudes of the Gulf of Finland. An apparent reason for the identified negative correlation between the average wave properties and the duration of the ice season is that a relatively large part of the ice season overlaps with the windy season at these latitudes.

Another possible conjecture from the established negative correlation is that the regions with a relatively short ice season may be more sensitive with respect to shortening of the ice season than more northern locations. This feature is likely when changes to the start of the ice season are systematically within the relatively windy season. On such occasions, any later appearance of ice will lead to an increase in both the average and cumulative wave properties.

## **4 Directional effects in the nearshore**

The combination of the complex shape of the Baltic Sea and the specific bi-directional structure of moderate and strong winds in the northern Baltic proper (Soomere, 2003) give rise to several beneficial features for this water body and its beaches. For example, several beaches in bays that are deeply cut into the mainland can be geometrically sheltered against the usual strong wave directions (Caliskan and Valle-Levinson, 2008). This feature leads to the presence of so-called almost equilibrium beaches even when there are very limited sand resources on the northern shore of Estonia (Soomere and Healy, 2011).

Changes in ice conditions addressed in Chapter 3 apparently have negligible impact on such beaches unless some other properties of waves play a role. For example, the situation may change if strong winds blow from an unusual direction or changes in the fetch length owing to the loss of winter ice lead to the generation of waves with period or length different from usual. As a result, the refraction properties of waves propagating over extensive shallow areas with a gently sloping seabed may change considerably. In both situations the existing implicit protection of beaches or coastal engineering structures will be less effective.

More broadly, the consequences of these changes in wave refraction properties may greatly augment the effect of losing protective ice cover in certain locations. The evidence provided in Chapter 3 suggests that such amplification is likely to occur at the latitudes of the Gulf of Finland in the near future. The situation is apparently similar in the Gulf of Riga that is located slightly to the south of the Gulf of Finland and that has relatively long ice season. As the Gulf of Riga is largely sheltered against waves generated in the Baltic proper, wave properties in this water body evidently follow changes to the local ice conditions. To shed some light on potential effects of loss of sea ice on the local wave properties, Paper III and Chapter 4 explore challenges for coastal engineering in terms of a possible need to re-design a small harbor in the Gulf of Riga in a future ice-free climate.

### **4.1 Wave fields in the Gulf of Riga and near Ruhnu**

The bi-directional and strongly anisotropic pattern of moderate and strong winds that usually blow from the south-west or north-north-west in the north-eastern Baltic Sea (Soomere, 2003) has substantially affected the planning and construction of ports in this part of the sea. In essence, port constructions must protect vessels against waves (Cairns et al., 2016). This condition has been met for millennia through careful choice of port location (Safadi, 2016). As the eastern shore of the Baltic Sea from the Sambian Peninsula to Cape Kolka has almost no naturally protected harbours (except for the Klaipėda Strait and Curonian Lagoon), large ports in this area such as Liepaja or Ventspils are sheltered against severe waves by massive breakwaters. The location of their entrances is chosen so that the most dangerous waves do not directly impact the quays. This geometric protection may become less effective if the wave approach direction changes in the future.

The situation with harbour locations is more favourable in the West Estonian Archipelago. Several bays provide naturally sheltered port locations against the strongly anisotropic wave climate at the northern, eastern and southern shores of these islands. Several ports (e.g., Heltermaa on the island of Hiiumaa) are left fully open to the east.

A core assumption for such a choice is that easterly and especially south-easterly winds are infrequent and weak in this part of the Baltic Sea (Soomere, 2003).

Geometric protection against waves from some directions (Caliskan and Valle-Levinson, 2008) is usually effective in situations when the sea deepens rapidly and depth-induced refraction is weak. However, the northern Baltic Sea has many underwater features and shoals that may render such protection insufficient. It is a common feature of the eastern Baltic Sea that wave refraction leads to relatively large levels of wave energy in seemingly well-sheltered areas (Kovaleva et al., 2017). The analysis of locations of the large harbour at Saaremaa (Soomere, 2001) revealed that the wave regime at one of the potential locations was much more severe than expected from geometrical considerations because of wave focusing owing to refraction. This process may redirect wave propagation direction in shallow water by more than 90°. Such ultra-refraction has been reported for south-west swells propagating towards San Francisco Bay (Hanes et al., 2013).

The downwind sides of small islands and shoals are particularly sensitive with respect to refraction of long storm waves. There are many examples reporting the entrance of refracted waves into seemingly sheltered bays or creating a crossing wave system. One location that is possibly affected by this mechanism is the Port of Ringsu at the south-eastern tip of the island of Ruhnu (Fig. 20) in the middle of the Gulf of Riga.

Similar to the interrelations of the Baltic Sea and North Sea in terms of wave properties, wave fields in the Gulf of Riga are weakly connected to those in the rest of the Baltic Sea. Only very limited amounts of wave energy excited in the Baltic proper propagate into the Gulf of Riga via the Irbe Strait. These waves propagate mostly to the north-east and thus almost do not affect the wave regime in the vicinity of Ruhnu. The other connection of the gulf to the rest of the Baltic Sea, the Suur Strait via Moonsund, is narrow and shallow. Waves excited by northerly winds in Moonsund also contribute insignificantly to wave energy around Ruhnu. Consequently, wave fields in

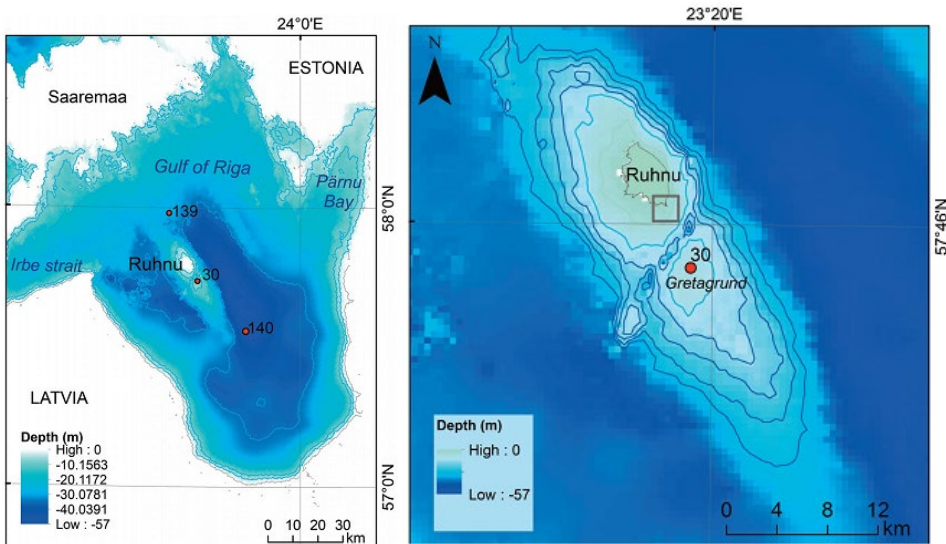


Figure 20. The Gulf of Riga in the Baltic Sea (left panel) and the island of Ruhnu (right panel). The right panel shows the second-level computational grid of the wave model and the grid points 30, 139, 140 selected for the analysis in Paper III. The right panel illustrates the nested grids of the third-level (entire panel) and fourth-level (small box at Ruhnu). Point 30 is located at Gretagrund, a shallow area to the south of Ruhnu. Modified from Paper III.

most of the gulf and specifically near Ruhnu are mostly locally generated and thus usually follow the local wind pattern.

The island of Ruhnu is open to all strong winds in the gulf. The pattern of such winds is apparently the same as in the northern Baltic proper (Soomere and Keevallik, 2001; Soomere, 2003), with strong winds from the south-west or north-north-west (Männikus et al., 2019). As is typical for the entire northern Baltic proper (except for the latitudes of the Gulf of Finland, Soomere and Keevallik, 2003), easterly winds are generally weaker and south-easterly winds are particularly infrequent (Männikus et al., 2019). On top of that, the western nearshore of Ruhnu is shallow and rocky, and apparently frequently impacted by ridge ice under strong westerly winds. The eastern shore is steeper, less rocky and partially sandy. It is therefore natural that historical landing places are mostly located at the eastern shore of the island even though the dwellings and fields are on its western part (Fig. 21). As described in Paper III, much relevant historical knowledge was lost after the Second World War when most of the local population fled to Sweden.

The contemporary Port of Ringsu (Fig. 21) was constructed at the south-eastern tip of Ruhnu in the 1950s (Orviku, 2018). This location to the east of Cape Ringsu had been used for lifting ships out of water and for loading operations using small boats (Orviku, 2018), but not as a harbour site. This choice was also made to ensure geometric shelter against waves excited by the local pattern of predominant strong winds described above. The breakwaters are designed to better protect the port waters and the entrance channel against waves that approach from the south-west, north, north-east and east. The entrance is open to the south-east. This is the direction from which winds are most infrequent and weak.

The port interior frequently, however, suffers from troublesomely high waves and rapid changes in the water level. Such phenomena also repeatedly occur during westerly winds even though the entire harbour area seems to be geometrically protected against waves excited by such winds. A possible reason for such phenomena is wave refraction along the underwater slopes of Ruhnu and neighbouring shallow

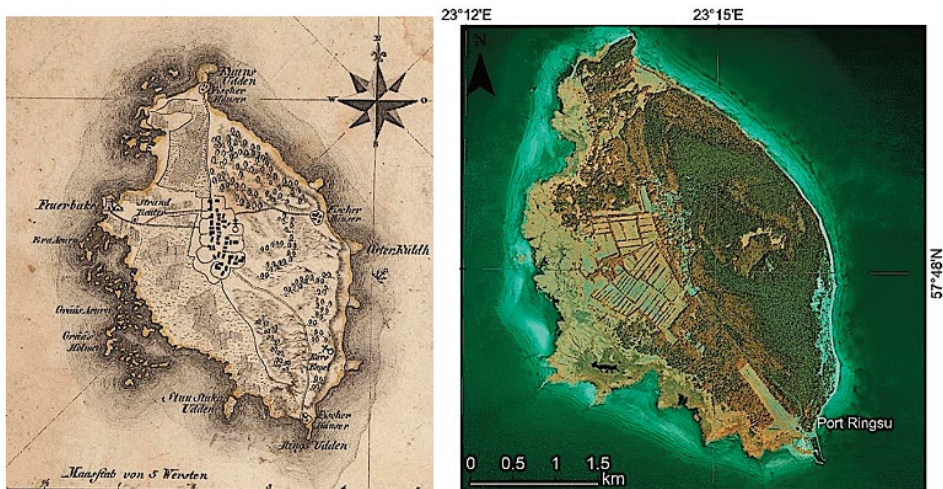


Figure 21. A map of Ruhnu 1798 (left panel) indicates also locations of the fishermen's houses (Fischer Häuser). One such house near Cape Ringsu (Rings-Udden) was located on the western shore of the cape, which is open to one of the predominant wind directions. The contemporary Port of Ringsu is located at the south-eastern tip of the island (right panel). From Paper III.

Gretagrund. To test this hypothesis, Paper III presents results of multi-nested wave model runs forced by a selection of moderate and strong wind conditions in the entire Gulf of Riga.

## 4.2 Simulation of local wave patterns

The properties of waves near the entrance to the Port of Ringsu are evaluated in Paper III using another contemporary wave model SWAN (Booij et al., 1999), version 40.11. This model provides a more realistic representation of wave-wave and wave-bottom interactions in the very shallow water environments of the eastern Baltic Sea (Alari and Raudsepp, 2010). The properties of waves are described in this third-generation phase-averaged spectral wave model by means of the two-dimensional wave action density spectrum  $N$ . This four-argument function is also the core of the WAM model used in Chapter 3 and presents information about how wave energy is distributed between components with different periods and propagating in different directions at every point of the sea. As there was no reliable information available about currents in the Gulf of Riga, the potential impact of currents was ignored. In this case the underlying wave action balance equation has the following form in Cartesian coordinates (Komen et al., 1994):

$$\frac{\partial N}{\partial t} + \frac{\partial c_x N}{\partial x} + \frac{\partial c_y N}{\partial y} + \frac{\partial c_\sigma N}{\partial \sigma} + \frac{\partial c_\theta N}{\partial \theta} = \frac{S_{tot}}{\sigma}. \quad (5)$$

The partial derivatives with respect to spatial coordinates  $x$  and  $y$  express the propagation of the energy of different wave components along the sea surface. This happens with group velocity and  $c_x$  and  $c_y$  are its  $x$ - and  $y$ -components. Alterations to the wave length and propagation direction owing to variations in water depth are described in terms of similar “propagation velocities” in the spectral spaces  $c_\sigma$  and  $c_\theta$ . These quantities describe how the angular frequency  $\sigma$  ( $\omega$  in Chapter 3) and the propagation direction  $\theta$  vary over the sea.

While the left-hand side of Eq. (5) is the same for WAM and SWAN, the core differences between these models are in the specification of its right-hand side. The term  $S_{tot}$  denotes the impact of the combination of all physical processes that affect wave generation, dissipation or redistribution in the particular model. These involve input by wind, the dissipation of waves by whitecapping, through bottom friction (Hasselmann et al., 1973), due to depth-induced wave breaking (Battjes and Janssen, 1978), and nonlinear transfer of wave energy.

While the WAM model only takes into account four-wave interactions (Komen et al., 1994) and is generally oriented to large-scale deep-water applications, the SWAN model also handles three-wave interactions (Eldeberky, 1996) in shallow areas and provides a larger variety of different options in shallow water environments. Paper III uses the following suite of settings: the whitecapping coefficient  $\delta$  was set to  $\delta = 1$  (Rogers et al., 2003; Pallares et al., 2014), the wind drag parameterisation as suggested by Wu (2012), the bottom friction coefficient was set to  $0.038 \text{ m}^2/\text{s}^3$  (Zijlema et al., 2012), and the parameters  $\alpha = 1$  and  $\gamma = 0.73$  for the depth-induced wave breaking source term. A similar configuration of the SWAN model has led to very small bias and root mean square difference between measured and simulated time series of wave parameters in the Baltic Sea (Björkqvist et al., 2018).

To reliably identify the wave properties near the Port of Ringsu, a four-level hierarchy of regular rectangular model grids was constructed. In order to account for

the possible propagation of waves generated in the Baltic proper into the Gulf of Riga, a coarse model was set up for the whole Baltic Sea with a step of 5000 m (251 × 271 grid points). The Gulf of Riga was covered with a step of 1000 m (171 × 181 grid points). The domains of these models are provided in Fig. 1 and Fig. 20. The model in the vicinity of Ruhnu had a step of 100 m and 211 × 171 grid points (Fig. 20). The finest model grid for the Port of Ringsu had a varying step from 11 m down to 3 m and 232 × 194 grid points. As usual, the properties of waves at the border of any inner model were taken from those evaluated using the relevant outer model. At each sea grid point, the energy of 864 spectrum components (36 directions and 24 frequency bins from 0.05 Hz to 1 Hz) was calculated. The bathymetry data for the outer grids was retrieved from the Baltic Sea Bathymetry Database (Baltic Sea Hydrographic Commission, 2013) and from the database of the Estonian Transport Administration for the inner grids. The resolution of the two innermost models allows replication of the changes in wave parameters near Ruhnu and at the entrance of the Port of Ringsu in detail.

The fetch length and propagation distance of waves that are excited in the Gulf of Riga and reach Ruhnu are in the range of 40–100 km (Fig. 20). The longest fetch (up to 100 km) corresponds to south-east storms and the shortest to south-west storms. Consequently, the wave fields become rapidly saturated near Ruhnu and almost do not evolve further after some time. The saturation time of wave fields in the Gulf of Riga is usually within 2–3 hours for wind speed 5 m/s, 3–5 hours for 10 m/s, and within 6 hours for a wind speed of 15 m/s. These time durations are even shorter for most wind conditions near Ruhnu. Consequently, an analysis of saturated wave fields near Ruhnu provides an adequate overview of potentially dangerous situations.

For these reasons this four-level version of the SWAN model was employed in Paper III as part of Delft3D suite to evaluate the properties of saturated wave fields. The model was forced with stationary (unidirectional steady) wind at speeds of 5, 10 and 15 m/s for the entire area covered by the grid and was run until the wave field became saturated. The wind direction was varied from 15° to 345° with a step of 30°. The outcome of these 36 runs allows the analysis of worst-case scenarios for a given wind speed and direction as changes to wind speed or direction usually lead to a decrease or a slower increase in the wave height.

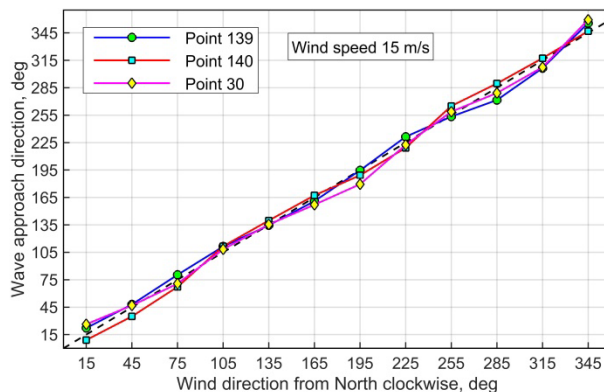


Figure 22. Comparison of the wind direction and the mean propagation direction of simulated waves in saturated wave fields for wind speeds of 15 m/s in the open part of the Gulf of Riga to the north (point 139, Fig. 20) and south (point 140, Fig. 20) of Ruhnu, and at the tip of Gretagrund (point 30, Fig. 20) to the south of Ruhnu. From Paper III. See reference on the next page.

### 4.3 Refraction-driven redirection of storm waves near Ruhnu

The modelled mean direction of saturated wave fields from the second-level computational grid (Fig. 20, left panel) closely follows the wind direction in the open part of the Gulf of Riga (points 139 and 140 in Fig. 20, left panel) and at the top of Gretagrund (point 30 in Fig. 20, right panel) for relatively low wind speed of 5 m/s (Paper III).

The mean modelled wave direction deviates from the wind direction up to 15° for some stronger (15 m/s) wind speeds (Fig. 22). This outcome from the second-level computational grid confirms the usual perception that wave fields in the open part of the Gulf of Riga mostly follow wind properties and that refraction plays a negligible role in their development. However, the results of the third level of computation with finer grid size reveal the wave refraction at the location of point 30 (Fig. 23B). This suggests that at local scales a finer spatial resolution can increase the level of accuracy for wave simulations greatly. The SWH at the three referred locations (points 139, 140, and 30) vary from 1.88 m to 2.73 m for a wind speed of 15 m/s. This variation apparently

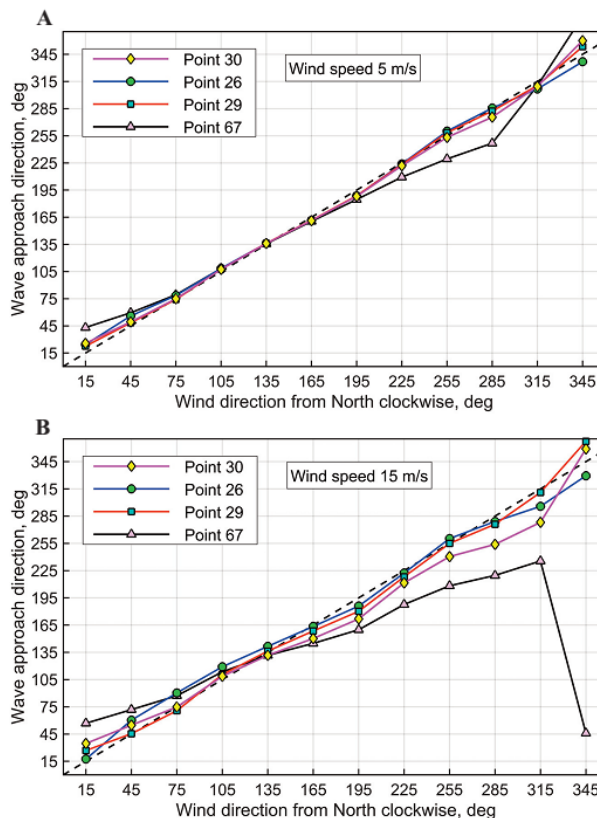


Figure 23. Comparison of the wind direction and the mean direction of simulated wave propagation in saturated wave fields for wind speeds of 5 m/s (A) and 15 m/s (B) on the northern slope of Gretagrund (point 30, water depth 7.7 m), in the shallow area to the west of the grid (point 26, water depth 13 m), in the deep channel (point 29, water depth 21 m), and in the fairway to the Port of Ringsu (point 67). The wave direction in panel (A) for wind from the direction of 345° is not distinguishable from the horizontal axis. The locations of grid points are indicated in Fig. 25. From Paper III.

follows the different fetch length for different wind directions. The mean period of saturated waves is in the range 4.0 to 5.1 s at these locations. This feature signals that the intensity of refraction of waves created by storms of this strength mostly depends on the angle between bottom isolines and wave vector rather than on wave period.

The difference between the wind and wave directions is larger, up to 20°, for some wind directions at locations near the top of Gretgrund and on the northern slope of the deep channel between Ruhnu and Gretgrund. The wave direction at these locations mostly follows the wind that blows from the south or east (Fig. 23). This difference becomes more significant closer to the Port of Ringsu. This is exemplified in Paper III by the example of point 67 at a distance of 0.5 km from the port entrance. The wave direction deviates by more than 30° from the wind direction even for weak (5 m/s) winds that blow from the west to the north. This deviation reaches 90° for strong (15 m/s) north-westerly and northerly winds.

The situation is different in the immediate vicinity of the Port of Ringsu (Fig. 24). Only waves driven by south-easterly winds (135°) that blow directly towards the port arrive at the port area aligned with the wind for any wind speed (Fig. 24 A, B). The wave direction largely follows the direction of weak (5 m/s) easterly, southerly and westerly

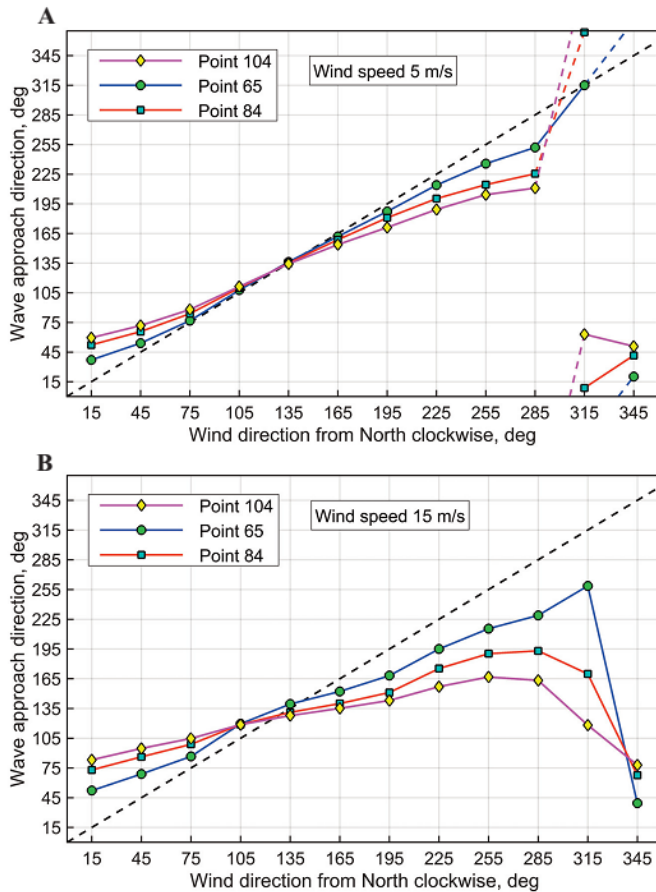


Figure 24. Comparison of the wind direction and the mean direction of simulated wave propagation for wind speeds of 5 m/s (A) and 15 m/s (B) in saturated wave fields to the south-east of Ruhnu (point 65), on the fairway to the Port of Ringsu (point 84), and at the entrance to the Port of Ringsu (point 104). The locations of grid points are indicated in Fig. 25. From Paper III.

winds. The mismatch of wave propagation and wind directions is larger for stronger winds. This is evidently because stronger winds excite longer waves and these experience more intense refraction. The deviation is about 30° at a distance 0.5 km (point 65) from the port for strong winds (15 m/s) from the east, south and west, and increases to 60°–90° for north-westerly and northerly winds (Fig. 24).

As demonstrated in Fig. 25, the reason for such deviations is the impact of refraction of approaching waves along their propagation. Part of their journey is almost parallel to the coastal area of Ruhnu. The impact of refraction is proportional to the phase speed of waves and is thus stronger for longer waves. Consequently, waves produced by stronger winds generally have a larger deviation from the original approach direction.

Underwater features around Ruhnu redirect waves excited by strong winds (15 m/s) in an interesting manner. The mean direction of waves that finally reach the port entrance is in the range of 80–190° for all wind directions (Fig. 24). Therefore, saturated waves generated by all strong (15 m/s) winds experience refraction so that they finally head directly into the port entrance. Therefore, refraction of wind waves that are generated in the open part of the Gulf of Riga and propagate along coastal slope of the island of Ruhnu systematically redirects storm waves directly into the entrance of the Port of Ringsu during virtually any strong wind event in the hypothetical ice-free climate. Consequently, further loss of sea ice may considerably increase the danger to the Port of Ringsu and its vicinity posed by storm waves.

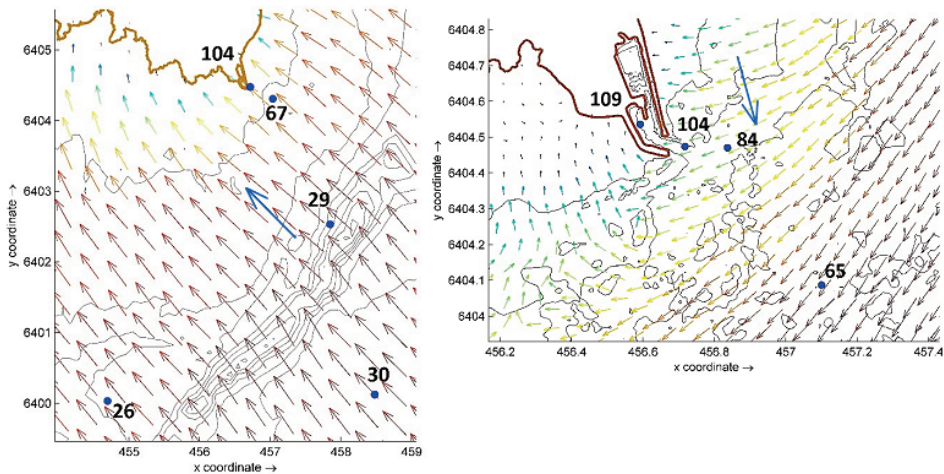


Figure 25. The wave model grid points for data used in Figs 23 and 24. Left panel: third-level grid, wind from the direction of 135°. Right panel: innermost fourth-level grid, wind from the direction of 345°. The wave pattern is presented for a wind speed of 15 m/s. The blue large arrows indicate the wind direction. The wave height is represented by colour (brown: the highest, yellow: medium, green and blue: lower waves) and the length of small arrows while the wave direction is indicated by the direction of small arrows. The scale is presented in kilometres. From Paper III.

## Conclusions

### Summary of the results

The presented studies address, for the first time, the possibility of retrieving new information about the wave climate of the Baltic Sea (almost importantly, significant wave height) and spatial patterns of its changes using estimates of wave heights based on satellite altimetry and the technique of Empirical Orthogonal Functions (EOF). This analysis includes extensive examination of the choice of the optimum set of parameters for analysis and the performance of this technique on noisy data sets. It also applies to situations when wave height estimates contain a considerable level of uncertainty. In this context, the ability of the EOF technique to resolve small-scale patterns, and the dependence of the variability retrieved by different modes of the EOF technique on the amount of noise in the data set are analysed.

The EOF technique is able to resolve patterns with a size of  $1.5^{\circ} \times 1.5^{\circ}$  for very low level of noise (5%). The performance of the technique decreases almost linearly with the increase in the level of noise. For the 20% noise level the smallest reliably detectable pattern is  $3^{\circ} \times 3^{\circ}$ .

The major established pattern of changes to the wave fields reveals a clear increase in wave heights in the western regions of the Baltic proper and almost no changes in the eastern part of the sea.

Further analysis made it possible to link some of the established patterns of changes to the major teleconnection patterns that characterise meteorological forcing in the Baltic Sea area. The detected linear trend in the wave height of the Baltic Sea displayed the strongest negative and statistically significant correlation (the relevant correlation coefficient  $-0.47 \pm 0.19$ ) with the SCAND climatic index, and somewhat less pronounced positive correlations with the North Atlantic Oscillation (NAO) index ( $0.31 \pm 0.22$ ) and the Atlantic Oscillation (AO) index ( $0.42 \pm 0.20$ ). The predominant wind is from the west during the positive phase of NAO and AO and from north-west during the negative phase of SCAND. No strong links were identified for other teleconnection patterns in the region.

This set of correlations indicates that the variations and trends in the Baltic Sea wave climate can be largely explained by the impact of atmospheric conditions that are expressed by these indices. The east-west asymmetry of changes to wave heights apparently stems from the interplay of north-westerly (characteristic to negative values of the SCAND index) and westerly (induced during periods with positive values of the NAO and AO indices) winds over the region.

An application of the running (sliding) correlation analysis revealed that the strength of the correlation of the Baltic Sea wave climate with the SCAND, NAO, and AO indices varies dramatically in time. Strong correlation of the first winter EOF with the three dominant climatic indices occurs in individual decades for different indices. The phenomena behind the SCAND pattern had a strong correlation (and apparently also influence) with the first winter EOF in 2000–2009. The similar correlation with the NAO and AO indices was weak during this decade. This correlation with the SCAND index significantly decreased afterwards whereas a strong correlation was observed with the NAO index. It is therefore likely that the Baltic Sea wave climate is driven jointly and alternately by several combinations of large-scale atmospheric processes whereas the link to each of these large systems may vary radically on a decadal scale.

The analysis of the interplay of ice conditions and wave properties replicates the well-known extensive variation in both mean and cumulative wave properties in space and time. Even though the duration of the ice season is several months, the usual statistical properties of wave fields, such as the annual average wave height evaluated for the idealised completely ice-free climate almost coincide with similar properties evaluated for the ice-free season at several locations. The difference in the two estimates is less than 1% at half of the studied locations. The mismatch is about 2–4% in the northern Sea of Bothnia and in the eastern Gulf of Finland. It is somewhat large for quadratic properties, up to 20–25% for energy and energy flux in the northernmost part of the study area.

The lack of correlation between the classic statistical properties of wave fields and the duration of the ice season apparently signals that the ice season overlaps with part of the relatively windy season and part of the relatively calm spring season. Variations in the length of the ice season generally have a smaller impact on the “classic” (Type F) statistical properties of the wave climate than the location of a particular site offshore or in a sheltered nearshore region.

The presented analysis in Paper II suggests that changes in ice conditions may lead to distinct reactions of wave properties in different regions. There is almost no correlation between the mean wave properties and the ice season duration in the Sea of Bothnia and the Bay of Bothnia. It is likely that the loss of sea ice will lead to limited changes to the mean wave properties in the near future in these regions. A statistically significant correlation (at a >99% level) of these quantities is evident at the latitudes of the Gulf of Finland. Therefore, the loss of sea ice is associated with an increase in the average wave height, energy and energy flux in this region.

The cumulative wave properties, such as energy and energy flux, grow rapidly when the ice season becomes shorter. The full loss of sea ice may lead to an increase by 30–50% in the wave energy and energy flux in the northern locations of the study area. Therefore, it is very likely that a warmer climate means much higher hydrodynamic loads in the nearshore of the north-eastern Baltic Sea. The rate of this increase follows the current length of the ice season.

The gradual decrease in ice season duration will eventually lead to a longer fetch length for wind waves and therefore to the generation of longer waves with different refraction properties. These variations to the wave fields may lead to considerable changes in the wave climate at sheltered shores and ports.

As an example showing the consequences of these variations, storm wave properties at the Port of Ringsu located on the south-east of the island of Ruhnu in the Gulf of Riga are investigated in the idealised no-ice climate. Underwater slopes of the island of Ruhnu and a nearby shallow (Gretagrund) may systematically redirect wind waves. The saturated wave fields for wind speeds of 15 m/s from any direction reach the geometrically sheltered Port of Ruhnu from a narrow range of directions between south and east, that is, from the direction from where storm winds are infrequent and weak.

## **Main conclusions proposed to defend**

1. The Empirical Orthogonal Function (EOF) technique reliably identifies spatial patterns with a size from  $1.5^{\circ} \times 1.5^{\circ}$  from the data set of significant wave heights produced by satellite altimetry in the Baltic Sea in ideal conditions of almost no noise.
2. The minimum size of the retrieved pattern increases and the level of explained temporal variability decreases almost linearly with the increase in the level of noise.
3. The pattern of the first EOF in winter matches the spatial distribution of the linear trend of significant wave height in the Baltic Sea. This mode of EOF has a strong negative correlation with the SCAND index in 2000–2009, and strong positive correlation with the North Atlantic Oscillation (NAO) and Arctic Oscillation (AO) climatic indices after this period. This behaviour is characteristic of regime shifts.
4. The link between these climatic indices with the wave climate of the Baltic Sea, evaluated in terms of the correlation of the first winter EOF mode and the relevant index, exhibits substantial decadal variation. When the link with the SCAND index is strong, the similar links with the NAO and AO indices are weak, and vice versa.
5. The main statistical properties of wave climate in the northern Baltic Sea, such as the annual average wave height, estimated from idealised ice-free simulations represent similar properties for the seasonally ice-covered sea.
6. The length of the ice season is negatively correlated with the average wave height, energy and energy flux. This correlation is strongest at the latitudes of the Gulf of Finland where the gradual loss of sea ice has led to rapid changes in the average wave properties.
7. The total loss of sea ice would lead to an increase in the average wave energy and its flux by maximally 20–25%. The annual cumulative wave energy and wave energy flux will greatly increase, on average more than 50% and up to 87% in single years in the Sea of Bothnia and Bay of Bothnia.
8. Refraction redirects storm waves near the island of Ruhnu in the Gulf of Riga up to  $180^{\circ}$ . As a result, for wind speeds of 15 m/s and all wind directions the saturated waves propagate almost directly into the entrance of the Port of Ringsu. This port is geometrically sheltered against the predominant wind directions and is open towards the south-east, from where winds are weak and infrequent.

## Recommendations for further work

While Chapters 1 and 2 provide important information about changes to wave properties in the Baltic Sea over a quarter of century, the time series used to extract this information are relatively short compared to the history of visual wave observations, instrumental measurements and modelling efforts. Further research should make clear whether the established patterns express systematic changes to the wave properties or reflect certain cyclic or decadal-scale variations.

The correlation between the wave properties and the major teleconnection indices should be considered for a longer time period. It would also be important to estimate whether the missing low wave heights in the satellite altimetry data play some role in the retrieved patterns or in the level of explained variability.

The role of sea ice on wave loads has only been established using a relatively crude approximation with no waves during the formal ice season. The resulting estimates can evidently be made much more accurate using wave models that incorporate ice information. Such estimates are particularly important for sedimentary segments of the Baltic Sea shore. The most sensitive areas in this respect currently seem to be those at the latitudes of the Gulf of Finland and, in particular, in the interior of this gulf. It is likely that ice is formed in the middle of the windy season at these locations in the current climate. Better estimates of the ice formation time would lead to better estimates of the cumulative wave energy that reaches such sedimentary segments. An additional threat is that the warmer climate with less sea ice will be more prone to the formation of storm surges. Estimates of the joint impact of waves and elevated water levels are a major challenge in this field.

The projected storm situations in the ice-free climate at the Port of Ringsu on Ruhnu raise several concerns and indicate a clear need for both theoretical studies and engineering solutions. As refraction becomes stronger for even longer waves, it is likely that very strong storms from virtually any direction will bring high waves directly into the harbour entrance, exactly from the direction from where winds are the weakest and least frequent.

Groeneweg et al. (2015) noted that the SWAN model sometimes underpredicts the energy of waves that propagate into shallow areas (like the vicinity of the Port of Ruhnu) after crossing deeper channels (such as the area between Ruhnu and Gretagrund). This feature basically reflects the classic effect of concentration of wave energy on the channel slopes (Li et al., 2000). This feature signals that the amount of wave energy reaching the Port of Ruhnu in southwestern storms might be even larger than predicted by the SWAN model. To understand what actually happens there, *in situ* measurements of wave properties in strong storms are definitely necessary.

From the engineering viewpoint, the entrance to the Port of Ringsu may need reshaping to ensure safety in the port. An extension of the existing breakwaters might be not sufficient as high waves systematically approach almost exactly along the fairway to the harbour. An artificial island or breakwater to the south-east of the port entrance is probably necessary. It could be a stationary (Cox and Czapinski, 2016) or a floating structure (Davis et al., 2013).

## References

- Alari V., Raudsepp U. 2010. Depth induced breaking of wind generated surface gravity waves in Estonian coastal waters. *Boreal Environment Research*, 15 (3), 295–300.
- Andersson H.C. 2002. Influence of long-term regional and large-scale atmospheric calculation on the Baltic sea level. *Tellus A: Dynamic Meteorology and Oceanography*, 54(1), 76–88, doi: 10.3402/tellusa.v54i1.12125.
- Ashton A., Murrey A.B., Arnault O. 2001. Formation of coastline features by large-scale instabilities induced by high-angle waves. *Nature*, 414, 296–300, doi: 10.1038/35104541.
- Baltic Sea Hydrographic Commission 2013. Baltic sea Bathymetry Database Version 0.9.3. <http://data.bshc.pro/>. Downloaded on 01.04.2021.
- Barbariol F., Bidlot J.R., Cavaleri L., Sclavo M., Thomson J., Benetazzo A. 2019. Maximum wave heights from global model reanalysis. *Progress in Oceanography*, 175, 139–160, doi: 10.1016/j.pocean.2019.03.009.
- Barnhart K.R., Overeem I., Anderson R.S. 2014. The effect of changing sea ice on the physical vulnerability of Arctic coasts. *Cryosphere*, 8(5), 1777–1799, doi: 10.5194/tc-8-1777-2014.
- Barnston A.G., Livezey R.E. 1987. Classification, seasonality and persistence of low-frequency atmospheric circulation patterns. *Monthly Weather Review*, 115(6), 1083–1126, doi: 10.1175/1520-0493(1987)115<1083:CSAPOL>2.0.CO;2.
- Battjes J.A., Janssen J.P.F.M. 1978. Energy loss and set-up due to breaking of random waves. *Coastal Engineering Proceedings*, 1(16), 32, doi: 10.9753/icce.v16.32.
- Bednorz E., Czernecki B., Tomczyk A.M., Pótrolniczak M. 2018. If not NAO then what?— regional circulation patterns governing summer air temperatures in Poland. *Theoretical and Applied Climatology*, 136(3), 1325–1337, doi: 10.1007/s00704-018-2562-x.
- Bednorz E., Pótrolniczak M., Czernecki B., Tomczyk A.M. 2019. Atmospheric forcing of coastal upwelling in the southern Baltic Sea basin. *Atmosphere*, 10(6), 327, doi: 10.3390/atmos10060327.
- Bertin X., Prouteau E., Letetrel C. 2013. A significant increase in wave height in the North Atlantic Ocean over the 20th century. *Global and Planetary Change*, 106, 77–83, doi: 10.1016/j.gloplacha.2013.03.009.
- Booij N., Ris R.C., Holthuijsen L.H. 1999. A third-generation wave model for coastal regions: 1. Model description and validation. *Journal of Geophysical Research-Oceans*, 104(C4), 7649–7666, doi: 10.1029/98JC02622.
- Björkqvist J.V., Tuomi L., Tollman N., Kangas A., Pettersson H., Marjamaa R., Jokinen H., Fortelius C. 2017. Brief communication: Characteristic properties of extreme wave events observed in the northern Baltic Proper, Baltic Sea. *Natural Hazards and Earth System Sciences*, 17(9), 1653–1658, doi: 10.5194/nhess-17-1653-2017.
- Björkqvist J.V., Lukas I., Alari V., van Vledder G.P., Hulst S., Pettersson H., Behrens A., Männik A. 2018. Comparing a 41-year model hindcast with decades of wave measurements from the Baltic Sea. *Ocean Engineering*, 152, 57–71, doi: 10.1016/j.oceaneng.2018.01.048.
- Björkqvist J.V., Rikka S., Alari V., Männik A., Tuomi L., Pettersson H. 2020. Wave height return periods from combined measurement-model data: a Baltic Sea case study. *Natural Hazards and Earth System Sciences*, 20(12), 3593–3609, doi: 10.5194/nhess-20-3593-2020.

- Björkqvist J.V., Pärt S., Alari V., Rikka S., Lindgren E., Tuomi L. 2021. Swell hindcast statistics for the Baltic Sea. *Ocean Science*, 17(6), 1815–1829, doi: 10.5194/os-17-1815-2021.
- Brenner A.C., Blndschadler R.A., Thomas R.H., Zwally H.J. 1983. Slope-induced errors in radar altimetry over continental ice sheets. *Journal of Geophysical Research-Oceans*, 88(C3), 1617–1623, doi: 10.1029/JC088iC03p01617.
- Broman B., Hammarklint T., Rannat K., Soomere T., Valdmann A. 2006. Trends and extremes of wave fields in the north-eastern part of the Baltic Proper. *Oceanologia*, 48(S), 165–184.
- Bueh C., Nakamura H. 2007. Scandinavian pattern and its climatic impact. *Quarterly Journal of the Royal Meteorological Society*, 133(629), 2117–2131, doi: 10.1002/qj.173.
- Buehner M., Caya A., Carrieres T., Pogson L. 2016. Assimilation of SSMIS and ASCAT data and the replacement of highly uncertain estimates in the Environment Canada Regional Ice Prediction System. *Quarterly Journal of the Royal Meteorological Society*, 142(695), 562–573, doi: 10.1002/qj.2408.
- Bärring L., von Storch H. 2004. Scandinavian storminess since about 1800. *Geophysical Research Letters*, 31(20), art no L20202, doi: 10.1029/2004GL020441.
- Cairns A., Carel J.M., Li X. 2016. Port and harbor design. In *Springer Handbook of Ocean Engineering* (Dhanak M.R., Xiros N.I., eds.), pp. 685–710. Springer, Cham, doi: 10.1007/978-3-319-16649-0\_31.
- Caliskan H., Valle-Levinson A. 2008. Wind-wave transformations in an elongated bay. *Continental Shelf Research*, 28, 1702–1710, doi: 10.1016/j.csr.2008.03.009.
- Cañellas B., Orfila Förster A., Méndez Incera F.J., Álvarez Díaz A., Tintoré Subirana J. 2010. Influence of the NAO on the northwestern Mediterranean wave climate. *Scientia Marina*, 74(1), 55–64, doi: 10.3989/scimar.2010.74n1055.
- Cavaleri L., Bertotti L. 1997. In search of the correct wind and wave fields in a minor basin. *Monthly Weather Review*, 125(8), 1964–1975, doi: 10.1175/1520-0493(1997)125<1964:ISOTCW>2.0.CO;2.
- Church J.A., White N.J., Coleman R., Lambeck K., Mitrovica J.X. 2004. Estimates of the regional distribution of sea level rise over the 1950–2000 period. *Journal of Climate*, 17(13), 2609–2625, doi: 10.1175/1520-0442(2004)017<2609:EOTRDO>2.0.CO;2.
- Ciešlikiewicz W., Paplińska-Swerpel B. 2008. A 44-year hindcast of wind wave fields over the Baltic Sea. *Coastal Engineering*, 55(11), 894–905, doi: 10.1016/j.coastaleng.2008.02.017.
- Collins III C.O., Rogers W.E., Marchenko A., Babanin A.V. 2015. In situ measurements of an energetic wave event in the Arctic marginal ice zone. *Geophysical Research Letters*, 42(6), 1863–1870, doi: 10.1002/2015GL063063.
- Cox J.C., Czapinski R.E. 2016. Engineering of an island-style breakwater system for the Fort Pierce marina. *Proceedings of the Institution of Civil Engineers-Maritime Engineering*, 169(1), 37–43, doi: 10.1680/jmaen.15.00014.
- Davis J., Phillips J., Czapinski R., Seissiger E., Cignarella P. 2013. Breakwater island creation: A 3-fold system. In *Design and Practice of Geosynthetic-Reinforced Soil Structures* (Ling H.I., Gottardi G., Cazzuffi D., Han J., Tatsuoka F. eds.), International Symposium on Design and Practice of Geosynthetic-Reinforced Soil Structures / 26th Italian National Conference on Geosynthetics, University of Bologna, Bologna, Italy, Oct 14–16, 2013, pp. 708–718.

- Dean R.G., Dalrymple R.A. 1991. Water wave mechanics for engineers and scientists. World Scientific, Singapore, 353 pp.
- Didenkulova I., Soomere T., Pindsoo K., Suuroja S. 2013. On the occurrence of non-reflecting cross-shore profiles along Estonian coasts of the Baltic Sea. *Estonian Journal of Engineering*, 19(2), 110–123, doi: 10.3176/eng.2013.2.02.
- Dinardo S., Fenoglio-Marc L., Buchhaupt C., Becker M., Scharroo R., Fernandes M.J., Benveniste J. 2018. Coastal SAR and PLRM altimetry in German Bight and West Baltic Sea. *Advances in Space Research*, 62(6), 1371–1404, doi: 10.1016/j.asr.2017.12.018.
- Eldeberky Y. 1996. Nonlinear Transformation of Wave Spectra in the Nearshore Zone. Ph.D. thesis, Department of Civil Engineering and Geosciences, Delft University of Technology, Netherlands, <http://resolver.tudelft.nl/uuid:707ca57d-81c3-4103-bc6e-aae1c90fce63>.
- [EUMETSAT] 2017. EUMETSAT Ocean and Sea Ice Satellite Application Facility. Global sea ice concentration climate data record 1979–2015 (v2.0, 2017), [Online]. Norwegian and Danish Meteorological Institutes, doi: 10.15770/EUM\_SAF\_OSI\_0008.
- Galanis G., Hayes D., Zodiatis G., Chu P.C., Kuo Y.H., Kallos G. 2012. Wave height characteristics in the Mediterranean Sea by means of numerical modeling, satellite data, statistical and geometrical techniques. *Marine Geophysical Research*, 33(1), 1–15, doi: 10.1007/s11001-011-9142-0.
- Gao T., Yu J.Y., Paek H. 2017. Impacts of four northern-hemisphere teleconnection patterns on atmospheric circulations over Eurasia and the Pacific. *Theoretical and Applied Climatology*, 129(3), 815–831, doi: 10.1007/s00704-016-1801-2.
- Gloersen P., Cavalieri D.J. 1986. Reduction of weather effects in the calculation of sea ice concentration from microwave radiances. *Journal of Geophysical Research: Oceans*, 91(C3), 3913–3919, doi: 10.1029/JC091iC03p03913.
- Goerlandt F., Montewka J., Zhang W., Kujala P. 2017. An analysis of ship escort and convoy operations in ice conditions. *Safety Science*, 95, 198–209, doi: 10.1016/j.ssci.2016.01.004.
- Granskog M., Kaartokallio H., Kuosa H., Thomas D.N., Vainio J. 2006. Sea ice in the Baltic Sea—a review. *Estuarine, Coastal and Shelf Science*, 70(1–2), 145–160, doi: 10.1016/j.ecss.2006.06.001.
- Groeneweg J., van Gent M., van Nieuwkoop J., Toledo Y. 2015. Wave Propagation into Complex Coastal Systems and the Role of Nonlinear Interactions. *Journal of Waterway Port, Coastal and Ocean Engineering*, 141(5), doi: 10.1061/(ASCE)WW.1943-5460.0000300.
- Haapala J., Leppäranta M. 1996. Simulating the Baltic Sea ice season with a coupled ice-ocean model. *Tellus A*, 48(5), 622–643, doi: 10.3402/tellusa.v48i5.12158.
- Haapala J., Leppäranta M. 1997. The Baltic Sea ice season in changing climate. *Boreal Environment Research*, 2(1), 93–108.
- Haapala J.J., Ronkainen I., Schmelzer N., Sztobryn M. 2015. Recent change—sea ice. In: The BACC II Author Team, Second Assessment of Climate Change for the Baltic Sea Basin, Regional Climate Studies, Springer, Cham, pp. 145–153, doi: 10.1007/978-3-319-16006-1\_8.
- Hanes D.M., Erikson L.H. 2013. The significance of ultra-refracted surface gravity waves on sheltered coasts, with application to San Francisco Bay. *Estuarine, Coastal and Shelf Science*, 133, 129–136, doi: 10.1016/j.ecss.2013.08.022.

- Hannachi A. 2004. A Primer for EOF Analysis of Climate Data. Department of Meteorology, University of Reading: Reading, UK. <http://www.o3d.org/eas-6490/lectures/EOFs/eofprimer.pdf>. Accessed 10 June 2019
- Harff J., Deng J., Dudzińska-Nowak J., Fröhle P., Groh A., Hünicke B., Soomere T., Zhang W. 2017. What determines the change of coastlines in the Baltic Sea?. In: Harff J., Furmańczyk K., von Storch H. (eds.), *Coastline Changes of the Baltic Sea from South to East*, Springer, Cham, pp. 15–35, doi: 10.1007/978-3-319-49894-2\_2.
- Hasselmann K., Barnett T.P., Bouws E., Carlson H., Cartwright D.E., Enke K., Ewing J.A., Gienapp H., Hasselmann D.E., Kruseman P., Meerburg A., Müller P., Olbers D.J., Richte K., Sell W., Walden H. 1973. Measurements of wind-wave growth and swell decay during the Joint North Sea Wave Project (JONSWAP). *Ergänzungsheft Deutsche Hydrographische Zeitung. Reihe A*, (8), 12.
- Hasselmann S., Hasselmann K., Bauer E., Janssen P.A.E.M., Komen G.J., Bertotti L., Lionello P., Guillaume A., Cardone V.C., Greenwood J.A., Reistad M., Zambresky L., Ewing J.A. 1988. The WAM Model—A third generation ocean wave prediction model. *Journal of Physical Oceanography*, 18(12), 1775–1810, doi: 10.1175/1520-0485(1988)018<1775:TWMTGO>2.0.CO;2.
- Hemer M.A., Church J.A., Hunter J.R. 2010. Variability and trends in the directional wave climate of the Southern Hemisphere. *International Journal of Climatology: A Journal of the Royal Meteorological Society*, 30(4), 475–491, doi: 10.1002/joc.1900.
- Hemer M.A., Fan Y., Mori N., Semedo A., Wang X.L. 2013. Projected changes in wave climate from a multi-model ensemble. *Nature Climate Change*, 3(5), 471–476, doi: 10.1038/nclimate1791.
- Hurrell J.W., Kushnir Y., Ottersen G., Visbeck M. 2003. The North Atlantic Oscillation: Climate Significance and Environmental Impact. *Geophysical Monograph Series*, 134, 279 pp.
- Hünicke B., Zorita E., Soomere T., Madsen K.S., Johansson M., Suursaar Ü. 2015. Recent change—sea level and wind waves. In: The BACC II Author Team, *Second Assessment of Climate Change for the Baltic Sea Basin, Regional Climate Studies*, Springer, Cham, pp. 155–185, doi: 10.1007/978-3-319-16006-1\_9.
- Irannezhad M., Marttila H., Kløve B. 2014. Long-term variations and trends in precipitation in Finland. *International Journal of Climatology*, 34(10), 3139–3153, doi: 10.1002/joc.3902.
- Izaguirre C., Méndez F.J., Menéndez M., Losada I.J. 2011. Global extreme wave height variability based on satellite data. *Geophysical Research Letters*, 38(10), L10607, doi: 10.1029/2011GL047302.
- Jaagus J. 2009. Regionalisation of the precipitation pattern in the Baltic Sea drainage basin and its dependence on large-scale atmospheric circulation. *Boreal Environment Research*, 14, 31–44.
- Jaagus J., Suursaar Ü. 2013. Long-term storminess and sea level variations on the Estonian coast of the Baltic Sea in relation to large-scale atmospheric circulation. *Estonian Journal of Earth Sciences*, 62(2), 73–92, doi: 10.3176/earth.2013.07.
- Jacobeit J., Jönsson P., Barring L., Beck C., Ekström M. 2001. Zonal indices for Europe 1780–1995 and running correlations with temperature. *Climatic Change*, 48(1), 219–241, doi: 10.1023/A:1005619023045.

- Jevrejeva S. 2001. Severity of winter seasons in the northern Baltic Sea between 1529 and 1990: reconstruction and analysis. *Climate Research*, 17(1), 55–62.
- Jevrejeva S., Moore J.C., Grinsted A. 2003. Influence of the Arctic Oscillation and El Niño-Southern Oscillation (ENSO) on ice conditions in the Baltic Sea: The wavelet approach. *Journal of Geophysical Research-Atmospheres*, 108(D21), 4677, doi: 10.1029/2003JD003417.
- Jevrejeva S., Drabkin V.V., Kostjukov J., Lebedev A.A., Leppäranta M., Mironov Y.U., Schmelzer N., Sztobryn M. 2004. Baltic Sea ice seasons in the twentieth century. *Climate Research*, 25(3), 217–227.
- Jevrejeva S., Moore J.C., Woodworth P.L., Grinsted A. 2005. Influence of large-scale atmospheric circulation on European sea level: results based on the wavelet transform method. *Tellus, Series A: Dynamic Meteorology and Oceanography*, 57(2), 183–193, doi: 10.3402/tellusa.v57i2.14609.
- Johansson M., Boman H., Kahma K., Launiainen J. 2001. Trends in sea level variability in the Baltic Sea. *Boreal Environment Research*, 6, 159–179.
- Jönsson A., Broman B., Rahm L. 2003. Variations in the Baltic Sea wave fields. *Ocean Engineering*, 30(1), 107–126, doi: 10.1016/S0029-8018(01)00103-2.
- Jönsson A., Danielsson Å., Rahm L. 2005. Bottom type distribution based on wave friction velocity in the Baltic Sea. *Continental Shelf Research*, 25(3), 419–435, doi: 10.1016/j.csr.2004.09.011.
- Keevallik S., Soomere T. 2008. Shifts in early spring wind regime in North-East Europe (1955–2007). *Climate of the Past*, 4(3), 147–152, doi:10.5194/cp-4-147-2008.
- Kelpšaitė L., Dailidienė I. 2011. Influence of wind wave climate change on coastal processes in the eastern Baltic Sea. *Journal of Coastal Research*, Special Issue 64, 220–224.
- Kelpšaitė L., Herrmann H., Soomere T. 2008. Wave regime differences along the eastern coast of the Baltic Proper. *Proceedings of the Estonian Academy of Sciences*, 57(4), 225–231, doi: 10.3176/proc.2008.4.04.
- Kelpšaitė-Rimkienė L., Parnell K.E., Žaromskis R., Kondrat V. 2021. Cross-shore profile evolution after an extreme erosion event–Palanga, Lithuania. *Journal of Marine Science and Engineering*, 9(1), 38, doi: 10.3390/jmse9010038.
- Kinsman B. 1965. *Wind Waves: Their Generation and Propagation on the Ocean Surface*. Prentice-Hall, 676 pp.
- Komen G.J., Cavaleri L., Donelan M., Hasselmann K., Hasselmann S., Janssen P.A.E.M. 1994. *Dynamics and Modelling of Ocean Waves*. Cambridge, UK: Cambridge University Press, 554 pp.
- Kovaleva O., Eelsalu M., Soomere T. 2017. Hot-spots of large wave energy resources in relatively sheltered sections of the Baltic Sea coast. *Renewable and Sustainable Energy Reviews*, 74, 424–437, doi: 10.1016/j.rser.2017.02.033.
- Kudryavtseva N.A., Soomere T. 2016. Validation of the multi-mission altimeter wave height data for the Baltic Sea region. *Estonian Journal of Earth Sciences*, 65(3), 161–175, doi: 10.3176/earth.2016.13.
- Kudryavtseva N., Soomere T. 2017. Satellite altimetry reveals spatial patterns of variations in the Baltic Sea wave climate. *Earth System Dynamics*, 8(3), 697–706, doi: 10.5194/esd-8-697-2017.
- Kudryavtseva N., Kussembayeva K., Rakisheva Z.B., Soomere T. 2019. Spatial variations in the Caspian Sea wave climate in 2002–2013 from satellite altimetry. *Estonian Journal of Earth Sciences*, 68(4), 225–240, doi: 10.3176/earth.2019.16.

- Kudryavtseva N., Räämet A., Soomere T. 2020. Coastal flooding: Joint probability of extreme water levels and waves along the Baltic Sea coast. *Journal of Coastal Research*, 95(SI), 1146–1151, doi: 10.2112/SI95-222.1.
- Kudryavtseva N., Soomere T., Männikus R. 2021. Non-stationary analysis of water level extremes in Latvian waters, Baltic Sea, during 1961–2018. *Natural Hazards and Earth System Sciences*, 21(4), 1279–1296, doi: 10.5194/nhess-21-1279-2021.
- Käyhkö J., Apsite E., Bolek A., Filatov N., Kondratyev S., Korhonen J., Kriaučiūnienė J., Lindström G., Nazarova L., Pyrh A., Sztobryn M. 2015. Recent change–river run-off and ice cover. In: The BACC II Author Team, Second Assessment of Climate Change for the Baltic Sea Basin, Regional Climate Studies, Springer, Cham, 99–116, doi: 10.1007/978-3-319-16006-1\_5.
- Łabuz T.A. 2015. Environmental impacts—coastal erosion and coastline changes. In: The BACC II Author Team, Second Assessment of Climate Change for the Baltic Sea Basin. Regional Climate Studies, Springer, Cham, pp. 381–396, doi: 10.1007/978-3-319-16006-1\_20.
- Lavergne T., Sørensen A.M., Kern S., Tonboe R., Notz D., Aaboe S., Bell L., Dybkjær G., Eastwood S., Gabarro C., Heygster G., Killie A.M., Kreiner B.M., Lavelle J., Saldo R., Sandven S., Pedersen L.T. 2019. Version 2 of the EUMETSAT OSI SAF and ESA CCI sea-ice concentration climate data records. *Cryosphere*, 13(1), 49–78, doi: 10.5194/tc-13-49-2019.
- Lehmann A., Getzlaff K., Harlaß J. 2011. Detailed assessment of climate variability in the Baltic Sea area for the period 1958 to 2009. *Climate Research*, 46(2), 185–196, doi: 10.3354/cr00876.
- Lensu M., Goerlandt F. 2019. Big maritime data for the Baltic Sea with a focus on the winter navigation system. *Marine Policy*, 104, 53–65, doi: 10.1016/j.marpol.2019.02.038.
- Leppäranta M. 2012. Ice season in the Baltic Sea and its climatic variability. In: Haapala I. (ed.), From the Earth's Core to Outer Space. Lecture Notes in Earth Sciences, 137. Springer, Berlin, Heidelberg, pp. 139–149, doi: 10.1007/978-3-642-25550-2\_9.
- Leppäranta M., Myrberg K. 2009. Physical Oceanography of the Baltic Sea. Springer Science & Business Media, Praxis, Berlin, Heidelberg, doi: 10.1007/978-3-540-79703-6.
- Levitus S., Antonov J., Boyer T. 2005. Warming of the world ocean, 1955–2003. *Geophysical research letters*, 32(2), doi: 10.1029/2004GL021592.
- Li Y.S., Liu S.X., Wai O.W.H., Yu Y.X. 2000. Wave concentration by a navigation channel. *Applied Ocean Research*, 22 (4), 199–213, doi: 10.1016/S0141-1187(00)00013-4.
- Lindsey R., Dahlman L. 2020. Climate change: ocean heat content. *Climate.Gov*, August 17, [Accessed September 2022].
- Lionello P., Sanna A. 2005. Mediterranean wave climate variability and its links with NAO and Indian Monsoon. *Climate Dynamics*, 25(6), 611–623, doi: 10.1007/s00382-005-0025-4.
- Liu A.K., Mollo-Christensen E. 1988. Wave propagation in a solid ice pack. *Journal of Physical Oceanography*, 18(11), 1702–1712, doi: 10.1175/1520-0485(1988)018<1702:WPIASI>2.0.CO;2.
- Madsen K.S., Høyer J.L., Tscherning C.C. 2007. Near-coastal satellite altimetry: Sea surface height variability in the North Sea-Baltic Sea area. *Geophysical Research Letters*, 34(14), L14601, doi: 10.1029/2007GL029965.

- Masselink G., Castelle B., Scott T., Dodet G., Suanez S., Jackson D., Floc'h F. 2016. Extreme wave activity during 2013/2014 winter and morphological impacts along the Atlantic coast of Europe. *Geophysical Research Letters*, 43(5), 2135–2143, doi: 10.1002/2015GL067492.
- Mäll M., Nakamura R., Suursaa Ü., Shibayama T. 2020. Pseudo-climate modelling study on projected changes in extreme extratropical cyclones, storm waves and surges under CMIP5 multi-model ensemble: Baltic Sea perspective. *Natural Hazards*, 102, 67–99, doi: 10.1007/s11069-020-03911-2.
- Männikus R., Soomere T., Kudryavtseva N. 2019. Identification of mechanisms that drive water level extremes from in situ measurements in the Gulf of Riga during 1961–2017. *Continental Shelf Research*, 182, 22–36, doi: 10.1016/j.csr.2019.05.014.
- Männikus R., Soomere T., Viška M. 2020. Variations in the mean, seasonal and extreme water level on the Latvian coast, the eastern Baltic Sea, during 1961–2018. *Estuarine, Coastal and Shelf Science*, 245, 106827, doi: 10.1016/j.ecss.2020.106827.
- Medvedeva A., Myslenkov S., Medvedev I., Arkhipkin V., Krechik V., Dobrolyubov S. 2016. Numerical modeling of the wind waves in the Baltic Sea using the rectangular and unstructured grids and the reanalysis NCEP/CFR. *Proceedings of the Hydrometeorological Research Center of the Russian Federation*, 362, 37–54 [in Russian with English summary].
- Mentaschi L., Vousdoukas M.I., Voukouvalas E., Dosio A., Feyen L. 2017. Global changes of extreme coastal wave energy fluxes triggered by intensified teleconnection patterns. *Geophysical Research Letters*, 44(5), 2416–2426, doi: 10.1002/2016GL072488.
- Merkouriadi I., Leppäranta M. 2014. Long-term analysis of hydrography and sea-ice data in Tvärminne, Gulf of Finland, Baltic Sea. *Climate Change*, 124(4), 849–859, doi: 10.1007/s10584-014-1130-3.
- Mietus M., von Storch H. 1997. Reconstruction of the wave climate in the proper Baltic basin, April 1947–March 1988. GKSS Report 97/E/28, Geesthacht.
- Minobe S., Mantua N. 1999. Interdecadal modulation of interannual atmospheric and oceanic variability over the North Pacific. *Progress in Oceanography*, 43(2–4), 163–192, doi: 10.1016/S0079-6611(99)00008-7.
- Mostert W., Deike L. 2020. Inertial energy dissipation in shallow-water breaking waves. *Journal of Fluid Mechanics*, 890, doi: 10.1017/jfm.2020.83.
- Myslenkov S.A., Medvedeva A., Arkhipkin V., Markina M., Surkova G., Krylov A., Dobrolyubov S., Zilitinkevich S., Koltermann P. 2018. Long-term statistics of storms in the Baltic, Barents and White seas and their future climate projections. *Geography, Environment, Sustainability*, 11(1), 93–112. doi: 10.24057/2071-9388-2018-11-1-93-112.
- Nezlin N.P., McWilliams J.C. 2003. Satellite data, Empirical Orthogonal Functions, and the 1997–1998 El Nino off California. *Remote Sensing of Environment*, 84(2), 234–254, doi: 10.1016/S0034-4257(02)00109-8.
- Nikolkina I., Soomere T., Räämet A. 2014. Multidecadal ensemble hindcast of wave fields in the Baltic Sea. 2014 IEEE/OES Baltic International Symposium (BALTIC), “Measuring and Modeling of Multi-Scale Interactions in the Marine Environment”, May 26–29, Tallinn, Estonia. IEEE Conference Publications, doi: 10.1109/BALTIC.2014.6887854.

- Nilsson E., Rutgersson A., Dingwell A., Björkqvist J.V., Pettersson H., Axell L., Nyberg J., Strömstedt. 2019. Characterization of wave energy potential for the Baltic Sea with focus on the Swedish Exclusive Economic Zone. *Energies*, 12(5), 793, doi: 10.3390/en12050793.
- Niroomandi A., Ma G., Ye X., Lou S., Xue P. 2018. Extreme value analysis of wave climate in Chesapeake Bay. *Ocean Engineering*, 159, 22–36. doi: 10.1016/j.oceaneng.2018.03.094.
- Omstedt A., Nyberg L. 1996. Response of Baltic Sea ice to seasonal, interannual forcing and climate change. *Tellus A*, 48(5), 644–662, doi: 10.3402/tellusa.v48i5.12160.
- Omstedt A., Pettersen C., Rodhe J., Winsor P. 2004. Baltic Sea climate: 200 yr of data on air temperature, sea level variation, ice cover, and atmospheric circulation. *Climate Research*, 25(3), 205–216, doi: 10.3354/cr025205.
- Omstedt A., Elken J., Lehmann A., Leppäranta M., Meier H.E.M., Myrberg K., Rutgersson A. 2014. Progress in physical oceanography of the Baltic Sea during the 2003–2014 period. *Progress in Oceanography*, 128, 139–171, doi: 10.1016/j.pocean.2014.08.010.
- Orviku K., Jaagus J., Kont A., Ratas U., Rivas R. 2003. Increasing activity of coastal processes associated with climate change in Estonia. *Journal of Coastal Research*, 19, 364–375.
- Orviku K. 2018. Rannad ja rannikud (Beaches and shores). Tallinna ülikooli kirjastus (Tallinn University Publishers), 349 pp. [in Estonian].
- OSI SAF 2017. Global Sea Ice Concentration Climate Data Record v2.0 – Multimission, EUMETSAT SAF on Ocean and Sea Ice, doi: 10.15770/EUM\_SAF\_OSI\_0008.
- Overeem I., Anderson R.S., Wobus C.W., Clow G.D., Urban F.E., Matell N. 2011. Sea ice loss enhances wave action at the Arctic coast. *Geophysical Research Letters*, 38(17), doi: 10.1029/2011GL048681.
- Pallares E., Sanchez-Arcilla A., Espino M. 2014. Wave energy balance in wave models (SWAN) for semi-enclosed domains application to the Catalan coast. *Continental Shelf Research*, 87, 41–53, doi: 10.1016/j.csr.2014.03.008.
- Patra A., Bhaskaran P.K. 2016. Trends in wind-wave climate over the head Bay of Bengal region. *International Journal of Climatology*, 36(13), 4222–4240, doi: 10.1002/joc.4627.
- Passaro M., Cipollini P., Benveniste J. 2015. Annual sea level variability of the coastal ocean: The Baltic Sea-North Sea transition zone. *Journal of Geophysical Research-Oceans*, 120(4), 3061–3078, doi: 10.1002/2014JC010510.
- Pindsoo K., Soomere T. 2015. Contribution of wave set-up into the total water level in the Tallinn area. *Proceedings of the Estonian Academy of Sciences*, 64(3S), doi: 10.3176/proc.2015.3S.03.
- Rakisheva Z., Kudryavtseva N., Kussembayeva K., Sakhayeva A. 2019. Studying the change of average waves of the Caspian Sea using the altimetry data. *Journal of Mathematics, Mechanics and Computer Science*, 101(1), 59–75, doi: 10.26577/JMMCS-2019-1-618.
- Reguero B.G., Losada I.J., Méndez F.J. 2019. A recent increase in global wave power as a consequence of oceanic warming. *Nature Communications*, 10(1), 1–14, doi: 10.1038/s41467-018-08066-0.
- Rikka S., Pleskachevsky A., Uiboupin R., Jacobsen S. 2018. Sea state in the Baltic Sea from space-borne high-resolution synthetic aperture radar imagery. *International Journal of Remote Sensing*, 39(4), 1256–1284, doi: 10.1080/01431161.2017.1399475.

- Rogers W.E., Hwang P.A., Wang D.W. 2003. Investigation of wave growth and decay in the SWAN model: three regional-scale applications. *Journal of Physical Oceanography*, 33 (2), 366–389, doi: 10.1175/1520-0485(2003)033<0366:LOWGAD>2.0.CO;2.
- Różyński G. 2010. Long-term evolution of Baltic Sea wave climate near a coastal segment in Poland; its drivers and impacts. *Ocean Engineering*, 37(2–3), 186–199, doi: 10.1016/j.oceaneng.2009.11.008.
- Ruosteenoja K., Vihma T., Venäläinen A. 2019. Projected Changes in European and North Atlantic Seasonal Wind Climate Derived from CMIP5 Simulations. *Journal of Climate*, 32(19), 6467–6490, doi: 10.1175/JCLI-D-19-0023.1.
- Rutgersson A., Kjellström E., Haapala J., Stendel M., Danilovich I., Drews M., Jylhä K., Kujala P., Guo Larsén X., Halsnæs K., Lehtonen I., Luomaranta A., Nilsson E., Olsson T., Särkkä J., Tuomi L., Wasmund N. 2022. Natural hazards and extreme events in the Baltic Sea region. *Earth System Dynamics*, 13(1), 251–301, doi: 10.5194/esd-13-251-2022.
- Ryabchuk D., Kolesov A., Chubarenko B., Spiridonov M., Kurennoy D., Soomere T. 2011a. Coastal erosion processes in the eastern Gulf of Finland and their links with geological and hydrometeorological factors. *Boreal Environment Research*, 16(Suppl. A), 117–137.
- Ryabchuk D., Leont'yev I., Sergeev A., Nesterova E., Sukhacheva L., Zhamoida V. 2011b. The morphology of sand spits and the genesis of longshore sand waves on the coast of the eastern Gulf of Finland. *Baltica*, 24(1), pp.13–24.
- Räämet A., Soomere T. 2010. The wave climate and its seasonal variability in the northeastern Baltic Sea. *Estonian Journal of Earth Sciences*, 59(1), 100–113, doi: 10.3176/earth.2010.1.08.
- Räämet A., Soomere T. 2021. Spatial pattern of quality of historical wave climate reconstructions for the Baltic Sea. *Boreal Environment Research*, 26, 29–41.
- Safadi C. 2016. Wind and wave modelling for the evaluation of the maritime accessibility and protection afforded by ancient harbours. *Journal of Archaeological Science: Reports*, 5, 348–360, doi: 10.1016/j.jasrep.2015.12.004.
- Sartini L., Besio G., Cassola F. 2017. Spatio-temporal modelling of extreme wave heights in the Mediterranean Sea. *Ocean Modelling*, 117, 52–69, doi: 10.1016/j.ocemod.2017.07.001
- Scharroo R. 2012. RADS version 3.1 User Manual and Format Specifications. Available at <http://rads.tudelft.nl/rads/radsmanual.pdf>. Accessed 6 March 2020
- Scharroo R., Leuliette E.W., Lillibridge J.L., Byrne D., Naeije M.C., Mitchum G.T. 2013. RADS: Consistent multi-mission products in Proc Symp on 20 Years of Progress in Radar Altimetry, 20–28 September 2012, Venice, Eur. Space Agency Spec. Publ., ESA SP-710.
- Shimura T., Mori N., Mase H. 2013. Ocean waves and teleconnection patterns in the northern hemisphere. *Journal of Climate*, 26(21), 8654–8670, doi: 10.1175/JCLI-D-12-00397.1.
- [SMHI and FIMR] 1982. Swedish Meteorological and Hydrological Institute, and Finnish Meteorological Institute. An Ice Atlas for the Baltic Sea, Kattegat, Skagerrak and Lake Vänern. Norrköping, Sjöfartsverket.
- Sooäär J., Jaagus J. 2007. Long-term changes in the sea ice regime in the Baltic Sea near the Estonian coast. *Estonian Journal of Engineering*, 13(3), 189–200.

- Soomere T. 2001. Wave regimes and anomalies off north-western Saaremaa Island. *Proceedings of the Estonian Academy of Sciences. Engineering*, 7 (2), 157–173, [http://vana.kirj.ee/public/va\\_te/t50-2-6.pdf](http://vana.kirj.ee/public/va_te/t50-2-6.pdf).
- Soomere T. 2013. Extending the observed Baltic Sea wave climate back to the 1940s. *Journal of Coastal Research*, 65(SI), 1969–1974, doi: 10.2112/SI65-333.1.
- Soomere T. 2022. Numerical simulations of wave climate in the Baltic Sea: a review. *Oceanologia*, doi: 10.1016/j.oceano.2022.01.004.
- Soomere T., Eelsalu M. 2014. On the wave energy potential along the eastern Baltic Sea coast. *Renewable Energy*, 71, 221–233, doi: 10.1016/j.renene.2014.05.025.
- Soomere T., Healy T. 2011. On the dynamics of “almost equilibrium” beaches in semi-sheltered bays along the southern coast of the Gulf of Finland. In: Harff J., Björck S., Hoth P. (eds.). *The Baltic Sea Basin. Central and Eastern European Development Studies, Part 5*, Springer, Heidelberg, Dordrecht, pp. 255–279.
- Soomere T., Keevallik S. 2001. Anisotropy of moderate and strong winds in the Baltic Proper. *Proceedings of the Estonian Academy of Sciences. Engineering*, 7(1), 35–49, doi: 10.3176/eng.2001.1.04.
- Soomere T., Keevallik S. 2003. Directional and extreme wind properties in the Gulf of Finland. *Proceedings of the Estonian Academy of Sciences. Engineering*, 9(2), 73–90, doi: 10.3176/eng.2003.2.01.
- Soomere T., Pindsoo K. 2016. Spatial variability in the trends in extreme storm surges and weekly-scale high water levels in the eastern Baltic Sea. *Continental Shelf Research*, 115, 53–64, doi: 10.1016/j.csr.2015.12.016.
- Soomere T., Räämet A. 2011. Long-term spatial variations in the Baltic Sea wave fields. *Ocean Science*, 7(1), 141–150, doi: 10.5194/os-7-141-2011.
- Soomere T., Räämet A. 2014. Decadal changes in the Baltic Sea wave heights. *Journal of Marine Systems*, 129, 86–95, doi: 10.1016/j.jmarsys.2013.03.009.
- Soomere T., Behrens A., Tuomi L., Nielsen J.W. 2008. Wave conditions in the Baltic Proper and in the Gulf of Finland during windstorm Gudrun. *Natural Hazards and Earth System Science*, 8(1), 37–46, doi: 10.5194/nhess-8-37-2008.
- Soomere T., Bishop S.R., Viška M., Räämet A. 2015. An abrupt change in winds that may radically affect the coasts and deep sections of the Baltic Sea. *Climate Research*, 62(2), 163–171, doi: 10.3354/cr01269.
- Soomere T., Weisse R., Behrens A. 2012. Wave climate in the Arkona basin, the Baltic Sea. *Ocean Science*, 8(2), 287–300, doi: 10.5194/os-8-287-2012.
- Surkova G.V., Arkhipkin V.S., Kislov A.V. 2015. Atmospheric circulation and storm events in the Baltic Sea. *Open Geosciences*, 7(1), 332–341, doi: 10.1515/geo-2015-0030.
- Suursaar Ü. 2013. Locally calibrated wave hindcasts in the Estonian coastal sea in 1966–2011. *Estonian Journal of Earth Sciences*, 62(1), 42–56, doi: 10.3176/earth.2013.05.
- Suursaar Ü. 2015. Analysis of wave time series in the Estonian coastal sea in 2003–2014. *Estonian Journal of Earth Sciences*, 64(4), 289–304, doi: 10.3176/earth.2015.35.
- Suursaar Ü., Kullas T. 2009. Decadal variations in wave heights off Cape Kelba, Saaremaa Island, and their relationships with changes in wind climate. *Oceanologia*, 51(1), 39–61, doi: 10.5697/oc.51-1.039.
- Suursaar Ü., Kullas T., Otsmann M. 2002. A model study of the sea level variations in the Gulf of Riga and the Väinameri Sea. *Continental Shelf Research*, 22, 2001–2019.
- Suursaar Ü., Kullas T., Otsmann M., Saaremäe I., Kuik J., Merilain M. 2006. Cyclone Gudrun in January 2005 and modelling its hydrodynamic consequences in the Estonian coastal waters. *Boreal Environment Research*, 11(2), 143–159.

- Suursaar Ü., Sooäär J., 2007. Decadal variations in mean and extreme sea level values along the Estonian coast of the Baltic Sea. *Tellus, Series A: Dynamic Meteorology and Oceanography*, 59(2), 249–260, doi: 10.1111/j.1600-0870.2006.00220.x.
- Suursaar Ü., Alari V., Tõnisson H. 2014. Multi-scale analysis of wave conditions and coastal changes in the north-eastern Baltic Sea. *Journal of Coastal Research*, 70, 223–228, doi: 10.2112/SI70-038.1.
- Tavakoli S., Babanin A.V. 2021. Wave energy attenuation by drifting and non-drifting floating rigid plates. *Ocean Engineering*, 226, 108717, doi: 10.1016/j.oceaneng.2021.108717.
- Thompson D.W., Wallace J.M. 1998. The Arctic Oscillation signature in the wintertime geopotential height and temperature fields. *Geophysical Research Letters*, 25(9), 1297–1300, doi: 10.1029/98GL00950.
- Tonboe R.T., Eastwood S., Lavergne T., Sørensen A.M., Rathmann N., Dybkjær G., Pedersen L.T., Høyer J.L., Kern S. 2016. The EUMETSAT sea ice concentration climate data record. *Cryosphere*, 10(5), 2275–2290, doi: 10.5194/tc-10-2275-2016.
- Trigo R.M., Osborn T.J., Corte-Real J.M. 2002. The North Atlantic Oscillation influence on Europe: climate impacts and associated physical mechanisms. *Climate Research*, 20(1), 9–17, doi: 10.3354/cr020009.
- Tuomi L., Kahma K.K., Pettersson H. 2011. Wave hindcast statistics in the seasonally ice-covered Baltic Sea. *Boreal Environment Research*, 16(6), 451–472.
- Tuomi L., Kanarik H., Björkqvist J.V., Marjamaa R., Vainio J., Hordoir R., Höglund A., Kahma K.K. 2019. Impact of ice data quality and treatment on wave hindcast statistics in seasonally ice-covered seas. *Frontiers in Earth Science*, 7, 166, doi: 10.3389/feart.2019.00166.
- Viška M., Soomere T. 2012. Hindcast of sediment flow along the Curonian Spit under different wave climates. In: Proceedings of the IEEE/OES Baltic 2012 International Symposium “Ocean: Past, Present and Future. Climate Change Research, Ocean Observation & Advanced Technologies for Regional Sustainability”, May 8–11, Klaipėda, Lithuania. IEEE Conference Publications, 7 pp., doi: 10.1109/BALTIC.2012.6249195.
- Von Storch H., Navarra A. (eds.) 1999. Analysis of climate variability: applications of statistical techniques. Springer Science & Business Media, doi: 10.1007/978-3-662-03744-7.
- Von Storch H., Omstedt A., Pawlak J., Reckermann M. 2015. Introduction and Summary. In: The BACC II Author Team, Second Assessment of Climate Change for the Baltic Sea Basin. Regional Climate Studies, Springer, Cham, pp. 1–22, doi: 10.1007/978-3-319-16006-1\_1.
- Wakelin S.L., Woodworth P.L., Flather R.A., Williams J.A. 2003. Sea-level dependence on the NAO over the NW European continental shelf. *Geophysical Research Letters*, 30(7), 1403, doi: 10.1029/2003GL017041.
- Walker G.T., Bliss E.W. 1932. World weather V. *Memoirs of the Royal Meteorological Society*, 4, 53–84.
- Wang X.L., Swail V.R. 2002. Trends of Atlantic wave extremes as simulated in a 40-yr wave hindcast using kinematically reanalyzed wind fields. *Journal of Climate*, 15(9), 1020–1035, doi: 10.1175/1520-0442(2002)015<1020:TOAWEA>2.0.CO;2.
- Wang X.L., Zwiers F.W., Swail V.R. 2004. North Atlantic ocean wave climate change scenarios for the twenty-first century. *Journal of Climate*, 17(12), 2368–2383, doi: 10.1175/1520-0442(2004)017<2368:NAOWCC>2.0.CO;2.

- Wiese A., Staneva J., Schulz-Stellenfleth J., Behrens A., Fenoglio-Marc L., Bidlot J.R. 2018. Synergy of wind wave model simulations and satellite observations during extreme events. *Ocean Science*, 14(6), 1503–1521, doi: 10.5194/os-14-1503-2018.
- Weisse R., von Storch H., Niemeyer H.D., Knaack H. 2012. Changing North Sea storm surge climate: An increasing hazard?. *Ocean & Coastal Management*, 68, 58–68, doi: 10.1016/j.ocecoaman.2011.09.005.
- Wolf J., Woolf D.K. 2006. Waves and climate change in the north-east Atlantic. *Geophysical Research Letters*, 33(6), L06604, doi: 10.1029/2005GL025113.
- Woolf D.K., Challenor P.G., Cotton P.D. 2002. Variability and predictability of the North Atlantic wave climate. *Journal of Geophysical Research-Oceans*, 107(C10), 3145, doi: 10.1029/2001JC001124.
- Wu J. 2012. Wind-stress coefficients over sea surface from breeze to hurricane. *Journal of Geophysical Research-Oceans*, 87(C12), 9704–9706, doi: 10.1029/JC087iC12p09704.
- Young I.R., Zieger S., Babanin A.V. 2011. Global trends in wind speed and wave height. *Science*, 332(6028), 451–455, doi: 10.1126/science.1197219.
- Young, I.R., Ribal A. 2022. Can multi-mission altimeter datasets accurately measure long-term trends in wave height?. *Remote Sensing*, 14(4), 974, doi: 10.3390/rs14040974.
- Zaitseva-Pärnaste I., Soomere T. 2013. Interannual variations of ice cover and wave energy flux in the northeastern Baltic Sea. *Annals of Glaciology*, 54(62), 175–182, doi: 10.3189/2013AoG62A228.
- Zhang N., Li S., Wu Y., Wang K.H., Zhang Q., You Z.J., Wang J. 2020. Effects of sea ice on wave energy flux distribution in the Bohai Sea. *Renewable Energy*, 162, 2330–2343, doi: 10.1016/j.renene.2020.10.036.
- Zijlema M., van Vledder G.Ph., Holthuijsen L.H. 2012. Bottom friction and wind drag for wave models. *Coastal Engineering*, 65, 19–26, doi: 10.1016/j.coastaleng.2012.03.002.
- Zujev M., Elken J., Lagema P. 2021. Data assimilation of sea surface temperature and salinity using basin-scale reconstruction from empirical orthogonal functions: a feasibility study in the northeastern Baltic Sea. *Ocean Science*, 17, 91–109, doi: 10.5194/os-17-91-2021.

## Acknowledgements

First of all, I express my sincere gratitude to my supervisor Prof. Tarmo Soomere. The door to his office was always open whenever I faced a problem or had a question about my research. He provided constant encouragement and was always willing and enthusiastic to assist in any way he could throughout my studies. I am so grateful for his support, guidance and deep insight into this field which have made my time here an inspiring experience.

I thank Dr. Nadezhda Kudryavtseva for her support, and the members of the Wave Engineering Laboratory for their consultation, guidance, and company during my studies. I thank Prof. Kevin Parnell, Dr. Nicole Delpeche-Ellmann, Dr. Maris Eelsalu, Dr. Rain Männikus, Dr. Andrea Giudici, Mikołaj Jankowski, Dr. Katri Pindsoo, and Margus Rätsep.

I extend a special thank you to Dr. Andrus Räämet for providing the modelled wave data for Paper II.

I thank Zahra Loghmannia who opened both her home and heart to me when I first arrived in the city.

I extend my profound gratitude to my father for providing me unfailing support. My sincerest thanks go to Chad Nester for all his love and sympathy. This thesis would not have been possible without them. Thank you.

The initial phase of research for Paper I was co-supported by institutional financing from the Estonian Ministry of Education and Research (grant IUT33-3) and the Flag-ERA project FuturiCT2.0. The further development of this paper and the work on Papers II and III was co-supported by the Estonian Research Council (grant PRG1129) and the European Economic Area (EEA) Financial Mechanism 2014–2021 Baltic Research Programme (grant EMP480).

The Radar Altimeter Database System (RADS), Finnish, Swedish, Norwegian and Danish Meteorological Institutes database and NOAA Center for Weather and Climate Prediction are gratefully acknowledged for providing data.

## Abstract

### Remote sensing and modelling of wind waves in semi-enclosed seas

The thesis addresses the quantification of wave properties, their dependence on the presence of ice and possible changes in the wave loads in the semi-enclosed and seasonally ice-covered Baltic Sea. The analysis is based on 25 years of satellite altimetry data (1992–2015) about wave height, satellite information about ice conditions and simulations of wave properties using the wave model WAM for the northern part of the sea, and wave modelling using the wave model SWAN in the Gulf of Riga.

The technique of Empirical Orthogonal Functions (EOF) is used for the first time for satellite-derived wave information in this water body. Simulations using synthetic data with various inserted patches and levels of noise demonstrated that this technique reliably recovers small patterns of changes, down to  $1.5 \times 1.5^\circ$  in idealised almost noise-free data. The minimum recognised pattern for the realistic 20% noise level is  $3^\circ \times 3^\circ$ .

The first winter EOF mode reveals the prominent east-west asymmetry of changes to the wave heights, with a faster increase in the western part of the sea. This mode has a strong link with the predominant teleconnection patterns in the area. It has a strong negative correlation with the Scandinavia pattern (SCAND) and equally sound positive correlation with the North Atlantic Oscillation (NAO) and Arctic Oscillation (AO) indices. The sliding analysis reveals substantial decadal variations in the correlation between this mode and the three indices. The SCAND pattern had a robust (statistically significant at a 95% level) strong correlation with, and strong influence on, Baltic Sea wave heights in the period 2000–2009. The correlation with the NAO and AO indices was weak during this decade. The situation was reversed in the 2010s.

Both satellite-based and *in situ* wave observations were employed together with the wave model WAM to explore the impact of the presence of sea ice on statistical properties of waves in the north-eastern Baltic Sea. The analysis is based on simulations of hypothetical ice-free wave climate for 1979–2007. The mean properties of waves (significant wave height, wave energy, energy flux) are passably represented by ice-free simulations. The presence of ice leads to relatively small changes (usually <5% and up to 20–25% at a few locations) in the average wave height, energy, and energy flux. The total loss of sea ice would lead to great (usually >50% and up to 82% for wave energy and 87% for wave energy flux) increase in the cumulative wave energy and energy flux. The average wave properties and the ice season duration are almost uncorrelated in the Sea of Bothnia and Bay of Bothnia. These quantities have a strong and statistically significant at a >99% level negative correlation at the latitudes of the Gulf of Finland where the later appearance of sea ice may lead to substantial increase in wave loads.

The impact of bathymetry-driven refraction on the wave propagation direction in totally ice-free climates is analysed for the Port of Ringsu port on the island of Ruhnu in the Gulf of Riga (Gulf of Livonia) based on simulations of saturated wave fields. The changes to wave propagation directions are minor (usually less than  $30^\circ$ ) for low wind speeds (5 m/s) but reach  $180^\circ$  for longer waves generated at wind speed of 15 m/s. Saturated waves excited by this wind speed are redirected by up to  $180^\circ$ . The waves propagate almost directly into the harbour entrance for any wind direction. Therefore, the port entrance has to be re-designed to provide shelter for ships in warmer climates with less sea ice.

## Lühikokkuvõte

### Tuulelainete kaugseire ja modelleerimine poolsuletud merealadel

Väitekiri käsitleb lainetuse ja lainekoormuste muutumist keeruka kujuga merealadel sõltuvalt kliimamuutusest ja sellega seonduvast jääolude teisenemisest, kombineerides kaugseire ja modelleerimise vahendeid. Analüüs toetub 25 aasta (1992–2015) satelliitaltimeetria andmetele lainekõrguse kohta Läänemerel, kaugseire teel saadud jääolude kirjeldusele, mudeliga WAM simuleeritud lainetuse parameetritele Läänemerel ning mudeliga SWAN simuleeritud lainetuse omadustele Liivi lahes.

Empiiriliste ortogonaalsete funktsioonide (EOF) tehnika on esmakordselt rakendatud altimeetria abil hinnatud Läänemere lainekõrguste ruumilise mustri muutuste analüüsimiseks. On näidatud, et EOF tehnika identifitseerib määravas andmestikus usaldusväärselt muutuste mustreid alates suurusel  $1.5 \times 1.5^\circ$ . Tugevama müra puhul meetodi lahutusvõime väheneb. Suhtelise mürataseme (mõõtmiste määramatuse) 20% puhul tunneb tehnika ära mustreid suurusega alates  $3^\circ \times 3^\circ$ .

Talviste lainetuse tingimuste EOF esimene mood (ehk tugevaim muster) näitab, et mere lääneosas on lainekõrgused kasvanud märksa kiiremini, kui idaosas. On näidatud, et muutused on seotud Läänemerd mõjutavate ilmapuustritega. On identifitseeritud selle moodi negatiivne korrelatsioon nn Skandinaavia võnkumise (SCAND) tugevusega ja sama tugev positiivne korrelatsioon Põhja-Atlandi võnkumise (NAO) ning Arktika võnkumise (AO) indeksitega. Korrelatsioonide tugevus on 1992–2015 radikaalselt muutunud. SCAND mustri indeks oli tugevas (>95% tasemel) korrelatsioonis Läänemere lainekõrgusega 2000–2009, mil lainekõrguse korrelatsioon NAO ja AO indeksitega oli ebaoluline. Kirjeldatud korrelatsioonide tugevus muutus vastupidiseks alates 2010.

Altimeetria andmestiku, mõõdetud ja mudeliga WAM rekonstrueeritud lainekõrguste ning merejää vaatluste alusel on hinnatud jääkatte mõju lainekliima statistilistele parameetritele Läänemere põhja- ja kirdeosas. On näidatud, et idealiseeritud jäävabal merel aastate 1979–2007 jaoks rekonstrueeritud lainekõrguste statistika esitab rahuldavalt ka lainetuse omadusi (nt keskmine lainekõrgus, lainetuse energia ja energia voog) situatsioonis, kus osa aastast on merel jää. Jääperioodi arvestamine modifitseeris keskmisi suurusid enamasti vähem kui 5% ning vaid üksikutes kohtades 20–25%. Demonstreeriti, et jää kadumine tähendab suuri muutusi lainetuse kumulatiivsetes omadustes, nagu summaarne lainetuse energia (mis kasvab üldiselt >50%; mõnedes kohtades kuni 82%) või energia voog (kuni 87%).

Botnia lahe põhjaosas praktiliselt puudub korrelatsioon lainetuse keskmiste parameetrite ja jääperioodi pikkuse vahel. Samas on nende suuruste vahel tugev korrelatsioon (statistilise usaldusväärsuse tase >99%) Soome lahe laiuskraadidel, kus jääperioodi lühenemine võib tähendada lainekoormuse kiiret kasvu.

Jääkatte kadumisega seonduvaid lokaalseid mõjusid hinnati Ringsu sadama jaoks Ruhnul. Jäävabal ajal esinevate tormidega tekkiva küllastunud lainetuse omadused rekonstrueeriti mudeliga SWAN. Näidati, et refraktsiooni mõju lainete levikusuunale on ebaoluline (üldiselt alla  $30^\circ$ ) nõrkade (5 m/s) ja mõõdukate (10 m/s) tuulte puhul. Tugevate tuultega (15 m/s) tekkinud lained võivad Ruhnul lähistel pöörduda  $180^\circ$  võrra. Selliste tuulte tekitatud lained levivad otse sadama sisse mistahes tuule suuna korral. See viitab vajadusele muuta sadama konfiguratsiooni, et tagada akvatooriumi turvalisus soojemas kliimas esinevate tormide puhul.



## Appendix: Papers constituting the thesis

### Publication I

**Najafzadeh F.**, Kudryavtseva N., Soomere T. 2021. Effects of large-scale atmospheric circulation on the Baltic Sea wave climate: application of the EOF method on multi-mission satellite altimetry data. *Climate Dynamics* 57(11), 3465–3478, doi: 10.1007/s00382-021-05874-x





# Effects of large-scale atmospheric circulation on the Baltic Sea wave climate: application of the EOF method on multi-mission satellite altimetry data

Fatemeh Najafzadeh<sup>1</sup> · Nadezhda Kudryavtseva<sup>1</sup> · Tarmo Soomere<sup>1,2</sup>

Received: 8 May 2020 / Accepted: 29 June 2021

© The Author(s), under exclusive licence to Springer-Verlag GmbH Germany, part of Springer Nature 2021

## Abstract

Wave heights in the Baltic Sea in the period 1992–2015 have mainly increased in the sea’s western parts. The linear trends in the winter wave heights exhibit a prominent meridional pattern. Using the technique of Empirical Orthogonal Functions (EOF) applied to multi-mission satellite altimetry data, we explain a large part of this increase with the Scandinavia pattern, North Atlantic Oscillation and Arctic Oscillation climatic indices. The winter trends show a statistically significant negative correlation (correlation coefficient  $-0.47 \pm 0.19$ ) with the Scandinavia pattern and a positive correlation with the North Atlantic Oscillation ( $0.31 \pm 0.22$ ) and Arctic Oscillation ( $0.42 \pm 0.20$ ). The meridional pattern is associated with more dominant north-westerly and westerly winds driven by the Scandinavia pattern and North Atlantic Oscillation, respectively. All three climatic indices show a statistically significant time-variable correlation with Baltic Sea wave heights during the winter season. When the Scandinavia pattern’s influence is strong, the North Atlantic and Arctic Oscillation effects are low and vice versa. The results are backed up by simulations using synthetic data that demonstrate that the percentage of variance explained using EOF analysis from the satellite-derived wave measurements is directly related to the percentage of noise in the data and that the retrieved spatial patterns are insensitive to the level of noise.

**Keywords** Baltic Sea · Wave climate · Satellite altimetry · Teleconnections · Wave heights · Empirical orthogonal functions

## 1 Introduction

The knowledge of both long-term changes and short-term variations in the wave climate has great importance for the safety of navigation (e.g., Barbariol et al. 2019), design purposes (e.g., Hemer et al. 2013), coastal protection (e.g., Weisse et al. 2012), and sediment transport (e.g., Masselink et al. 2016). In semi-sheltered seas, such as the Baltic Sea (Fig. 1), due to the limited size of the water body, small changes in the wind direction can lead to large spatio-temporal variations in the wave climate (e.g., Jönsson et al. 2003; Soomere and Räämet 2011; Kudryavtseva and Soomere

2017; Kudryavtseva et al. 2019) and alongshore transport patterns (Soomere et al. 2015). Therefore, to minimise coastal hazards and economic losses, and to provide adequate information for engineering and coastal planning in the future, it is crucial to determine the spatial and temporal variability of the wave climate.

Wave properties in different locations of the Baltic Sea have varied significantly over the decades (Suursaar and Kullas 2009; Różyński 2010; Soomere and Räämet 2014). For example, wave intensity showed a rapid drop in the northern part of the Baltic proper at the beginning of the 1980s, while it had a small increase along the Lithuanian coast (Kelpšaitė et al. 2008). The average significant wave height (SWH) in this basin, estimated using satellite altimetry, was in the range of 0.44–1.94 m during the period 1993–2015 with an increasing trend of 0.005 m/year (Kudryavtseva and Soomere 2017). The largest mean SWH of 1.2 m occurred in the Baltic proper (Nikolkina et al. 2014; Björkqvist et al. 2018) and also in the Sea of Bothnia, even though the seasonal appearance of ice in the Baltic Sea affected wave growth in this subbasin (Fig. 1). As expected, semi-enclosed

✉ Nadezhda Kudryavtseva  
nadezhda.kudryavtseva@taltech.ee

<sup>1</sup> Wave Engineering Laboratory, Department of Cybernetics, School of Science, Tallinn University of Technology, Akadeemia tee 21, 12618 Tallinn, Estonia

<sup>2</sup> Estonian Academy of Sciences, Kohtu 6, 10130 Tallinn, Estonia

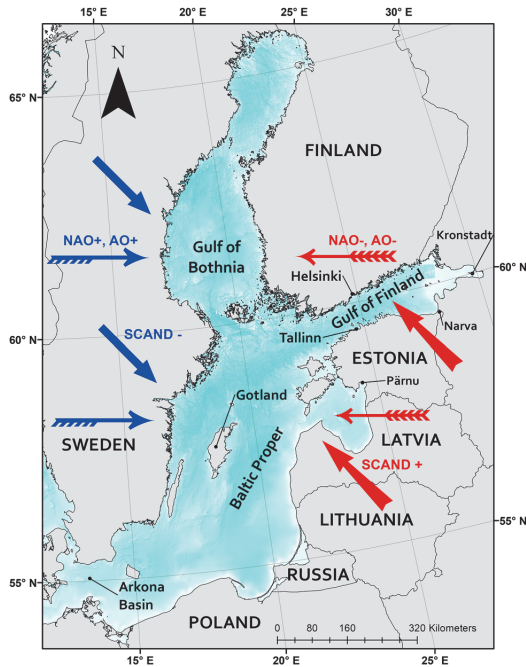


**Fig. 1** The study area, showing the predominant wind direction during the positive (red) and negative (blue) phases of the SCAND, and the positive (blue) and negative (red) phases of NAO and AO patterns. The figure was created using ArcMap software using the bathymetry data from Baltic Sea Hydrographic Commission, 2013, Baltic Sea Bathymetry Database version 0.9.3. Downloaded from <http://data.bshc.pro/> on 07.10.2019

areas of this basin, such as the Gulf of Finland, the Gulf of Riga, and the Bay of Bothnia were characterised by a lower range of the mean SWH, of 0.5–1.0 m (Tuomi et al. 2011; Nikolchina et al. 2014; Kudryavtseva and Soomere 2017).

The maximum SWH and peak periods reached ~8 m and 10–12 s respectively, in the northern part of the Baltic proper (Tuomi et al. 2011) and in the Sea of Bothnia (Björkqvist et al. 2020), ~6 m and 8–11 s at the entrance to the Gulf of Finland, and ~4 m and 6–8 s in the eastern part of this gulf (Räämet et al. 2010). Most of the wave events with SWH more than 7 m occurred from November to January (Björkqvist et al. 2018), and the roughest wave storms were in January 2005 (Suursaar and Kullas 2009) and January 2019 (Björkqvist et al. 2020). During the wave storm in January 2005, the measured SWH reached 7.2 m in the northern Baltic proper and 4.5 m in the Gulf of Finland (Soomere et al. 2008), while in January 2019, the SWH reached 8.1 m in the Sea of Bothnia (Björkqvist et al. 2020).

One of the main drivers of wind properties is the different phases of atmospheric circulation, which can be explained

in connection with climate change (Wang et al. 2004). The Baltic Sea is located in a transition area between the North Atlantic Ocean and the continental area of Eurasia. Consequently, the wave climate in this basin is highly influenced by processes that are represented by the North Atlantic Oscillation (NAO), Arctic Oscillation (AO), and Scandinavia pattern (SCAND, previously Eurasia-1, Barnston and Livezey 1987) climate indices.

The NAO pattern is one of the most prominent teleconnection patterns over the North Atlantic and European regions in all seasons (e.g., Walker and Bliss 1932). However, it had the strongest influence over the Baltic Sea in winter (Różyński 2010) explaining an essential part of SWH variability from December to February. This climatic index reflects the intensity of the north–south dipole of anomalies with one centre located over Greenland and another in the North Atlantic at latitudes ~40° N. In terms of the wind direction, the positive phase of the NAO corresponds to stronger westerly winds. During the negative phase, westerly winds are weaker, and the winds from the east and north-east are more frequent (Fig. 1; e.g., Trigo et al. 2002).

The AO characterises the air circulating counter-clockwise at ~55° N latitude, in the Arctic. The AO is strongly related to the NAO. When the AO is in its positive phase, a belt of strong winds circulating the North Pole confines colder air inside the polar regions (e.g., Thompson and Wallace 1998). In the AO's negative phase, this belt becomes weaker, resulting in a southward movement of colder arctic air into the mid-latitudes, accompanied by increased storminess (Fig. 1). The positive phase of the AO, similar to the analogous phase of the NAO, corresponds to strong westerly winds over the Baltic Sea region. The negative phase of the AO results in a shift of storm tracks to the south and the winds from the east are more frequent in the region. The NAO and AO are widely used to connect regional climate variability to sea level (Andersson 2002; Jevrejeva et al. 2005; Passaro et al. 2015), storm events (Surkova et al. 2015; Kudryavtseva et al. 2021), SWH (Różyński 2010), and ice conditions (Jevrejeva et al. 2003) in the Baltic Sea.

The processes reflected by the NAO and AO have a time variable effect on the Baltic Sea region. A significant change in the frequency of cyclonic circulation occurred at the end of the nineteenth century, which presumably coincided with the retreat of the Little Ice Age (e.g., Omstedt et al. 2004). The sea-level records showed a changing effect of the NAO and AO on the Baltic Sea water level with a decrease in the correlation of the relevant time series with these indices in the period 1900–1954 (Andersson 2002; Jevrejeva et al. 2005), and an increase in the period 1980–2000 (Wakelin et al. 2003; Jevrejeva et al. 2005; Suursaar and Sooäär 2007). There are also indications of spatial dependence of the correlation between the NAO index and sea level. The reported correlations were

very low in the period 1961–1980 at Narva and Pärnu tide gauges (Suursaar and Sooäär 2007) but much stronger at Wismar, Kronstadt, and Cuxhaven during the same time period (Jevrejeva et al. 2005). The time variability of the correlation with the NAO index is also prominent in the temperature (e.g., Jacobeit et al. 2001) and ice conditions (e.g., Jevrejeva et al. 2003). However, the possibility of a time variable relationship between the NAO and AO or the other climatic indices with the Baltic Sea wave climate is currently not studied.

The SCAND pattern consists of a main circulation centre over Scandinavia, with weaker centres of an opposite sign over eastern Russia and Western Europe. This pattern affects regional weather conditions and westerlies mostly in winter (Gao et al. 2017). During the negative phase of the SCAND, the wind rotates anticlockwise around the midpoint of the anomaly, creating strong westerly or north-westerly winds over northern Europe, Scandinavia, and the Baltic Sea region. During the SCAND positive phase, the wind reverses its direction, rotating clockwise, which results in a belt of strong easterly and south-easterly winds (Bueh and Nakamura 2007; Gao et al. 2017). Figure 1 shows wind directions during the positive and negative phases of the SCAND over the Baltic Sea (Bueh and Nakamura 2007). This pattern's positive phase blocks the cold air in central Eurasia with below-average temperatures across central Russia and Western Europe.

While the most influential atmospheric teleconnections in the Baltic Sea region are NAO, AO, and SCAND, in some studies, the East-Atlantic West-Russia (EAWR), the East Atlantic (EA), the Polar-Eurasia (POL), and the Atlantic Multidecadal Oscillation (AMO) are considered as the drivers of precipitation patterns (Jaagus 2009; Irannezhad et al. 2014) and coastal upwelling (Bednorz et al. 2018). However, it is still unclear what the links between these climatic indices and the wave climate are.

There are three different data collecting methods for wave climate studies: modelling, in situ measurements and remote sensing. The most common wave models used in the Baltic Sea are the third-generation models WAM (Hasselmann et al. 1988; Komen et al. 1994; Cavaleri and Bertotti 1997) and SWAN (Booij et al. 1999). Based on these models, several hindcasts of the wave climate (Soomere 2005; Cieřlikiewicz and Paplińska-Swerpel 2008; Björkqvist et al. 2018; Tuomi et al. 2019) and studies of the annual and decadal changes of SWH in the Baltic Sea (Soomere and Räämet 2014) were performed. Due to different model parameters and, in particular, depending on the wind forcing, there are mismatches between different model outputs (Tuomi et al. 2011; Soomere and Räämet 2011; Räämet and Soomere 2021). In situ measurements are the primary source in the assessment of the local wave climate. However, relevant devices do not cover the whole area of interest,

and the wave measurements are limited to the ice-free time (Madsen et al. 2007; Cieřlikiewicz and Paplińska-Swerpel 2008; Tuomi et al. 2011). Hence, in situ measurements are restricted only to a few locations and provide a limited knowledge of wave field spatial variability.

Significant advances in satellite technology made it possible to obtain homogeneous and continuous wave data over vast areas. SWH derived from high-resolution satellite-based techniques such as Synthetic Aperture Radar (SAR) in 2012–2017 were compared with in situ data over the Baltic Sea (Rikka et al. 2018). Although there is a good agreement between the SAR and in situ wave height data, the SAR data cover only a short period of 5 years and cannot be used to reconstruct long-term wave climate variability. Satellite altimetry has become a powerful tool for studying the global wave climate and its relation to the climatic indices (Hannachi 2004). For example, a strong relationship between the interannual variability of SWH (including trends) and both the AO and NAO revealed a connection between these climate indices and the interannual extreme wave climate in the North Atlantic (Izaguirre et al. 2011).

However, the use of satellite altimetry is problematic in coastal areas (e.g., Madsen et al. 2007) and in partially ice-covered (e.g., Brenner et al. 1983) water bodies like the Baltic Sea. For these reasons, the wave height data from satellites has been used scarcely in this region until recently. A significant effort towards validating the long-term multi-mission SWH data with the available in situ wave measurements in the Baltic Sea region was performed by Kudryavtseva and Soomere (2016). This validation made it possible to study in detail spatial and temporal variations of the Baltic Sea wave climate over the last few decades. Significant spatial variability was detected over this basin, which can be explained by a rotation of predominant strong wind directions rather than an increase in the wind speed (Kudryavtseva and Soomere 2017). However, more effort is needed to identify the main drivers behind the spatial variability of wave heights in the Baltic Sea.

To examine this question in detail, the EOF method (Hannachi 2004) is applied in this study to the wave properties retrieved from satellite altimetry. The EOFs produce an expansion of data in a series of functions that separate the spatio-temporal variations (Niroomandi et al. 2018) and facilitate variability analysis in this domain. The EOF method is a robust tool to determine correlations between the wave climate and climatic indices. It has been widely used to study major modes of climate variability such as the NAO and the El Niño indices (Lionello and Sanna 2005; Nezlin and McWilliams 2003) and to estimate monthly distributions of large-scale sea-level variability on the global scale (Church et al. 2004). The EOF analysis extracted the predominant spatial patterns of monthly averaged wave height variability in wintertime in the northern hemisphere

(Shimura et al. 2013) and determined the “climate” of seasonal directional wave energy flux in the southern hemisphere (Hemer et al. 2010).

Several recent studies have addressed the options for the use of this technique in different regions. For example, EOFs helped establish an annual cycle and validate the Mediterranean Sea’s spatial wave distribution (Lionello and Sanna 2005; Cañellas et al. 2010; Sartini et al. 2017), to represent interseasonal variations in the Bengal region (Patra and Bhaskaran 2016) and to analyse the patterns of sea surface temperature and salinity in the Baltic Sea (Zujev et al. 2021). It has also been used to define long-term trends and spatio-temporal variability of SWH in Chesapeake Bay (Niroomandi et al. 2018). In the Baltic Sea, this method was applied to evaluate the main properties of the wave climate of the Baltic Sea using a 5-year hindcast dataset in the period 1988–1993 (Mietus and von Storch 1997). The first EOF of the wave properties revealed a significant anomaly of SWH in the eastern part of the Baltic Sea. The second and the third EOFs described an anomaly of SWH from the southwest to the northeast and an oscillation between the eastern and western parts of the basin, respectively (Mietus and von Storch 1997).

In this study, a multi-mission satellite altimetry SWH dataset is used, which was previously validated against all available in situ wave measurements for the Baltic Sea basin (Kudryavtseva and Soomere 2016). Based on these data, spatial and temporal variations of monthly averages of the SWH in the Baltic Sea are analysed by applying the EOF method, and a correlation analysis is performed between the EOF modes and various climatic indices.

The manuscript is organised as follows. First, a description of the data and the methodology is introduced in Sect. 2. In Sect. 3, the EOF technique is used to retrieve the SWH pattern in the Baltic Sea. Discussion and conclusions are presented in Sect. 4.

## 2 Materials and methods

### 2.1 Satellite altimetry data

The satellite altimetry SWH data from nine satellite missions, namely GEOSAT, ERS-1, TOPEX, ERS-2, ENVISAT, JASON-1, JASON-2, CRYOSAT-2, and SARAL, covering the period 1992–2015 (24 years) with 710,344 measurements in total, were used in this study. The data were obtained from the Radar Altimeter Dataset System (RADS) database (Scharroo 2012; Scharroo et al. 2013) and are available for download at <http://rads.tudelft.nl/rads/rads.shtml> (accessed 1 March 2021).

Several features of the Baltic Sea, such as the seasonal ice cover (Tuomi et al. 2011), complicated geometry and

the presence of extensive archipelago areas in this relatively small basin (Madsen et al. 2007) can significantly affect the quality of satellite data (Kudryavtseva and Soomere 2016). Therefore, data with backscatter coefficient > 13.5 cdb, large errors in SWH normalised standard deviation, data closer than 0.2° to the coast, or measured over the sea areas with more than 30% ice concentration were eliminated from further analysis and all measurements were corrected for biases (Kudryavtseva and Soomere 2016). Finally, the data were thoroughly checked for consistency and possible erroneous measurements and validated against the in situ wave records (Kudryavtseva and Soomere 2016).

The resulting dataset (Fig. 2) proved to be well suitable for the analysis of the Baltic Sea wave climate (Kudryavtseva and Soomere 2017). More than two decades of satellite altimetry data with a large number of measurements provide excellent spatial and temporal coverage over the Baltic Sea. The wave fields here exhibit intricate variability patterns in both temporal and spatial domain (e.g., Jönsson et al. 2003; Soomere and Räämet 2011; Kudryavtseva and Soomere 2017). To extract these patterns, an EOF analysis, which separates individual modes of variability, was performed on monthly-averaged SWHs. The analysis was implemented using the software package “spacetime” (version 1.2–1) in R (version 3.4.4).

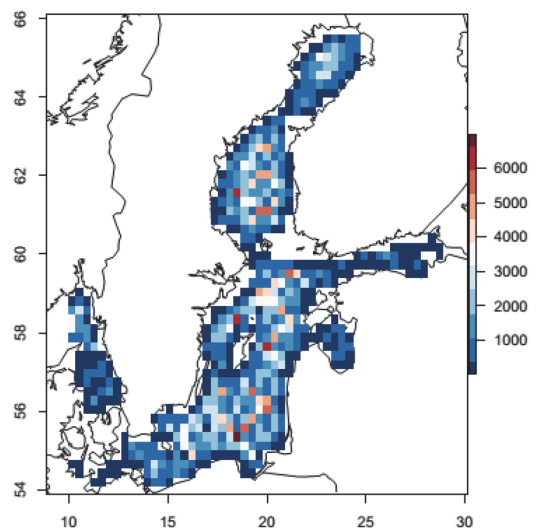


**Fig. 2** Spatial distribution of the number of satellite altimetry SWH data in the Baltic Sea for the period 1992–2015. The figure was created using R software (version 3.4.4, using “mapdata” and “maps” packages)

## 2.2 Data gridding

Each satellite altimetry mission measures continuous data only along a specific line. Merging the measurements from different missions into a combined dataset provides much better spatial and temporal coverage but can be prone to gaps. Due to differences in orbits of various missions, the gaps are not regular, which significantly complicates further analysis.

A monthly averaged dataset with a regular rectangular grid was created. The latitudes and longitudes ranged from 54.11° N to 65.57° N and from 10° E to 28.83° E, respectively. Different grid sizes and their effect on the results were thoroughly tested, and the cell size of 0.8° × 0.8° showed the optimal performance. Additionally, the grid size effect on the percentage of temporal variability retrieved by EOF was studied. No dependency of the resulting EOFs on the grid resolution was detected. Despite an increase in resolution, no significant change in the magnitude of reconstructed temporal variability was found.

Due to the nature of the satellite altimetry data, each grid cell has a different number of measurements (Fig. 2). A small number of observations in a particular cell can lead to errors in the EOF results. Hence, the cells with less than a certain number of measurements should be omitted from the analysis. To test the optimal lower cut-off value, the distribution of the number of measurements per grid cell was examined. Interestingly, it was very close to a uniform distribution. To calculate the minimum number of measurements in a single grid cell that does not cause errors in the EOF results, the cut-off values varied in the range from 2%-iles to 5%-iles and the EOF analysis results were compared. This test was performed for the whole dataset and for several subsets containing measurements during various seasons. The 2nd percentile cut-off provided consistent results and was used in further analysis. As a result, the grid cells that have less than 645 (whole dataset), 181 (winter), 141 (spring), 145 (summer), and 180 (autumn) measurements were omitted, leaving more than 99.1% of the data available for the analysis. Most of the omitted data were from the Gulf of Finland, a narrow gulf with a rugged coastline. The spatial distribution of the other omitted data points appeared to be random and therefore does not affect the retrieved wave climate spatial patterns.

## 2.3 Averaging errors

To create a more complete dataset, a monthly average SWH was calculated for each grid cell before applying the EOF method. Due to the natural variability of wave heights on timescales shorter than a month in this water body (Soomere

and Eelsalu 2014), each monthly average has an uncertainty. This uncertainty  $\sigma$  was estimated as an error of the mean:

$$\sigma = \frac{sd(SWH_t)}{\sqrt{N}}, \quad (1)$$

where  $SWH_t$  is a set of SWH measured for one month in one grid cell, and  $N$  is the number of the data points in each grid cell for that month. A characteristic error of the mean for the whole dataset was estimated as the median of  $\sigma$ . The typical error of the mean in the dataset of interest is ~9%.

## 2.4 Simulated data sets

To characterise the effect of spatial and temporal gaps (that are inherent in the satellite altimetry data) on the resulting EOFs, simulated data were created and thoroughly tested. The gaps in the data appear due to the variable ice cover, proximity to the coast and satellite tracks. Synthetic data with distinct zonal and meridional patterns were generated and classified as:

*Scenario A:* A simulated dataset with a distinct zonal (north-south) variation of wave heights, where the wave heights in the northern part (to the north of 59° N) follow a linear trend of 0.005 m/year and the SWH in the southern part has no distinct long-term variability (Fig. 3). The northern part includes the Bay of Bothnia, the Sea of Bothnia and the Gulf of Finland and the southern part comprises the Gotland Basin, the Gulf of Riga, the Bornholm Basin and the Arkona Basin.

*Scenario B:* A simulated dataset with a prominent meridional (west-east) variation of wave heights. The SWH in the western part (to the west of 19.4° E) follows a linear trend of 0.005 m/year, and in the eastern part, the wave heights have no long-term variability (Fig. 4). The eastern part covers the Bay of Bothnia, eastern Sea of Bothnia, the Gulf of Finland, the Gulf of Riga and the Eastern Gotland Basin.

These created datasets emulated precisely the same timings and locations as the actual multi-mission satellite measurements. The trend of 0.005 m/year was assigned as a measured SWH trend in the Baltic Sea (Kudryavtseva and Soomere 2017). Gaussian random noise was added to all the simulated data. To test the effect of noise level on the retrieval of the wave height spatial distribution, the width of the relevant (Gaussian noise) distribution was varied from 5 to 30% of the total average of the simulated wave heights.

The EOF analysis results on the simulated data are shown in Fig. 3 for the zonal and Fig. 4 for the meridional spatial

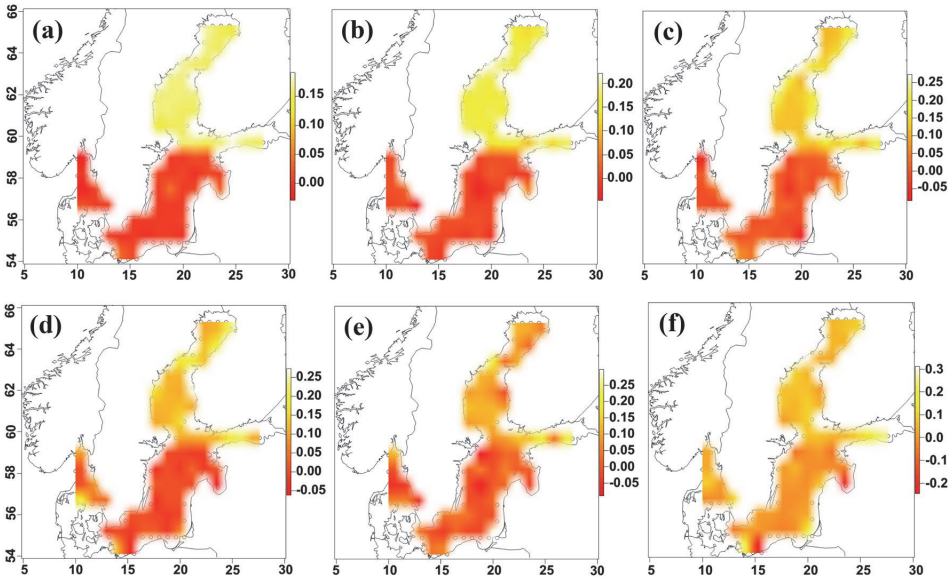


**Fig. 3** The first EOF patterns for simulated datasets (Scenario A) with introduced random noise at the level of 5% (a), 10% (b), 20% (c), 25% (d), 27% (e), and 30% (f). The data were interpolated for

ease of interpretation. The figure was created using R software (version 3.4.4, using “mapdata” and “maps” packages)

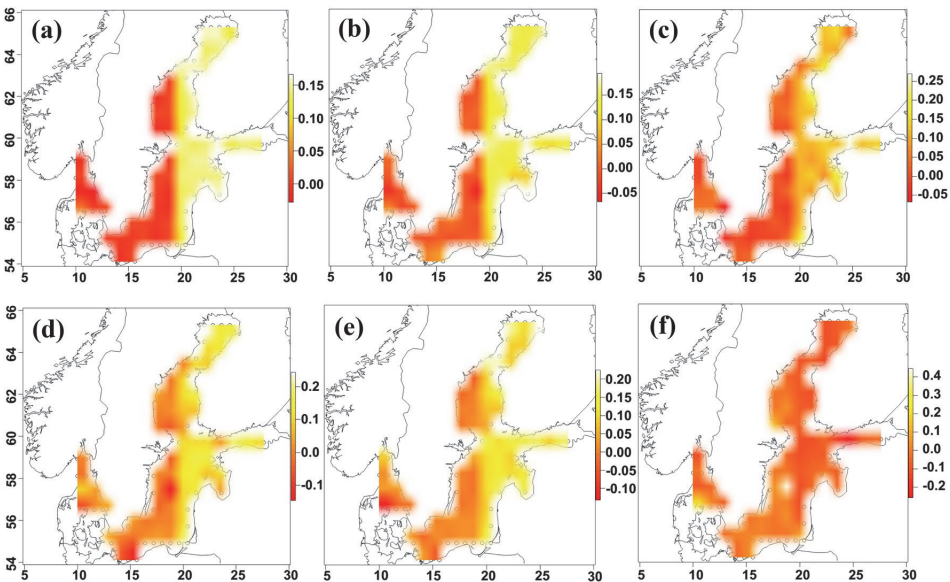
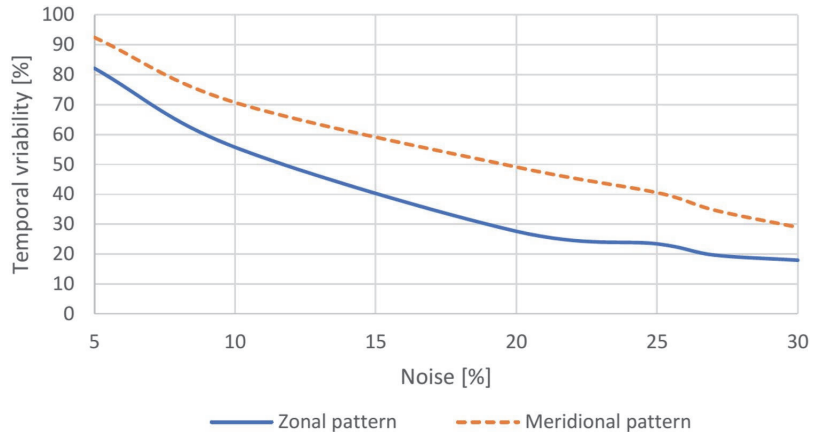


**Fig. 4** The first EOF patterns for simulated data (Scenario B) with introduced random noise at the level of 5% (a), 10% (b), 20% (c), 25% (d), 27% (e), and 30% (f). The data were interpolated for ease of

interpretation. The figure was created using R software (version 3.4.4, using “mapdata” and “maps” packages)

**Fig. 5** Reconstructed percentage of variability of the first EOF mode versus a percentage of introduced uncertainty in the synthetic datasets. The solid blue line represents the dataset with the introduced zonal pattern (Scenario A), and the orange dashed line is the dataset with the meridional pattern (Scenario B)



patterns. The first EOF pattern between northern and southern parts as well as eastern and western parts of the Baltic Sea is visible when the noise level is less than 30%. However, at the noise level higher than 30%, the spatial pattern disappears. These features indicate that (i) spatial and temporal gaps of the satellite altimetry data do not significantly affect the EOF results and (ii) the results of the EOF analysis are susceptible to the noise level.

The percentage of retrieved variance explained by the first EOF mode diminishes with an increase in the noise level (Fig. 5). The low level of introduced noise (5%) results in high variance of ~90% for the simulated datasets in both spatial patterns. However, the highest level of introduced uncertainty (30%) leads to only 18% and 29% of retrieved temporal variabilities for zonal and meridional patterns, respectively. Therefore, this indicates that the temporal signal's strength obtained with the EOF technique highly depends on the noise level. In particular, the noise in the data can substantially reduce the percentage of variability reflected by the first EOF, even for clearly visible and defined spatial patterns. For example, in Fig. 3d, e and Fig. 4d, e the observed patterns are quite prominent, but the percentage of the recovered variability is less than 30% and 40% for zonal and meridional patterns, respectively. This indicates that even when the retrieved percentage of variability by the EOF method is relatively low, the method can detect correct patterns.

Considering that no other pattern was introduced in the simulated data, all the retrieved temporal variabilities by the 2nd and 3rd EOF modes should not be real as they are evidently caused by fake patterns picked up in the random noise. The second and third EOF modes for both scenarios retrieve less than 10% of the variance. This percentage then can be used as an indication of the reliability of the EOF method. Therefore, it is natural to assume that, for our

analysis, any EOF mode with a percentage of less than 10% variability is unreliable.

To test whether there is any preference in detecting the meridional pattern better than the zonal pattern, the variance retrieved by the EOF method for both scenarios was compared. The difference of retrieved variance for scenarios A and B varies between 10 and 21% (Fig. 5). At low noise levels, the difference is marginal (10%). It increases with the introduced uncertainty until the noise level reaches 20% when the difference starts to decrease. Overall, the method exhibits a slight preference for detecting the meridional pattern compared to the zonal pattern. This feature reflects a higher density of satellite measurements in the east–west direction at the Baltic Sea latitudes.

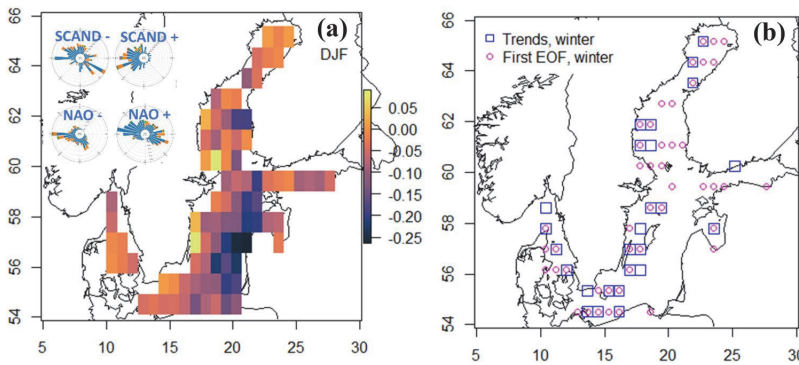
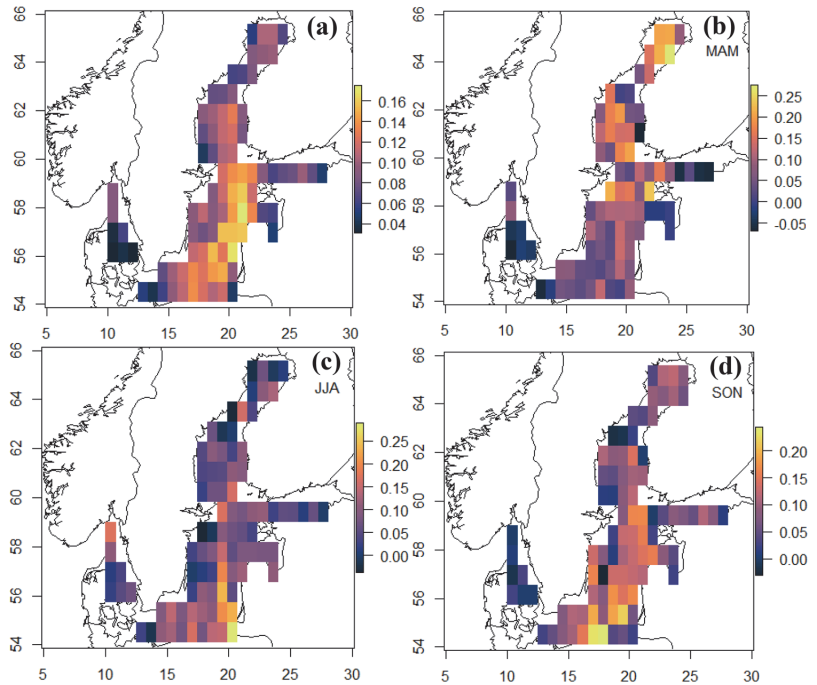
### 3 Results

#### 3.1 Spatial distribution of wave heights

The first EOF mode of the Baltic Sea wave heights over the whole study period (Fig. 6a) shows high values in the Baltic proper, both in the southern and eastern parts. The lower values are observed in the Gulf of Finland, the Gulf of Riga, the Danish straits, and the Gulf of Bothnia. This spatial pattern in the central Baltic Sea qualitatively matches the results of the EOF analysis of the modelled wave climate (Mietus and von Storch 1997), where the first EOF mode also showed higher values in the eastern part of the Baltic proper.

To study the seasonality of wave patterns, two approaches are used. The first approach uses the classification of the seasons into a “stormy” period, which includes the months from January to March and from August to December and a “calm” period, which lasts from April to July (Soomere and Pindsoo 2016; Männikus et al. 2020). The EOFs are also

**Fig. 6** First EOFs describing the main patterns in the Baltic Sea wave heights retrieved for the entire SWH data set in (a), spring (b), summer (c), and autumn (d) seasons. The figure was created using R software (version 3.4.4, using “mapdata” and “maps” packages)

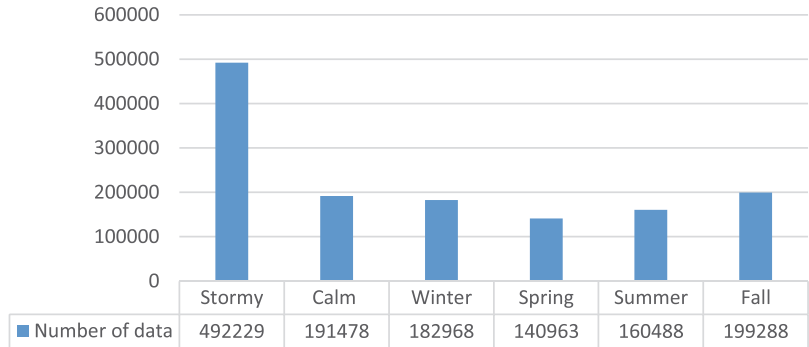


**Fig. 7** a The first EOF pattern for the winter season (DJF). The wind roses show typical winter wind direction during the SCAND positive (01 Dec 1998–26 Feb 1999) and negative (01 Dec 2005–28 Feb 2006) phases and the NAO positive (01 Dec 1994–28 Feb 1995) and negative (01 Dec 1995–28 Feb 1996) phases at Hultsfred station 57.53° N, 15.82° E (obtained from Swedish automatic wind measurement data, <https://mesonet.agron.iastate.edu/sites/locate.php>, last

accessed 01 Feb 2021). b The spatial coincidence of the linear trends in SWH in winter and the first EOF mode in winter. The trends were fitted for the 1996–2015 period using the same grid as the one used for the EOF method and are significant at 95% confidence level. Only the EOF values above  $-0.07$  are shown. The figure was created using R software (version 3.4.4, using “mapdata” and “maps” packages)

considered for usual seasons, such as winter (DJF, Fig. 7a), spring (MAM, Fig. 6b), summer (JJA, Fig. 6c), and autumn (SON, Fig. 6d). The spring and autumn seasons reveal a north–south structure, the spring showing higher values of the first EOF in the northern parts of the Baltic Sea, in the

Bay of Bothnia (Fig. 6b), whereas the autumn exhibits an EOF structure with the maxima in the southern Baltic and the Baltic proper (Fig. 6d). The EOFs for the summer season (Fig. 6c) reveal strong patchiness without a prominent large-scale pattern. The autumn and spring have the most and the

**Fig. 8** The total number of satellite altimetry measurements in each season**Table 1** Temporal variability explained by EOF modes for different seasons. The percentage of retrieved variance for the first three EOFs and the total variability are shown in each column

Seasons	First EOF (%)	Second EOF (%)	Third EOF (%)	Total variability (%)
Winter	27	9	8	44
Spring	17	14	12	43
Summer	22	9	8	39
Autumn	23	9	7	39
Stormy	19	12	8	39
Calm	17	11	10	38
All seasons	17	13	10	40

least number of satellite altimetry snapshots, respectively (Fig. 8). The percentages of retrieved variance with the EOF analysis are shown for different seasons and the whole year in Table 1. The total temporal variability, explained by the first three EOF functions, ranges from 38% for the calm period up to 44% in winter.

The winter season shows the strongest signal in the first EOF. Additionally, this season reveals a prominent meridional pattern (Fig. 7a). The first EOF mode is negative in the eastern part of the Baltic proper and the eastern part of the Gulf of Bothnia, whereas it shows positive values in the western parts of these water bodies. The meridional pattern is remarkably similar to the spatial distribution of linear trends (Fig. 7b) fitted to the winter season yearly averages for the 1996–2015 period (the detailed description of trends is discussed in Kudryavtseva and Soomere 2017).

The linear trends shown in Fig. 7b are fitted using the same grid as used for the EOF analysis (Sect. 2.2) for better comparison of the results. Instead of monthly averaging, seasonal averaging was performed. The trends were fitted for each grid cell, however, only the trends with the statistical significance > 95% are shown in Fig. 7b. The probability of the coincidence that statistically significant linear trends are detected in the same cell where the first

EOF has a value higher than a particular cut-off value was thoroughly tested. The selection of values above the cut-off value of  $-0.07$  provides the highest probability of coincidence. This cut-off value results in 77% of grid cells with the detected linear trends coinciding with the first winter EOF pattern. In other words, that 77% of grid cells with the significant linear trend are located precisely at the same locations as the grid cells with winter EOF above  $-0.07$ . Therefore, the loci of sea areas with statistically significant trends in the wave height is remarkably similar to the expression of the first EOF function, meaning *that the first winter EOF is associated with the linear trends in SWH*.

### 3.2 Reliability of spatial patterns

In this study, the variance explained by the first EOF is only ~27% for the winter season. The model-based studies of wave climate with the EOF method revealed a much stronger signal in the Baltic Sea (Mietus and von Storch 1997; Shimura et al. 2013). However, similar satellite-based studies also reported a low percentage of retrieved variance of the first EOF. For example, Hemer et al. (2010) using multi-mission altimeter data, found that the first EOFs of the wave climate explain only 17–19% of the wave climate variability. Similarly, Woolf et al. (2002) found that for the North Atlantic satellite-derived wave climate, the first EOF explains 41% of the variance, while the other EOFs each explain < 19% of temporal variability. The dependence of this proportion on the gaps and noise in the satellite altimetry data are not widely discussed.

The detailed analysis of the simulated datasets performed in Sect. 2.4 demonstrates that the noise level in the satellite data significantly affects the percentage of retrieved variance but that the shape of the retrieved spatial patterns is practically not affected (Fig. 5). With the considerable noise level, the amount of temporal variability explained by the first EOF can become as low as 20% even for a very distinctive

and robust pattern in simulated data. However, even with high noise levels and the low percentage of variability, the EOF method can still reconstruct the correct spatial pattern (Figs. 3e, 4e). Therefore, the relatively low variance retrieved with the EOF method from satellite altimetry data (e.g., Hemer et al. 2010) is most likely caused by substantial uncertainty in the data. Hence, it is likely that the observed meridional pattern in the first EOF (Fig. 7a) does represent a real pattern of the wave climate, even if it has a relatively low percentage of retrieved variance.

### 3.3 Relation between SWH trends and large-scale atmospheric teleconnections

To study whether the Baltic Sea wave climate and trends in SWH are driven by changes in the large-scale atmospheric circulation, a correlation analysis was performed between the first three EOFs, signifying the spatio-temporal modes of the Baltic Sea wave climate, and various climatic indices. To match the satellite altimetry data's monthly timescales, the monthly time series of the climatic indices were used. The climatic records were obtained from the NOAA Center for Weather and Climate Prediction.

The strongest correlation between the first EOF for the winter season and the SCAND climatic index is negative, with a correlation coefficient of  $-0.47 \pm 0.19$  (Table 2). The SCAND pattern exhibits substantial seasonal variability. Interestingly, the correlation of the first EOF mode with the SCAND also shows variability over different seasons. It is the lowest throughout the spring season ( $0.24 \pm 0.22$ ). During the summer and autumn the correlation is positive,  $0.38 \pm 0.20$  and  $0.36 \pm 0.21$ , respectively, reflecting a prevailing (south-)easterly wind direction during these seasons.

The uncertainty of the correlation, evaluated in terms of the 95% confidence intervals, was used as a measure of reliability. Only three studied climatic indices exhibit a correlation larger than the uncertainty intervals for the winter season, namely the SCAND, the AO, and the NAO indices. Contrary to the SCAND index, the AO and NAO indices show positive correlations, with the coefficients of  $0.42 \pm 0.20$  (AO) and  $0.31 \pm 0.22$  (NAO). Both the AO and NAO indices have a significant correlation with the first EOF

mode during the winter season. For all other seasons, this mode reveals no correlations larger than the uncertainty. The correlation analysis performed between the other climatic indices, namely AMO, EA, EAWR, POLEUR and the first three EOFs indicated no significant correlation. The EAWR index shows a correlation coefficient of  $0.26 \pm 0.22$  with the first winter EOF, which is slightly higher than the associated uncertainty.

The estimated values of correlation coefficients are close to similar values from correlation analysis between the annual number of storms in the Baltic Sea with the SWH larger than 2 m and various teleconnections reported by Myslenkov et al. (2018) and Medvedeva et al. (2016) where they found a correlation of  $-0.59$  with the SCAND,  $0.32$  with the AO, and  $0.12$  with the NAO index based on the wave modelling results and NCAR reanalysis. This similarity indicates that the first winter EOF and the SWH trends are affected by the same processes as the storminess. Slightly stronger positive correlations with the NAO and AO indices and a weaker negative correlation with the SCAND index were obtained for SWH > 4 m using wave hindcast for a more extended period 1950–2010 (Surkova et al. 2015). A stronger positive correlation in Surkova et al. (2015) was most likely caused by the rapid reaction of wave fields to the time variability of the main teleconnection patterns' influence over the Baltic Sea region.

The relationship between the wave height variability and the climatic indices was also studied at a few wave measurement locations. Wave records at Vilsandi in the West Estonian Archipelago showed a correlation coefficient of the SWH with the NAO indices at the level of 0.7 during the period 1966–2006 (Suursaar and Kullas 2009). However, only a mild relationship between the NAO index and SWH was found in the southern Baltic (e.g., at Lubiatowo in January (Różyński 2010)). Therefore, it is likely that the impact of phenomena that govern the NAO index effects on the Baltic Sea wave fields dramatically varies in different locations and periods. This feature is not unexpected because the Baltic Sea wave climate's severity substantially depends on the match of predominant strong wind directions with the water body's geometry.

### 3.4 Time variable correlation with climatic indices

To study possible time variability of the influence of the processes behind climatic indices on the wave climate of the Baltic Sea, a sliding correlation analysis was performed. A Pearson's product-moment correlation implemented in the "stats" package (R version 3.4.4) was used for the correlation analysis between the first three dominant climatic indices (SCAND, AO, and NAO) during the winter months and the first EOF in winter. The use of Kendall and Spearman correlations leads to the same results. Different window

**Table 2** Correlation coefficients between climatic indices and first three EOFs for the winter season. The correlation of the most prominent climatic indices is presented

Climatic Index	First EOF	Second EOF	Third EOF
SCAND	$-0.47 \pm 0.19$	$0.01 \pm 0.24$	$-0.07 \pm 0.24$
AO	$0.42 \pm 0.20$	$0.19 \pm 0.23$	$-0.03 \pm 0.24$
NAO	$0.31 \pm 0.22$	$0.19 \pm 0.23$	$-0.09 \pm 0.24$

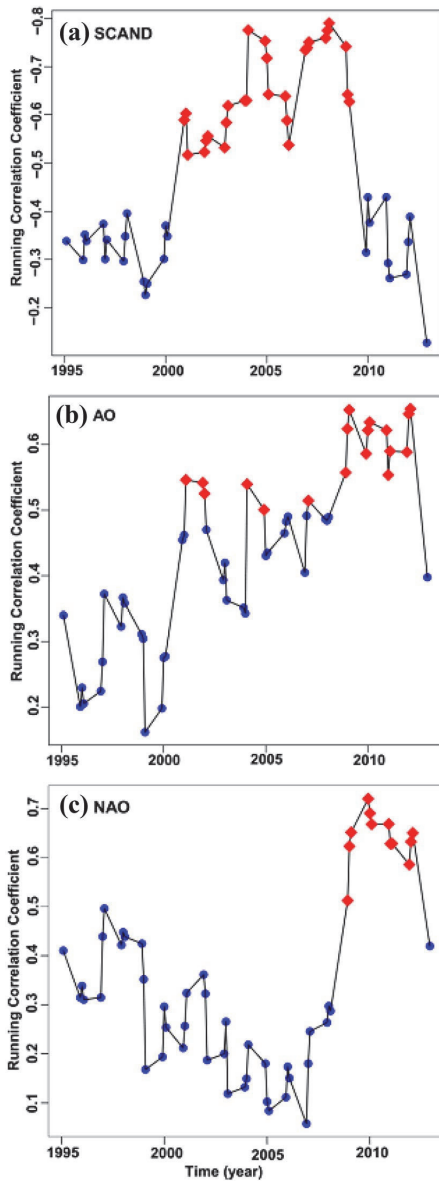


**Fig. 9** Sliding correlation coefficient between the first EOF and **a** Scandinavia pattern, **b** Arctic Oscillation, and **c** the North Atlantic Oscillation with 5-year window size. The correlations with >95% level of statistical significance are indicated in red

lengths from 2 to 9 years were tested (with one-year step), and the window with a length of 5 years was selected as it provided the optimal noise level.

For all three climatic indices, the sliding correlation coefficients (called correlations below for brevity) with the first winter EOF exhibit significant time variability (Fig. 9). The SCAND index revealed the highest values (between  $-0.5$  and  $-0.8$ ) from 2000 to 2009. The correlation with the SCAND index was statistically significant at a >95% level during these years. The significance was calculated in a classical manner using the Pearson  $p$  value criteria of  $<0.05$ , which considers both the magnitude of correlation and the number of entries in the time series. The SCAND index has a predominantly negative correlation with the first winter EOF mode. After 2009 the correlation between the index and the wave climate in the Baltic Sea drastically diminishes.

The sliding correlation between the AO index and the first winter EOF is in the range of  $0.16$ – $0.66$ , reaching a maximum in 2012. Throughout 2008–2012, the correlation had a robust value of  $\sim 0.55$  and was statistically significant at a 95% level. The maximum correlation for the NAO index was  $0.72$  in 2010. Between 2009 and 2012, the correlation surged and had the largest values (above  $>0.5$ ) and was consistently statistically significant at a 95% level. The correlation of the first winter EOF with the AO and NAO indices gradually increased from 2008 until 2012. The correlation of NAO index surged to the highest value in 2009 and fluctuated until 2012, while the AO index correlation increased more slowly than the NAO index correlation over this period.

The NAO and AO indices' correlation with the winter first EOF was relatively low in the 1995–2009 period. A significant change occurred after 2009 when the correlation with the SCAND index diminished, and the NAO and AO indices exhibited a strong correlation with the winter wave climate. Similar to other studies, the AO and NAO indices showed related behaviour. Among these climatic indices, the SCAND index had a stronger correlation with the winter wave climate between 2000 and 2009, and after this year, its effect reduced. The years 2008–2009 seem to represent a turning moment in the Baltic Sea wave climate when the correlation with the SCAND index drastically diminished, and, at the same time, the correlation with the NAO and AO indices became statistically significant at a >95% significance level and stayed at the same level after 2009.

## 4 Discussion and conclusions

In order to interpret the appearance of various modes and parameters of the EOF modes of the Baltic Sea wave climate derived from satellite altimetry, it was demonstrated that (i) the percentage of variability in the retrieved wave fields is directly related to the percentage of noise in the data and that (ii) the retrieved spatial patterns are practically not affected by the noise. Low variance is generally observed in the EOF analysis of the wave climate derived

from the satellite altimetry (e.g., Woolf et al. 2002; Hemer et al. 2010). However, the reasons behind the low retrieved variance of EOFs were not studied in detail. In this study, a thorough analysis was performed on how the measurement noise affects the retrieved variance of EOF modes.

The connection between the NAO index and trends in the wave heights for the North Atlantic and the North Sea is well-established and widely discussed (e.g., Woolf et al. 2002; Wolf and Woolf 2006; Hemer et al. 2010). The phenomena behind the NAO index are driving processes in those bodies of water. For example, the long-term positive trend in the wave heights in the North Atlantic (Bertin et al. 2013) is related to the corresponding trend in the NAO index (e.g., Wolf and Woolf 2006). However, it is not clear if there is a connection between the wave climate trends and climatic indices in the Baltic Sea region. The results of our study show a strong anti-correlation between the linear trends in the Baltic Sea wave climate and the SCAND climatic index ( $-0.47 \pm 0.19$ ) and a positive correlation with the NAO ( $0.31 \pm 0.22$ ) and AO ( $0.42 \pm 0.20$ ) indices. During the NAO and AO's positive phase, strong westerly winds are predominant in the Baltic Sea area (Fig. 7b). This negative correlation with the SCAND index and a positive correlation with the NAO and AO indices agrees well with the explanation that the trends in the Baltic Sea wave climate are due to the interplay of north-westerly (driven by the SCAND pattern) and westerly (driven by the NAO and AO) winds over the region.

Most importantly, using the running correlation analysis, we demonstrated for the first time that the Baltic Sea wave climate has a significant time variable correlation with the SCAND, NAO, and AO indices. The phenomena that govern the SCAND pattern had a strong influence on the Baltic Sea waves between 2000 and 2009 when the effect of the NAO and AO indices was weak. Interestingly, after the year 2009, the correlation of the wave height with the SCAND index significantly diminished, and the NAO and AO indices exhibited a strong correlation with the winter wave climate.

This feature can be interpreted as an indication that the Baltic Sea wave climate is driven alternately by several sets of processes that are characterised by the listed three indices. The strength of correlation between the wave properties and a single index dramatically varies in time. When north-westerly winds are stronger during the negative phase of the SCAND index, the effect of the processes that drive the NAO index is weaker. Alternatively, when the correlation with the NAO index is more substantial, the westerly winds are stronger, and the effect of phenomena that make up the SCAND index is weaker.

**Acknowledgements** The research was co-supported by the institutional financing by the Estonian Ministry of Education and Research (Grant

IUT33-3), the Flag-ERA project FuturiCT2.0, the Estonian Research Council (Grant PRG1129) and the European Economic Area (EEA) Financial Mechanism 2014–2021 Baltic Research Programme (Grant EMP480). We also acknowledge the support of the Horizon2020 Erasmus+ project CUPAGIS in terms of institutional collaboration. We thank the Radar Altimeter Database System (RADS) database and NOAA Center for Weather and Climate Prediction for providing the data. Comments on the manuscript from anonymous referees are greatly acknowledged.

**Funding** The research was co-supported by the institutional financing by the Estonian Ministry of Education and Research (grant IUT33-3), the Flag-ERA project FuturiCT2.0, the Estonian Research Council (grant PRG1129) and the European Economic Area (EEA) Financial Mechanism 2014–2021 Baltic Research Programme (grant EMP480).

**Availability of data and material** The RADS satellite altimetry data are available at <http://rads.tudelft.nl/rads/rads.shtml> (accessed 1 March 2021).

**Code availability** From the authors on request.

## Declarations

**Conflict of interest** The authors declare that they have no conflict of interest.

## References

- Andersson HC (2002) Influence of long-term regional and large-scale atmospheric calculation on the Baltic sea level. *Tellus A Dyn Meteorol Oceanogr* 54(1):76–88. <https://doi.org/10.3402/tellusa.v54i1.12125>
- Barbariol F, Bidlot J-R, Cavaleri L, Sclavo M, Thomson J, Benetazzo A (2019) Maximum wave heights from global model reanalysis. *Prog Oceanogr* 175:139–160. <https://doi.org/10.1016/j.pocean.2019.03.009>
- Barnston AG, Livezey RE (1987) Classification, seasonality and persistence of low-frequency atmospheric circulation patterns. *Mon Weather Rev* 115(6):1083–1126. [https://doi.org/10.1175/1520-0493\(1987\)115%3c1083:CSAPOL%3e2.0.CO;2](https://doi.org/10.1175/1520-0493(1987)115%3c1083:CSAPOL%3e2.0.CO;2)
- Bednorz E, Czernecki B, Tomczyk AM, Pórolniczak M (2018) If not NAO then what?—regional circulation patterns governing summer air temperatures in Poland. *Theoret Appl Climatol* 136(3):1325–1337. <https://doi.org/10.1007/s00704-018-2562-x>
- Bertin X, Prouteau E, Letetrel C (2013) A significant increase in wave height in the North Atlantic Ocean over the 20th century. *Global Planet Change* 106:77–83. <https://doi.org/10.1016/j.gloplacha.2013.03.009>
- Björkqvist J-V, Lukas I, Alari V, van Vledder GP, Hulst S, Pettersson H, Behrens A, Männik A (2018) Comparing a 41-year model hindcast with decades of wave measurements from the Baltic Sea. *Ocean Eng* 152:57–71. <https://doi.org/10.1016/j.oceaneng.2018.01.048>
- Björkqvist J-V, Rikka S, Alari V, Männik A, Tuomi L, Pettersson H (2020) Wave height return periods from combined measurement-model data: a Baltic Sea case study. *Nat Hazard* 20(12):3593–3609. <https://doi.org/10.5194/nhess-20-3593-2020>
- Booij N, Ris RC, Holthuijsen LH (1999) A third-generation wave model for coastal regions: 1. Model description and validation. *J Geophys Res Oceans* 104(4):7649–7666. <https://doi.org/10.1029/98JC02622>

- Brenner AC, Blndschadler RA, Thomas RH, Zwally HJ (1983) Slope-induced errors in radar altimetry over continental ice sheets. *J Geophys Res Oceans* 88(C3):1617–1623. <https://doi.org/10.1029/JC088iC03p01617>
- Bueh C, Nakamura H (2007) Scandinavian pattern and its climatic impact. *Q J R Meteorol Soc* 133(629):2117–2131. <https://doi.org/10.1002/qj.173>
- Cañellas B, Orfila A, Méndez F, Álvarez A, Tintoré J (2010) Influence of the NAO on the northwestern Mediterranean wave climate. *Sci Mar* 74(1):55–64. <https://doi.org/10.3989/scimar.2010.74n1055>
- Cavaleri L, Bertotti L (1997) In search of the correct wind and wave fields in a minor basin. *Mon Weather Rev* 125(8):1964–1975. [https://doi.org/10.1175/1520-0493\(1997\)125<1964:ISOTCW>2.0.CO;2](https://doi.org/10.1175/1520-0493(1997)125<1964:ISOTCW>2.0.CO;2)
- Church JA, White NJ, Coleman R, Lambeck K, Mitrovica JX (2004) Estimates of the regional distribution of sea level rise over the 1950–2000 period. *J Clim* 17(13):2609–2625. [https://doi.org/10.1175/1520-0442\(2004\)017<2609:EOTRDO>2.0.CO;2](https://doi.org/10.1175/1520-0442(2004)017<2609:EOTRDO>2.0.CO;2)
- Cieślakiewicz W, Paplińska-Swempel B (2008) A 44-year hindcast of wind wave fields over the Baltic Sea. *Coast Eng* 55(11):894–905. <https://doi.org/10.1016/j.coastaleng.2008.02.017>
- Gao T, Yu J-Y, Paek H (2017) Impacts of four northern-hemisphere teleconnection patterns on atmospheric circulations over Eurasia and the Pacific. *Theoret Appl Climatol* 129(3):815–831. <https://doi.org/10.1007/s00704-016-1801-2>
- Hannachi A (2004) A Primer for EOF Analysis of Climate Data. Department of Meteorology, University of Reading: Reading, UK. <http://www.o3d.org/eas-6490/lectures/EOFs/cofprimer.pdf>. Accessed 10 Jun 2019
- Hasselmann K, Hasselmann S, Bauer E et al (1988) The WAM Model—A third generation ocean wave prediction model. *J Phys Oceanogr* 18(12):1775–1810. [https://doi.org/10.1175/1520-0485\(1988\)018<1775:TWMTO>2.0.CO;2](https://doi.org/10.1175/1520-0485(1988)018<1775:TWMTO>2.0.CO;2)
- Hemer MA, Church JA, Hunter JR (2010) Variability and trends in the directional wave climate of the Southern Hemisphere. *Int J Climatol* 30(4):475–491. <https://doi.org/10.1002/joc.1900>
- Hemer MA, Fan Y, Mori N, Semedo A, Wang XL (2013) Projected changes in wave climate from a multi-model ensemble. *Nat Clim Chang* 3(5):471–476. <https://doi.org/10.1038/nclimate1791>
- Irannezhad M, Marttila H, Kløve B (2014) Long-term variations and trends in precipitation in Finland. *Int J Climatol* 34(10):3139–3153. <https://doi.org/10.1002/joc.3902>
- Izaguirre C, Méndez FJ, Menéndez M, Losada IJ (2011) Global extreme wave height variability based on satellite data. *Geophys Res Lett* 38(10):L10607. <https://doi.org/10.1029/2011GL047302>
- Jaagus J (2009) Regionalisation of the precipitation pattern in the Baltic Sea drainage basin and its dependence on large-scale atmospheric circulation. *Boreal Environ Res* 14:31–44
- Jacobbeit J, Jönsson P, Barring L, Beck C, Ekström M (2001) Zonal indices for Europe 1780–1995 and running correlations with temperature. *Clim Change* 48(1):219–241. <https://doi.org/10.1023/A:1005619023045>
- Jevrejeva S, Moore JC, Grinsted A (2003) Influence of the Arctic Oscillation and El Niño–Southern Oscillation (ENSO) on ice conditions in the Baltic Sea: the wavelet approach. *J Gerontol Ser A Biol Med Sci* 108(D21):4677. <https://doi.org/10.1029/2003JD003417>
- Jevrejeva S, Moore JC, Woodworth PL, Grinsted A (2005) Influence of large-scale atmospheric circulation on European sea level: results based on the wavelet transform method. *Tellus Ser A Dyn Meteorol Oceanogr* 57(2):183–193. <https://doi.org/10.3402/tellusa.v57i2.14609>
- Jönsson A, Broman B, Rahm L (2003) Variations in the Baltic Sea wave fields. *Ocean Eng* 30(1):107–126. [https://doi.org/10.1016/S0029-8018\(01\)00103-2](https://doi.org/10.1016/S0029-8018(01)00103-2)
- Kelpšaitė L, Herrmann H, Soomere T (2008) Wave regime differences along the eastern coast of the Baltic Proper. *Proc Est Acad Sci* 57(4):225–231. <https://doi.org/10.3176/proc.2008.4.04>
- Komen GJ, Cavaleri L, Donelan M, Hasselmann K, Hasselmann S, Janssen PAEM (1994) Dynamics and modelling of ocean waves. Cambridge University Press, Cambridge
- Kudryavtseva NA, Soomere T (2016) Validation of the multi-mission altimeter wave height data for the Baltic Sea region. *Estonian J Earth Sci* 65(3):161–175. <https://doi.org/10.3176/earth.2016.13>
- Kudryavtseva N, Soomere T (2017) Satellite altimetry reveals spatial patterns of variations in the Baltic Sea wave climate. *Earth Syst Dyn* 8(3):697–706. <https://doi.org/10.5194/esd-8-697-2017>
- Kudryavtseva N, Kussembayeva K, Rakisheva ZB, Soomere T (2019) Spatial variations in the Caspian Sea wave climate in 2002–2013 from satellite altimetry. *Estonian J Earth Sci* 68(4):225–240. <https://doi.org/10.3176/earth.2019.16>
- Kudryavtseva N, Soomere T, Männikus R (2021) Non-stationary analysis of water level extremes in Latvian waters, Baltic Sea, during 1961–2018. *Nat Hazard* 21(4):1279–1296. <https://doi.org/10.5194/nhess-21-1279-2021>
- Lionello P, Sanna A (2005) Mediterranean wave climate variability and its links with NAO and Indian Monsoon. *Clim Dyn* 25(6):611–623. <https://doi.org/10.1007/s00382-005-0025-4>
- Madsen KS, Høyer JL, Tscherning CC (2007) Near-coastal satellite altimetry: Sea surface height variability in the North Sea–Baltic Sea area. *Geophys Res Lett* 34(14):L14601. <https://doi.org/10.1029/2007GL029965>
- Männikus R, Soomere T, Viška M (2020) Variations in the mean, seasonal and extreme water level on the Latvian coast, the eastern Baltic Sea, during 1961–2018. *Estuar Coast Shelf Sci* 245:106827. <https://doi.org/10.1016/j.ecss.2020.106827>
- Masselink G, Castello B, Scott T, Dodet G, Suarez S, Jackson D, Floc'h F (2016) Extreme wave activity during 2013/2014 winter and morphological impacts along the Atlantic coast of Europe. *Geophys Res Lett* 43(5):2135–2143. <https://doi.org/10.1002/2015GL067492>
- Medvedeva A, Myslenkov S, Medvedev I, Arkhipkin V, Krechik V, Dobrolyubov S (2016) Numerical modeling of the wind waves in the Baltic Sea using the rectangular and unstructured grids and the reanalysis NCEP/CFRSR. In: Proceedings of the Hydrometeorological Research Center of the Russian Federation 362:37–54 (in Russian with English summary)
- Mietus M, von Storch H (1997) Reconstruction of the wave climate in the proper Baltic basin, April 1947–March 1988. *GKSS Report* 97/E/28, Geesthacht.
- Myslenkov SA, Medvedeva A, Arkhipkin V, Markina M, Surkova G, Krylov A, Dobrolyubov S, Zilitinkevich S, Koltermann P (2018) Long-term statistics of storms in the Baltic, Barents and White seas and their future climate projections. *Geogr Environ Sustain* 11(1):93–112. <https://doi.org/10.24057/2071-9388-2018-11-1-93-112>
- Nezlin NP, McWilliams JC (2003) Satellite data, empirical orthogonal functions, and the 1997–1998 El Niño off California. *Remote Sens Environ* 84(2):234–254. [https://doi.org/10.1016/S0034-4257\(02\)00109-8](https://doi.org/10.1016/S0034-4257(02)00109-8)
- Nikolkina I, Soomere T, Räämet A (2014) Multidecadal ensemble hindcast of wave fields in the Baltic Sea. *IEEE/OES Baltic Int Symp (BALTIC)*. <https://doi.org/10.1109/BALTIC.2014.6887854>
- Niroomandi A, Ma G, Ye X, Lou S, Xue P (2018) Extreme value analysis of wave climate in Chesapeake Bay. *Ocean Eng* 159:22–36. <https://doi.org/10.1016/j.oceaneng.2018.03.094>
- Omstedt A, Pettersen C, Rodhe J, Winsor P (2004) Baltic Sea climate: 200 yr of data on air temperature, sea level variation, ice cover, and atmospheric circulation. *Climate Res* 25(3):205–216. <https://doi.org/10.3354/cr025205>

- Passaro M, Cipollini P, Benveniste J (2015) Annual sea level variability of the coastal ocean: the Baltic Sea-North Sea transition zone. *J Geophys Res Oceans* 120(4):3061–3078. <https://doi.org/10.1002/2014JC010510>
- Patra A, Bhaskaran PK (2016) Trends in wind-wave climate over the head Bay of Bengal region. *Int J Climatol* 36(13):4222–4240. <https://doi.org/10.1002/joc.4627>
- Räämet A, Soomere T (2021) Spatial pattern of quality of historical wave climate reconstructions for the Baltic Sea. *Boreal Environ Res* 26:29–41
- Räämet A, Soomere T, Zaitseva-Pärnaste I (2010) Variations in extreme wave heights and wave directions in the north-eastern Baltic Sea. *Proc Est Acad Sci* 59(2):182–192. <https://doi.org/10.3176/proc.2010.2.18>
- Rikka S, Pleskachevsky A, Uiboupin R, Jacobsen S (2018) Sea state in the Baltic Sea from space-borne high-resolution synthetic aperture radar imagery. *Int J Remote Sens* 39(4):1256–1284. <https://doi.org/10.1080/01431161.2017.1399475>
- Różyński G (2010) Long-term evolution of Baltic Sea wave climate near a coastal segment in Poland; its drivers and impacts. *Ocean Eng* 37(2–3):186–199. <https://doi.org/10.1016/j.oceaneng.2009.11.008>
- Sartini L, Besio G, Cassola F (2017) Spatio-temporal modelling of extreme wave heights in the Mediterranean Sea. *Ocean Model* 117:52–69. <https://doi.org/10.1016/j.ocemod.2017.07.001>
- Scharroo R (2012) RADS version 3.1 user manual and format specifications. <http://rads.tudelft.nl/rads/radsmanual.pdf>. Accessed 6 Mar 2020
- Scharroo R, Leuliette EW, Lillibridge JL, Byrne D, Naeije MC, Mitchum GT (2013) RADS: Consistent multi-mission products in Proc Symp on 20 Years of Progress in Radar Altimetry, 20–28 September 2012, Venice, Eur. Space Agency Spec. Publ., ESA SP-710
- Shimura T, Mori N, Mase H (2013) Ocean waves and teleconnection patterns in the northern hemisphere. *J Clim* 26(21):8654–8670. <https://doi.org/10.1175/JCLI-D-12-00397.1>
- Soomere T (2005) Wind wave statistics in Tallinn Bay. *Boreal Environ Res* 10(2):103–118
- Soomere T, Eelsalu M (2014) On the wave energy potential along the eastern Baltic Sea coast. *Renew Energy* 71:221–233. <https://doi.org/10.1016/j.renene.2014.05.025>
- Soomere T, Pindsoo K (2016) Spatial variability in the trends in extreme storm surges and weekly-scale high water levels in the eastern Baltic Sea. *Cont Shelf Res* 115:53–64. <https://doi.org/10.1016/j.csr.2015.12.016>
- Soomere T, Räämet A (2011) Long-term spatial variations in the Baltic Sea wave fields. *Ocean Sci* 7(1):141–150. <https://doi.org/10.5194/os-7-141-2011>
- Soomere T, Räämet A (2014) Decadal changes in the Baltic Sea wave heights. *J Mar Syst* 129:86–95. <https://doi.org/10.1016/j.jmarsys.2013.03.009>
- Soomere T, Behrens A, Tuomi L, Nielsen JW (2008) Wave conditions in the Baltic Proper and in the Gulf of Finland during windstorm Gudrun. *Nat Hazards Earth Syst Sci* 8(1):37–46. <https://doi.org/10.5194/nhess-8-37-2008>
- Soomere T, Bishop SR, Viška M, Räämet A (2015) An abrupt change in winds that may radically affect the coasts and deep sections of the Baltic Sea. *Clim Res* 62(2):163–171. <https://doi.org/10.3354/cr01269>
- Surkova GV, Arkhipkin VS, Kislov AV (2015) Atmospheric circulation and storm events in the Baltic Sea. *Open Geosci* 7(1):332–341. <https://doi.org/10.1515/geo-2015-0030>
- Suursaar Ü, Kullas T (2009) Decadal variations in wave heights off Cape Kelba, Saaremaa Island, and their relationships with changes in wind climate. *Oceanologia* 51(1):39–61. <https://doi.org/10.5697/oc.51-1.039>
- Suursaar Ü, Sooäär J (2007) Decadal variations in mean and extreme sea level values along the Estonian coast of the Baltic Sea. *Tellus Ser A Dyn Meteorol Oceanogr* 59(2):249–260. <https://doi.org/10.1111/j.1600-0870.2006.00220.x>
- Thompson DWJ, Wallace JM (1998) The Arctic Oscillation signature in the wintertime geopotential height and temperature fields. *Geophys Res Lett* 25(9):1297–1300. <https://doi.org/10.1029/98GL00950>
- Trigo RM, Osborn TJ, Corte-Real JM (2002) The North Atlantic Oscillation influence on Europe: climate impacts and associated physical mechanisms. *Clim Res* 20(1):9–17. <https://doi.org/10.3354/cr020009>
- Tuomi L, Kahma KK, Pettersson H (2011) Wave hindcast statistics in the seasonally ice-covered Baltic Sea. *Boreal Environ Res* 16(6):451–472
- Tuomi L, Kanarik H, Björkqvist J-V, Marjamaa R, Vainio J, Hordoir R, Höglund A, Kahma KK (2019) Impact of ice data quality and treatment on wave hindcast statistics in seasonally ice-covered seas. *Front Earth Sci* 7:166. <https://doi.org/10.3389/feart.2019.00166>
- Wakelin SL, Woodworth PL, Flather RA, Williams JA (2003) Sea-level dependence on the NAO over the NW European continental shelf. *Geophys Res Lett* 30(7):1403. <https://doi.org/10.1029/2003GL017041>
- Walker GT, Bliss EW (1932) World weather V. *Memoirs R Meteorol Soc* 4:53–84
- Wang XL, Zwiers FW, Swail VR (2004) North Atlantic ocean wave climate change scenarios for the twenty-first century. *J Clim* 17(12):2368–2383. [https://doi.org/10.1175/1520-0442\(2004\)017<2368:NAOWCC>2.0.CO;2](https://doi.org/10.1175/1520-0442(2004)017<2368:NAOWCC>2.0.CO;2)
- Weisse R, von Storch H, Niemeier HD, Knaack H (2012) Changing North Sea storm surge climate: an increasing hazard? *Ocean Coast Manag* 68:58–68. <https://doi.org/10.1016/j.ocecoaman.2011.09.005>
- Wolf J, Woolf DK (2006) Waves and climate change in the north-east Atlantic. *Geophys Res Lett* 33(6):L06604. <https://doi.org/10.1029/2005GL025113>
- Woolf DK, Challenor PG, Cotton PD (2002) Variability and predictability of the North Atlantic wave climate. *J Geophys Res Oceans* 107(C10):3145. <https://doi.org/10.1029/2001JC001124>
- Zujev M, Elken J, Lagema P (2021) Data assimilation of sea surface temperature and salinity using basin-scale reconstruction from empirical orthogonal functions: a feasibility study in the north-eastern Baltic Sea. *Ocean Sci* 17:91–109. <https://doi.org/10.5194/os-17-91-2021>

**Publisher's Note** Springer Nature remains neutral with regard to jurisdictional claims in published maps and institutional affiliations.

## Publication II

**Najafzadeh F.**, Kudryavtseva N., Soomere T., Giudici A. 2022. Effect of ice cover on wave statistics and wave-driven processes in the northern Baltic Sea. *Boreal Environment Research*, 27, 97–116.



# Effect of ice cover on wave statistics and wave-driven processes in the northern Baltic Sea

Fatemeh Najafzadeh<sup>1)\*</sup>, Nadezhda Kudryavtseva<sup>1)</sup>, Tarmo Soomere<sup>1)2)</sup> and Andrea Giudici<sup>1)</sup>

<sup>1)</sup> Wave Engineering Laboratory, Department of Cybernetics, School of Science, Tallinn University of Technology, Akadeemia tee 21, Tallinn, 12618, Estonia  
(\*corresponding author's e-mail: fatemeh@ioc.ee)

<sup>2)</sup> Estonian Academy of Sciences, Kohtu 6, Tallinn, 10130, Estonia

Received 11 Aug. 2021, final version received 21 Feb. 2022, accepted 17 Mar. 2022

Najafzadeh F., Kudryavtseva N., Soomere T. & Giudici A. 2022: Effect of ice cover on wave statistics and wave-driven processes in the northern Baltic Sea. *Boreal Env. Res.* 27: 97–116.

We explore the effect of sea ice on wind wave statistics and wave-driven hydrodynamic loads in a seasonally ice-covered sea. We compare the results of hypothetical ice-free wave simulations for 1979–2007 in the northern Baltic Sea with *in-situ* wave time series and with truncated simulations in which waves during the ice season are ignored. The ice cover impacts the mean wave properties usually less than 5% and up to 10–20% at a few locations. The cumulative annual wave energy and energy flux are greatly (up to 82%) influenced. The mean wave properties and the ice season duration are almost uncorrelated in the Sea of Bothnia and Bay of Bothnia but have a statistically significant (at a > 99% level) negative correlation at the latitudes of the Gulf of Finland. This feature implies that climate-driven changes, first of all, the later appearance of ice in the relatively windy late autumn and winter season, may considerably add energy to coastal processes at these latitudes.

## Introduction

Variations in the wave climate have a broad impact, from shaping coastlines (e.g., Łabuz 2015, Kelpšaitė-Rimkienė *et al.* 2021) and coastal erosion (Ryabchuk *et al.* 2011, Suursaar *et al.* 2014, Harff *et al.* 2017) to the safety of navigation and shipping (Goerlandt *et al.* 2017, Lensu and Goerlandt 2019). These variations are largely driven by similar variations in the weather conditions, first of all wind forcing and air temperature. Sea ice also has a great influence on wave properties. They both have extensive seasonal and interannual variability and they both are eventually impacted by climate change

in boreal marginal seas, such as the Baltic Sea (Fig. 1).

The weather conditions of the Baltic Sea are mostly controlled by two dominant atmospheric circulation systems; the North Atlantic Oscillation and the Scandinavian mode (e.g., von Storch *et al.* 2015). Their extensive variability leads to large spatial and temporal variations in the mean and extreme Baltic Sea wave properties. These changes exhibit a complicated spatial pattern (Soomere and Räämet 2011). The mean significant wave height,  $H_s$ , evaluated using satellite altimetry data 1993–2015, varied in the range of 1–1.3 m in the Baltic proper (Kudryavtseva and Soomere 2016, 2017). This value may be slightly

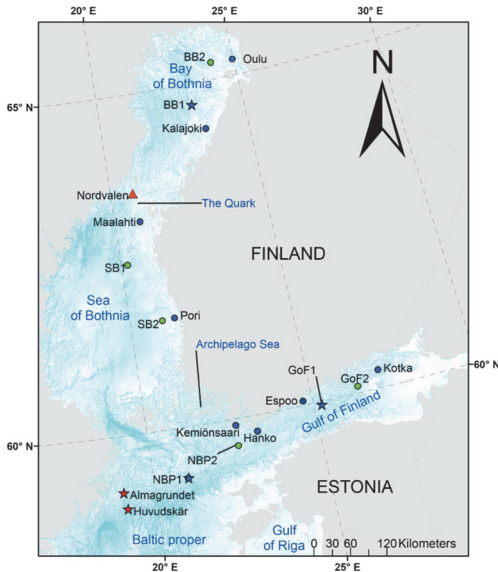


**Fig 1.** Map of the study area and the discussed locations. The wave measurement devices operated by the Swedish Meteorological and Hydrological Institute (SMHI) and Finnish Meteorological Institute (FMI) are marked with red and blue stars, respectively. The locations of FMI temperature buoys are shown by blue circles, WAM model grid points used in the analysis by green circles, and the south-west SMHI location Nordvalen by a red triangle.

overestimated because satellite altimetry does not recognise very low wave heights. In semi-enclosed areas like the Bay of Bothnia, the Gulf of Finland, and the Gulf of Riga, the mean  $H_s$  had lower values in the range of 0.5–1 m (Tuomi et al. 2011, Nikolkina et al. 2014).

The most disruptive storms in the Baltic Sea basin usually happen in late autumn or early winter (Suursaar et al. 2006, Björkqvist et al. 2017, 2020). The severest wave events are found in the northern part of the Baltic proper where the maximum measured  $H_s$  and peak period reached 8.2 m and over 12 s, respectively, in December 2004 (Soomere et al. 2008, Tuomi et al. 2011, Björkqvist et al. 2018). Waves can also be very high in the Sea of Bothnia; for example, in January 2019, the maximum  $H_s$  and the peak period in the southern part of this basin reached 8.1 m and 12 s, respectively (Björkqvist et al. 2020).

The long-term changes in the wind and wave properties in the Baltic Sea region are less reli-

ably known than their short-term variations. Wind speeds have increased at an 850 hPa level over the Atlantic Ocean (Pryor and Barthelmie 2003, Torralba et al. 2017) and strong westerly winds have become more frequent in the Baltic region (Ruostenoja et al. 2019). These trends, however, seem to be controversial in the Baltic Sea also in terms of wave heights (Hünicke et al. 2015, Rutgersson et al. 2022). Estimated by the satellite altimetry, the mean significant wave height  $H_s$  increased by  $0.005 \text{ m yr}^{-1}$  from 1993 to 2015 over the Baltic Sea. This trend is more discernible in the western part of this basin (Kudryavtseva and Soomere 2017). A large part of this change is controlled by the two above-mentioned atmospheric circulation systems (Najafzadeh et al. 2021). Even though the average wave heights have increased only marginally, unexpectedly severe wave conditions have been recorded in the 21st century (Björkqvist et al. 2017, 2020). Other analyses also indicate that extremes may increase (Mäll et al. 2020) and become more frequent (Kudryavtseva et al. 2020).

The properties of waves and sea ice cover are strongly interrelated. The presence of ice affects wave growth and the generation of longer waves implicitly via reduction of the free propagation distance (Liu and Mollo-Christensen 1988) and explicitly by dissipation of wave energy (Collins et al. 2015, Mostert and Deike 2020, Tavakoli and Babanin 2021). Even though wind speeds may be even higher during the ice season, the ice cover damps wave fields and wave impact on the shore (Orviku et al. 2003, Ryabchuk et al. 2011). For example, the mean wave energy flux decreased by up to 80% due to the effects of ice in the Bohai Sea, the innermost gulf of the Yellow Sea, in winter 2011–2012 (Zhang et al. 2020).

Ice conditions in the Baltic Sea are highly variable in different years (SMHI and FIMR 1982, Haapala and Leppäranta 1996). During a mild winter, the ice extends only over the Bay of Bothnia, the Archipelago Sea, and some parts of the Gulf of Finland (Fig. 1). During an average winter, ice covers about 45% of the sea (Jevrejeva 2001). In a severe winter (e.g., in 1947), the entire sea may be covered by ice (Jevrejeva 2001, Leppäranta and Myrberg 2009,

Section 7.1). The ice season's length varies from 5 to 7 months and the ice may cover 10–100% of the total area of the Baltic Sea (Jevrejeva 2001, Leppäranta and Myrberg 2009, Section 7.2).

Sea ice and its extent are highly susceptible to rising temperature. An increase in winter air temperature by 1°C over the Baltic Sea reduces the ice season's length by 1–2 weeks and the ice-covered area by 2.5% of the basin area (Leppäranta 2012). The current climate change has led to a shorter ice season in the Arctic (Overeem *et al.* 2011) and milder (ice) winters in the Baltic Sea (Omstedt *et al.* 2004, Haapala *et al.* 2015).

The ice season duration has decreased by 10–30 days per century in the southern Baltic proper in the period 1896–1993 (Sztobryn 1994, Vihma and Haapala 2009). The ice breakup has shifted by two days per century in severe winters in the Gulf of Riga in the period 1529–1990 (Jevrejeva 2001). The changes in the ice season duration (Omstedt *et al.* 2004, Käyhkö *et al.* 2015) are slower in the northern Baltic proper or the Gulf of Finland (Haapala and Leppäranta 1997, Jevrejeva *et al.* 2004). The duration of ice season in the northern Bay of Bothnia and southern Sea of Bothnia (Fig. 1) has decreased by 18 and 47 days per century, respectively (Haapala *et al.* 2015, Section 8.3). This process is even faster in the Gulf of Finland (Sooäär and Jaagus 2007, Merkouriadi and Leppäranta 2014).

The combination of a shorter ice season and more severe wave conditions imply that, the coastlines of the Baltic Sea are systematically more exposed to the surges and waves (Omstedt and Nyberg 1996, Barnhart *et al.* 2014). This shift may cause rapid erosion or alteration in some coastal areas (Orviku *et al.* 2003, Overeem *et al.* 2011) even though the impact of ice ridges on the nearshore seabed may decrease. It is thus important to consider, at least qualitatively, the consequences of the changes to the properties of the ice season on the future of the seasonally ice-covered Baltic Sea.

Tuomi *et al.* (2011) introduced five approaches for wave statistics under such conditions. Type M statistics include only measurements (e.g., Broman *et al.* 2006). Type F only includes the data during the ice-free season that is usually normalised due to the different number of ice-free data points. Type N statistics

reflect the idealised ice-free conditions during the whole year (e.g., Suursaar and Kullas 2009). The latter approximation has been used in simulations of wave climate of the Baltic Sea using the WAM model and geostrophic winds (Räämet and Soomere 2010).

All these approaches generally introduce a systematic alteration in the established wave features (Tuomi *et al.* 2019). Type N statistics leads to an overestimation of the cumulative wave energy and energy flux. The magnitude and even the sign of the difference between estimates of mean wave properties using different approaches depend on whether the ice season is windier or calmer than the rest of the year. Björkqvist *et al.* (2018) noted that the mean  $H_s$  in the Bay of Bothnia was reduced by 30% when the ice time was included in the statistics, but the impact of ice was negligible to the south of latitude 59.5°, that is, to the south of the mid-latitude of the Gulf of Finland.

Here, we make an attempt to evaluate the potential impact of changes in the sea ice season duration on the wave statistics based on a comparison of the WAM model data during the ice-free time (Type F) and over the whole year in idealised ice-free conditions (Type N). The difference between the two estimates is used to characterise to a first approximation the impact of ice using only idealised ice-free simulations. The focus is on the potential changes in the cumulative wave energy and energy flux over certain time intervals and seasons in the northern Baltic Sea.

Specifically, we explore how the presence of seasonal ice cover impacts some widely used categories of wave statistics, how much the presence of ice reduces the wave impact compared to an idealised ice-free climate, whether this reduction has changed over the years, and at which locations the reduced ice cover in the near future may substantially modify wave-driven hydrodynamic loads.

We employ the new satellite-derived OSI-450 (Lavergne *et al.* 2019) ice concentration measurements to identify the ice season. The time series of wave height, wave energy, and wave energy flux are hindcast by the WAM model. The results are validated using available *in-situ* wave data. We start from a short descrip-

tion of data used in this study and the method of calculating wave energy flux. We then provide wave statistics and their changes introduced by the variations in the length of the ice season, and discuss which parameters influence the difference between Type F and N statistics for model and *in-situ* data, respectively. Finally, we discuss the outcome and formulate the conclusions.

## Data and methods

The analysis is based on the concentration of ice cover in the Baltic Sea retrieved from satellite microwave radiometry, validated using the classic ice charts and represented in terms of the start, end and duration of the ice season for each winter at selected locations. This data set is complemented by *in situ* measured and numerically modelled time series of wave properties. The mean and cumulative (total) wave energy and wave energy flux for each year and ice season are used to characterise the potential impact of climatic changes to the ice properties on wave loads in the nearshore.

A typical ice season in the Baltic Sea starts in early winter and continues until the spring of the following year. Most of the extreme wave events and thus conditions that provide large portions of wave energy flux occur from September to February (e.g., Björkqvist *et al.* 2018). Therefore, the windiest months often overlap with the ice season in the northern Baltic Sea. For this reason, even small changes in the start or duration of the ice season may lead to considerable changes in the wave impact at some locations.

### Sea ice

The sea ice concentration data used for this study are OSI-450 (Lavergne *et al.* 2019), which is the second major version of the EUMETSAT Ocean and Sea Ice Satellite Application Facility (OSI SAF) global Sea-Ice Concentration (SIC) Climate Data Record (v2.0 2017). The data provided by Norwegian and Danish Meteorological Institutes are accessible at <http://osisaf.met.no> [accessed in February 2021]. The first version of the OSI SAF SIC (OSI-409, the predecessor of

OSI-450) started in 2006. The main difference between these two datasets is a new Open Water (Weather) Filter (Gloersen and Cavalieri 1986, Buehner *et al.* 2016) which is applied on OSI-450. It removes the false sea ice over open water regions that exhibited weather-induced noise while protecting the records of low ice concentration values. Moreover, the implemented algorithms for OSI-450 are more precise (Lavergne *et al.* 2019) and new sources of satellite input data (from the EUMETSAT Climate Monitoring Satellite Application Facility) are used. A thorough description of the processes is presented in Tonboe *et al.* (2016). The detailed list of similarities and differences between the two versions is described in the product user manual (available on <http://osisaf.met.no>) [accessed in February 2021].

The global collection of sea ice concentrations, OSI-450, has daily records from 1979 to 2015 with a spatial resolution of 25×25 km. The dataset provides the ice concentration, flags, and uncertainty estimations. Ice concentration is the share of the grid area covered by ice (%). Each ice concentration value is associated with a flag and a measure of uncertainty. The flags present information about the processing steps and levels that may have an effect on the ice concentration value. The uncertainty estimation for each sea ice concentration is given as standard deviation (%). The entries with this flag equal to 0 present a nominal ice concentration value (%) which is modified for sea ice concentration and uncertainties (%). The values in the database were thoroughly checked for outliers and possibly erroneous data. To remove unreliable measurements, we only use the data with flag 0. Selecting only the data with the flag values equal to 0 drastically improved the quality of OSI-450 ice maps in the Baltic Sea region.

Following the classic notion of the duration of ice cover (e.g., Jevrejeva 2001), we use only two dates for each year: the beginning and end of the ice season. The entire time period between these dates is interpreted as the ice season. This interpretation may overlook a few days when open-sea ice has drifted to another location. However, coastal regions of the north-eastern Baltic Sea have numerous small islands, peninsulas and bays cut into the mainland. This region

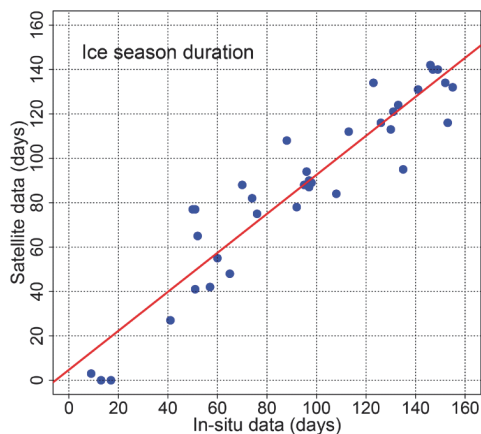


**Fig 2.** Satellite-derived ice season duration from OSI-450 ( $\zeta = 50\%$ ) versus in-situ ice season duration observed at SMHI Nordvalen station. The red line represents the linear regression line.

usually has non-moving (fast) ice during the entire time period when ice is observed in the offshore. Therefore, even though this approximation may be not be exact for offshore sea areas, it apparently is adequate in terms of waves and wave energy that reaches the nearshore.

The beginning of the ice season at a particular location was estimated as the time of the first reliable measurement with the ice concentration exceeding a certain threshold,  $\zeta$ , after the 1<sup>st</sup> of July. The end of the ice season is considered as the time of the last measurement with the ice concentration  $> \zeta$  before the 1<sup>st</sup> of July the following year. The algorithm was implemented in the R (ver. 4.0.3) programming language (Kabacoff 2011).

To find the most suitable ice concentration cutoff  $\zeta$ , the ice season duration retrieved from OSI-450 at an observation location near Storskäret in the Quark area in the waters of Maa-lahti municipality (referred to as Maa-lahti below, Fig. 1) is compared with the one derived from the Swedish Meteorological and Hydrological Institute (SMHI) ice charts for a range of cutoff values. The satellite-derived duration of the ice season is sensitive to the selected values of  $\zeta$ . The best match was achieved using  $\zeta = 50\%$ , resulting in a correlation coefficient of 0.91 between the two estimates. The bias and root-mean-square of the two estimates are 10.53% and 21.35 days, respectively. Therefore, the ice

concentration cutoff of 50% was used in the analysis.

The satellite-derived estimates of the ice season duration obtained from OSI-450 ice data were compared with similar estimates retrieved from the SMHI ice charts. The ice season's summary observed by the SMHI since 1970, charts and reports are available at [http://www.smhi.se/oceanografi/istjanst/havsis\\_en.php](http://www.smhi.se/oceanografi/istjanst/havsis_en.php) [accessed in February 2021]. This data set reflects information from SMHI ice observers, pilot stations, ice-breakers, coastguard observations, and satellite images. The ice season duration is defined as the total number of days with ice. To compare the satellite-derived ice season data with the direct ice observations, we used the data from the SMHI south-west Nordvalen (63.54°N, 20.73°E) ice observation location and its nearest OSI-450 satellite ice measurement location at 63.54°N, 20.76°E.

The estimates of the ice season duration based on SMHI observations and OSI-450 at Nordvalen showed good correspondence (Fig. 2; correlation coefficient 0.94) and almost no bias (intercept of the linear regression line at 4.7 days; slope 0.88). Three ice-free winters from OSI-450 correspond to less than 20 locally observed ice days per year. This mismatch suggests that satellite information tends to overlook small ice concentrations that are spotted by other means. This feature may also reflect relatively large intervals and gaps in the satellite data.

The further analysis uses only the properties of ice seasons retrieved using satellite information. The longest average ice season lasts about 107 days in the Bay of Bothnia (Fig. 3). This is up to two months longer than in the lower-latitude sub-basins, such the Sea of Bothnia (Maa-lahti, also Storskäret, mean duration 86 days), the Gulf of Finland (GoF1, 53 days), and Kemiön-saari (Kalvören) in the Baltic proper (53 days).

Many areas in the western part of the Baltic Sea, including SMHI wave buoys and observation locations, experience ice only during average and severe winters. The satellite OSI-450 ice data rarely indicate ice in these areas and the satellite-derived ice season duration is zero in most of the years. Therefore, the effect of sea ice on wave properties and wave loads in the nearshore are generally small at such locations

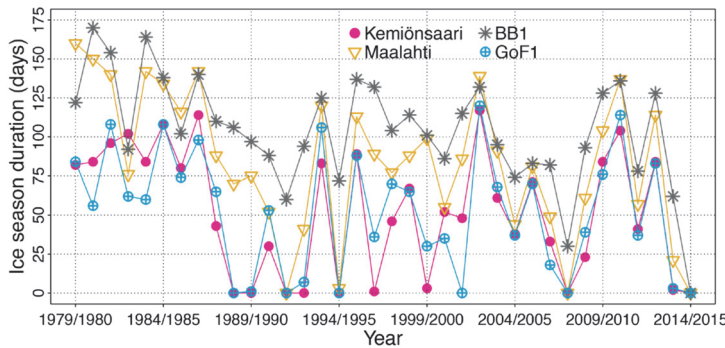


**Fig 3.** Ice season duration at different locations based on OSI-450 satellite data.

and apparently cannot be reliably identified from the data set used for this study.

### Wave data

To select the areas where our analysis is meaningful, we calculate the percentage of years with nonzero ice season from the total number of years (27). Considering seven measurements per covariate (ice season duration and the wave statistics), at least 20 years with nonzero-ice season duration are necessary for an adequate estimate. For this reason, we only consider locations where  $> 52\%$  of the years have nonzero ice season duration. Such areas are concentrated in the north-eastern part of the Baltic Sea; mostly in the Gulf of Finland, Sea of Bothnia and Gulf of Bothnia, and to lesser extent in the north-eastern Baltic proper.

We select for the analysis eight Finnish Meteorological Institute (FMI) buoy stations that have various purposes near the shores of Finland (Table 1): Oulu and Kalajoki in the Bay of Bothnia, Maalahti in the Quark area, Pori in the Sea of Bothnia, Kemiönsaari and Hanko in the northern Baltic proper and at the entrance to the Gulf of Finland, and Espoo and Kotka in the Gulf of Finland (Fig. 1). In order to reflect the difference in offshore and nearshore ice and wave properties, we include the location of the FMI wave buoy in the central Gulf of Finland (denoted GoF1 below for brevity), and a buoy in the central part of the Bay of Bothnia (BB1) (Fig. 1).

Several of the above locations are in very shallow water or located close to the shore where the modelled wave data may not necessarily

adequately reflect the real situation. To complement the analysis using more offshore locations, we add into consideration modelled wave data at another offshore location (BB2) in the Bay of Bothnia, two offshore locations (SB1 and SB2) in the Sea of Bothnia, and one location (NBP2) in the northern Baltic Proper and one (GoF2) in the Gulf of Finland (Fig. 1, Table 1). In addition, we employ wave data from two SMHI measurement locations at Almagrundet and Huvudskär, and from the FMI wave buoy in the northern Baltic proper (NBP1) for limited time periods.

The analysis in this study relies on the significant wave height  $H_s$  and peak period  $T_p$  of wave fields. Estimates of wave energy flux generally also require wave propagation direction. As this parameter is less frequently available, we only address the magnitude of wave energy flux. The main properties of the measurement locations and time series of  $H_s$  and  $T_p$  are provided in Table 1. More detailed information about these locations and devices is available, e.g., in Björkqvist *et al.* (2018), Nilsson *et al.* (2019). Datasets were retrieved through open data interfaces (<https://opendata-download-ocobs.smhi.se/>, <https://en.ilmatieteenlaitos.fi/open-data>) [accessed in August 2021].

The time resolution of the measured wave time series varies. The most frequent measurements (once in 0.5 h) exist for BB1, GoF1, and NBP1. The rest of the buoys (Table 1) provide data once an hour. The buoys have to be taken out of water for maintenance and also before the ice season to avoid damage by freezing. Therefore, the number of measurements and the coverage of the measured time series are different at each station.

We employ the time series of wave properties reconstructed for the Baltic Sea for 38 years (1970–2007) by Räämet and Soomere (2010) using the third-generation wave model WAM Cycle 4 (Komen *et al.* 1996). We use the wave properties at the nearest WAM model grid point to the locations in Table 1. The typical mismatch is  $0.02^\circ$  in both north-south and east-west directions.

The simulated data set with about 3 nautical miles spatial and one-hour temporal resolutions is based on the hypothetical condition of no-ice and thus represents Type N statistics. This data set has been produced using SMHI geostrophic winds with a spatial resolution of  $1^\circ$  and a temporal resolution of 6 h before September 1977 and 3 h after September 1977 that are adjusted for the surface wind at 10 m level by multiplying the speed by 0.6 and rotating the direction by  $15^\circ$  counter-clockwise (cf. Bumke and Hasse 1989).

This low spatio-temporal resolution of wind data and the simplified scheme for the construction of surface-level winds leads to a systematic underestimation of wave heights in some parts of

the Baltic Sea. The quality of the reconstructed wave properties varies spatially. They have a relatively good correlation with measured data and with the output of simulations using COSMO winds at the latitudes of the Gulf of Finland (Räämet and Soomere, 2021), whereas the match is much worse in the southern Baltic Sea. As the largest changes to wave conditions due to changes in the ice conditions have occurred in the northern Baltic Sea (Jevrejeva 2001) and we basically look at the currently occurring suppression of the wave impact caused by the presence of ice compared to the hypothetical ice-free conditions, this set of wave properties is generally suitable for our purposes.

## Methods

We are interested in how much the presence of ice reduces the wave impact and how much this kind of reduction has changed over the years. Different viewpoints are possible for the analysis of interrelations between wave prop-

**Table 1.** Main parameters of locations used in this study. Water depth for the locations was estimated from (Seifert *et al.* 2001). All temperature buoys are MetOcean iCVP type.

Location and/or station name	Data Source	Device	Lat °N	Lon °E	Depth (m)	$H_s$ ( $T_p$ ) observations
Almagrundet	SMHI	Echosounder	59.15	19.13	29	1987–2003
Huvudskär	SMHI	Directional waverider	58.93	19.17	103	From 2001 (2010)
Bay of Bothnia 1 (BB1)	FMI	Directional waverider	64.68	23.24	74	From 2012 (2012)
Bay of Bothnia 2 (BB2)	WAM	WAM model output	65.25	24.20	12	
Northern Baltic proper 1 (NBP1)	FMI	Directional waverider	59.25	21.00	71	From 1996 (1996)
Northern Baltic proper 2 (NBP2)	WAM	WAM model output	59.60	22.60	46	
Gulf of Finland 1 (GoF1)	FMI	Directional waverider	59.96	25.24	55	From 2000 (2000)
Gulf of Finland 2 (GoF2)	WAM	WAM model output	60.10	26.40	58	
Espoo Kytö	FMI	Temperature buoy	60.06	24.72	25	
Hanko Längden	FMI	Temperature buoy	59.76	23.22	23	
Kalajoki Maakalla	FMI	Temperature buoy	64.30	23.55	12	
Kemiönsaari Kalvören	FMI	Temperature buoy	59.90	22.63	6	
Kotka Kuusenkari	FMI	Temperature buoy	60.27	27.11	8	
Maalahti Storskäret	FMI	Temperature buoy	63.11	20.82	3	
Oulu Santapankki	FMI	Temperature buoy	65.23	24.97	6	
Pori Kajakari	FMI	Temperature buoy	61.62	21.39	6	
Sea of Bothnia 1 (SB1)	WAM	WAM model output	62.50	20.20	114	
Sea of Bothnia 2 (SB2)	WAM	WAM model output	61.60	21.00	48	
South-west Nordvalen	SMHI	Ice observations	63.54	20.73	25	
—	OSI-540	Satellite ice data	63.54	20.76	18	

erties and ice conditions, the latter expressed here in terms of the ice season duration. One way is to evaluate these ice-driven changes within a calendar year by comparison, for example, the cumulative wave energy flux to the shores in hypothetical ice-free conditions versus this flux over the ice-free season (Zaitseva-Pärnaste and Soomere 2013).

However, it is natural to consider the impact of the presence of ice on the wave field over whole ice seasons. This approach is extensively used in the analysis of changes to average and extreme water levels. Following Männikus *et al.* (2019), we call the time period from July of a certain year to the end of June of the subsequent year a stormy season. Such 12-month time periods contain the entire ice season for each winter and also the entire relatively windy autumn-winter season. As mentioned above, we employ the simplest proxy of the ice season where the wave data during its whole duration are discarded from the calculation.

The instantaneous values of the wave energy  $E$  (KJ m<sup>-2</sup>) are calculated as:

$$E = \frac{\rho g H^2}{16}, \quad (1)$$

where  $\rho$  is the density of water (taken here constant 998 kg m<sup>-3</sup>),  $g$  is acceleration due to gravity (9.81 m s<sup>-2</sup>),  $H$  is the measured significant wave height of *in-situ* data and the hindcast  $H_s$  for modelled data. The wave energy flux  $P$  (KW m<sup>-1</sup>) is calculated as (Guilou 2020):

$$P = E c_g, \quad (2)$$

$$c_g = \frac{\omega}{2k} \left(1 + \frac{2kd}{\sinh 2kd}\right). \quad (3)$$

Here,  $c_g$  is the group speed,  $\omega$  is the angular wave frequency (rad s<sup>-1</sup>),  $d$  is the water depth (m),  $k = 2\pi/\lambda$  is the wave number, the wavelength,  $\lambda$ , is calculated from the general dispersion relation of water waves  $\omega^2 = gk \tanh(kd)$  that is expressed as:

$$\lambda = \frac{gT^2}{2\pi} \tanh\left(\frac{2\pi d}{\lambda}\right). \quad (4)$$

As the energy period is often not available,  $T$  is interpreted here as the peak period. The wavelength is estimated for the approximate water depth  $d$  at each station.

The mean significant wave height  $\overline{H_{sy}}$ , wave energy  $\overline{E_y}$  and wave energy flux  $\overline{P_y}$  during a particular stormy season are calculated in a classic (Type F) manner; for example, the mean wave energy  $\overline{E_y}$  in a particular stormy season is

$$\overline{E_y} = \frac{1}{N_y} \sum_{\text{year}} E_i, \quad (5)$$

where  $E_i$  is the instantaneous wave energy and  $N_y$  is the number of available measurements or modelled values of wave energy in this stormy season. Note that these estimates do not contain any information about the ice season duration. This information is reflected by the ratio of  $N_y$  and the total number of measurement instants or modelled data points during the entire stormy season.

The total (or cumulative) wave energy and especially energy flux are richer in content measures of the impact of ice cover on hydrodynamic loads in the nearshore. The wave energy goes as squared wave height and the wave energy flux in shallow water as wave energy to the power of 2.5. For example, the total stormy season wave energy flux  $P_{\text{tot}}$  was calculated as a sum of instantaneous values of energy flux  $P_i$  calculated once an hour during the two subsequent half-years (stormy season):

$$P_{\text{tot}} = \sum_{\text{year}} P_i. \quad (6)$$

The cumulative wave energy  $P_{\text{tot}}$  is calculated similarly to Eq. (6). As the time series of modelled wave data (1970–2007) and ice information in OSI-450 (from 1979) cover different time periods, we use in comparisons mostly the overlapping part of these data sets, that is, 27 stormy seasons from 1979/1980 to 2006/2007.

## Results

### Wave statistics during ice-free time (Type F)

We start from the analysis of temporal and spatial variability of the main wave properties in the selected locations over 27 stormy seasons (1979/1980–2006/2007). The annual mean  $H_s$  during the ice-free time of single stormy seasons (Type F statistics) for the selected stations (Fig. 4) varies by a factor of two at the study sites. The Bay of Bothnia, Oulu, with the longest ice season, is characterised by the lowest range of the mean  $H_s$  in single stormy seasons (0.38–0.55 m). This feature apparently reflects the combination of a relatively sheltered location of the particular site and well-known seasonality of wind patterns in the Baltic Sea region. Namely, the ice-free time in this part of the Baltic Sea usually matches the spring and summer seasons that have the lowest wind speed. The mean  $H_s$  in single stormy seasons at three other stations in this subbasin (BB1, BB2, and Kalajoki) varied between 0.50 m and 0.77 m. Both these locations (BB1, Kalajoki) are open to the predominant moderate and strong south-western winds in this region. The somewhat larger mean  $H_s$  at BB1 (0.72 m) evidently reflects its more open position compared to Kalajoki.

Stations in the Sea of Bothnia have a higher mean  $H_s$  (0.51–1.01 m) and shorter ice season duration than in the Bay of Bothnia. It is natural that the mean  $H_s$  is higher at the offshore locations SB1 and SB2 than in more sheltered nearshore locations at Maalahti and Pori.

Kemiönsaari, on the north-eastern shore of the Baltic proper, has the second-lowest mean  $H_s$  (0.46–0.62 m). This feature might also be due to the station's location, which is sheltered against westerly winds by islands in the Archipelago Sea (Fig. 1). The Hanko station is located to the south of Kemiönsaari. It is open to the predominant moderate and strong westerly winds over the Baltic proper and has higher mean  $H_s$  values (0.54–0.77 m). As expected, the much more open location in the northern Baltic proper (NBP2) has clearly higher mean  $H_s$  values than those hindcast for Kemiönsaari or Hanko.

In the Gulf of Finland, the GoF1 wave buoy in the central Gulf of Finland has a higher mean  $H_s$  (0.55–0.87 m) compared to similar estimates for Espoo, GoF2, and Kotka (0.44–0.73 m). Generally, the farther the station is located from the coast, the higher is the mean  $H_s$  at this station. This feature becomes evident in each sub-basin, except for the GoF2 location. The calculated values of mean  $H_s$  are consistent with the results provided by Björkqvist *et al.* (2018), who estimate the ice-free (Type F) mean  $H_s$  for the Baltic Sea from a 41-year SWAN model hindcast. It can be therefore concluded that variations in the ice season duration have a clearly smaller impact on Type F statistics of mean wave properties than the location of the particular site.

The boxplots of magnitude and scatter of other mean Type F properties of wave fields (not shown) evaluated using the WAM model are similar to those presented in Fig. 4. As expected, the stormy season mean of wave energy during ice-free time (Fig. 5) calculated using Eq. (5) has much larger interannual and spatial variation than the mean  $H_s$ . Its magnitude varies by a factor of up to 3 at all locations in 1979/1980–2006/2007. The mean wave energy over all the years also varies by a factor of 3 at different stations. It reaches a maximum of 0.79 KJ m<sup>-2</sup> at GoF1, is less than ~0.71 KJ m<sup>-2</sup> at BB1 and mostly between 0.2 and 0.3 KJ m<sup>-2</sup> at Kemiönsaari.

Both interannual and spatial variations in the ice-free (Type F) mean wave energy flux (Fig. 6) are, as expected, even larger than similar variations in the wave energy (Fig. 5). The long-term mean of this quantity varies from about 1 KW m<sup>-1</sup> at Kemiönsaari up to 2.5 KW m<sup>-1</sup> at Maalahti, BB1 and GoF1. This level is almost the same as the relevant Type N values for nearshore areas of the western Baltic proper (Soomere and Eelsalu 2014). A natural reason for relatively large wave energy flux at the sites in question is that they are located at a larger distance from the shore and in deeper areas than the "converter line" locations addressed by Soomere and Eelsalu (2014). The patterns of interannual variations in the mean energy and energy flux (Figs. 5 and 6) are almost identical at all locations. This feature indicates that wave periods in the storms that provide the largest contribution

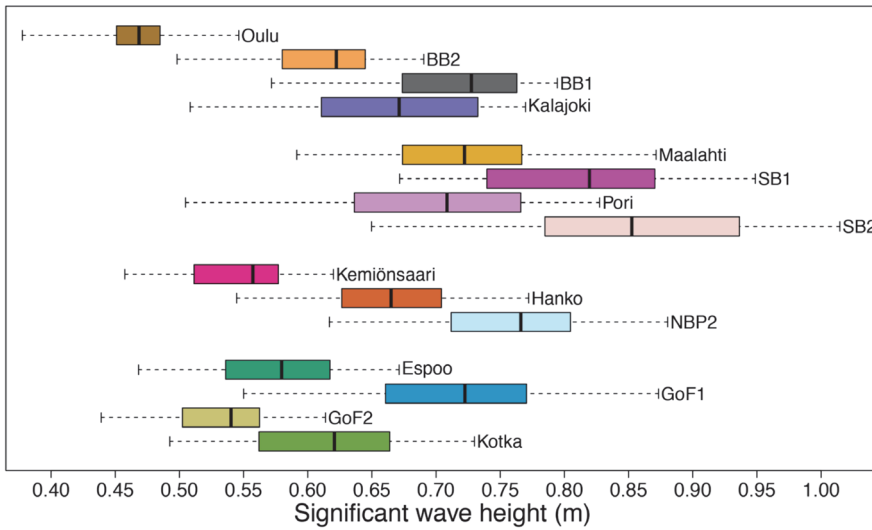


**Fig 4.** Boxplot of ice-free modelled mean  $H_s$  (Type F statistics) during 27 stormy seasons from 1979/1980 to 2006/2007. The coloured area reflects the two middle quartiles of stormy season mean  $H_s$ . The vertical line in this area represents the median  $H_s$  (in terms of mean  $H_s$  in single stormy seasons). The sections denoted by dashed lines represent the lowest and the highest quartiles. The maximum and minimum  $H_s$  at the particular location are shown using small vertical lines.

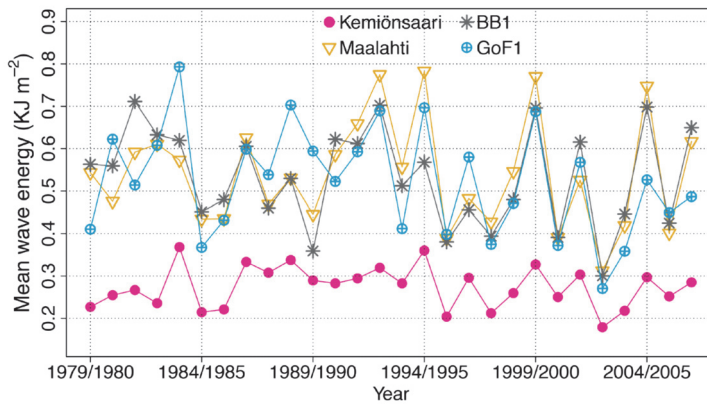


**Fig 5.** Mean ice-free wave energy (Type F statistics) evaluated from the WAM model output during stormy seasons 1979/1980–2006/2007.

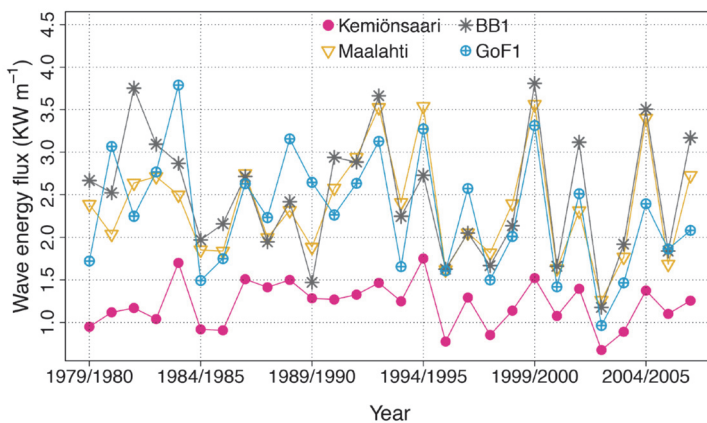


**Fig 6.** Mean ice-free wave energy flux (Type F) evaluated from the WAM model output during stormy seasons 1979/1980–2006/2007.

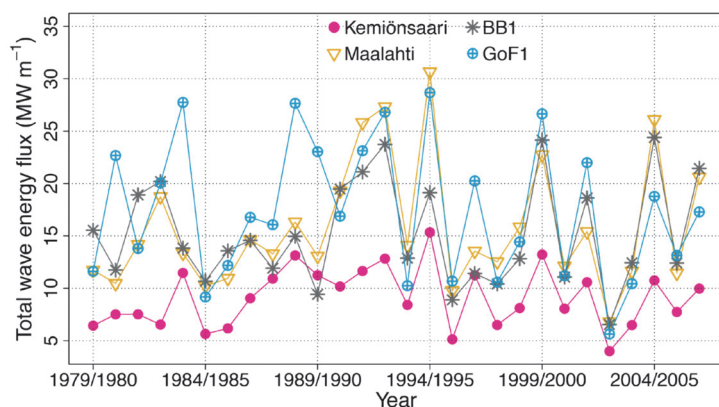


**Fig 7.** Mean ice-free total (cumulative) wave energy flux (Type F) evaluated from the WAM model output during stormy seasons 1979/1980–2006/2007.

to the wave energy flux vary insignificantly. This conjecture is consistent with the perception that severe wave fields in the study area are generally fetch-limited.

Spatio-temporal variations in the cumulative Type F properties of wave fields at the locations in question are even larger. For example, the cumulative wave energy flux  $P_{tot}$  at GoF1 varies almost by a factor of 6 in individual stormy seasons (Fig. 7). This feature indicates that intermittency of wave properties is evident not only between single storms and seasons (Soomere and Eelsalu 2014) but also in terms of different years.

Interestingly, spatial differences in this quantity at separate locations are smaller than similar differences for wave energy or energy flux. The mean  $P_{tot}$  varies only by a factor of 2 at locations represented in Fig. 7. In the light of the normally fetch-limited nature of the Baltic Sea wave fields (that suppresses differences in wave periods under severe wave conditions), this feature may indicate that the strongest wave storms that provide a very large contribution to the total wave energy flux (Soomere and Eelsalu 2014) impact simultaneously all considered locations and occur before the ice season starts even at the northernmost locations.

To validate the described ice-free wave statistics to some extent, we compared wave statistics derived from *in-situ* measurements (Type M; Tuomi *et al.* 2011) with similar statistics obtained from wave simulations. The beginning and the end of the ice season were estimated from the satellite observations as described

above. Wave buoys are removed before the ice season starts. Thus, in the northern part of the Baltic Sea, the measurement period is typically from May/early June until December/early January (Tuomi *et al.* 2019), and only a few locations and years are suitable for such a comparison. Some buoy measurements have been made with ice concentration up to 40%, according to satellite data, which possibly indicates an invalid interpretation of satellite information. The only station in the study area that experiences frequent and long ice cover with an overlap of more than 5 years of our model data and the measurements is at GoF1. Simultaneous observations and model data are available during the period 2001/2002–2006/2007. Based on OSI-450 ice data, the ice season duration varied in the range of 0–120 days during these years (Fig. 3). The wave properties during the ice-free time, based on simulations (Type F) and *in-situ* (Type M) data, considerably varied during these years, showing the difference in wave energy flux in the range of 3% to 48% (in 2002/2003, which has the longest ice season, 120 days).

The difference is even larger for single stormy seasons at locations in BB1 that allow a comparison of this kind. At Almagrundet the difference in the wave energy flux  $P_{tot}$  is 62% with 22 days of ice for 1994/1995. Huvudskär and the FMI buoy (NBPI) location in the northern Baltic proper have wave measurements in 2002/2003 with 12 and 34 day ice season duration, respectively. The difference between Type F and M wave energy flux is 47% and 34%, respectively, at these locations. This estimate of the difference

between the ice-free (Type F) and the measurement statistics (Type M) matches a similar estimate by Björkqvist *et al.* (2018) for the Bay of Bothnia and apparently characterises years with long and extensive ice cover in the northern Baltic Proper.

### Impact of the presence of ice on mean wave properties

A first-order perception of the impact of the presence of ice cover on wave properties can be inferred from a comparison of the box and scatter plots of the difference in modelled wave properties that reflect statistics Type F and N. The relevant quantities characterise to some extent the impact of the presence of ice in the current climate against a hypothetical ice-free climate that has the same wind regime as the climate today. The magnitude of this difference exemplifies, to a first approximation, changes to hydrodynamic loads that could be expected in a much warmer climate. The addressed properties (mean  $H_s$ , mean and cumulative wave energy and energy flux) for stormy seasons from 1979/1980 to 2006/2007 show the impact of ice from different viewpoints.

The difference in  $H_s$  calculated for the selected stations in each subbasin (Fig. 8) first of all indicates that the mean  $H_s$  in totally ice-free conditions would generally exceed that in the current climate. The only exception is Pori, where the evaluated difference is  $-0.25\%$ . Virtually no changes are projected at SB1, SB2, Kemiönsaari, Hanko, Espoo, GoF1 and GoF2. The ice season is relatively short at these locations and the sites are open to the predominant strong wind directions (Fig. 1). At locations with longer ice season duration, the completely ice-free wave regime would lead to an increase by 3–5% in the mean  $H_s$ . The largest increase ( $> 10\%$ ) is projected to the locations at higher latitudes, such as Oulu in the Bay of Bothnia. The rate of increase in the mean  $H_s$  in single stormy seasons could be much larger, up to 28% at Oulu. Kalajoki and BB1, with the longest ice season duration after Oulu, also host very large rates of increase in the stormy season mean  $H_s$ , 24% and 23%, respectively. Interestingly, on many occasions, the mean single stormy season

$H_s$  may decrease in the completely ice-free statistics. As mentioned above, this feature apparently reflects the (mis)match of the relatively windy season with the ice season.

The situation is generally the same with the stormy season mean wave energy and energy flux (Figs. 9 and 10). The impact of the presence of ice on these quantities is negligible at Pori, somewhat unexpectedly in the offshore of the Sea of Bothnia (at SB1 and SB2) and generally at all locations where the ice season is relatively short. The magnitude of this impact increases towards the North and East. This gradient matches the increase in the ice season duration. The impact of ice is, as expected, the largest in the Bay of Bothnia, especially in the coastal area (Oulu), where the mean wave energy in the ice-free climate may be 20% larger than now.

The difference between the increase rates for mean wave energy (Fig. 9) and energy flux (Fig. 10) is just a few per cent. Therefore, the existing Type F estimates of annual mean wave energy and energy flux adequately (within a few per cent) represent also the hypothetical ice-free situation in the northern Baltic Sea, except in the Bay of Bothnia and the eastern Gulf of Finland, where the difference may reach 20% for wave energy and almost 30% for the wave energy flux. Interestingly, the pattern of differences is asymmetric: large positive differences (equivalently, underestimation of mean wave energy in Type N statistics) are more likely than large negative differences.

The difference between Type F and N statistics for energy in single stormy seasons is much larger, up to 54% (Fig. 9) at Oulu. This feature suggests that the shift to completely ice-free conditions in a future climate will probably lead to large changes in the wave energy and energy flux in single stormy seasons, but the mean wave properties are represented adequately by Type F statistics in most of the Baltic Sea as indicated also by Björkqvist *et al.* (2018).

### Impact of the presence of ice on cumulative wave statistics

The impact of sea ice on cumulative properties of the wave climate is much larger compared to

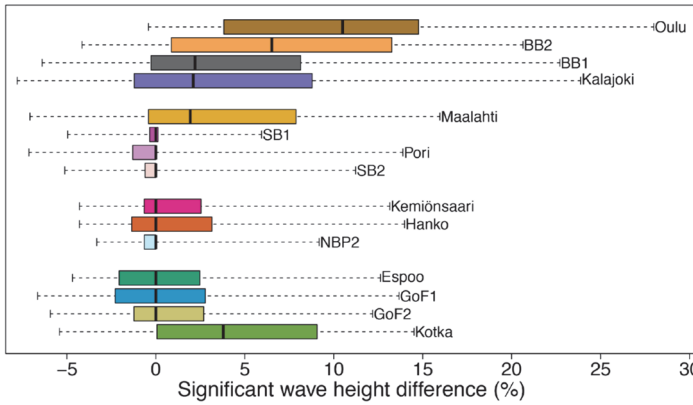


**Fig 8.** The difference of Type F and N estimates of mean  $H_s$  in single stormy seasons.

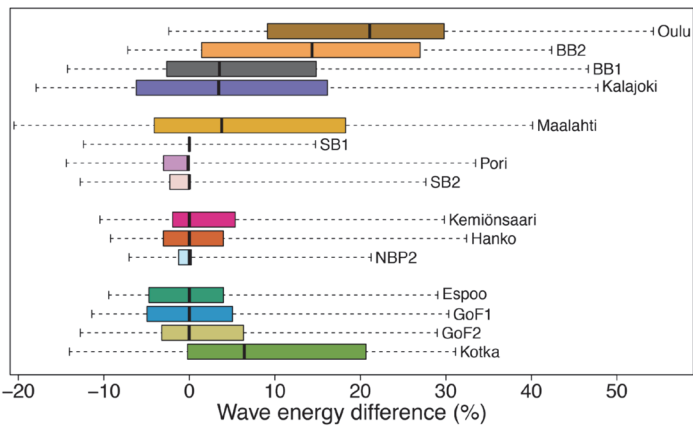


**Fig 9.** The difference of Type F and N estimates of mean wave energy in single stormy seasons.

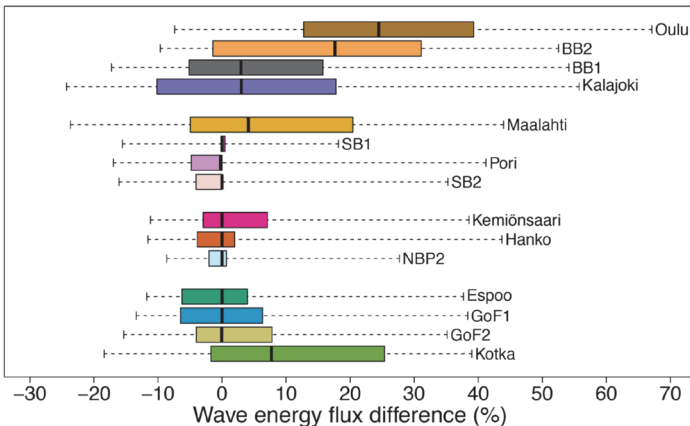


**Fig 10.** The difference of Type F and N estimates of mean wave energy flux in single stormy seasons.

the above. Its magnitude at a particular site obviously depends on the ice season duration and the least (zero) difference characterises the years with no ice.

The largest mean difference of cumulative wave energy  $E_{tot}$  (Fig. 11) between Type F and Type N estimates is 57% at Oulu where and it can reach up to 82% in a single stormy season.

For other locations in the Bay of Bothnia it reaches about 47% for BB2 and 37% for BB1 and Kalajoki, which are the largest values for differences in  $E_{tot}$  among the considered subbasins.

Although the ice season is shorter in the northern Baltic proper and Gulf of Finland than in the Sea of Bothnia, the existence of ice leads to a decrease in the  $E_{tot}$  by up to 59% in

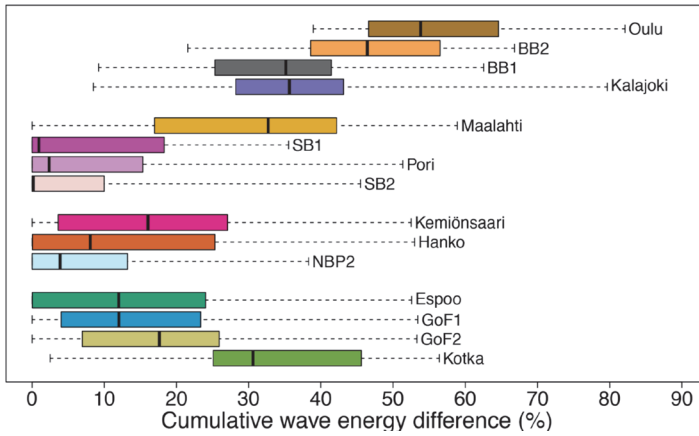


**Fig 11.** The difference of Type F and N estimates of cumulative wave energy in single stormy seasons from 1979/1980 to 2006/2007.

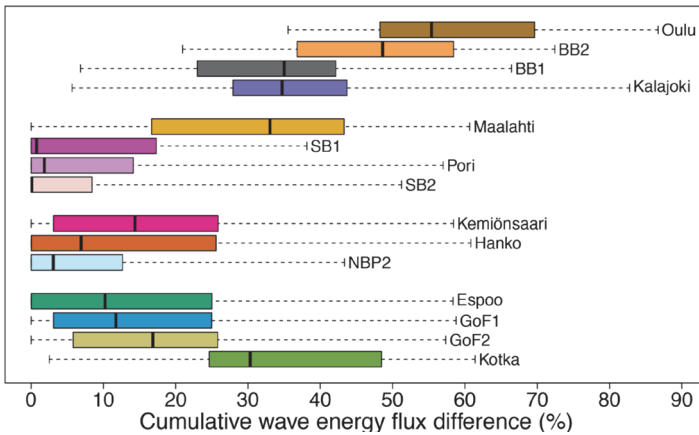


**Fig 12.** The difference of Type F and N estimates of cumulative wave energy flux in single stormy seasons.

single stormy seasons (Fig. 11). Interestingly, the decrease in this quantity is relatively small, below 15% on average, at several locations of the Sea of Bothnia and the Gulf of Finland. The ice-driven decrease in  $E_{tot}$  is smallest (8.5%) at SB1 in the Sea of Bothnia.

The patterns of differences between Type F and Type N statistics for cumulative wave energy flux  $P_{tot}$  (Fig. 12) insignificantly (usually no more than by a few per cent) differ from those evaluated for cumulative wave energy  $E_{tot}$ . This small difference in the estimates in Figs. 11 and 12 again indicates that wave periods (and thus group velocities) in strong storms mostly depend on the fetch length and less on the wind speed.

The above has shown that Type F statistics gives on most occasions an adequate estimate of mean wave properties in the idealised ice-free climate. However, quantities based on cumulative wave properties substantially underestimate

the total wave energy and especially energy flux to the coastal areas. It is thus essential to consider the ice season's duration when using wave statistics in coastal or other applications where cumulative properties of waves are decisive.

### Wave statistics and ice season duration

The natural dependence of cumulative properties of wave fields on the presence of sea ice obviously reflects the different number of modelled (or measured) snapshots of wave properties during the ice-free time and during the entire year or stormy season. The longer the ice season, the fewer wave measurements are included in the Type F statistics. However, the interrelations between the number of wave data entries and the mean  $H_s$ , wave energy and energy flux are not straightforward.

The mean ice season duration at the considered locations (Table 1) varies from 25 (SB2) to 167 (Oulu) days. A scatter diagram of ice season duration and mean wave height at four locations (Fig. 13) shows that a longer ice season duration generally corresponds to a lower value of stormy season  $H_s$ . In other words, interannual variations in the wave energy are in counter-phase with the ice season duration. The mean  $H_s$  decreases when the ice season becomes longer at all considered locations (Table 2) even though at some locations (e.g., BB1, Fig. 13) the slope of the relevant trend is very small. This decrease is statistically significant at a 99% level at five locations in or at the entrance of the Gulf of Finland: Espoo, Hanko, Kemiönsaari, Kotka and central Gulf of Finland (GoF1).

Compared with Kemiönsaari, the correlation between these two parameters is much weaker at Maalahti (the mean ice season duration 1979–2007 is 90 days), Oulu and Pori. No correlation exists at BB1 (where the mean ice season duration is 110 days) and Kalajoki. The spatial pattern of similar correlation coefficients between the ice season duration, wave energy and energy flux for ice-free time is almost the same (Table 2). The values of correlation coefficients are also almost the same for  $H_s$ , wave

energy and energy flux. The correlation coefficient between the ice season duration and the wave energy at Espoo, Hanko, Kemiönsaari, Kotka, and GoF1 reveal a statistically significant negative correlation at a > 99% confidence level (Table 2). Only at Oulu are these correlations for energy and energy flux clearly stronger than the correlation for  $H_s$ . A similar pattern of interrelations becomes evident for the ice season duration and mean wave energy flux (Fig. 14).

The presence of ice at these five locations in and near the Gulf of Finland, therefore, impacts not only the cumulative quantities but also the addressed mean properties of wave fields. The above has shown that, somewhat unexpectedly, the existing Type F statistics would remain correct also in some future ice-free climates. However, not unexpectedly, at the latitudes of the Gulf of Finland some properties of Type F statistics of the idealised ice-free wave climate apparently will differ from the similar properties of the current wave climate.

As spring is relatively calm in the study area, the presented material indicates that the time instant of ice formation at the latitudes of the Gulf of Finland often falls into the middle of a relatively windy winter. Derived from satellite data, the ice season at these latitudes typically

**Table 2.** Pearson correlation coefficients and relevant  $p$ -values between ice season duration and mean  $H_s$ , wave energy ( $E$ ) and wave energy flux ( $P$ ) for the ice-free season. Locations with  $p$ -values indicating statistical significance of the correlation at a > 99% level are shown with bold font. Note that adjusted  $R^2$  may take small negative values.

Location	Ice season duration vs. $H_s$			Ice season duration vs. $E$			Ice season duration vs. $P$		
	Correlation	Adj. $R^2$	$p$	Correlation	Adj. $R^2$	$p$	Correlation	Adj. $R^2$	$p$
<b>Espoo</b>	<b>-0.63±0.12</b>	<b>0.37</b>	<b>0.00</b>	<b>-0.62±0.12</b>	<b>0.36</b>	<b>0.00</b>	<b>-0.60±0.13</b>	<b>0.33</b>	<b>0.00</b>
<b>Hanko</b>	<b>-0.66±0.11</b>	<b>0.42</b>	<b>0.00</b>	<b>-0.64±0.12</b>	<b>0.39</b>	<b>0.00</b>	<b>-0.61±0.12</b>	<b>0.34</b>	<b>0.00</b>
Kalajoki	-0.19±0.18	-0.00	0.33	-0.16±0.18	-0.01	0.42	-0.16±0.18	-0.01	0.41
<b>Kemiönsaari</b>	<b>-0.59±0.13</b>	<b>0.32</b>	<b>0.00</b>	<b>-0.55±0.14</b>	<b>0.27</b>	<b>0.00</b>	<b>-0.54±0.14</b>	<b>0.27</b>	<b>0.00</b>
<b>Kotka</b>	<b>-0.54±0.14</b>	<b>0.27</b>	<b>0.00</b>	<b>-0.55±0.13</b>	<b>0.28</b>	<b>0.00</b>	<b>-0.55±0.14</b>	<b>0.27</b>	<b>0.00</b>
Maalahti	-0.43±0.16	0.16	0.02	-0.44±0.16	0.16	0.02	-0.43±0.16	0.16	0.02
Oulu	-0.37±0.16	0.10	0.05	-0.43±0.16	0.16	0.02	-0.46±0.15	0.18	0.01
BB1	-0.08±0.19	-0.03	0.69	-0.09±0.18	-0.03	0.65	-0.11±0.18	-0.03	0.58
BB2	-0.35±0.17	0.09	0.07	-0.29±0.17	0.05	0.13	-0.26±0.18	0.03	0.17
Pori	-0.31±0.17	0.07	0.09	-0.28±0.17	0.04	0.15	-0.27±0.17	0.04	0.16
<b>GoF1</b>	<b>-0.62±0.12</b>	<b>0.36</b>	<b>0.00</b>	<b>-0.61±0.12</b>	<b>0.34</b>	<b>0.00</b>	<b>-0.59±0.13</b>	<b>0.32</b>	<b>0.00</b>
<b>GoF2</b>	<b>-0.53±0.14</b>	<b>0.25</b>	<b>0.00</b>	<b>-0.50±0.15</b>	<b>0.22</b>	<b>0.00</b>	<b>-0.44±0.15</b>	0.16	0.02
<b>NBP2</b>	<b>-0.53±0.14</b>	<b>0.26</b>	<b>0.00</b>	<b>-0.51±0.14</b>	<b>0.23</b>	<b>0.00</b>	<b>-0.48±0.15</b>	<b>0.20</b>	<b>0.00</b>
SB1	-0.32±0.17	0.07	0.09	-0.35±0.17	0.09	0.07	-0.34±0.17	0.08	0.07
SB2	-0.36±0.16	0.10	0.06	-0.33±0.17	0.07	0.09	-0.30±0.17	0.06	0.12

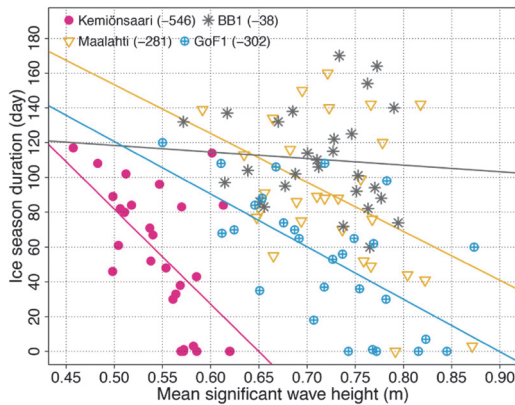


**Fig 13.** Scatter diagram of ice season duration and mean  $H_s$  during ice-free times at four locations of Fig. 1. The slopes of the relevant regression lines are presented in the legend.

starts at the beginning of February. The formation of ice in the Sea of Bothnia and Bay of Bothnia occurs one or two months earlier, at the beginning of January and December, respectively. Therefore a large proportion of strong winds that are frequent in winter overlap with the ice season. These features together suggest that the regions of the Baltic Sea that have a relatively short ice season (especially those on the northern shore of the Gulf of Finland) may be even more sensitive with respect to changes in ice conditions under current climate change than locations in the far North where ice season lasts 3–4 months. With a longer perspective, however, a similar sensitivity will appear for the locations in the Sea of Bothnia and Bay of Bothnia.

## Discussion

The main purpose of this research was to estimate how the presence of seasonal ice cover impacts the widely used categories of wave statistics, such as mean significant wave height, mean and cumulative wave energy and energy flux in the northern Baltic Sea. Specifically, we are interested in how much the presence of ice reduces the wave impact compared to an idealised ice-free climate and whether this reduction has changed over the years. An associated task was to understand whether and/or in which loca-

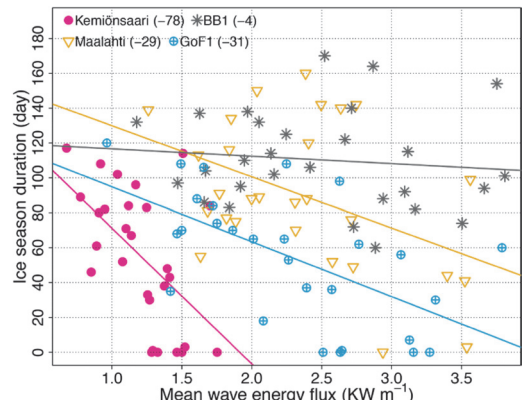


**Fig 14.** Scatter diagram of ice season duration and mean wave energy flux during ice-free times at four locations of Fig. 1. The slopes of the relevant regression lines are presented in the legend.

tions the reduced ice cover in the near future may substantially modify wave-driven hydrodynamic loads in the coastal zone. The research has been mostly performed using simulated wave data for 1970–2007 and satellite information about ice conditions since 1979. The analysis is focused on nearshore areas of the north-eastern Baltic Sea that are commonly ice-covered in winter.

The extensive variation in ice conditions and in the length of ice season in both time and space, as well as the overall shortening of the ice season in the Baltic Sea (Fig. 3), are extensively described in detail in the literature (e.g., Granskog *et al.* 2006, Omstedt *et al.* 2014, Käyhkö *et al.* 2015). Our analysis replicates this spatio-temporal variability in both mean and cumulative wave properties. It is somewhat counter-intuitive that the common statistical properties derived from idealised completely ice-free conditions (Type N) match well with similar properties evaluated for actual ice-free time (Type F) in the north of the study area. The difference in the listed mean properties of wave fields is negligible ( $< 1\%$ ) at half the locations. It reaches the level of 2–4% in the northern Gulf of Bothnia and in the eastern Gulf of Finland, and up to 10% for energy and 20% for energy flux in the far North.

This invariance of these statistical properties of wave fields on the presence of sea ice apparently reflects a specific match of the windy and

ice seasons in the study area. The ice season starts in the relatively windy late autumn and early winter and ends in a relatively calm spring season. The described feature may be explained as a balance between statistical properties of waves during ice-free times and properties of hypothetical waves during the ice season.

It is natural that the cumulative energy and energy flux greatly depend on the presence of sea ice. These quantities grow rapidly when the ice season becomes shorter. The potential climate change driven variations in ice conditions alone may thus lead to an increase by 30–50% of the wave energy and energy flux and thus to a substantial escalation of the hydrodynamic loads in the nearshore of the study area in a long-term. An almost trivial conjecture is that the longer the ice season is today, the larger is the potential impact of sea waves in a hypothetical ice-free future climate.

A different picture becomes evident for a part of the study area. The mean wave properties are almost uncorrelated with the ice season duration in the northern part of the study area, in the Sea of Bothnia and the Bay of Bothnia. There is, however, a statistically significant correlation (at a > 99% level) of these quantities at the latitudes of the Gulf of Finland. A decrease in the ice season duration is associated with a rapid increase in the mean wave properties in this region. The rate of this rise is almost the same for mean wave height, energy and energy flux.

This established correlation reiterates the results of Zaitseva-Pärnaste and Soomere (2013), where the modelled data at three locations in the eastern Baltic Sea showed a similar negative correlation. Our analysis shed further light on this property and revealed large spatial variations of this feature in different parts of the Baltic Sea.

This spatial variability suggests that recent changes in ice conditions may lead to a radically distinct reaction of wave properties and impacted coastal areas in different regions. The invariance of mean wave parameters on the ice season duration in the northern part of the study area suggests that climate warming and the associated loss of sea ice will have a limited impact on the mean wave properties and even on wave-driven loads in the near future at the scale of a few years to a few decades. This seems to

be the situation in the middle and northern part of the Sea of Bothnia and in the Bay of Bothnia. We note that this conjecture only applies to the changes in wave conditions in a hypothetical future climate that has the wind climate of today.

On the contrary, locations at the latitudes of the Gulf of Finland may be greatly affected also at time scales of a few years, should the ice season continue to shorten at the existing pace. A simple explanation is that at these locations the ice is formed somewhere in the middle of the relatively windy season. Any delay in the ice formation time would thus open the likelihood of more wave energy impacting the coastal area. This shift will eventually be associated with increased water levels compared to the circumstances with ice cover. If such situations are frequent, high waves will attack unprotected and unfrozen sediment on the upper parts of the beaches for much longer times and eventually cause massive coastal erosion and fine sediment relocation (Orviku *et al.* 2003, Overeem *et al.* 2011, Ryabchuk *et al.* 2011).

## Conclusions

Mean properties of wave fields (significant wave height, wave energy, energy flux) in the seasonally ice-covered northern Baltic Sea can be passably estimated using hypothetical completely ice-free models while similar cumulative properties of the wave climate are overestimated by up to 82% for wave energy and 87% for wave energy flux.

The mean wave properties are almost uncorrelated with the ice season duration in the Sea of Bothnia and the Bay of Bothnia but have a statistically significant (at a > 99% level) negative correlation with the ice season duration at the latitudes of the Gulf of Finland. In other words, the longer the ice season, the lower is the mean wave height in the Gulf of Finland and adjacent areas. Another reflection of this feature is that the interannual variations in wave energy are in counter-phase with the ice season duration.

Recent climate change driven variations in the ice cover duration are unlikely to significantly impact hydrodynamic loads on the nearshore in the Sea of Bothnia and the Gulf

of Bothnia in the near future. However, these changes may considerably add energy to coastal processes at the latitudes of the Gulf of Finland.

*Acknowledgements:* The research was co-supported by the Estonian Research Council (grant PRG1129) and the European Economic Area (EEA) Financial Mechanism 2014–2021 Baltic Research Programme (grant EMP480). We thank the Radar Altimeter Database System (RADS), Finnish, Swedish, Norwegian and Danish Meteorological Institutes database and NOAA Center for Weather and Climate Prediction for providing the data, and Prof Kevin Parnell for suggestions towards improvement of the manuscript.

## References

- Barnhart K.R., Overeem I. & Anderson R.S. 2014. The effect of changing sea ice on the physical vulnerability of Arctic coasts. *Cryosphere* 8(5): 1777–1799, doi: 10.5194/tc-8-1777-2014.
- Björkqvist J.-V., Tuomi L., Tollman N., Kangas A., Pettersson H., Marjamaa R., Jokinen H. & Fortelius C. 2017. Brief communication: Characteristic properties of extreme wave events observed in the northern Baltic Proper, Baltic Sea. *Nat. Hazards Earth Syst. Sci.* 17(9): 1653–1658, doi: 10.5194/nhess-17-1653-2017.
- Björkqvist J.-V., Lukas I., Alari V., van Vledder G. P., Hulst S., Pettersson H., Behrens A. & Männik A. 2018. Comparing a 41-year model hindcast with decades of wave measurements from the Baltic Sea. *Ocean Eng.* 152: 57–71, doi: 10.1016/j.oceaneng.2018.01.048.
- Björkqvist J.-V., Rikka S., Alari V., Männik A., Tuomi L. & Pettersson H. 2020. Wave height return periods from combined measurement-model data: a Baltic Sea case study. *Nat. Hazards Earth Syst. Sci.* 20(12): 3593–3609, doi: 10.5194/nhess-20-3593-2020.
- Broman B., Hammarklint T., Rannat K., Soomere T. & Valdmann A. 2006. Trends and extremes of wave fields in the north-eastern part of the Baltic Proper. *Oceanologia* 48(S): 165–184.
- Buehner M., Caya A., Carrieres T. & Pogson L. 2016. Assimilation of SSMIS and ASCAT data and the replacement of highly uncertain estimates in the Environment Canada Regional Ice Prediction System. *Q. J. R. Meteorol. Soc.* 142(695): 562–573, doi:10.1002/qj.2408.
- Bumke K. & Hasse L. 1989. An analysis scheme for determination of true surface winds at sea from ship synoptic wind and pressure observations. In: Munn R. E. (ed.), *Boundary Layer Studies and Applications*, Springer, Dordrecht, pp. 295–308, doi: 10.1007/978-94-009-0975-5\_18.
- Collins III C.O., Rogers W.E., Marchenko A. & Babanin A.V. 2015. In situ measurements of an energetic wave event in the Arctic marginal ice zone. *Geophys. Res. Lett.* 42(6): 1863–1870, doi: 10.1002/2015GL063063.
- [EUMETSAT] 2017. EUMETSAT Ocean and Sea Ice Satellite Application Facility. *Global sea ice concentration climate data record 1979–2015* (v2.0, 2017), [Online]. Norwegian and Danish Meteorological Institutes, doi: 10.15770/EUM\_SAF\_OSI\_0008.
- Gloersen P. & Cavalieri D.J. 1986. Reduction of weather effects in the calculation of sea ice concentration from microwave radiances. *J. Geophys. Res.-Oceans* 91(C3): 3913–3919, doi: 10.1029/JC091iC03p03913.
- Goerlandt F., Montewka J., Zhang W. & Kujala P. 2017. An analysis of ship escort and convoy operations in ice conditions. *Saf. Sci.* 95: 198–209, doi: 10.1016/j.ssci.2016.01.004.
- Granskog M., Kaartokallio H., Kuosa H., Thomas D. N. & Vainio J. 2006. Sea ice in the Baltic Sea – A review. *Estuar. Coast. Shelf Sci.* 70(1–2): 145–160, doi: 10.1016/j.ecss.2006.06.001.
- Guillou N. 2020. Estimating wave energy flux from significant wave height and peak period. *Renew. Energy* 155: 1383–1393, doi:10.1016/j.renene.2020.03.124.
- Haapala J. & Leppäranta M. 1996. Simulating the Baltic Sea ice season with a coupled ice-ocean model. *Tellus A* 48(5): 622–643, doi:10.3402/tellusa.v48i5.12158.
- Haapala J. & Leppäranta M. 1997. The Baltic Sea ice season in changing climate. *Boreal Environ. Res.* 2(1): 93–108.
- Haapala J.J., Ronkainen I., Schmelzer N. & Sztobryn M. 2015. Recent change—sea ice. In: The BACC II Author Team, *Second Assessment of Climate Change for the Baltic Sea Basin*, Regional Climate Studies, Springer, Cham, pp. 145–153, doi: 10.1007/978-3-319-16006-1\_8.
- Harff J., Deng J., Dudzińska-Nowak J., Fröhle P., Groh A., Hünicke B., Soomere T. & Zhang W. 2017. What determines the change of coastlines in the Baltic Sea? In: Harff J., Furmańczyk K., von Storch H. (eds.), *Coastline Changes of the Baltic Sea from South to East*, Springer, Cham, pp. 15–35, doi: 10.1007/978-3-319-49894-2\_2.
- Hünicke B., Zorita E., Soomere T., Madsen K.S., Johansson M. & Suursaar Ü. 2015. Recent change—sea level and wind waves. In: The BACC II Author Team, *Second Assessment of Climate Change for the Baltic Sea Basin*, Regional Climate Studies, Springer, Cham, pp. 155–185, doi: 10.1007/978-3-319-16006-1\_9.
- Jevrejeva S. 2001. Severity of winter seasons in the northern Baltic Sea between 1529 and 1990: reconstruction and analysis. *Clim. Res.* 17(1): 55–62.
- Jevrejeva S., Drabkin V.V., Kostjukov J., Lebedev A.A., Leppäranta M., Mironov Y.U., Schmelzer N. & Sztobryn M. 2004. Baltic Sea ice seasons in the twentieth century. *Clim. Res.* 25(3): 217–227.
- Kabacoff R. 2011. *R in Action: Data analysis and graphics with R*. Shelter Island, NY, USA: Manning publications.
- Käyhkö J., Apsite E., Bolek A., Filatov N., Kondratyev S., Korhonen J., Kriaučiūnienė J., Lindström G., Nazarova L., Pyrh A. & Sztobryn M. 2015. Recent change—river run-off and ice cover. In: The BACC II Author Team, *Second Assessment of Climate Change for the Baltic Sea Basin*, Regional Climate Studies, Springer, Cham, pp. 99–116, doi: 10.1007/978-3-319-16006-1\_5.
- Kelpšaitė-Rimkienė L., Parnell K.E., Žaromskis R. & Kon-

- drat V. 2021. Cross-shore profile evolution after an extreme erosion event—Palanga, Lithuania. *J. Mar. Sci. Eng.* 9(1): 38, doi:10.3390/jmse9010038.
- Komen G.J., Cavaleri L., Donelan M., Hasselmann K., Hasselmann S. & Janssen P.A.E.M. 1996. *Dynamics and Modelling of Ocean Waves*. Cambridge University Press, Cambridge, UK.
- Kudryavtseva N.A. & Soomere T. 2016. Validation of the multi-mission altimeter data for the Baltic Sea region. *Estonian J. Earth Sci.* 65: 161–175, doi: 10.3176/earth.2016.13.
- Kudryavtseva N. & Soomere T. 2017. Satellite altimetry reveals spatial patterns of variations in the Baltic Sea wave climate. *Earth Syst. Dyn.* 8(3): 697–706, doi: 10.5194/esd-8-697-2017.
- Kudryavtseva N., Räämet A. & Soomere T. 2020. Coastal flooding: Joint probability of extreme water levels and waves along the Baltic Sea coast. *J. Coast. Res.* 95(SI): 1146–1151, doi: 10.2112/SI95-222.1.
- Labuz T.A. 2015. Environmental impacts—coastal erosion and coastline changes. In: The BACC II Author Team, *Second Assessment of Climate Change for the Baltic Sea Basin*. Regional Climate Studies, Springer, Cham, pp. 381–396, doi: 10.1007/978-3-319-16006-1\_20.
- Lavergne T., Sørensen A. M., Kern S., Tonboe R., Notz D., Aaboe S., Bell L., Dybkjær G., Eastwood S., Gabarro C., Heygster G., Killie A. M., Kreiner B. M., Lavelle J., Saldo R., Sandven S. & Pedersen L.T. 2019. Version 2 of the EUMETSAT OSI SAF and ESA CCI sea-ice concentration climate data records. *Cryosphere* 13(1): 49–78, doi: 10.5194/tc-13-49-2019.
- Lensu M. & Goerlandt F. 2019. Big maritime data for the Baltic Sea with a focus on the winter navigation system. *Mar. Policy* 104: 53–65, doi:10.1016/j.marpol.2019.02.038.
- Leppäranta M. 2012. Ice Season in the Baltic Sea and Its Climatic Variability. In: Haapala I. (ed.), *From the Earth's Core to Outer Space*. Lecture Notes in Earth Sciences, 137. Springer, Berlin, Heidelberg, pp. 139–149, doi:10.1007/978-3-642-25550-2\_9.
- Leppäranta M. & Myrberg K. 2009. The ice of the Baltic Sea. In: *Physical Oceanography of the Baltic Sea*. Springer Praxis, Berlin, Heidelberg, pp. 219–260, doi: 10.1007/978-3-540-79703-6\_7.
- Liu A.K. & Mollo-Christensen E. 1988. Wave propagation in a solid ice pack. *J. Phys. Oceanogr.* 18(11): 1702–1712, doi: 10.1175/1520-0485(1988)018<1702:WPIASI>2.0.CO;2
- Mäll, M., Nakamura, R., Suursaar, Ü. & Shibayama, T. 2020. Pseudo-climate modelling study on projected changes in extreme extratropical cyclones, storm waves and surges under CMIP5 multi-model ensemble: Baltic Sea perspective. *Nat. Hazards* 102: 67–99, doi: 10.1007/s11069-020-03911-2.
- Männikus R., Soomere T. & Kudryavtseva N. 2019. Identification of mechanisms that drive water level extremes from in situ measurements in the Gulf of Riga during 1961–2017. *Cont. Shelf Res.* 182: 22–36, doi: 10.1016/j.csr.2019.05.014.
- Merkouriadi I. & Leppäranta M. 2014. Long-term analysis of hydrography and sea-ice data in Tvärminne, Gulf of Finland, Baltic Sea. *Clim. Change* 124(4): 849–859, doi:10.1007/s10584-014-1130-3.
- Mostert W. & Deike L. 2020. Inertial energy dissipation in shallow-water breaking waves. *J. Fluid Mech.* 890: A12, doi: 10.1017/jfm.2020.83.
- Najafzadeh F., Kudryavtseva N. & Soomere T. 2021. Effects of large-scale atmospheric circulation on the Baltic Sea wave climate: application of the EOF method on multi-mission satellite altimetry data. *Clim. Dyn.* 57(3–4), doi: 10.1007/s00382-021-05874-x.
- Nikolkina I., Soomere T. & Räämet A. 2014. Multidecadal ensemble hindcast of wave fields in the Baltic Sea. *2014 IEEE/OES Baltic International Symposium (BALTIC)*, “Measuring and Modeling of Multi-Scale Interactions in the Marine Environment”, May 26–29, Tallinn, Estonia. IEEE Conference Publications, doi: 10.1109/BALTIC.2014.6887854.
- Nilsson E., Rutgersson A., Dingwell A., Björkqvist J.-V., Pettersson H., Axell L., Nyberg J. & Strömstedt E. 2019. Characterization of wave energy potential for the Baltic Sea with focus on the Swedish Exclusive Economic Zone. *Energies* 12(5): 793, doi: 10.3390/en12050793.
- Omstedt A. & Nyberg L. 1996. Response of Baltic Sea ice to seasonal, interannual forcing and climate change. *Tellus A* 48(5): 644–662, doi: 10.3402/tellusa.v48i5.12160.
- Omstedt A., Pettersson C., Rodhe J. & Winsor P. 2004. Baltic Sea climate: 200 yr of data on air temperature, sea level variation, ice cover, and atmospheric circulation. *Clim. Res.* 25(3): 205–216, doi: 10.3354/cr025205.
- Omstedt A., Elken J., Lehmann A., Leppäranta M., Meier H.E.M., Myrberg K. & Rutgersson A. 2014. Progress in physical oceanography of the Baltic Sea during the 2003–2014 period. *Prog. Oceanogr.* 128: 139–171, doi: 10.1016/j.pocean.2014.08.010.
- Orviku K., Jaagus J., Kont A., Ratas U. & Rivis R. 2003. Increasing activity of coastal processes associated with climate change in Estonia. *J. Coast. Res.* 19: 364–375.
- OSI SAF 2017. *Global Sea Ice Concentration Climate Data Record v2.0 — Multimission, EUMETSAT SAF on Ocean and Sea Ice*, doi: 10.15770/EUM\_SAF\_OSI\_0008.
- Overeem I., Anderson R.S., Wobus C.W., Clow G.D., Urban F.E. & Matell N. 2011. Sea ice loss enhances wave action at the Arctic coast. *Geophys. Res. Lett.* 38(17), doi: 10.1029/2011GL048681.
- Pryor S.C. & Barthelmie R.J. 2003. Long-term trends in near-surface flow over the Baltic. *Int. J. Climatol.* 23(3): 271–289, doi: 10.1002/joc.878.
- Räämet A. & Soomere T. 2010. The wave climate and its seasonal variability in the northeastern Baltic Sea. *Estonian J. Earth Sci.* 59(1): 100–113, doi: 10.3176/earth.2010.1.08.
- Räämet A. & Soomere T. 2021. Spatial pattern of quality of historical wave climate reconstructions for the Baltic Sea. *Boreal Environ. Res.* 26: 29–41.
- Ruosteenoja K., Vihma T. & Venäläinen A. 2019. Projected Changes in European and North Atlantic Seasonal Wind Climate Derived from CMIP5 Simulations. *J. Clim.* 32(19): 6467–6490, doi: 10.1175/JCLI-D-19-0023.1.

- Rutgersson A., Kjellström E., Haapala J., Stendel M., Danilovich I., Drews M., Jylhä K., Kujala P., Guo Larsén X., Halsnæs K., Lehtonen I., Luomaranta A., Nilsson E., Olsson T., Särkkä J., Tuomi L. & Wasmund N. 2022. Natural hazards and extreme events in the Baltic Sea region. *Earth Syst. Dynam.* 13(1): 251–301, doi: 10.5194/esd-13-251-2022.
- Ryabchuk D., Kolesov A., Chubarenko B., Spiridonov M., Kurennoy D. & Soomere T. 2011. Coastal erosion processes in the eastern Gulf of Finland and their links with geological and hydrometeorological factors. *Boreal Environ. Res.* 16(Suppl. A): 117–137.
- Seifert T., Tauber F. & Kayser B. 2001. A high resolution spherical grid topography of the Baltic Sea—revised edition. In: *Baltic Sea Science Congress, November 25–29, 2001, Stockholm, Sweden*, Poster 147.
- Sztobryn M. 1994. Long-term changes in ice conditions at the Polish coast of the Baltic Sea. In: *Proc. 12th Int. Symp. on Ice, Norwegian Inst. Techn., Trondheim, Norway, August 23–26, 1994*, 345–354.
- [SMHI and FIMR] 1982. Swedish Meteorological and Hydrological Institute, and Finnish Meteorological Institute. *An Ice Atlas for the Baltic Sea, Kattegat, Skagerrak and Lake Vänern*. Norrköping, Sjöfartsverket.
- Sooäär J. & Jaagus J. 2007. Long-term changes in the sea ice regime in the Baltic Sea near the Estonian coast. *Estonian J. Eng.* 13(3): 189–200.
- Soomere T., Behrens A., Tuomi L. & Nielsen J.W. 2008. Wave conditions in the Baltic Proper and in the Gulf of Finland during windstorm Gudrun. *Nat. Hazards Earth Syst. Sci.* 8(1): 37–46, doi: 10.5194/nhess-8-37-2008.
- Soomere T. & Räämet A. 2011. Long-term spatial variations in the Baltic Sea wave fields. *Ocean Sci.* 7(1): 141–150, doi: 10.5194/os-7-141-2011.
- Soomere T. & Eelsalu M. 2014. On the wave energy potential along the eastern Baltic Sea coast. *Renew. Energy* 71: 221–233, doi: 10.1016/j.renene.2014.05.025.
- Suursaar Ü. & Kullas T. 2009. Decadal variations in wave heights off Cape Kelba, Saaremaa Island, and their relationships with changes in wind climate. *Oceanologia* 51(1): 39–61.
- Suursaar Ü., Kullas T., Otsmann M., Saaremäe I., Kuik J. & Merilain M. 2006. Cyclone Gudrun in January 2005 and modelling its hydrodynamic consequences in the Estonian coastal waters. *Boreal Environ. Res.* 11 (2): 143–159.
- Suursaar Ü., Alari V. & Tõnisson H. 2014. Multi-scale analysis of wave conditions and coastal changes in the north-eastern Baltic Sea. *J. Coast. Res.* 70: 223–228, doi: 10.2112/SI70-038.1.
- Tavakoli S. & Babanin A.V. 2021. Wave energy attenuation by drifting and non-drifting floating rigid plates. *Ocean Eng.* 226: 108717, doi: 10.1016/j.oceaneng.2021.108717.
- Tonboe R.T., Eastwood S., Laverigne T., Sørensen A.M., Rathmann N., Dybkjær G., Pedersen L.T., Høyer J.L. & Kern S. 2016. The EUMETSAT sea ice concentration climate data record. *Cryosphere* 10(5): 2275–2290, doi: 10.5194/tc-10-2275-2016.
- Torralba V., Doblas-Reyes F. J. & Gonzalez-Reviriego N. 2017. Uncertainty in recent near-surface wind speed trends: a global reanalysis intercomparison. *Environ. Res. Lett.* 12(11): 114019, doi: 10.1088/1748-9326/aa8a58.
- Tuomi L., Kahma K. K. & Pettersson H. 2011. Wave hindcast statistics in the seasonally ice-covered Baltic Sea. *Boreal Environ. Res.* 16(6): 451–472.
- Tuomi L., Kanarik H., Björkqvist J.-V., Marjamaa R., Vainio J., Hordoier R., Höglund A. & Kahma K.K. 2019. Impact of ice data quality and treatment on wave hindcast statistics in seasonally ice-covered seas. *Front. Earth Sci.* 7: 166, doi: 10.3389/feart.2019.00166.
- Vihma T. & Haapala J. 2009. Geophysics of sea ice in the Baltic Sea: A review. *Prog. Oceanogr.* 80(3–4): 129–148, doi: 10.1016/j.pocean.2009.02.002.
- Von Storch H., Omstedt A., Pawlak J. & Reckermann M. 2015. Introduction and Summary. In: The BACC II Author Team, *Second Assessment of Climate Change for the Baltic Sea Basin*. Regional Climate Studies, Springer, Cham, pp. 1–22, doi: 10.1007/978-3-319-16006-1\_1.
- Zaitseva-Pärnaste I. & Soomere T. 2013. Interannual variations of ice cover and wave energy flux in the north-eastern Baltic Sea. *Ann. Glaciol.* 54(62): 175–182, doi: 10.3189/2013AoG62A228.
- Zhang N., Li S., Wu Y., Wang K.H., Zhang Q., You Z.J. & Wang J. 2020. Effects of sea ice on wave energy flux distribution in the Bohai Sea. *Renew. Energy* 162: 2330–2343, doi: 10.1016/j.renene.2020.10.036.

### Publication III

Männikus R., Soomere T., **Najafzadeh F.** 2022. Refraction may redirect waves from multiple directions into a harbour: a case study in the Gulf of Riga, eastern Baltic Sea. *Estonian Journal of Earth Sciences*, 71(2), 80–88, doi: 10.3176/earth.2022.06.



## Refraction may redirect waves from multiple directions into a harbour: a case study in the Gulf of Riga, eastern Baltic Sea

Rain Männikus<sup>a\*</sup>, Tarmo Soomere<sup>a,b</sup> and Fatemeh Najafzadeh<sup>a</sup>

<sup>a</sup>Laboratory of Wave Engineering, Department of Cybernetics, School of Science, Tallinn University of Technology, Akadeemia tee 21, 12618 Tallinn, Estonia; soomere@cs.ioc.ee

<sup>b</sup>Estonian Academy of Sciences, Kohtu 6, 10130 Tallinn, Estonia

\* Corresponding author, rain.mannikus@gmail.com

Received 14 January 2022, accepted 18 April 2022, available online 12 May 2022

**Abstract.** We analyse the impact of bathymetry on the propagation direction of wind waves near the Port of Ringsu on the island of Ruhnu in the central part of the Gulf of Riga (Gulf of Livonia). Waves propagating towards this port are systematically redirected by underwater features. On most occasions the main direction of the refracted saturated wave fields is towards the harbour entrance. This shows that the port entrance needs a complicated set of breakwaters to cope with wind generated waves from most directions.

**Keywords:** wave modelling, wave direction, SWAN model, port planning, Gulf of Riga, Baltic Sea.

### INTRODUCTION

The main task of both large and small harbours is to provide effective protection for vessels from the impact of wind, waves and currents (Cairns et al. 2016), as well as to offer a safe haven for various operations. Since ancient times (Safadi 2016) this requirement has usually been achieved by a smart choice of the location of the harbour entrance so that it is naturally sheltered against severe waves and/or by the construction of a system of breakwaters that protect the port interior from marine impacts.

Wave refraction may convert seemingly well-sheltered coastal areas into hot spots of wave energy (Kovaleva et al. 2017). In some cases, waves can undergo substantial changes from their deep-water direction of propagation. This kind of ultra-refraction by more than 90 degrees redirects, for example, south-west swells into San Francisco Bay (Hanes and Erikson 2013).

This phenomenon occurs frequently on the downwind side of small islands and shoals where refracted waves may cross each other or enter seemingly sheltered bays. However, the related effects usually do not impact the interior of small ports and marinas that are located on the downwind side of such islands or headlands.

The small island of Ruhnu (Fig. 1) lies in the middle of the Gulf of Riga (Gulf of Livonia in Estonian tradition) and is thus open to all wind directions. In this region, strong winds blow usually either from the south-west or less frequently from the north/north-west (Soomere and Keevallik 2001; Männikus et al. 2019). Easterly winds are much weaker and south-east winds are infrequent and mild. Very little wave energy generated in the Baltic Proper penetrates into the Gulf of Riga. Wave fields in this water body are thus mostly locally generated and, on most occasions, follow the wind patterns. The nearshore of the western side of this island is shallow, rocky and unwelcoming for landing while the eastern shore is steeper, less rocky and more easily accessible from the sea.

The described anisotropy of wind (and wave) fields together with the different characteristics of the shores are evidently the main reasons why all historical boat landing sites were located on the eastern coast of Ruhnu (Fig. 2). Interestingly, one such site lay to the west of natural Cape Ringsu (Rings-Udden), the southern tip of the island, in an area that seems to be fully open to one of the predominant wind directions. Much of historical knowledge about these sites was lost after the 1940s. According to a census taken in 1934, Ruhnu had a

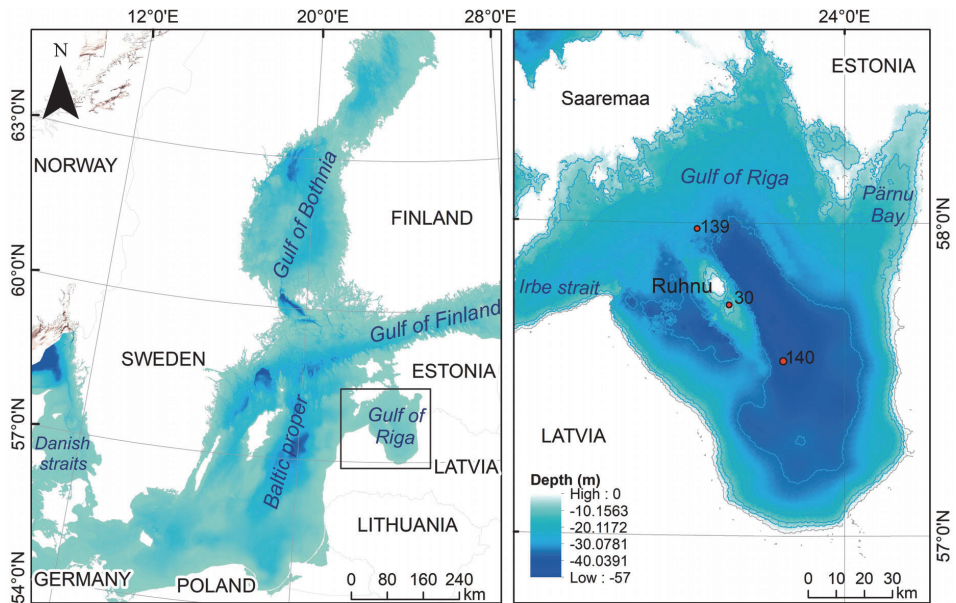


**Fig. 1.** The Gulf of Riga in the Baltic Sea (left panel) and the island of Ruhnu in the Gulf of Riga (right panel). The right panel shows the area covered by the second-level computational grid of the wave model and the selected grid points (30, 139, 140) for the analysis of wave directions. Point 30 is located at Gretagrund, a shallow area to the south of Ruhnu.

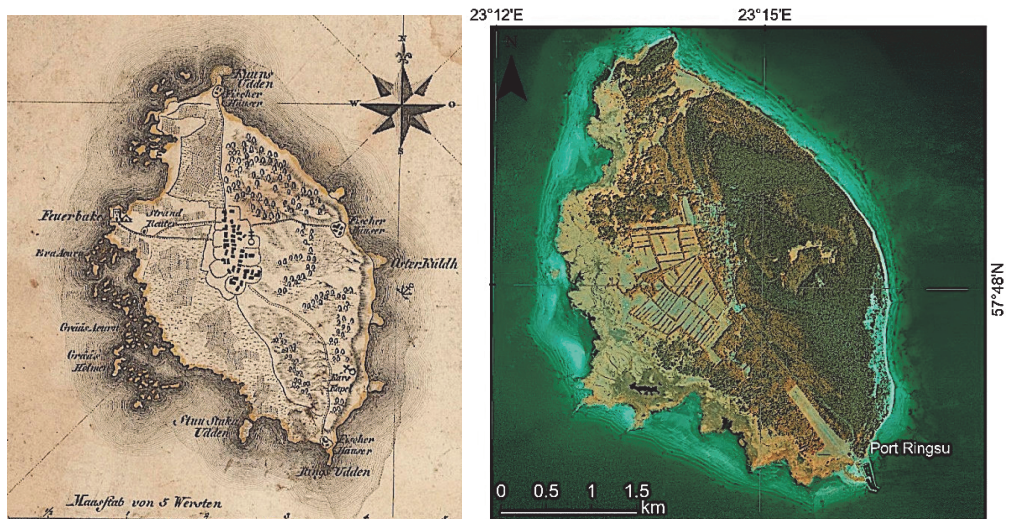


**Fig. 2.** The island of Ruhnu from the Atlas of Livland (Livonia) by Ludwig August von Mellin in 1798 (left panel). It is likely that boat landing sites were located by the fishermen's houses (Fischer Häuser). Note that the fishermen's house near Cape Ringsu (Ringsu-Udden) was located on the western coast of the cape, which is open to one of the predominant wind directions. The Port of Ringsu is located at the south-eastern tip of the island (right panel).

population of 282, among these 277 ethnic Swedes and 5 ethnic Estonians (LinkFang 2021). Most locals (except for two families) had fled from Ruhnu to Sweden by the end of the Second World War.

The contemporary Port of Ringsu was constructed at the end of the 1950s (Orviku 2018). This was the time when knowledge about wave properties was scarce in Estonia and planning activities in the Soviet Union were dictated by military and political considerations rather than economic or scientific reasons. The location along the eastern shore of Cape Ringsu had been used for lifting ships out of water and for unloading ships by using small boats in the past (Orviku 2018), but not as a harbour site.

The contemporary harbour (Fig. 2) was designed to meet the above description of predominant wind patterns. The port and its approach are geometrically sheltered against waves coming from the north-west and north. The port interior is protected from waves that approach from the south-west and west by a shallow-water area and a breakwater. To protect the port waters even better, the tip of the southern breakwater is turned to the south-east. Another breakwater protects the port and its entrance channel from waves from the north, north-east and east. The entrance is oriented to the south-east (about 120° clockwise from the north), that is, to the direction from which winds are infrequent and weak.

In spite of this careful design, the port interior often suffers from inconveniently high waves and sudden changes in the water level. Undesirable wave conditions often occur even during westerly winds, against which the harbour seems to be perfectly protected.

In this article we demonstrate that wave conditions that annoy the port visitors and endanger small vessels in the port are created systematically by wave refraction and perhaps ultra-refraction. To that end, we employ a sequence of wave model runs forced by stationary and homogeneous wind conditions across the entire study area. The simulations are performed until the wave field becomes stationary.

## THE WAVE MODEL

We used wave model SWAN (version 40.11) in Delft3D suite to replicate waves under a variety of stationary wind conditions. As the fetch length and propagation distance of waves that reach Ruhnu are both less than 100 km (Fig. 1), this approach gives a reasonable estimate of wind conditions during which waves may affect the harbour interior.

The wave model SWAN (Booij et al. 1999) is a third-generation phase-averaged spectral wave model that was developed at Delft University of Technology. The waves are described via the two-dimensional wave action density

spectrum  $N$ , the evolution of which is governed by the wave action balance equation. This equation, in Cartesian coordinates without ambient currents, takes the following form:

$$\frac{\partial N}{\partial t} + \frac{\partial c_x N}{\partial x} + \frac{\partial c_y N}{\partial y} + \frac{\partial c_\sigma N}{\partial \sigma} + \frac{\partial c_\theta N}{\partial \theta} = \frac{S_{tot}}{\sigma}.$$

The terms on the left side of this equation represent the rate of change and the propagation of wave energy in two-dimensional geographical space, as well as the shifting of the angular frequency caused by variations in depth and depth-induced refraction. The  $x$ - and  $y$ -components of the group velocity are denoted by  $c_x$  and  $c_y$ . The propagation velocities in the spectral space, which are defined by the angular frequency  $\sigma$  and the propagation direction  $\theta$ , are  $c_\sigma$  and  $c_\theta$ , respectively. Expressions for the spectral velocities can be found in the SWAN technical manual (The SWAN team 2021).

The core quantity on the right-hand side  $S_{tot}$  denotes the sum of all physical processes that represent generation, dissipation or redistribution of wave energy in SWAN. The deep-water source terms include energy input by wind (Komen et al. 1984), dissipation of waves by white-capping (Komen et al. 1984) and nonlinear transfer of wave energy due to four-wave interactions using the Discrete Interaction Approximation (DIA) (Hasselmann et al. 1985). The whitecapping coefficient  $\delta$  was set at  $\delta = 1$  following Rogers et al. (2003) and Pallares et al. (2014). We used the wind drag parameterisation suggested by Wu (1982). The shallow-water source terms are energy dissipation through bottom friction (Hasselmann et al. 1973), dissipation due to depth-induced wave breaking (Battjes and Janssen 1978) and nonlinear transfer of wave energy through three-wave interactions using the Lumped Triad Approximation (LTA) (Eldeberky 1996). The bottom friction coefficient was set at  $0.038 \text{ m}^2/\text{s}^3$ , as suggested by Zijlema et al. (2012). The values of parameters  $\alpha$  and  $\gamma$  for the depth-induced wave breaking source term were set at  $\alpha = 1$  and  $\delta = 0.73$ , respectively. A very similar configuration of the SWAN model has shown excellent results in calculations of the Baltic Sea wave fields (Björkqvist et al. 2018).

We used a four-level nested scheme of rectangular model grids. Even though only very little wave energy created in the Baltic Proper enters the Gulf of Riga, propagation of specific swells into the gulf cannot be excluded. For this reason, a coarse model was run for the whole Baltic Sea on a regular grid with a step of 5000 m ( $251 \times 271$  grid points). The second-level regular grid covered the Gulf of Riga with a step of 1000 m ( $171 \times 181$  grid points). The third-level grid (Fig. 3) covered the island of Ruhnu with neighbouring waters with a regular step of 100 m ( $211 \times 171$  grid points). The innermost (finest) model focused on the Port of Ringsu (Fig. 3) with

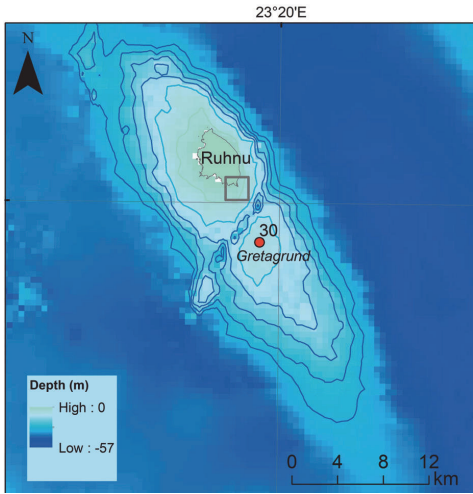


**Fig. 3.** The location scheme of the third-level (entire panel) and fourth-level (small box on Ruhnu) nested grids.

a varying step of 11 to 3 m ( $232 \times 194$  grid points). The resolution of the third- and fourth-level grids is evidently sufficiently fine to replicate refraction of waves in the vicinity of Ruhnu and the Port of Ringsu. The bathymetry was taken from the database of the Estonian Transport Administration and from the Baltic Sea Bathymetry Database by the Baltic Sea Hydrographic Commission (Baltic Sea Hydrographic Commission 2013). At each sea grid point, 864 spectrum components (36 equally spaced directions and 24 frequency bins from 0.05 Hz to 1 Hz) were calculated.

The model was forced with stationary (unidirectional steady) wind at a speed of 5, 10 or 15 m/s until the wave field became saturated. This happens in the Gulf of Riga usually within 2–3 hours for 5 m/s, 3–5 hours for 10 m/s, and within 6 hours for a wind speed of 15 m/s. The wind direction was varied from  $15^\circ$  to  $345^\circ$  with a step of  $30^\circ$ . Hence, there were 36 different situations. The spatial pattern of the resulting wave directions is provided below, mainly from the third-level grid. The location of wave model grid points used below to quantify the impact of refraction on the wave fields in the vicinity of the southern tip of Ruhnu and around Gretagrund (Fig. 3) is presented in Fig. 4.

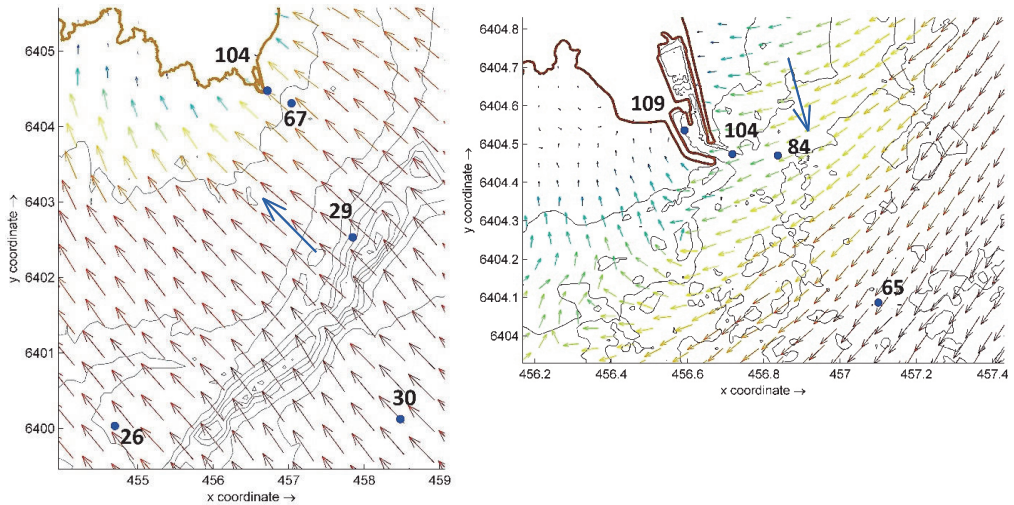


**Fig. 4.** The wave model grid points for data used in Fig. 4 and in Figs 5–7. Left panel: third-level grid, wind from the direction of  $135^\circ$ . Right panel: innermost fourth-level grid, wind from the direction of  $345^\circ$ . The wave pattern is presented for a wind speed of 15 m/s. The blue large arrows indicate the wind direction. The wave height is represented by colour (brown and red: the highest, yellow: medium, green and blue: lower waves) and the length of small arrows while the wave direction is indicated by the direction of small arrows. The scale is presented in kilometres.

## RESULTS

As expected, the simulated wave direction in saturated fetch-limited situations with a relatively low wind speed of 5 m/s follows almost exactly the wind direction in the open area of the Gulf of Riga (Fig. 5A). The deviation of the mean wave direction from the forcing wind direction provided by the SWAN model slightly increases for strong winds (15 m/s) and reaches up to 15° for some wind directions (Fig. 5B). The mean wave direction corresponds even better to the wind direction at the tip of Gretagrund to the south of Ruhnu (Fig. 5). While wave heights at these three locations vary substantially (from

1.88 to 2.73 m for a wind speed of 15 m/s) for different wind directions, the mean period only varies from 4.0 to 5.1 s.

The situation is similar to that in the deep channel between Ruhnu and Gretagrund described above. On most occasions, the mean wave direction follows the wind direction (Fig. 6). The deviation of the wave propagation from the wind direction is up to 20° on both slopes of this channel (Fig. 6). Wave direction on the coastal slope of Ruhnu at a distance of 0.5 km from the entrance of the Port of Ringsu (point 67 in Fig. 4, left panel) corresponds less closely to the wind direction. The deviation of waves from the wind direction exceeds 30° for winds from the

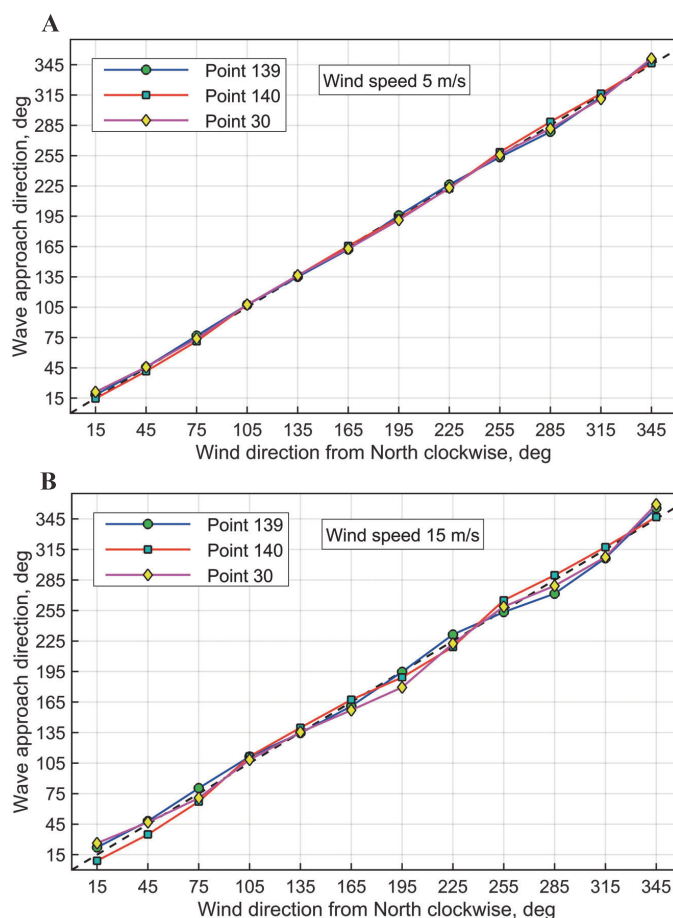


**Fig. 5.** Comparison of the wind direction and the mean propagation direction of simulated waves in saturated wave fields for wind speeds of 5 m/s (A) and 15 m/s (B) in the open part of the Gulf of Riga to the north (point 139, Fig. 1) and south (point 140, Fig. 1) of Ruhnu, and at the tip of Gretagrund (point 30, Fig. 4) to the south of Ruhnu.

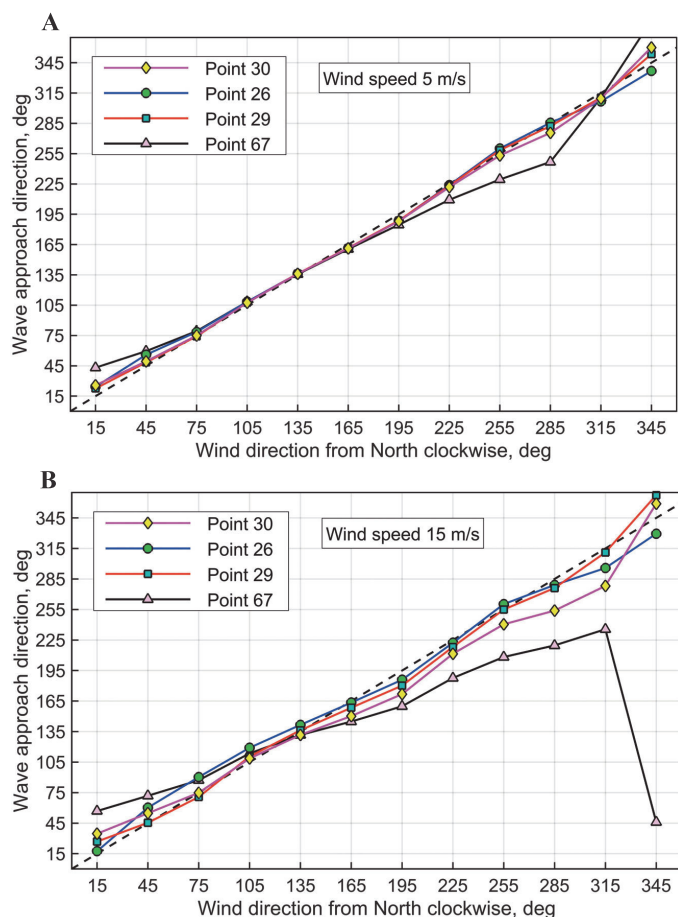


**Fig. 6.** Comparison of the wind direction and the mean direction of simulated wave propagation in saturated wave fields for wind speeds of 5 m/s (A) and 15 m/s (B) on the northern slope of Gretagrund (point 30, water depth 7.7 m), in the shallow area to the west of the grid (point 26, water depth 13 m), in the deep channel (point 29, water depth 21 m), and on the fairway to the Port of Ringsu (point 67). The locations of grid points are indicated in Fig. 4.

west to the north at this particular point (point 67 in Fig. 4, left panel). As expected, the deviation is larger for stronger winds and reaches  $90^\circ$  for north-west and north winds.

Wave propagation direction often deviates significantly from the wind direction in the immediate vicinity of the Port of Ringsu, even for weak winds (Fig. 7A). The mean wave direction corresponds to the wind direction only for south-east winds ( $115^\circ$ ) near the entrance to the Port of Ringsu (Fig. 7). Basically, these winds blow right into the port entrance. For a low wind speed (5 m/s), the wave direction follows the wind direction to some extent

for east, south and west winds. The deviation of wave propagation from the wind direction increases with the increase in wind speed because longer waves driven by stronger winds experience more intense refraction. This deviation is usually of the order of  $30^\circ$  at a distance of about 0.5 km (point 65 in Fig. 4, right panel) from the port entrance for winds of 15 m/s from the east, south and west. The deviation increases to  $60^\circ$ – $90^\circ$  for north-west and north winds (Fig. 7). This pattern of changes evidently represents the impact of refraction on wave propagation in the shallow nearshore of Ruhnu.

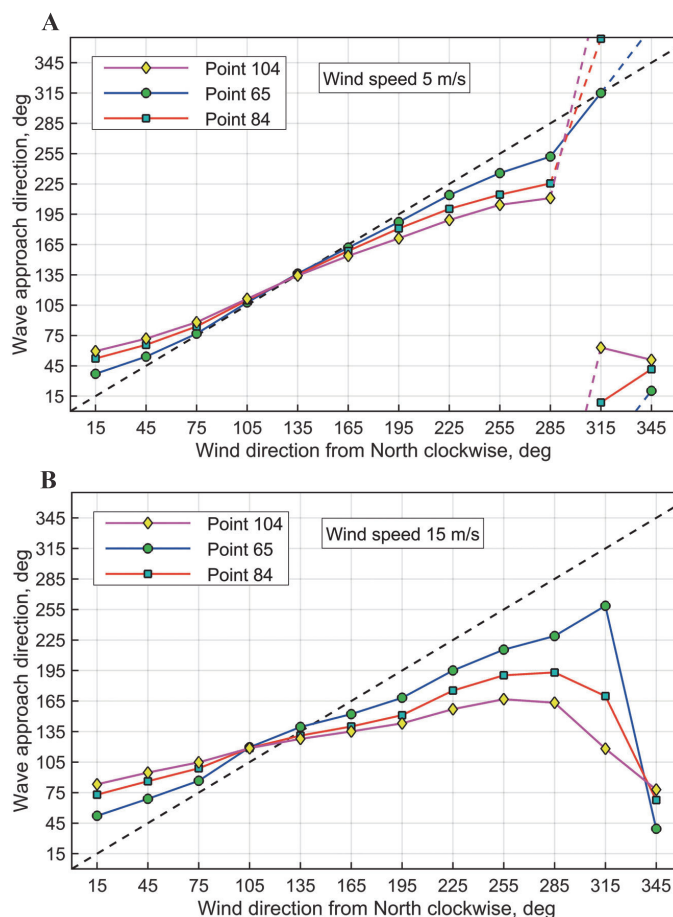


**Fig. 7.** Comparison of the wind direction and the mean direction of simulated wave propagation for wind speeds of 5 m/s (A) and 15 m/s (B) in saturated wave fields to the south-east of Ruhnu (point 65), on the fairway to the Port of Ringsu (point 84), and at the entrance to the Port of Ringsu (point 104). The locations of grid points are indicated in Fig. 4.

The impact of refraction becomes, as expected, stronger for higher and longer waves produced by higher wind speeds. Refraction redirects waves excited by wind speeds of 15 m/s so that the mean direction of waves is confined to the range of directions 80–190° (Fig. 7B). Only waves excited by easterly winds follow the wind direction towards the entrance to the Port of Ringsu. Importantly, wave directions generated by most strong (15 m/s) winds are reshaped by the bathymetry so that waves approach the fairway and the port entrance from the south-east, that is, heading directly for the port entrance.

## DISCUSSION

The central conjecture from the presented analysis is that refraction of wind waves on underwater slopes of the island of Ruhnu and possibly on the slopes of Gretagrund to the south of Ruhnu systematically redirects the waves so that intense waves enter the Port of Ringsu during virtually any strong wind event. This transformation is relatively mild for weak winds but becomes more significant for strong winds. This feature simply reflects an increase in the wave period and length under stronger

winds, which leads to an associated increase in refraction. It is therefore likely that in the case of very strong storms the range of wave approach directions is even narrower, converging around 120°, that is, along the fairway that enters the port.

This outcome is not completely unexpected as refraction often reshapes nearshore wave fields. This phenomenon may cause an inhomogeneous distribution of wave heights along some coastal segments as demonstrated, e.g., by the classic ray diagram for the mouth of the Hudson River on the Atlantic coast of the USA (Kinsman 1965). It is, however, surprising and instructive that this mechanism can create a massive wave energy flux, on average, straight from the direction where winds are the weakest and least frequent.

It might be necessary to design more extensive protection of the entrance to the Port of Ringsu to ensure safety in its interior. It could be realised, for example, in the form of an island-style breakwater located in the prevailing approach direction of waves. Such an island or breakwater could be either a stationary (Cox and Czlapinski 2016) or anchored floating structure (Davis et al. 2013). The existing harbour jetties have also been designed to avoid siltation of the port. A modified shelter structure will eventually influence the sediment transport pattern in the vicinity of the harbour. It is therefore important to check whether it could lead to silting of the harbour entrance.

Finally, we note that the wave heights approaching from the south and south-west could, to some extent, be underestimated by the SWAN model as this model tends to underpredict wave energy when waves are penetrating into bathymetries with shallow areas traversed by channels (Groeneweg et al. 2015). Such effects are characteristic of tidal inlets. They can occur here because of the presence of a deep channel between Ruhnu and Gretgrund to the south of the island. This channel evidently plays a role similar to that of dredged navigation channels where refraction leads to the concentration of wave energy on the sides of the channel (Li et al. 2000). The energy of waves approaching from the south, south-west or west is redirected to the south along the southern side of the channel. The concentrated wave energy that propagates along the northern side of the channel, on the other hand, may propagate directly towards the entrance to the Port of Ringsu.

## CONCLUSION

We have shown that underwater slopes of small islands and nearby shallows may systematically and radically redirect wind waves so that they regularly impact coastlines and

coastal engineering structures from an unexpected direction, independent of the wind direction. In the case of the Port of Ringsu located on the island of Ruhnu, it is the direction from which storm winds are infrequent and weak.

**Acknowledgements.** The research was co-supported by the Estonian Research Council (grant PRG1129) and the European Economic Area (EEA) Financial Mechanism 2014–2021 Baltic Research Programme (grant EMP480). Rain Männikus acknowledges the support by Saarte Liinid AS, contract LTEE21048. We are very grateful to Maris Eelsalu who produced the maps and to Prof. Kevin Parnell for suggestions towards improvement of the manuscript. The authors also thank the reviewers Hannes Tõnisson and Peter Fröhle for their valuable comments. The publication costs of this article were covered by the Estonian Academy of Sciences.

## REFERENCES

- Baltic Sea Hydrographic Commission. 2013. *Baltic Sea Bathymetry Database Version 0.9.3*. <http://data.bshc.pro/legal> (accessed 2121-04-01).
- Battjes, J. A. and Janssen, J. P. F. M. 1978. Energy loss and set-up due to breaking of random waves. In *Proceedings of the 16th International Conference on Coastal Engineering, Hamburg, Germany, August 27 – September 3, 1978*. American Society of Civil Engineers, 569–587. <https://doi.org/10.1061/9780872621909.034>
- Björkqvist, J.-V., Lukas, I., Alari, V., van Vledder, G. Ph., Hulst, S., Pettersson, H., Behrens, A. and Männik A. 2018. Comparing a 41-year model hindcast with decades of wave measurements from the Baltic Sea. *Ocean Engineering*, **152**, 57–71. <https://doi.org/10.1016/j.oceaneng.2018.01.048>
- Booij, N., Ris, R. C. and Holthuijsen, L. H. 1999. A third-generation wave model for coastal regions: 1. model description and validation. *Journal of Geophysical Research – Oceans*, **104**(C4), 7649–7666. <https://doi.org/10.1029/98JC02622>
- Cairns, A., Carel, J. M. and Li, X. 2016. Port and harbor design. In *Springer Handbook of Ocean Engineering* (Dhanak, M. R. and Xiros, N. I., eds). Springer, Cham, 685–710. [https://doi.org/10.1007/978-3-319-16649-0\\_31](https://doi.org/10.1007/978-3-319-16649-0_31)
- Cox, J. C. and Czlapinski, R. E. 2016. Engineering of an island-style breakwater system for the Fort Pierce marina. *Proceedings of the Institution of Civil Engineers – Maritime Engineering*, **169**(1), 37–43. <https://doi.org/10.1680/jmaen.15.00014>
- Davis, J., Phillips, J., Czlapinski, R., Seissiger, E. and Cignarella, P. 2013. Breakwater island creation: A 3-fold system. In *Design and Practice of Geosynthetic-Reinforced Soil Structures. International Symposium on Design and Practice of Geosynthetic-Reinforced Soil Structures / 26th Italian National Conference on Geosynthetics, Bologna, Italy, October 14–16, 2013* (Ling, H. I., Gottardi, G., Cazzuffi, D., Han, J. and Tatsuoka, F., eds). DEStech Publications, Lancaster, PA, 708–718.

- Eldeberky, Y. 1996. *Nonlinear transformation of wave spectra in the nearshore zone*. PhD Thesis. Delft University of Technology, Netherlands.
- Groeneweg, J., van Gent, M., van Nieuwkoop, J. and Toledo, Y. 2015. Wave propagation into complex coastal systems and the role of nonlinear interactions. *Journal of Waterway, Port, Coastal, and Ocean Engineering*, **141**(5). [https://doi.org/10.1061/\(ASCE\)WW.1943-5460.0000300](https://doi.org/10.1061/(ASCE)WW.1943-5460.0000300)
- Hanes, D. M. and Erikson, L. H. 2013. The significance of ultra-refracted surface gravity waves on sheltered coasts, with application to San Francisco Bay. *Estuarine, Coastal and Shelf Science*, **133**, 129–136. <https://doi.org/10.1016/j.ecss.2013.08.022>
- Hasselmann, K., Barnett, T. P., Bouws, E., Carlson, H., Cartwright, D. E., Enke, K. et al. 1973. Measurements of wind-wave growth and swell decay during the Joint North Sea Wave Project (JONSWAP). *Deutsche Hydrographische Zeitung*, **8**(12).
- Hasselmann, S., Hasselmann, K., Allender, J. H. and Barnett, T. P. 1985. Computations and parameterizations of the nonlinear energy transfer in a gravity-wave spectrum. Part II: parameterizations of the nonlinear energy transfer for application in wave models. *Journal of Physical Oceanography*, **15**(11), 1378–1391. [https://doi.org/10.1175/1520-0485\(1985\)015<1378:CAPOTN>2.0.CO;2](https://doi.org/10.1175/1520-0485(1985)015<1378:CAPOTN>2.0.CO;2)
- Kinsman, B. 1965. *Wind Waves: Their Generation and Propagation on the Ocean Surface*. Prentice-Hall, Englewood Cliffs, NJ.
- Komen, G. J., Hasselmann, S. and Hasselmann, K. 1984. On the existence of a fully developed wind-sea spectrum. *Journal of Physical Oceanography*, **14**(8), 1271–1285. [https://doi.org/10.1175/1520-0485\(1984\)014<1271:OTEQAF>2.0.CO;2](https://doi.org/10.1175/1520-0485(1984)014<1271:OTEQAF>2.0.CO;2)
- Kovaleva, O., Eelsalu, M. and Soomere, T. 2017. Hot-spots of large wave energy resources in relatively sheltered sections of the Baltic Sea coast. *Renewable and Sustainable Energy Reviews*, **74**, 424–437. <https://doi.org/10.1016/j.rser.2017.02.033>
- Li, Y. S., Liu, S.-X., Wai, O. W. H. and Yu, Y.-X. 2000. Wave concentration by a navigation channel. *Applied Ocean Research*, **22**(4), 199–213. [https://doi.org/10.1016/S0141-1187\(00\)00013-4](https://doi.org/10.1016/S0141-1187(00)00013-4)
- LinkFang. 2021. *Ruhnu*. <https://en.linkfang.org/wiki/Ruhnu> (accessed 2021-12-21).
- Männikus, R., Soomere, T. and Kudryavtseva, N. 2019. Identification of mechanisms that drive water level extremes from in situ measurements in the Gulf of Riga during 1961–2017. *Continental Shelf Research*, **182**, 22–36. <https://doi.org/10.1016/j.csr.2019.05.014>
- Orviku, K. 2018. *Rannad ja rannikud (Beaches and Shores)*. Tallinna ülikooli kirjastus, Tallinn (in Estonian).
- Pallares, E., Sánchez-Arcilla, A. and Espino, M. 2014. Wave energy balance in wave models (SWAN) for semi-enclosed domains – Application to the Catalan coast. *Continental Shelf Research*, **87**, 41–53. <https://doi.org/10.1016/j.csr.2014.03.008>
- Rogers, W. E., Hwang, P. A. and Wang, D. W. 2003. Investigation of wave growth and decay in the SWAN model: three regional-scale applications. *Journal of Physical Oceanography*, **33**(2), 366–389. [https://doi.org/10.1175/1520-0485\(2003\)033<0366:IOWGAD>2.0.CO;2](https://doi.org/10.1175/1520-0485(2003)033<0366:IOWGAD>2.0.CO;2)
- Safadi, C. 2016. Wind and wave modelling for the evaluation of the maritime accessibility and protection afforded by ancient harbours. *Journal of Archaeological Science: Reports*, **5**, 348–360. <https://doi.org/10.1016/j.jasrep.2015.12.004>
- Soomere, T. and Keevallik, S. 2001. Anisotropy of moderate and strong winds in the Baltic Proper. *Proceedings of the Estonian Academy of Sciences. Engineering*, **7**(1), 35–49. <https://doi.org/10.3176/ENG.2001.1.04>
- The SWAN team. 2021. *SWAN scientific and technical documentation*. Technical Report. Delft University of Technology. <http://swanmodel.sourceforge.net/download/zip/swantech.pdf> (accessed 2021-12-20).
- Wu, J. 1982. Wind-stress coefficients over sea surface from breeze to hurricane. *Journal of Geophysical Research – Oceans*, **87**(C12), 9704–9706. <https://doi.org/10.1029/JC087iC12p09704>
- Zijlema, M., van Vledder, G. Ph. and Holthuijsen, L. H. 2012. Bottom friction and wind drag for wave models. *Coastal Engineering*, **65**, 19–26. <https://doi.org/10.1016/j.coastaleng.2012.03.002>

## Näiliselt kaitstud väikesadamat võib ohustada lainete refraktsioon: Ringsu sadam Ruhnu saarel Liivi lahes

Rain Männikus, Tarmo Soomere ja Fatemeh Najafzadeh

Madalmeres levivate lainete suund muutub refraktsiooni tõttu süstemaatiliselt nõnda, et laineharjad muutuvad järjest enam paralleelseks mere samasügavusjoontega. Ringsu sadam Ruhnu saarel on avatud kagusse, kust tugevaid tuuli puhub harva. Ruhnu saart ümbritsev madalmeri ja sellest lõunas paiknev Gretagrundi madal mõjutavad aga lainelevi suunda nii, et Liivi lahel mistahes suunast puhuvate tugevamate tuulte (15 m/s) korral levivad kõrged lained valdavalt otse Ringsu sadamasse. Ohutuse tagamiseks tuleb sadama suuet kaitsta just kagu poolt.

# Curriculum Vitae

## 1. Personal data

Name Fatemeh Najafzadeh  
Date of birth 11.06.1990  
Place of birth Mashhad, Iran  
Citizenship Iran

## 2. Contact data

Address Ehitajate tee 5, 12616 Tallinn  
Phone (+372) 51813370  
E-mail Fatemeh.Najafzadeh@taltech.ee

## 3. Education

Educational institution	Graduation year	Education (field of study / degree)
Amirkabir University of technology	2013–2016	Naval Architecture / Master of Science
Chabahar Maritime University	2008–2013	Naval Architecture /Bachelor of Sciences
Shahed Varesane Noor	2004–2008	High school

## 4. Language competence/skills

Language	Level
English	Fluent – C1
Persian	Native
Arabic	Beginner
Estonian	Beginner
German	Beginner

## 5. Special courses and further training

Period	Educational or other organisation
January 2020	Visit to Finnish Meteorological Institute, Helsinki, Finland
September 2019	<i>Applications of Remote Sensing in the Baltic Sea region</i> , Võru, Estonia
March 2019	<i>Analysis of Climate Variability</i> , Rostock, Germany
August 2018	<i>Climate of the Baltic Sea</i> , Summer school, Trosa, Sweden

## 6. Professional employment

Period	Organisation	Position
March 2018–to date	Tallinn University of Technology, Department of Cybernetics	Early stage researcher
March–June 2013	Chabahar Maritime University	Teaching assistant

## 7. Research activity

*Articles indexed by the Web of Science database (1.1):*

**Najafzadeh F.**, Kudryavtseva N., Soomere T., Giudici A. 2022. Effect of ice cover on wave statistics and wave-driven processes in the northern Baltic Sea. *Boreal Environment Research*, 27, 97–116.

Männikus R., Soomere T., **Najafzadeh F.** 2022. Refraction may redirect waves from multiple directions into a harbour: a case study in the Gulf of Riga, eastern Baltic Sea. *Estonian Journal of Earth Sciences*, 71 (2), 80–88, doi: 10.3176/earth.2022.06.

**Najafzadeh F.**, Kudryavtseva N., Soomere T. 2021. Effects of large-scale atmospheric circulation on the Baltic Sea wave climate: application of the EOF method on multi-mission satellite altimetry data. *Climate Dynamics*, 57, 3465–3478, doi: 10.1007/s00382-021-05874-x.

*Articles published in other conference proceedings (3.4):*

Giudici A., Männikus R., **Najafzadeh F.**, Jankowski M.Z., Soomere T., Suursaar Ü. 2022. High-resolution wave model for coastal management and engineering in the eastern Baltic Sea. *4<sup>th</sup> Baltic Earth Conference Assessing the Baltic Sea Earth System* (30 May to 3 June 2022, Jastarnia, Poland. Presented by Jankowski M.Z.).

**Najafzadeh F.**, Giudici A., Soomere T., Männikus R., Jankowski M.Z. 2021. High-Resolution Wave Climate Calculations in the Baltic Sea using SWAN with a 3-nested grid system. *The Gulf of Finland Science Days* (29–30 November 2021, Tallinn, Estonia).

**Najafzadeh F.**, Kudryavtseva N., Giudici A., Soomere T., 2020. Estimating the wave statistics bias in the partially ice-covered regions of the Baltic Sea. *3<sup>rd</sup> Baltic Earth Conference Earth system changes and Baltic Sea coasts* (2–3 June 2020, online).

*Abstracts of conference presentations (5.2):*

**Najafzadeh F.**, Kudryavtseva N., Soomere T. 2020. Contribution of Atmospheric Teleconnections in Regional Wave Climate Variability Based on EOF Application: Baltic Sea Case. *AGU Advancing Earth and Space Science* (11–17 December 2020, online).

**Najafzadeh F.**, Kudryavtseva N., Soomere T. 2019. Effects of the sampling bias on retrieved modes of wave climate variations from satellite altimetry: Baltic Sea case study. *ESA Living Planet Symposium* (13–17 May 2019, Milan, Italy).

**Najafzadeh F.**, Kudryavtseva N., Soomere T. 2019. Baltic Sea wave climate variability and its connection with climatic indices deduced from Empirical Orthogonal Functions. *Baltic Sea Science Congress 2019* (19–23 August 2019, Stockholm, Sweden).

**Najafzadeh F.**, Kudryavtseva N., Soomere T. 2018. Baltic Sea wave climate via empirical orthogonal function analysis. *Baltic Earth Workshop on Multiple drivers for Earth system changes in the Baltic Sea region* (26–27 November 2018, Tallinn, Estonia).

**Najafzadeh F.**, Kudryavtseva N., Soomere T. 2018. Application of empirical orthogonal functions reveals multiple modes of variations in the Baltic Sea wave climate. *7<sup>th</sup> IEEE/OES Baltic Symposium Clean and Safe Baltic Sea and Energy Security for the Baltic countries* (12–15 June 2018, Klaipėda, Lithuania).

# Elulookirjeldus

## 1. Isikuandmed

Nimi: Fatemeh Najafzadeh  
Sünniaeg: 11.06.1990  
Sünnikoht: Mashhad, Iraan  
Kodakondsus: Iraan

## 2. Kontaktandmed

Aadress Ehitajate tee 5, 12616 Tallinn  
Telefon (+372) 51813370  
E-post Fatemeh.Najafzadeh@taltech.ee

## 3. Education

Hariduasutus	Õppimise aeg	Haridus (eriala / kraad)
Amirkabir University of technology	2013–2016	Laevaehitus / teadusmagister
Chabahr Maritime University	2008–2013	Laevaehitus / bakalaureus
Shahed Varesane Noor	2004–2008	Keskool

## 4. Keelteoskus

Keel	Tase
Inglise	C1
Pärsia	Emakeel
Araabia	Algaja
Eesti	Algaja
Saksa	Algaja

## 5. Täiendõpe

Õppimise aeg	Täiendõppe nimi ja läbiviija
Jaanuar 2020	Õppereis Soome meteoroloogia Instituuti, Helsingi, Soome
September 2019	<i>Kaugseire rakendused Läänemere regioonis, Võru</i>
Märts 2019	<i>Kliima muutlikkuse analüüs, Rostock, Saksamaa</i>
August 2018	<i>Läänemere kliima, rahvusvaheline suvekool, Trosa, Rootsi</i>

## 6. Teenistuskäik

Period	Organisatsioon	Ametikoht
Märts 2018–tänapäev	Tallinna tehnikaülikool, loodusteaduskond, küberneetika instituut	Doktorant-nooremteadur
Märts–juuni 2013	Chabahr Maritime University	Õppeülesannete täitja

## 7. Teadustegevus

Avaldatud teadusartiklite, muude publikatsioonide ja peetud konverentsiettekannete loetelu on toodud ingliskeelse elulookirjelduse juures.

ISSN 2585-6901 (PDF)  
ISBN 978-9949-83-918-6 (PDF)